NEUTRAL AND CATIONIC MAIN GROUP LEWIS ACIDS-SYNTHESIS, CHARACTERIZATION AND ANION COMPLEXATION

A Dissertation

by

TODD WILLIAM HUDNALL

Submitted to the Office of Graduate Studies of
Texas A&M University
in partial fulfillment of the requirements for the degree of

DOCTOR OF PHILOSOPHY

December 2008

Major Subject: Chemistry

NEUTRAL AND CATIONIC MAIN GROUP LEWIS ACIDS-SYNTHESIS, CHARACTERIZATION AND ANION COMPLEXATION

A Dissertation

by

TODD WILLIAM HUDNALL

Submitted to the Office of Graduate Studies of
Texas A&M University
in partial fulfillment of the requirements for the degree of

DOCTOR OF PHILOSOPHY

Approved by:

Chair of Committee,	François P. Gabbaï
Committee Members,	Donald J. Darensbourg
	John A. Gladysz
	Daniel F. Shantz
Head of Department,	David H. Russell

December 2008

Major Subject: Chemistry

ABSTRACT

Neutral and Cationic Main Group Lewis Acids-Synthesis, Characterization and Anion Complexation. (December 2008)

Todd William Hudnall, B.S., Texas State University-San Marcos

Chair of Advisory Committee: Dr. François P. Gabbaï

The molecular recognition of fluoride and cyanide anions has become an increasingly pertinent objective in research due to the toxicity associated with these anions, as well as their widespread use. Fluoride is commonly added to drinking water and toothpastes to promote dental health, and often used in the treatment of osteoporosis, however, high doses can lead to skeletal fluorosis, an incurable condition. Cyanide is also an extremely toxic anion, which binds to and deactivates the cytochrome-c oxidase enzyme, often leading to fatality. The molecular recognition of these anions in water has proven to be challenging. For fluoride, the anion is small, and thus, efficiently hydrated ($\Delta H°_{hyd}$ = -504 KJ/mol), making its complexation in aqueous environments particularly difficult. In addition to being small and efficiently hydrated like the fluoride anion, cyanide has a $pK_{a(HCN)}$ of 9.3 making its competing protonation in neutral water a further complication. Recent efforts to complex fluoride and cyanide have utilized triarylboranes, which covalently bind the anion. Monofunctional triarylboranes display a high affinity for fluoride with binding constants in the range of 10^5-10^6 M^{-1} in organic solvents, and chelating triarylboranes exhibit markedly higher anion affinities. These species, however, remain challenged in the presence of water.

This dissertation focuses on the synthesis and properties of novel Lewis acids designed for the molecular recognition of fluoride or cyanide in aqueous environments. To this end, a group 15 element will be incorporated into a main group Lewis acid-containing molecule for the purpose of: i) increasing the Lewis acidity of the molecule via incorporation of a cationic group, and ii) increasing the water compatibility of the host. Specifically, a pair of isomeric ammonium boranes has been synthesized. These boranes are selective sensors which selectively bind either fluoride or cyanide anions in

water. The study of phosphonium boranes has revealed that the latent Lewis acidity of the phosphonium moiety is capable of aiding triarylboranes in the chelation of small anions. Finally, my research shows that Brönsted acidic H-bond donors such as amides, when paired with triarylboranes, are capable of forming chelate complexes with fluoride.

DEDICATION

For you mom:

This dissertation is the best garbage man that I can be; but of course you wouldn't expect any less from me.

ACKNOWLEDGMENTS

I would first like to thank Mr. Larry Anderson, my high school chemistry teacher, for introducing me to the fantastic world of chemistry, and to both Dr. Chad J. Booth and Dr. Michael T. Blanda who served as undergraduate research advisors to me. In addition to easing me into a research setting, they gave me the confidence to pursue my doctoral degree. I would like to acknowledge my research committee. In particular, I would like to thank Dr. Donald J. Darensbourg and Dr. Stephen A. Miller for taking time out of their busy schedules for me. Additionally, I'd like to acknowledge Dr. Daniel F. Shantz for sitting on my committee, and Dr. John A. Gladysz for replacing Dr. Miller during my final defense.

The Gabbaï research group has been pivotal in helping me complete my Ph.D. Christopher Dorsey, who has been my colleague and good friend these past four years, has spent countless hours mulling over ideas about our research. His friendship during our graduate career has been invaluable. I would also like to thank Dr. Mohand A. Melaimi, who helped me greatly as a first year graduate student, and the entire Gabbaï group: Dr. Ching-Wen Chiu, Casey Wade, Dr. Mieock Kim, Youngmin Kim, Dr. Min Hyung Lee, Dr. Thomas Taylor, Dr. Charlotte Burress, Dr. Takeshi Matsumoto, Dr. Chammi Gamage, Haiyan Zhao, Tzu-Pin Lin, Bryan Carroll, Sirinan Kulchat and James Bondi.

A special thanks goes out to my mom Patti for always teaching me to persevere in all of life's endeavors, and to my sister Michelle and my fiancé Erin for their love and patience while I finished my Ph.D.

I would like to acknowledge the NSF, the Welch Foundation, the U.S. Army Institute for Chemical Defense for research funding, and the Department of Chemistry and Office of Graduate Studies for travel grants.

Finally, I would like to thank my research advisor, Professor François P. Gabbaï, for always having an open door and for the exhaustive time he has spent with me discussing my research. In addition to his time, I am thankful for the opportunity he has given me

to work in his laboratory and for his tremendous help in preparing this dissertation. He has always exhibited an enthusiastic and unrelenting approach to chemistry, and I owe any future success to his influence. I will forever be greatful for the time he has spent with me during my tenure at Texas A&M.

TABLE OF CONTENTS

CHAPTER Page

CHAPTER Page

Page

LIST OF FIGURES

Page

Page

Page

Page

Page

Page

Page

LIST OF TABLES

Page

CHAPTER I

INTRODUCTION TO BORON AND SILICON-BASED LEWIS ACIDS FOR THE MOLECULAR RECOGNITION OF FLUORIDE OR CYANIDE ANIONS

1.1 Introduction

The molecular recognition of fluoride continues to attract a great deal of attention because of the importance of this anion in dental health[1] and in the treatment of osteoporosis.[2] In 2002, the Centers for Disease Control and Prevention, stated that 60% of the U.S. population received fluoridated water.[3] In addition to water treatment, fluoride is also found in toothpastes and is often used as an anabolic drug in the treatment of osteoporosis. While the beneficial effects of fluoride are well documented, excessive intake can result in loss of calcium from the tooth matrix, thereby leading to cavity formation and ultimately dental fluorosis. Chronic exposure to high levels of fluoride can lead to skeletal fluorosis; an incurable condition resulting from the hardening and calcifying of the bones and joints.[4,5] The detrimental effects caused by excessive fluoride intake has become an impetus for the careful monitoring of fluoride concentration in drinking water. At the academic level, fluoride displays a high hydration enthalpy (ΔH^o = -504 kJ/mol)[6], causing its molecular recognition by abiotic hosts to be a definite challenge. In most cases, the binding sites of the sensors consist of amide, urea, thiourea, guanidinium, or pyrrole functionalities that are capable of hydrogen bonding with the anionic guest. [6-21] Implementation of this strategy has led to the design of very selective fluoride receptors and sensors. However, as noted by Fabbrizzi, fluoride recognition by these derivatives mostly takes place in organic solvents, which greatly limits the scope of their application.[22] The fluoride anion is effectively solvated in part due to its small size. The small size, and subsequently, the efficient solvation of fluoride, render the selective recognition of this anion over various

---

This dissertation follows the style and format of the *Journal of the American Chemical Society*.

other anions problematic. To circumvent the limitations experienced by molecules which hydrogen bond with the fluoride anion, several groups have investigated Lewis acidic receptors that can covalently bind fluoride ions such as triarylboranes.

In addition to the fluoride anion, another biologically relevant anion is the cyanide anion. Cyanide is a toxic anion which binds to and deactivates the cytochrome-c oxidase enzyme with sometimes fatal consequences.[23] Because cyanide is widely available in both research and industrial settings, its use for harmful purposes or its release in the environment are sources of concern.[24] Thus, as for the fluoride anion, the development of cyanide sensors which are competent in aqueous media has become a contemporary research objective for many groups. Another similarity shared by the fluoride and the cyanide anion is efficient solvation in water. For cyanide, an additional complication arises from the competitive protonation ($pK_{a(HCN)} = 9.3$) which occurs in water.

Despite these challenges, a number of receptors which effect cyanide recognition in water have been reported. The receptors typically are electrophilic organic compounds which undergo C-C bond forming reactions with cyanide.[25-28] This paradigm has been exploited by taking advantage of the cyanide anion's inherent nucleophilicity. Cyanide recognition in these species typically necessitates basic pH to overcome HCN formation and the reversibility in these systems is not well documented. Receptors which give rise to a colorimetric or fluorometric response in the presence of cyanide would also be advantageous for sensing applications. To date, several receptors, which give a colorimetric or fluorometric response to cyanide and employ ketones or amides as the receptor site, have been developed.[25-28] Most of these receptors only function in organic solvents; as such, several groups have turned their attention to Lewis acidic molecules which may serve as competent hosts for cyanide anions.

1.2 Neutral, monofunctional triarylboranes for anion recognition

Since boron is intrinsically fluorophilic, a great deal of work has been focused on the utilization of Lewis acidic boron compounds for the complexation of fluoride.[29-40] A large part of the recent research has been focused on neutral monofunctional

triarylboranes which readily complex fluoride anions in organic solvents (Figure 1).[41-44] In addition to fluoride complexation, it has long been established that triarylboranes react with cyanide to generate cyanoborate complexes (Figure 1). In particular, the cyanoborate anion $[Ph_3BCN]^-$ has been used to precipitate cesium ions from water.[45] This observation suggests that water stable triarylboranes may be well suited for the recognition of cyanide in water.

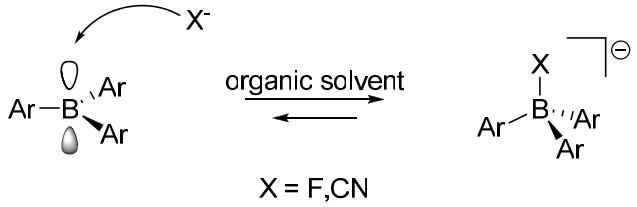

Figure 1: Fluoride or cyanide complexation of triarylboranes.

While these properties of triarylboranes have long been overlooked in the context of anion sensing, Tamao and Yamaguchi made a seminal contribution in which they showed that tri(9-anthryl)borane, **1**, complexes fluoride ions with a binding constant of 2.8×10^5 M^{-1} in THF.[46] This process has also been shown to be reversible upon the addition of water into THF solutions of the fluoroborate [**1**-F]$^-$.

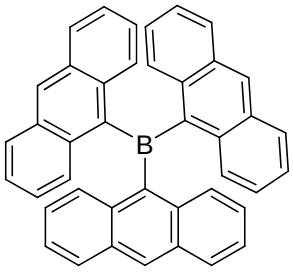

1

Another attractive feature of their discovery pertains to the photophysical response observed upon fluoride binding. Indeed, fluoride binding interrupts the extended electronic conjugation mediated by the boron empty p-orbital leading to a blue shift of the absorbance (Figure 2).

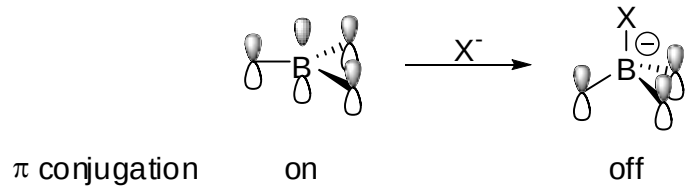

Figure 2: Change in π-conjugation of triarylboranes upon complexation.

Yamaguchi has also prepared triarylborane derivatives containing borafluorene moieties (**2a-c)**.[47] These receptors behave similarly to **1** and also display a visible response upon fluoride binding. Because of the antiaromatic character of the borafluorene moiety, compounds of type **2** are more electron deficient than **1** and display higher fluoride binding constants (Table 1).

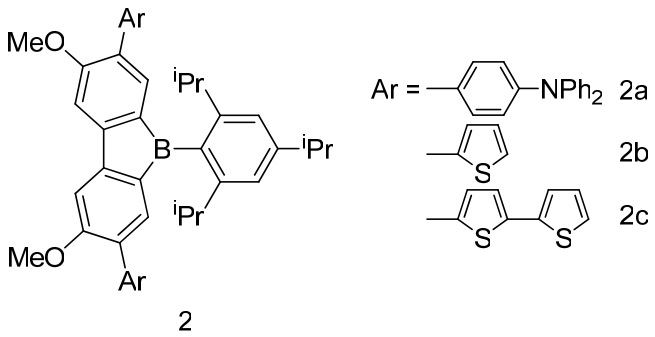

2

Since the advent of these profound contributions, a number of other groups have reported other tri-arylborane based fluoride receptors whose fluoride binding constants are given in Table 1.[48-54] These compounds are discussed in more detail in the following paragraphs.

1.2.1 Neutral, monofunctional triarylboranes which exhibit charge transfer character

In the presence of appropriate electron donors, triarylboranes tend to display an intramolecular charge-transfer transition.[42] Although this property has been extensively studied, the use of these types of molecules in fluoride sensing was not investigated until recently. Wang and co-workers have developed a series of anion receptors featuring triarylamino and triarylboryl moieties (**3**, **4** and **5**) that respectively serve as electron donor and acceptor units.[52,54]

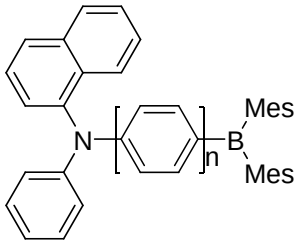

3a: n = 1
3b: n = 2

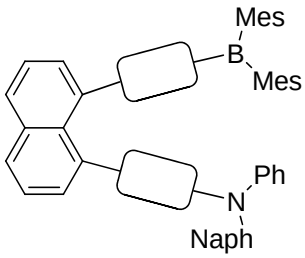

4

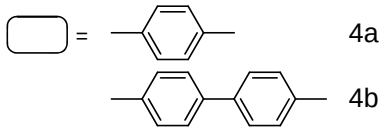

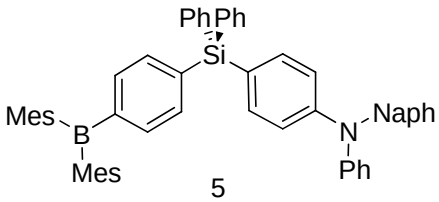

5

Photo-excitation of these molecules results in an intramolecular charge-transfer emission, which can be quenched or perturbed by fluoride binding at the boron center. Since the luminescence of the molecule is altered due to the formation of a fluoroborate,

the fluoride binding constant of the borane receptor can be determined via fluorescence titration.

The effect of the relative position of the donor and acceptor groups has also been investigated. In the linear molecule **3**, fluoride addition results in the quenching of the luminescence in THF.[52] However, in the U-shaped molecule **4**, two emission mechanisms are observed, the through space donor-acceptor charge-transfer emission and the π-π* transition localized on the triarylamino moiety. In the presence of fluoride, the quantum yield of the π-π* transition is enhanced because of a quenching of the charge-transfer emission pathway. Moreover, the B-N separation in these molecules affects not only the efficiency of the charge transfer, but also the fluoride binding ability of the triarylboryl moiety. For example, compounds **4a** and **4b** exhibit much lower fluoride binding constants when compared to the linear molecules **3** and the V-shaped molecule **5** . This weaker binding is the consequence of strong steric interactions between the donor and acceptor groups imposed by the U-shaped geometry (Table 1). Analogously, the V-shaped receptors, **5**, exhibit two luminescence mechanisms similar to their U-shaped analogues, but with higher sensitivity toward fluoride binding.[54]

1.2.2 Neutral, monofunctional triarylboranes which exhibit two-photon excited fluorescence

Triarylboranes which display unusual two-photon excited fluorescence (TPEF) have been recently investigated. TPEF is especially attractive for imaging purposes in biological systems because the low energy light needed to excite the chromophore has a greater penetration depth in biological tissues. With this type of applications in mind, Li and Fang have monitored the fluoride ion binding ability of **6** using its TPEF properties.[51] The resulting fluoride binding constant of 2×10^5 M^{-1} is identical to that obtained from single-photon excited fluorescence (SPEF) (Table 1).[51]

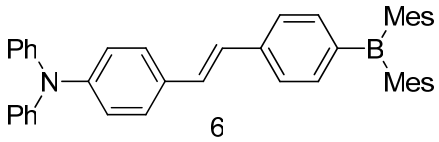

6

1.3 Neutral, polyfunctional, non-chelating triarylboranes

1.3.1 Pyridyl-based polyfunctional triarylboranes and their transition metal complexes

In addition to simple monofunctional boranes, several polyfunctional boranes containing various molecular linkers have been investigated. Wang and co-workers have reported a strategy used to increase the fluoride affinity of diboranes by incorporating an electron withdrawing molecular linker between two boryl groups. Diborane **7** contains a 2,2'-bipyridyl linker and displays enhanced fluoride affinity due to the presence of electronegative nitrogen atoms.[55] As indicated by cyclic voltammetry, **7** is reduced at a potential which is 270 mV more positive than that of its biphenyl analog **8**. Moreover, the separation between the first and second reduction waves in the cyclic voltammogram of **7** is 130 mV greater than that observed for **8**. This observation indicates that the bipyridyl linker is more efficient in mediating electronic communication between the two boryl units.

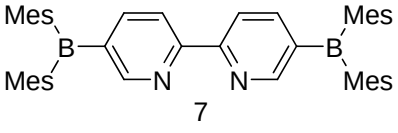

7

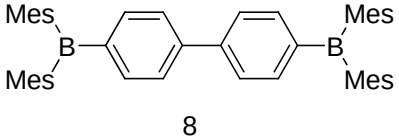

8

7Ma: M = Pt, R = Ph
7Mb: M = Pt, R = Me
7Mc: M = Cu, R = PPh_3

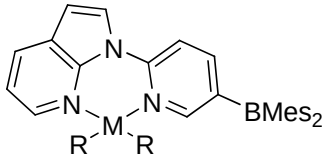

9a: M = Pt, R = Ph
9b: M = Pt, R = Cl
9c: M = Cu, R = PPh_3

The higher Lewis acidity of **7** is also manifested by its unusually high fluoride affinity. This diborane first binds a single fluoride anion with a binding constant greater than 10^8 M^{-1} followed by a second one at 10^6 M^{-1} (Table 1). These values are much higher than those typically measured for triarylboranes. Coordination of Cu(I) or Pt(II) moieties to the bipyridyl ligand of this diborane leads to the formation of orange complexes **7**Ma-c, which feature Metal to Ligand Charge Transfer bands that can be used to monitor fluoride complexation.[55] The bipyridine complexes **9a-c** were also reported by Wang in the same year as compounds **7** and **8**. These molecules are unique in that they exhibit room temperature phosphorescence which can be used to monitor anion binding. The copper(I) derivative, **9**c exhibits a quenching of the phosphorescence, which is concomitant with ligand dissociation from the metal. The emission quantum yield of the copper species is very high (0.88), and thus its response to fluoride is very sensitive. Complexes **9**a and **9**b don't suffer from ligand dissociation, and rather than phosphorescence quenching, a colorimetric shift from yellow to green is observed in the presence of fluoride anions.[56]

1.3.2 Multistage fluoride binding by neutral polyfunctional triarylboranes

Yamaguchi has also reported a polyfunctional borane, **10**, that contains four boron atoms capable of binding fluoride. The fluoride binding constants were determined to be 6.9×10^4 M^{-1}, 9.0×10^2 M^{-1}, and 2.1×10^2 M^{-1} for the first, second and third fluoride ion, respectively (Table 1).[41] This result indicates that the fluoride affinity of **10** is significantly decreased after the first fluoride binding event. This can be attributed to an increase in Coulombic repulsion which results from the formation of increasingly anionic fluoroborate species. It is also noteworthy that the UV-vis spectrum of $[\mathbf{10}\text{-}\mathbf{F_3}]^{3-}$ is very close to that observed for **1**, suggesting that fluoride complexation only occurs at the terminal boron sites.

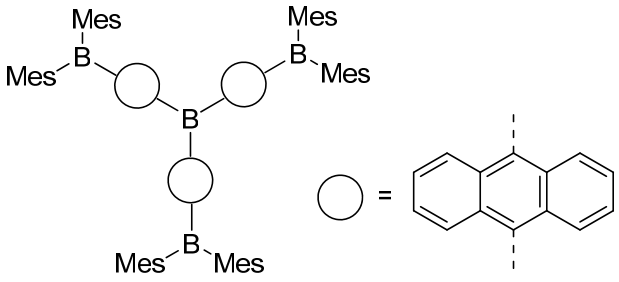

10

Like compound **10**, diborane **11** exhibits two distinct stages of fluoride complexation which can be observed by UV-vis spectroscopy.[51] From the UV-vis titration experiments carried out in THF, the first and second fluoride binding constants were determined to be 3.2 x 10^5 M^{-1} and 1.3 x 10^5 M^{-1} for first and second binding sites, respectively (Table 1).

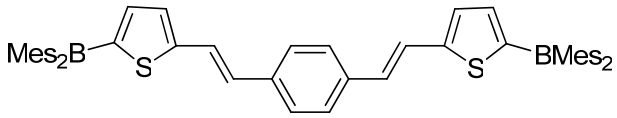

11

Compound **11** also displays strong SPEF and TPEF which along with absorption spectroscopy, can be used to monitor fluoride binding. However, only the first stage of fluoride complexation can be observed using SPEF and TPEF. Indeed, after addition of one equivalent of fluoride, no further changes can be observed in the luminescence spectrum due to the low quantum yield of [**11**-F]$^-$.[51]

More recently, Fang and coworkers have synthesized a series of polydimesitylboryl-substituted truxenes, **12**, which serve as fluorometric probes for fluoride anions.[57] Molecules **12** display fluoride binding constants in THF which average 3 × 10^5 M^{-1} for

complexation of a single fluoride anion and approximately 10^4 M^{-1} for complexation of the second and third fluoride anions (Table 1).

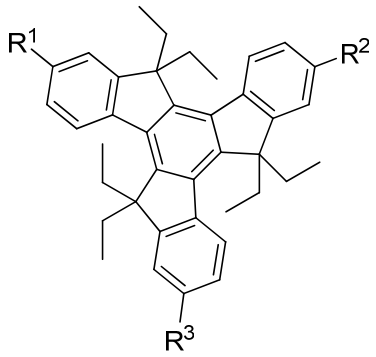

12a: $R^1 = R^2 = H$; $R^3 = BMes_2$
12b: $R^1 = R^3 = BMes_2$; $R^2 = H$
12c: $R^1 = R^2 = R^3 = BMes_2$
12d: $R^1 = R^2 = BMes_2$; $R^3 = NPh_2$
12e: $R^1 = R^2 = NPh_2$; $R^3 = BMes_2$

Compounds **12**a-c display very similar absorption and emission spectra at approximately 360 and 385 nm respectively. These three molecules exhibit a modest Stokes shift and short fluorescence lifetimes ($\tau < 5$ ns), characteristic of these acceptor substituted truxenes. Interestingly, as the boryl substitution is increased on going from **12**a to **12**c, the molar extinction coefficient (ε_{max}) increases proportionally. This is also observed in the emission spectrum of these molecules (ie. **12**c exhibits a higher quantum yield than **12**a). Because of the presence of donor triarylamino groups, compounds **12**d and **12**e exhibit charge-transfer transitions which are quenched upon fluoride complexation as is seen in the compounds developed by Wang (**3**-**5**).[52,54,57]

1.3.3 Polystyrene supported neutral, polyfunctional triarylboranes

Jäkle has synthesized a series of luminescent triarylborane-functionalized polystyrene derivatives (**13**).[49] These three polymers display broad absorption bands in the 365-440 nm range both in CH_2Cl_2 solutions or when cast as thin films from toluene. They are also highly fluorescent giving rise to emission bands which range from 442-537 nm. The observed red-shift in the absorption and emission spectra can be correlated

to the increasing electron-donating ability of the R group on the thienyl moiety. Thus, as the R group becomes more electron-donating on going from hydrogen to hexyl, and then diphenylamino, the absorption and emission spectra are increasingly red-shifted.

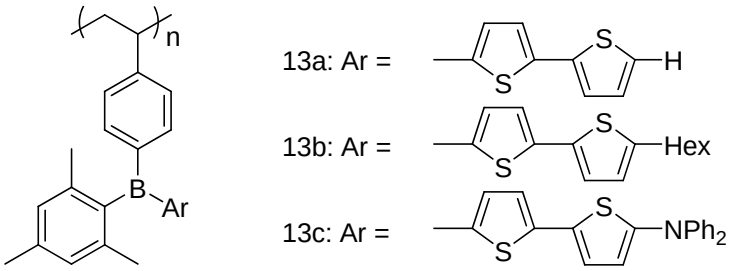

The fluoride binding properties of the substituted bithiophene polymers (**13b** and **13c**) were studied in THF. For **13b**, upon incremental addition of fluoride anions, a gradual decrease in the absorption band at 378 nm was observed. This spectral change coincided with the appearance of a new band at 338 nm (attributed to the absorbance of a bithiophene with a fluoroborate moiety $[B(Mes)ArF]^-$). Similarly, fluoride addition to **13c** led to the appearance of band at 362 nm, blue-shifted by 70 nm relative to the uncomplexed polymer. Using these spectral changes, a fluoride binding constant of logK = 6.9 is obtained for each of the polymers (Table 1). Similar values could be obtained by monitoring the intensity of the emission bands of **13b** and **13c** at 461 and 532 nm, respectively, upon fluoride addition.[49]

These polymers were screened against several anions including chloride, bromide, nitrate and cyanide in order to determine if fluoride complexation was selective. It was shown that the presence of a 10-fold excess of either fluoride or cyanide induced a quenching of the fluorescence of these polymers, indicating that they may potentially serve as sensors for fluoride or cyanide anions. Interestingly, it was also noted that upon addition of either of these two anions to a solution of **13b** in THF the appearance of a weaker, new emission band at 405 nm was concomitant with the disappearance of the

band at 461 nm when exciting at 330 nm. This new band was attributed to the emission of the bithiophene moieties decorated by borate groups (Figure 3). Likewise, **13c** exhibits a new blue emission band at 457 nm with a shoulder extending to ca. 430 nm with simultaneous loss of the green emission at 537 nm (Figure 3). This colorimetric turn-on response is unusual for triarylboryl anion sensors and is desirable in the context of developing wavelength-ratiometric probes for fluoride or cyanide.[49]

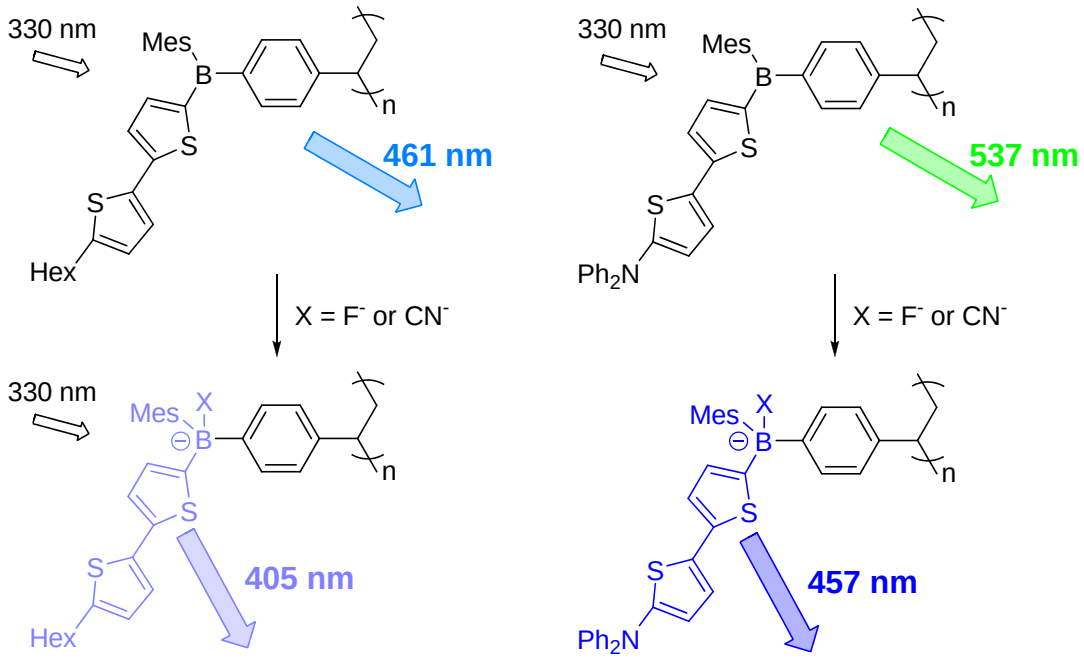

Figure 3 Changes in the emission wavelength of 13b and 13c in THF (3×10^{-5} M in borane) in the presence of fluoride or cyanide anions (λ_{ex} = 330 nm).

1.4 Neutral, bidentate polyfunctional triarylboranes

In order to increase the binding constant of borane based receptors, several groups, including ours, have explored the use of bidentate boranes that chelate fluoride[48,58-67] (Figure 4). Our efforts in this area have focused on the design of naphthalene based derivatives such as **14** and **15**. The UV-vis titration of **14** in THF reveals that the

absorbance decreases linearly with an increase in fluoride concentration and reaches the baseline after addition of one equivalent of fluoride. This result indicates the formation of a 1:1 complex between **14** and fluoride with a binding constant exceeding the measurable range ($>10^9$ M^{-1}). This enhancement is attributed to chelation of the fluoride anion which occurs in this type of system. There is also a drastic relief of steric repulsion between two boryl groups upon fluoride binding which favors complexation of the anion.[68] Unlike the fluoroborate derivative [**1**-F]$^-$, addition of water to THF solutions of [**14**-F]$^-$ does not result in dissociation of the B-F bond. Although the fluoride binding constants of such receptors exceed those of monofunctional analogs by 3 or 4 orders of magnitude, their use in protic environments remains problematic. For example, chelating diboranes such as **14** will undergo a slow hydrolysis in the presence of water or methanol.[48]

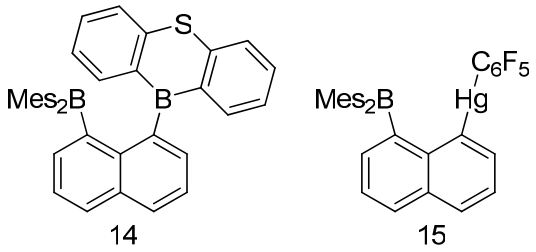

Figure 4: Chelating bifunctional Lewis acids **14** and **15**.

The heteronuclear B/Hg derivative **15** is also capable of chelating fluoride anions in 90/10 (vol.) THF/water[61], but not in pure water. Chelation of the fluoride anion indicates that the mercury(II) center is sufficiently fluorophilic and aids in enhancing the fluoride affinity of the Lewis acidic boron atom. The X-ray crystallographic analysis of [**15**-F]$^-$ indicates that there is a weak interaction between the fluoride anion and the fluorophilic mercury(II) Lewis acid (B-F = 1.483(4) Å, F-Hg = 2.589(2) Å, Figure 5).

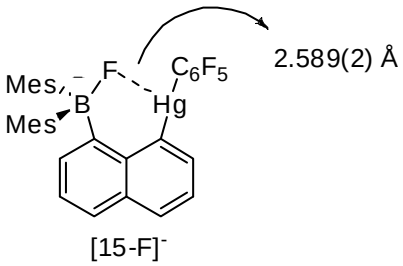

Figure 5: Fluoride anion chelation observed in [**15**-F]$^-$.

Besides participating in fluoride binding,[69,70] mercury(II) can also serve to induce the room temperature phosphorescence of hydrocarbon chromophores via spin-orbit coupling effects.[71] Photoexcitation of **15** gives rise to an emission at λ_{max} = 531 nm in the solid state corresponding to the phosphorescence of the dimesitylboryl-naphthalenediyl chromophore. Upon fluoride complexation, a new intense signal appears at 480 nm whose energy and vibronic progressions resemble those observed in the phosphorescence spectrum of pure naphthalene. This indicates that fluoride binding results in the loss of conjugation and isolates the naphthalenediyl chromophore, which readily phosphoresces due to the spin-orbit coupling induced by the mercury atom. The fluoride binding constant of **15** was determined to be greater than 10^8 M^{-1} in organic solvent and 2.3 x 10^4 M^{-1} in a 9:1 THF/H_2O mixed solvent system (Table 1), which substantiates the cooperative binding of fluoride by the boron and mercury atoms. At the time of its report, **15** was the first triarylborane capable of binding fluoride ions in water containing media.

1.4.1 Perfluorinated bidentate diboranes for anion complexation

Piers's group has also reported bidentate diboranes which are capable of anion chelation. For example, 1,2-bis(bis(pentafluorophenyl)boryl)benzene (**16**) has been prepared, and its use as a Lewis activator in olefin polymerization reactions investigated. This diborane complexes a number of anions including hydroxide, methoxide[72], azide[73],

chloride[74] and fluoride[72]. Although the stability constant of these adducts have not been reported, it can be assumed that these anionic chelate complexes are highly stable (Figure 6).

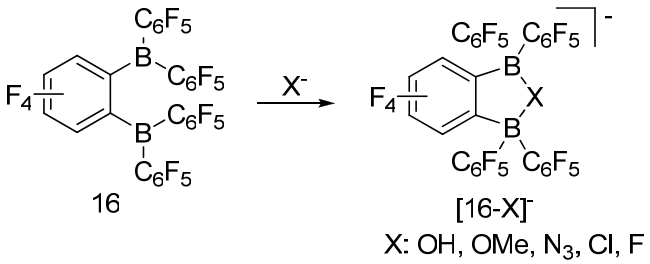

Figure 6: Anion complexation of **16**.

1.4.2 Heteronuclear boron/tin bidentate Lewis acids

The group of Jäkle has also made several interesting contributions in the area of borane based fluoride probes. Numerous derivatives synthesized by their group consist of ferrocene-based heteronuclear bidentate Lewis acids which contain neighboring boryl and stannyl Lewis acidic moieties. These molecules (**17**) show a variety of fluoride complexation modes including: anion chelation, multiple anion complexation to each Lewis acid site, and anion complexation induced aryl (or alkyl) group migration (observed in **17**c and **17**d).

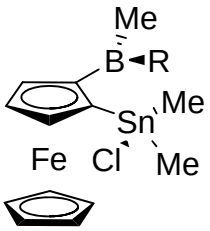

17a: R = Cl 17c: R = Th
17b: R = Ph 17d: R = All

In 2007, Jäkle reported compounds **17a** and **17b** which serve to chelate fluoride anions between the Lewis acidic boron and tin atoms.[75] Indeed, treatment of **17a** or **17b** with 1.7 equivalents of KF and 18-crown-6-ether (18-c-6) in THF at ambient temperature for two days leads to formation of [**17a**-F_2]$^-$ and [**17b**-F]$^-$ respectively, whereas addition of an excess of KF at elevated temperatures (50 °C) leads to formation of the adducts [**17a**-F_3]$^-$ and [**17b**-F_2]$^-$ (Figure 7).[75]

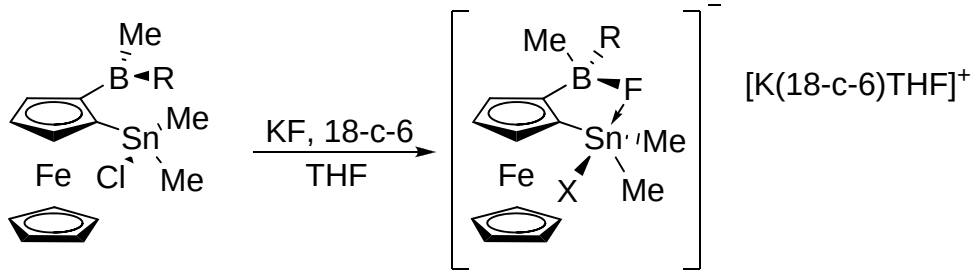

17a: R = Cl
17b: R = Ph

[17a-F_2]$^-$: R = F, X = Cl
[17b-F]$^-$: R = Ph, X = Cl
[17a-F_3]$^-$: R = F, X = F
[17b-F_2]$^-$: R = Ph, X = F

Figure 7: Formation of fluoride adducts with compounds **17**a and **17**b.

Despite the attractive photophysical properties and the substantial fluoride affinity of triarylboranes (Table 1), their use for practical applications remains problematic. In particular, none of the aforementioned boranes are capable of binding fluoride in aqueous media, nor are they able to overcome the hydration energy of fluoride. For example, although the fluoride adduct of compound [**1**-F]$^-$ shows a stability constant of 10^5 in organic solvents, addition of water into the system leads to complete dissociation of the fluoroborate. The chelating diborane **14**, whose fluoride binding constant exceeds that of mono-functional boranes by at least 3 orders of magnitude, cannot bind fluoride in protic environments and undergoes hydrolysis in the presence of water. The heteronuclear bidentate receptor **15**, which captures fluoride in a 9:1 THF/H_2O mixed solvent system, does not capture fluoride from pure water. For these reasons, an alternantive strategy based on the use of cationic triarylboranes has been recently considered.

1.5 Fluoride complexation by cationic triarylboranes

1.5.1 Monofunctional ammonium and phosphonium triarylboranes

Hoping to increase the fluoride affinity of the borane based receptor via Coulombic effects, recent efforts have been devoted to the study of cationic boranes (Figure 8).[76-84,85,86]

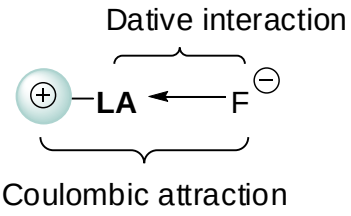

Figure 8: Conceptual drawing illustrating the favored interaction between cationic Lewis acids and fluoride anions (LA = Lewis acid).

The first reported example of a cationic borane from the Gabbaï group is inspired by compounds such as **14** and **15**, featuring ammonium and triarylboryl moieties fashioned to a rigid naphthalene scaffold. Ammonium borane [**18**]$^+$ (isolated as a triflate (OTf^-) salt) readily complexes fluoride in a variety of organic solvents; in particular, the fluoride binding constant obtained in $CHCl_3$ is greater than $10^6\ M^{-1}$ (Table 1) which is at least two orders of magnitude greater than what is observed for **15** ($K = 2.1 \pm 0.2 \times 10^4\ M^{-1}$ in $CHCl_3$).[85]

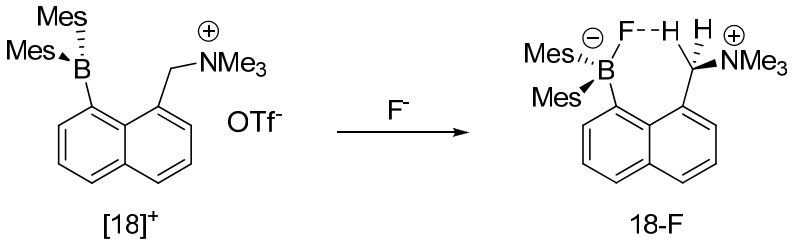

Figure 9: Fluoride complexation by the cationic borane [**18**]$^+$ to form the zwitterion **18**-F.

As depicted in the structure of the zwitterionic **18**-F (Figure 9), the fluoride anion forms a weak hydrogen bond with a proton on the adjacent methylene group. The presence of this interaction was confirmed by single crystal X-ray diffraction analysis of **18**-F.[85] Remarkably, ammonium borane [**18**]$^+$ is capable of extracting fluoride anions from water biphasically. Indeed, when a chloroform solution containing [**18**]$^+$ is shaken with an aqueous solution of fluoride anions (KF), fluoride is transferred from the water layer to the organic layer as corroborated by multinuclear NMR spectroscopy. The significance of this discovery lies in the fact that [**18**]$^+$ was the first reported triarylborane able to overcome the hydration enthalpy of the fluoride anion.[85]

Like [**18**]$^+$, phosphonium boranes of type [**19**]$^+$, are capable of capturing fluoride anions under biphasic conditions.[87] In addition to being able to induce fluoride transfer in solution, fluoride ions can be transferred to the phosphonium boranes in the solid state.

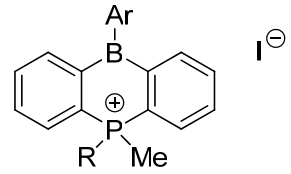

19a$^+$: Ar = Mes, R = Ph
19b$^+$: Ar = Tip, R = Me

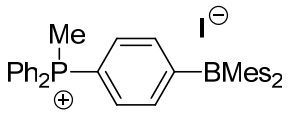

20^+

These results were obtained by washing powders of [**19**]$^+$ with aqueous solutions of KF.[87] Complex **19a**-F was relatively unstable, precluding isolation of this complex. Fluoride binding was observed, however, in solution by multinuclear NMR. For cation [**19b**]$^+$, the introduction of the 2,4,6-triisopropylphenyl (Tip) group imparts substantial stability to the corresponding fluoroborate complex **19b**-F, allowing for isolation and structural characterization.

The *para*-phenylyene substituted phosphonium borane [**20**]$^+$ is the first reported example of a triarylborane which functions in aqueous media as a fluoride receptor.[88] Moreover, [**20**]$^+$ binds fluoride at neutral pH. It is also exceptionally selective for fluoride over chloride, bromide, nitrate, sulfate and phosphate anions. Indeed, titration experiments carried out in H_2O/MeOH (9:1, v/v) mixed solvent allowed for the determination of a stability constant for the zwitterion **20**-F of 1000 M^{-1} (Table 1). Fluoride complexation can be monitored by a decrease in the absorbance of the band at 321 nm, or by monitoring a decrease in the emission spectrum of [**20**]$^+$ at 495 nm.

Addition of fluoride anions to an aqueous solution of [**20**]$^+$ induces a rapid quenching of the bright green fluorescence, providing a nice fluorometric response for fluoride sensing in water. This turn-off sensing approach has been well established for triarylboranes, and the potential application of compounds such as [**20**]$^+$ in biological systems remains attractive.[88]

1.5.2 Heteronuclear cationic boron/mercury Lewis acids

Additional work with cationic boranes for fluoride sensing has been completed by our group. Ammonium borane [**21**]$^+$ is the first attempt by the group of Gabbaï at incorporating a cationic functionality into a bidentate heteronuclear Lewis acid.[89] This effort was aimed at determining if fluoride anion chelation by bidentate Lewis acids could be complemented by favorable Coulombic attractions. In order to test this hypothesis, the fluoride binding constants for the cationic borane [**21**]$^+$ and its neutral precursor **22** were obtained in THF/H_2O (9/1 vol.) mixed solvent. Spectroscopic and structural studies confirm the presence of a bridging fluoride anion in the fluoroborate complexes **21**-F and [**22**-F]$^-$. The ^{199}Hg NMR resonances for each molecule appear as a doublet at -759.8 ppm ($^1J_{Hg\text{-}F}$ = 122 Hz) and -708.6 ($^1J_{Hg\text{-}F}$ = 109.8 Hz) for **21**-F and [**22**-F]$^-$ respectively. This assessment is further substantiated by the X-ray crystal structure obtained for **21**-F which clearly features a B-F-Hg bridging unit (B-F = 1.474(8) Å, Hg-F = 2.618(3) Å) that is structurally similar to that observed in [**15**-F]$^-$.[89]

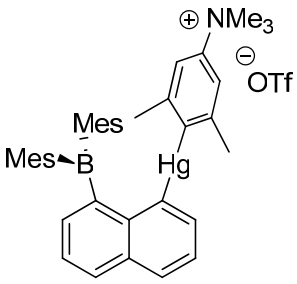

[21]$^+$

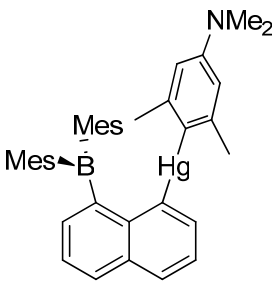

22

Table 1: Fluoride binding constants of triarylboranes.

	Solvent	K_1 (M^{-1})	K_2 (M^{-2})	K_3 (M^{-3})
1	THF	$2.8(\pm0.3) \times 10^5$	---	---
2c	THF	$1.4(\pm0.3) \times 10^6$	---	---
3	THF	N.A.	---	---
4a	THF	1.4×10^4	---	---
4b	THF	4×10^4	---	---
5	THF	N.A.	---	---
6	THF(SPEF)	$2.1(\pm0.4) \times 10^5$	---	---
7	CH_2Cl_2	$\geq 10^8$	$\sim 10^6$	---
	THF/EtOH 7:3	6×10^4	---	---
7Ma	CH_2Cl_2	$\geq 10^9$	$\sim 10^6$	---
	CH_2Cl_2/MeOH 4:1	4×10^3	---	---
10	THF	$6.9(\pm0.2) \times 10^4$	$9.0(\pm0.6) \times 10^2$	$2.1(\pm0.4) \times 10^2$
11	THF	$3.2(\pm0.3) \times 10^5$	$1.3(\pm0.2) \times 10^5$	---
12a	THF	3.1×10^5	---	---
12b	THF	2.9×10^5	2.8×10^4	---
12c	THF	3.9×10^5	2.5×10^4	1.6×10^4
12d	THF	2.5×10^5	---	---
12e	THF	3.1×10^5	2.2×10^4	---
14	THF	$\geq 10^8$	---	---
15	THF/H_2O 9:1	2.3×10^4	---	---
13b,c	THF	$\sim 10^7$	---	---
[**18**]$^+$	$CHCl_3$	$\geq 10^6$	---	---
[**20**]$^+$	H_2O/MeOH 9:1	1000	---	---
[**21**]$^+$	THF/H_2O 9:1	$6.2(\pm0.2) \times 10^4$	---	---
22	THF/H_2O 9:1	$1.3(\pm0.1) \times 10^2$	---	---

In accordance with the prediction that favorable Coulombic effects resulting from the introduction of a cationic center can complement chelation of fluoride anion in bidentate Lewis acid derivatives, it was found that the stability constant of **21**-F ($6.2 \pm 0.2 \times 10^4$ M^{-1}) exceeds that of [**22**-F]$^-$ ($1.3 \pm 0.1 \times 10^2$ M^-) by two orders of magnitude in the THF/H_2O mixed solvent system (Table 1).[89]

1.6 Introduction to fluoride complexation by boronic acids and esters

In addition to triarylboranes, the three-coordinate boronic acids/esters have been extensively investigated for the molecular recognition of fluoride anions. The inherent unsaturation at the boron center effectively makes complexation with Lewis bases possible. While selective binding of fluoride can be achieved, competitive complexation of diols, sugars and other halides is often observed. One of the first examples concerning the use of boronic esters for anion recognition was reported in 1991 by Reetz and coworkers.[90] In this report, the authors synthesized crown-ether molecules featuring a pendant boronic ester. These molecules were used for the recognition of potassium salts (Figure 10). Although not very selective, these species brought attention to the practical use of boron based systems for anion recognition.[90]

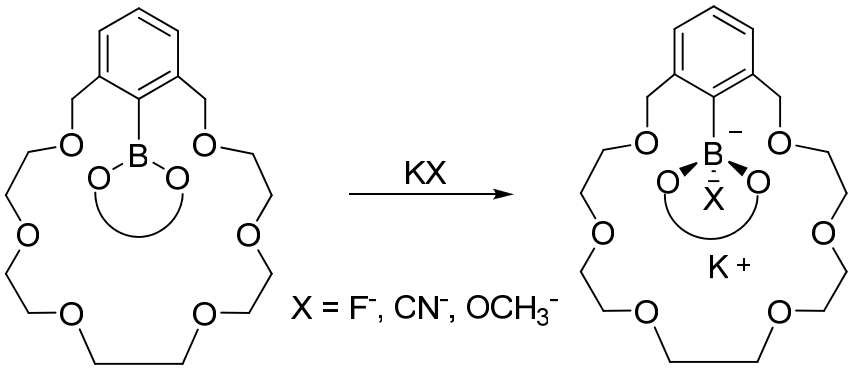

Figure 10: Crown-ether boronic ester potassium salt receptors.

1.7 Arylboronic acid-based receptors for fluoride anions

1.7.1 Simple arylboronic acids for fluoride sensing

Some of the simplest known examples of boron based fluoride receptors are aryl boronic acids such as phenyl boronic acid (**23**). Unlike triarylboranes which bind only a single fluoride anion per boron atom, boronic acids can bind up to three fluoride anions to form the corresponding trifluoroborates. This three step equilibrium involving the boronic acid group and fluoride anions has been nicely delineated by the group of Lakowicz (Figure 11).[35,37]

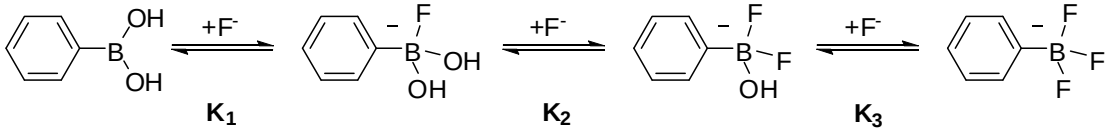

Figure 11: Equilibrium involved in the interaction between the boronic acid group and fluoride.

In 1998, James and coworkers investigated the fluorescence detection of fluoride using phenylboronic acid, 2-napthylboronic acid (**24**), and an amino substituted phenylboronic acid (**25**).[33]

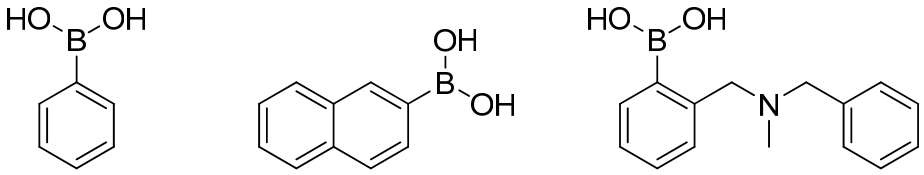

23 24 25

Compounds **23-25** behave as selective fluoride probes whose fluorescence is quenched upon formation of the corresponding aryltrifluoroborates. The fluorescence quenching phenomenon is similar to that observed in triarylboranes where the conjugation of a chromophore through the empty p-orbital on boron is disrupted upon rehyrbidization of the boron atom in the presence of fluoride anions. This method of detection is often challenged in water as boronic acids exist as four-coordinate boronate anions at pH values above their pK_a. Formation of tetrahedral boronate species also quenches directly attached fluorophores, which limits their application for fluoride sensing at neutral pH.

When **23** and **24** are titrated with KF at pH 5.5 in 50% (w/w) methanol-water buffer, the fluorescence of the phenyl and 2-napthyl fluorophores decreases. The experimental curves can be fitted based on the formation of a trifluoroborate species with K_3 values of 1.04×10^4 and 1.08×10^4 M^{-3} respectively. In the case of compound **25**, fluoride binding may be assisted by a hydrogen-bonding interaction involving the protonated amine and the boron-bound fluorine atom. (Figure 12).[33] Titrations of **25** carried out using the same conditions described for **23** and **24** provided data which could be fitted by hand to obtain a fluoride binding constant K_1 for the formation of a $[ArB(OH)_2F]^-$ anion of 101 M^{-1}.

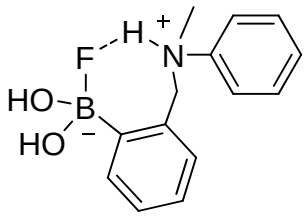

Figure 12: Proposed B-F---HN bridge in fluoride adduct of **25**.

Lakowicz has also developed colorimetric probes for the detection of fluoride anions based on quinolinium boronic acids (**26 a-c**, **27 a-c** and **28 a-c**).[35,91] The quinolinium scaffold is readily soluble in water and compounds **26-28** are all fluorescent derivatives, hence the interest for anion sensors based on this design.

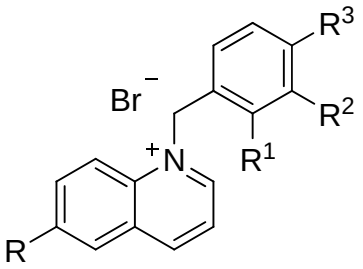

26a: R= Me, R^1= $B(OH)_2$, R^2= H, R^3=H
26b: R= Me, R^1= H, R^2= $B(OH)_2$, R^3=H
26c: R= Me, R^1= H, R^2= H, R^3=$B(OH)_2$

27a: R= MeO, R^1= $B(OH)_2$, R^2= H, R^3=H
27b: R= MeO, R^1= H, R^2= $B(OH)_2$, R^3=H
27c: R= MeO, R^1= H, R^2= H, R^3=$B(OH)_2$

28a: R= NH_2, R^1= $B(OH)_2$, R^2= H, R^3=H
28b: R= NH_2, R^1= H, R^2= $B(OH)_2$, R^3=H
28c: R= NH_2, R^1= H, R^2= H, R^3=$B(OH)_2$

These cationic derivatives are well adapted for anion binding in water; however, these probes do not exhibit any appreciable selectivity for fluoride, interacting with other anions including chloride, bromide, iodide and cyanide. The quinolinium functionality is highly fluorescent and as such is sensitive to quenching by halides. It is well documented that the halides quench organic fluorophores effectively. For dynamic quenching, fluorophore sensitivity to halide is known to be $I^- > Br^- > Cl^-$, with fluoride displaying no appreciable quenching. This ordering is best rationalized by invoking heavy-atom-effect where the efficiency of intersystem crossing to the excited triplet state increases with the mass of the halide.

The mechanism by which the quinolinium probes interact with fluoride and cyanide differs from that of the other halides. While dynamic quenching is observed upon contact of the quinolinium receptors with chloride, bromide or iodide; quenching in the presence of fluoride or cyanide can be attributed to complexation of the anion to the empty-p_z orbital of the boron atom as observed with other boron-based probes. The fluoride binding constants of compounds **26-28** range from 10-1000 mM^3, and the cyanide binding constants were found to be between 5 mM^3-100 mM^3 in water (Table 2).[35,91]

Table 2: Stability constants for compounds **26-28** with fluoride and cyanide in water.

	Fluoride K_3 (mM^{-3})	Cyanide K_3 (mM^{-3})
26a	530	16.7
26b	330	16.9
26c	500	15.9
27a	960	52.9
27b	900	84.0
27c	1000	20.8
28a	40.0	8.33
28b	10.8	5.88
28c	55.6	7.14

Lakowicz has investigated a variety of fluoride probes which feature intramolecular charge transfer (ICT) transition. These ICT transitions are very sensitive to slight perturbations in the structure/environment of the molecule. For the boronic acid probes, **29 a-b**, **30** , **31** and **32 a-b**, an ICT state is induced by combining a boronic acid functionality with a conjugated electron-donating group.[37] The ICT state in these molecules renders them highly fluorescent. Upon fluoride complexation, the formally neutral boronic acid becomes negatively charged and behaves as an electron donor, thus the ICT state is altered. Since the ICT state in these probes is very sensitive to the change in the hybridization of the boron atom, anion complexation to the boron results in a fluorometric response.

The dimethylamino substituted probes **29a** and **29b** feature emission bands in the visible spectrum which arise from intramolecular charge transfer from the dimethylamino group to the boronic acid moiety. Addition of fluoride to these molecules leads to a blue shift in their emission spectra (Table 3).[37] This shift can be attributed to a loss of ICT character in the excited state upon rehybridization of the boron from sp^2 to sp^3 (Figure 13).

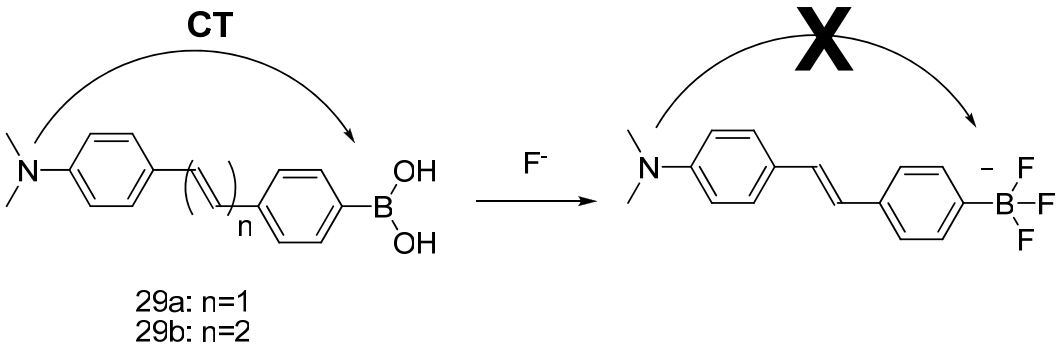

Figure 13: Fluoride ion complexation of **29**a and **29**b.

For the cyano-substituted probe **30**, the inverse of this phenomenon is observed. A red shift in the emission spectrum of **30** as well as a decrease in the intensity of the emission band is observed upon addition of fluoride anions (Table 3), resulting from the generation of an electron-donating borate functionality, leading to the appearance of an ICT transition (Figure 14).[37]

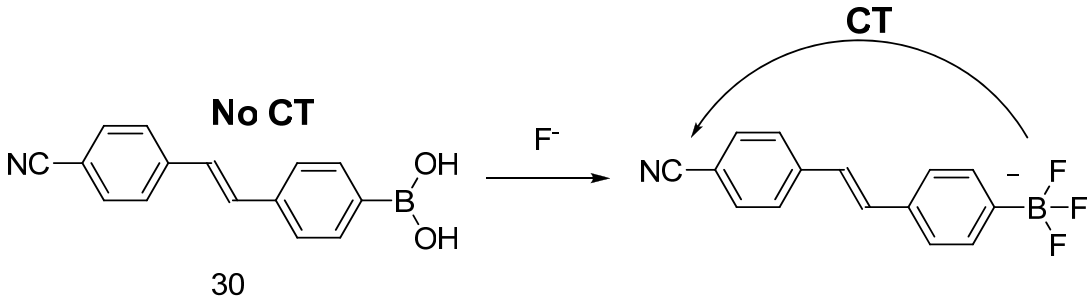

Figure 14: Fluoride ion complexation of **30**.

Probes **31**, **32a** and **32b** feature the dimethylamino functionality, and thus exhibit charge-transfer character. Like compounds **29** these molecules all undergo a blue shift in their respective emission spectra in the presence of fluoride anions. In **31,** the diphenyloxazole linker, with electron donor and acceptor groups, is highly sensitive to the charge-transfer and shows diagnostic spectral changes following perturbation of the ICT.[37]

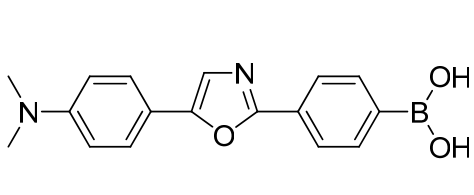

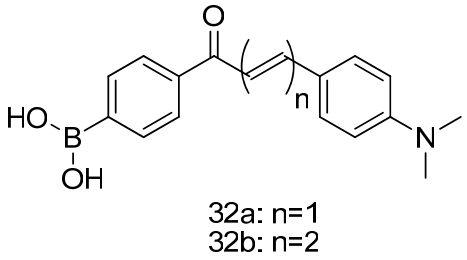

In compounds **32a** and **32b**, the boronic acid functionality does not directly participate in the ICT, but rather the ICT involves the dimethylamino and carbonyl groups. The boronic acid is in conjugation with the carbonyl and rehybridization from sp^2 to sp^3 increases the electronic density of the carbonyl functionality leading to changes in the ICT character of the excited state. This is evidenced by a very small blue shift (~ 15 nm) in the emission band upon fluoride binding accompanied by a large increase in the emission band intensity.

These probes display fluoride binding constants for formation of the trifluoroborate species ranging from 2×10^2- 2×10^4 M^{-3} in water-methanol mixed solvent systems and are capable of detecting fluoride in the 40-200 mM range. Remarkably, compounds **29-32** are selective for fluoride over chloride and bromide, exhibiting no appreciable spectral changes upon addition of the other halogens. The scope of their application in water is limited, however, as the boronic acid functionality also interacts with hydroxide and diols; therefore, fluoride sensing at high pH or in the presence of catechols or sugars would be severely compromised.[37]

Table 3: Spectroscopic properties and stability constants for compounds **29-32**.

	Solvent	λ_{Em} (no F^-) (nm)	λ_{Em} (F^-) (nm)	K_3 (M^{-3})
29a	H_2O/MeOH 2:1	497	455	3.0×10^2
29b	H_2O/MeOH 2:1	531	488	1.9×10^2
30	H_2O/MeOH 2:1	389	420	2.9×10^3
31	H_2O/MeOH 2:1	554	490	6.6×10^3
32[a]	H_2O/MeOH 2:1	585	570	1.3×10^4
32b	H_2O/MeOH 2:1	668	654	1.5×10^4

The most recent work using arylboronic acids as fluoride probes comes from the group of James. Compounds **33** and **34** exhibit a colorimetric response in the presence of fluoride via generation of a highly colored phenoxy radical species (Figure 15) in addition to the typical fluorescence/absorbance quenching.[92]

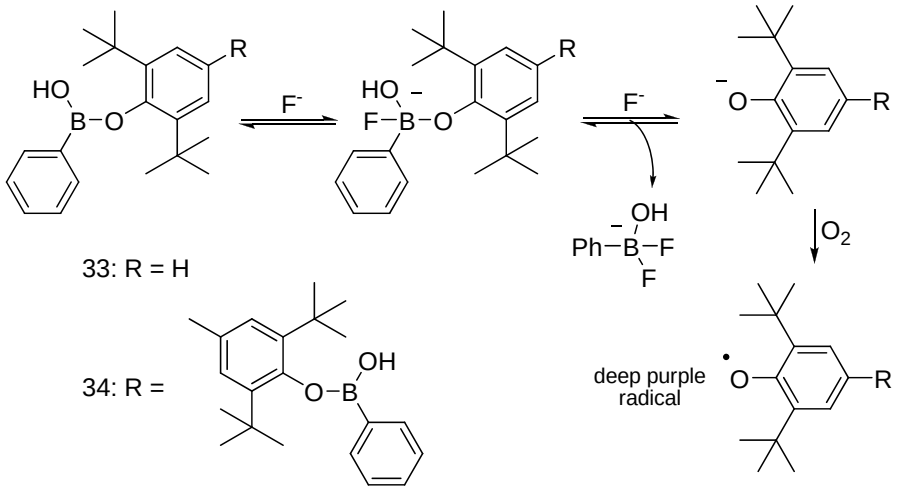

Figure 15: Formation of a phenoxy radical upon reaction of fluoride anions with compounds **33** and **34**.

Each molecule coordinates two fluoride anions per boron atom to release a $[ArBF_2OH]^-$ species, consequently generating a phenoxide anion that is readily oxidized aerobically to produce a dark purple-colored phenoxy radical species. For compound **33**, a high degree of selectivity for fluoride is observed with no spectral changes in the absorption or emission spectra in the presence of Cl^-, Br^- or $H_2PO_4^-$. Compound **34**, however, is not selective for fluoride like **33**. In the presence of chloride anions, a rapid quenching of the emission band is observed. The quenching observed is nonlinear, and could be fitted to a 2:1 (**34**:Cl^-) stoichiometry. The origin of this observation is believed to result from a conformational change from a staggered structure of **34** in solution to one where a chloride anion is hydrogen-bound to four B-OH groups.[92]

1.7.2 Transition metal complexes featuring boronic acids for fluoride detection

Another strategy that can be used to monitor the fluoride affinity of boronic acids is the incorporation of a transition metal into the backbone of the receptor. This often times leads to an increase in the Lewis acidity of the boron center if the transition metal containing moiety is strongly electron withdrawing. Incorporation of a transition metal is also advantageous as fluoride binding can often be observed electrochemically. An example related to the work of Wang[55], concerns the bipyridine iron (II) boronic acid (**35**) reported by Simonet and Fabre.[93]

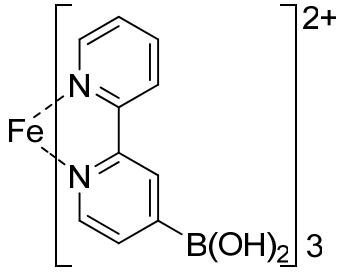

35

Fluoride complexation to compound **35** can be monitored by cyclic voltametry (CV). Indeed, the oxidation potential of **35** experiences a cathodic shift of up to 153 mV depending on pH. Compound **35** is also highly selective for fluoride over chloride and bromide, but suffers from boronate ester formation in the presence of sugars.[93]

In addition to pyridine based transition metal complexes, several ferrocene based boronic acids have been investigated for fluoride recognition. Ferroceneboronic acid[94] (**36**) was the first borylated ferrocene derivative to be investigated for fluoride recognition by Shinkai and coworkers.[31] Compound **36** is remarkably stable in methanol-water mixed solvents and water at neutral pH. The redox properties of **36** are drastically altered in the presence of fluoride anions. By monitoring the shift of the reduction wave with respect to fluoride concentration, the stability constants for fluoride

and various other anions was determined. It was found that the oxidized ferrocenium derivative [**36**]$^{+}$ binds fluoride with stability constants of 1000 ± 50 M^{-1} and 700 ± 50 M^{-1} (in MeOH/H_2O (1:9) and pure water respectively) which are at least three orders of magnitude greater than that observed for the neutral species **36** (Figure 16). Both the oxidized and neutral forms of **36** display remarkable selectivity for fluoride over Cl^-, Br^-, SCN^-, SO_4^{2-} and $H_2PO_4^-$, whose binding constants were less than 20 M^{-1}.

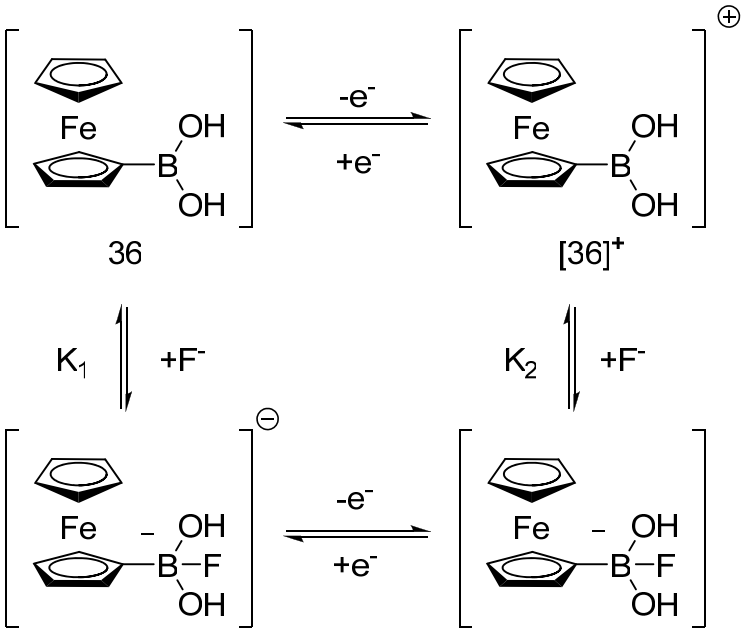

Figure 16: Fluoride binding of **36** and its oxidized analog [**36**]$^{+}$.

Also of notable importance, is while both the neutral ferroceneboronic acid **36** and its oxidized form [**36**]$^{+}$ are selective for fluoride over the aforementioned anions, they are not selective over hydroxide which binds to the boron center. This interference occurs only in strongly alkaline media. For this reason, these two ferrocene derivatives remain ideal for fluoride recognition at neutral pH or under physiological conditions.[31]

The group of Aldridge has also investigated ferrocenylboronic acid such as compound **37**. Remarkably, **37** is not only capable of binding fluoride anions, but it has also been shown to activate hydrofluoric acid (HF). Indeed, **37** adds HF (from collidine-HF) to form a zwitterionic complex (**38**) with an unusual N-H---F-B bridging interaction (Figure 17).[30] Compound **38** is the first reported structural example of a fluoroborate functionality which features a fluorine atom that is hydrogen bonded to an adjacent hydrogen-bond donor group. Formation of **38** has been verified by multinuclear NMR (^{11}B NMR: 3.0 ppm, q, J_{BF} = 49 Hz; ^{19}F NMR: -133.9 ppm, q, J_{FB} = 49 Hz), cyclic voltammetry [-43 mV (75 mV)], and single crystal X-ray analysis.[30] Compound **37** is also highly selective for fluoride and thus selective for HF. Indeed, the reaction of **37** with HCl, HBr, and HI results only in protonation of the amino functionality and complexation of the halide is not observed.[30]

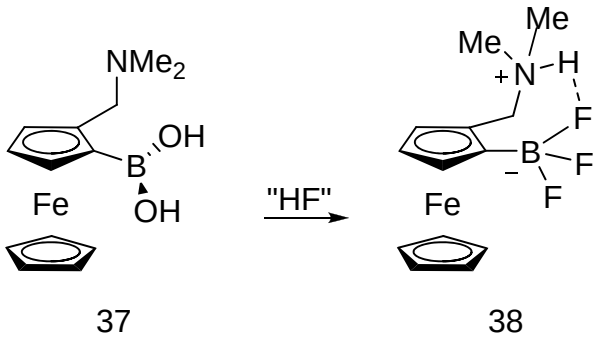

Figure 17: Complexation of HF by **37** to form zwitterion **38**.

1.8 Arylboronic ester-based receptors for fluoride anions

1.8.1 Monofunctional arylboronic ester-based fluoride sensors

Simple arylboronic esters such as **39**, **40**, **41**, **42**, and **43** have also been used for the molecular recognition of fluoride ions. The stillbene derivatives, **39**-**42**, developed by Spange and coworkers in 2007 are examples of boronic ester derivatives which function as colorimetric sensors for fluoride ions. Molecules **40**-**42** contain increasingly stronger

electron-withdrawing nitro-substituted functionalities, whereas **39** lacks this feature. Upon fluoride complexation, the boronic ester moiety rehybridizes and becomes an electron-rich (donating) fluoroborate group. For **40**, **41** and **42**, fluoride binding generates a push-pull scenario inducing an ICT state characterized by a red shifted emission.[95] The observed red-shift increases directly with the increasing number of nitro substituents, indicative of a larger "pull" character of the nitro-arene moiety. For the control compound **39**, no change is observed in the absorption spectrum upon addition of fluoride. Altogether, this phenomenon is similar to that discussed previously in the case of arylboronic acids bearing electron-withdrawing functionalities.[95] Spange has not reported any binding constants for these pinacolboronic esters. However, he was also able to show that these compounds were selective for fluoride over the other halogens, a characteristic which is common among receptors featuring this moiety.[95]

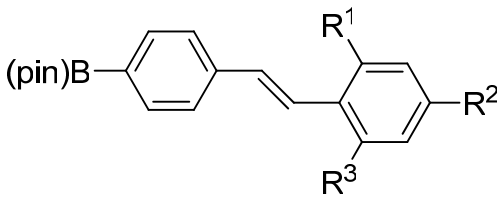

39: $R^1 = R^2 = R^3 = H$
40: $R^1 = R^3 = H$, $R^2 = NO_2$
41: $R^1 = H$, $R^2 = R^3 = NO_2$
42: $R^1 = R^2 = R^3 = NO_2$

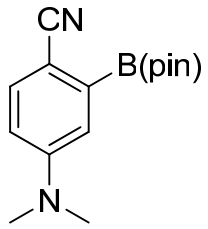

43

The 4-(*N*,*N*-Dimethylamino)benzonitrile (DMABN) derivative **43** reported in 2007 by Zhu *et al.* gives rise to a ratiometric fluorescent response upon addition of fluoride.[96] In THF, incremental addition of fluoride anions to **43** results in a blue shift observed in the absorption spectrum of approximately 10 nm. This data can be fitted by hand to a 1:1 isotherm to obtain a binding constant $K = 3.4 \pm 0.2 \times 10^5\ M^{-1}$. The fluoride binding constant can also be obtained via fluorescence spectroscopy. Upon incremental addition

of fluoride to a THF solution of **43** (5.0×10^{-5} M) the band at λ_{em} = 402 nm is quenched while a new band grows in at λ_{em} = 343 nm. Monitoring the intensity at either wavelength yields *K* values which are consistent with that obtained by UV/vis methods. Compound **43** is also highly selective for fluoride over the other halogens and exhibits no appreciable change in either the absorption or emission spectra in the presence of Cl^-, Br^- or I^-.[96]

1.8.2 Polyfunctional boronic ester-based fluoride sensors

Several polyfunctional boronic esters have also been investigated for fluoride recognition. One simple derivative reported by Baumgartner in 2006 is the highly fluorescent dithienophosphole-bis-pinacolboronic ester **44**.[38] Like other bisborylated species, **44** is capable of binding two equivalents of fluoride anions (one per boron center). The dithienophosphole chromophore exhibits a broad emission band in CH_2Cl_2 which undergoes a red shift in the presence of excess fluoride. This shift is ratiometric, and as a result, fluorescence titration measurements can be used to determine the two fluoride binding constants K_1 and K_2 (1.1×10^4 M^{-1} and 6.3×10^3 M^{-2} respectively). Stepwise formation of [**44**-F]$^-$ is observed in solution by ^{11}B NMR which features two independent resonances at δ = 5.8 (borate) and 28.5 (boronic ester) functionalities. Compound **44** is not water soluble, but the difluoride species [**44**-F_2]$^{2-}$ displays a broad emission band at λ_{em} = 478 nm in water which is very close to that observed in CH_2Cl_2. For this reason Baumgartner was able to show that **44** is suitable for fluoride sensing in water. For example, when solid **44** is added to water containing fluoride, the resulting solution exhibits a blue-green fluorescence (λ_{em} = 478 nm). **44** is also selective for fluoride over the other halides and exhibits high sensitivity to this analyte.[38]

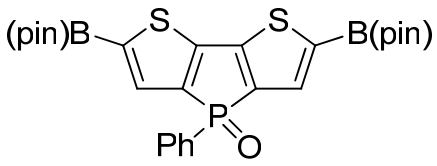

44

Simonet and Fabre have also synthesized derivatives which incorporate pinacolboronic ester functionalities into triphenylamines. These derivatives do not exhibit any charge-transfer character like other amino-functionalized boron compounds.[37] Instead, fluoride binding to compounds **45**, **46**, and **47** can be monitored electrochemically.[97] Cathodic shifts in the oxidation potential, which correspond to the formation of a stable radical cation at the nitrogen atom, are observed upon fluoride complexation to these molecules. Formation of a stable radical cation is facilitated upon fluoride binding due to the anionic nature of the fluoroborate which favors formation of neutral zwitterionic species. It is interesting to note that the free receptors **45** and **46** display characteristic irreversible oxidation waves at $E_{1/2}$ = 0.69 and 0.74 V (vs Ag^{+}/Ag) in acetonitrile, indicative of the formation of an unstable radical cation species. In contrast, the triboryl substituted derivative **47** exhibits a reversible wave at $E_{1/2}$ = 0.72 V corresponding to the formation of a stable radical cation species. Differential pulsed voltametry (DPV) was used to monitor the fluoride binding in dichloromethane. Upon addition of fluoride anions, the oxidation potentials decreased in intensity while one (for compound **45**), two (**46**) or three (**47**) new waves which were shifted cathodically grew in. These new oxidation waves each correspond to one of the fluoride complexes, namely [**45**-F]$^{-}$, [**46**-F]$^{-}$, [**46**-F_2]$^{2-}$, [**47**-F]$^{-}$, [**47**-F_2]$^{2-}$ and [**47**-F_3]$^{3-}$ respectively.

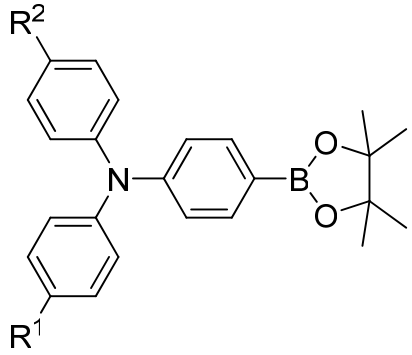

45: $R^1 = R^2 = H$
46: $R^1 = H$, $R^2 = B(pin)$
47: $R^1 = R^2 = B(pin)$

Each of these receptors showed selectivity for fluoride over the other halides and CV experiments indicate that upon fluoride complexation all three compounds exhibit reversible oxidation waves, indicating the formation of stable radicals. From this data, fluoride binding constants have been obtained for the neutral (K_1, K_2 and K_3) and oxidized (K_1', K_2' and K_3') form of compounds **45**, **46** and **47** (Table 4). As one would predict, the oxidized (cationic species) all displayed higher stability constants than their neutral counterparts.[97] The fluoride binding of these molecules has also been shown to be reversible. Indeed, addition of Me_3SiCl to a solution of the fluoroborates leads to complete regeneration of the oxidation wave for the free receptor.[97]

Table 4: Binding constants corresponding to the complexation of F^- by the neutral and oxidized forms of **45**, **46** and **47**.

	K_1 (M^{-1})	K_1' (M^{-1})	K_2 (M^{-2})	K_2' (M^{-2})	K_3 (M^{-2})	K_3' (M^{-3})
45	2.4×10^2	1.6×10^7	---	---	---	---
46	2.8×10^2	1.2×10^7	3.9×10^2	1.1×10^6	---	---
47	2.1×10^2	0.9×10^7	1.6×10^2	3.0×10^5	1.0×10^2	3.4×10^5

James has also contributed to the area of polyfunctional diboronic esters for fluoride recognition by studying compound **48** in which the respective arrangement of the pinacolboronic ester moiety should facilitate fluoride ion chelation (Figure 18).[34,34] By monitoring the emission quenching (λ_{em} = 395) of **48** upon the addition of TBAF in chloroform, James proposed formation of [**48**-μ_2-F]$^-$ with a stability constant $10^{6.3}$ M^{-1}. These results have however been recently disputed by Aldridge who showed that fluoride ions induce a B-O bond cleavage.[34,29]

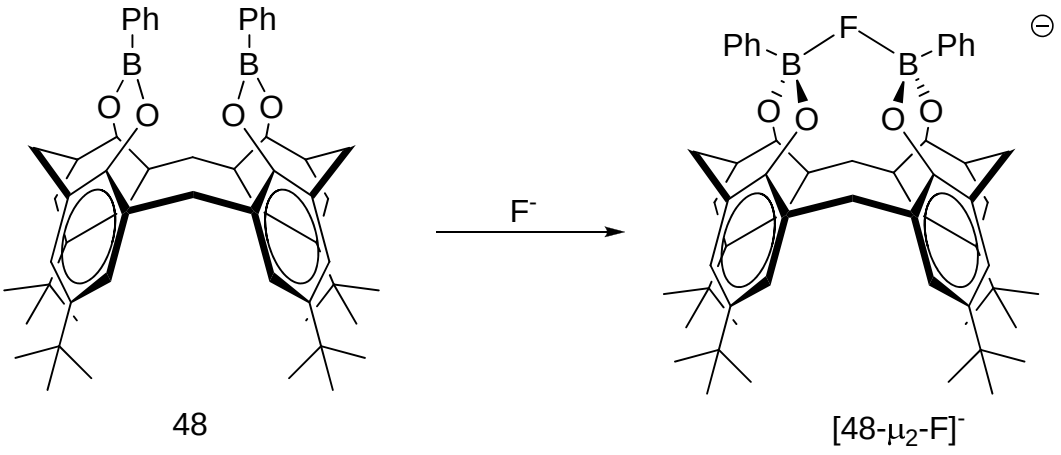

Figure 18: Proposed fluoride binding mode of **48**.

In an effort to enforce fluoride ion chelation in polyborylated ferrocene derivatives, the more preorganized borylated ferrocene derivatives **49** and **50** have been synthesized and investigated by Aldridge.[98] Unfortunately, however, compounds **49** and **50** undergo facile cleavage of the B-O bonds in the presence of fluoride sources such as TBAF and KF/18-crown-6 to yield the parent calixarene compound as evidenced by multinuclear NMR spectroscopy.[29]

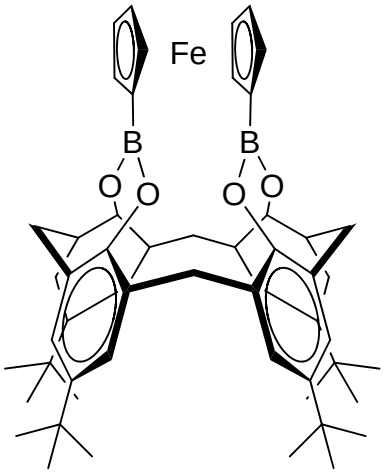

49

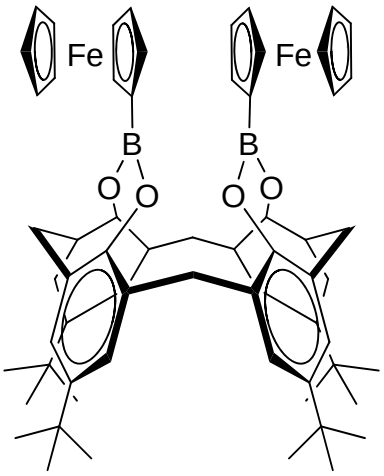

50

1.9 Transition metal complexes featuring boronic esters for fluoride detection

Several examples of transition metal complexes which feature boronic ester functionalites have also been developed for the purpose of fluoride recognition. Schlüter and Fabre have reported a terpyridine iron(II) complex which is functionalized by two pinacolboronic ester moieties.[99]

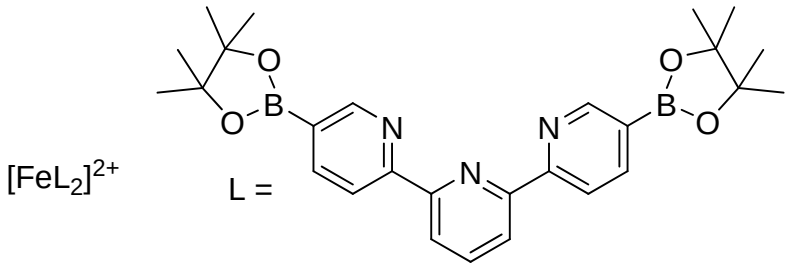

51

Compound **51** is very similar to derivative **35** and also experiences a cathodic shift of (-160 mV) in the oxidation potential upon fluoride complexation to the boronic ester

group.[93] Like compound **35**, this cathodic shift can be attributed to formation of a more electron rich metal complex which is more easily oxidized than the free Lewis acid receptor. Compound **51** is somewhat more selective for fluoride than **35** showing no appreciable redox shifts in the presence of Br^-, NO_3^- and SO_4^{2-} and only a small shift (-22 mV) in the presence of Cl^-.[99] The binding constant for formation of the monofluoroboronate species [**51**-F]$^-$ (K_1 = 500 M^{-1}) has been determined by UV-vis spectroscopy. While the data obtained from these spectroscopic measurements could also be fitted to the formation of the corresponding bisfluoroborate species **51**-F_2, the binding constant K_2 could not be accurately determined.[99]

1.9.1 Monoborylated ferrocene boronic esters

In the area of transition metal complex-based boronic ester derivatives, Aldridge has undoubtedly made the largest contribution. Aldridge has reported numerous ferrocene-based boronic esters including mono-, bis-, tris- and tetrakis- borylated species. In addition the ferrocene boronic acid **37**, Aldridge and coworkers also reported the ambiphilic aminoboronic ester ferrocene derivatives **52** and **53**. Like **37**, these molecules are capable of selectively activating HF.[30]

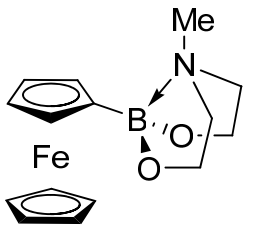

52

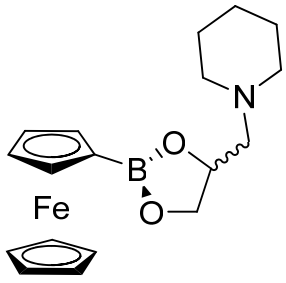

53

Upon addition of three equivalents of HF (as the collidine complex 2,4,6-trimethylpyridine•$(HF)_{1.5}$) to compounds **52** and **53**, complete conversion to the corresponding ferrocene trifluoroborate complex [**54**]$^-$ is observed (Figure 19).[30]

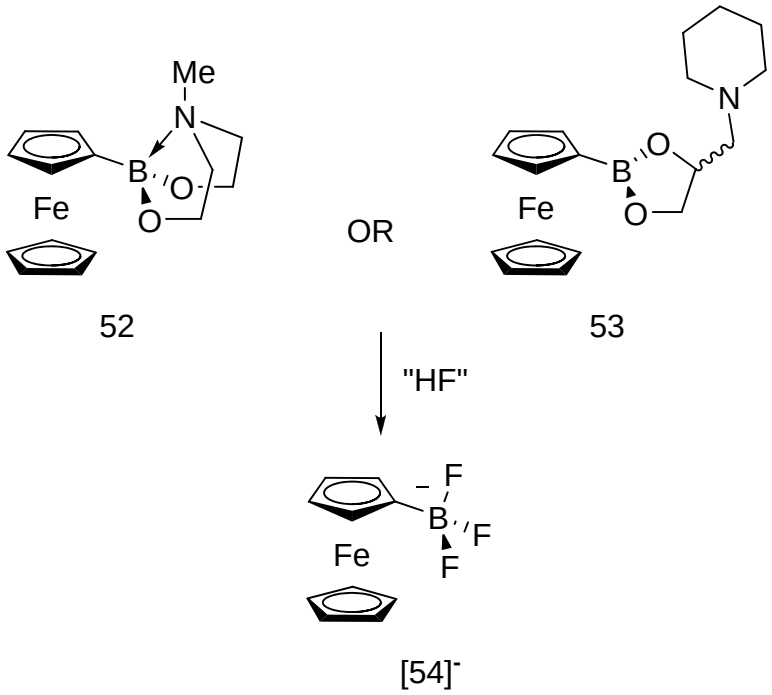

Figure 19: Complexation of HF by **52** and **53** to form [**54**]$^-$.

Formation of the same common boron containing species [**54**]$^-$ is corroborated by ^{11}B NMR spectroscopy which features a quartet (δ_B = 3.7 ppm, J_{BF} = 49.8 Hz) and by electrochemical analysis [CV; $E_{1/2}$ = -320 mV] after addition of the collidine complex to either **52** or **53**. The $[HN(CH_3)(CH_2CH_2OH)_2]^+$ salt of [**54**]$^-$, obtained from the reaction of **52** with HF, has also been characterized by single crystal X-ray diffraction analysis.[30]

Aldridge and coworkers have recently reported a series of simple monofunctional ferrocene boronic esters.[98,100] Compounds **55**, **56**, **57**, **58** and **59** behave as previously reported ferrocene functionalized boronic esters, complexing fluoride to form the

corresponding fluoroboronate species. Fluoride binding is readily observed by ^{11}B NMR and cyclic voltammetry. Upon addition of 1 equivalent of TBAF to compounds **55-59** in acetonitrile, the ^{11}B NMR signal undergoes an upfield shift from (δ_B = 28.6-34.1 ppm) for the free boronic ester to δ_B = 7.8-10.2 ppm which is characteristic of a four-coordinate boron atom.[98]

In addition to a large upfield shift in the ^{11}B NMR spectrum upon coordination of the anion, there is a cathodic shift (~ 530 mV) of the oxidation wave in dichloromethane observed for these receptors which is consistent with the change from an electron-withdrawing boronic ester functionality to the anionic fluoroboronate. The fluoride binding can also be quantified for these receptors using NMR spectroscopy. For example, monitoring the ^1H NMR resonance of the methine in **56** upon addition of TBAF in $CDCl_3$ affords a binding constant of 35.8 ± 9.8 M^{-1}.[98]

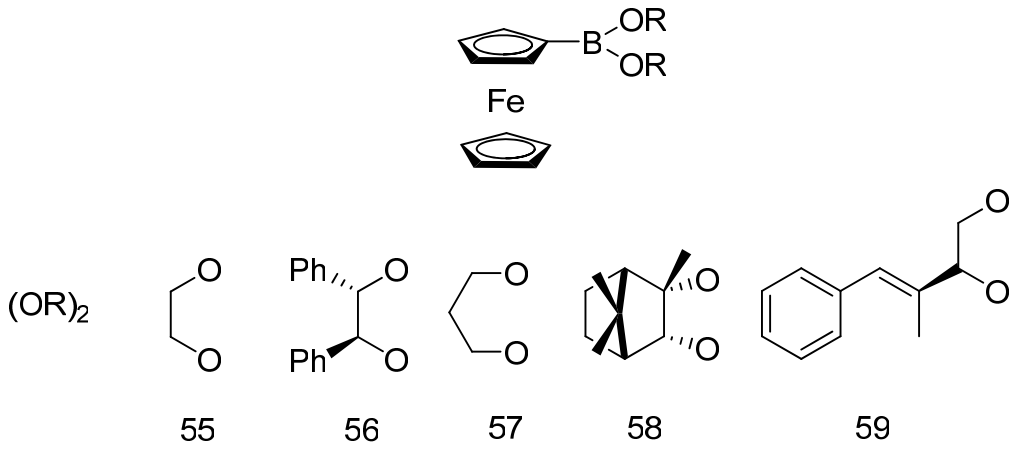

Although the binding constants of receptors of this type are indicative of weak Lewis acid/base interaction, it is precisely this weak interaction which inherently leads to a remarkable selectivity for fluoride over several other anions (Cl^-, Br^-, I^-, BF_4^-, PF_6^-, $H_2PO_4^-$, HSO_4^- and NO_3^-) observed for compounds **55-59**. It is well documented that

boronic acids display fluoride binding constants which are at least two orders of magnitude greater than chloride and bromide. Thus if the fluoride binding is weak, then other anions would be expected to display negligible interaction with the boron center.[98]

Another monofunctional derivative which has been synthesized by Aldridge is the pentamethylated ferrocene boronic ester **60**.[98] Compound **60** was synthesized to see what affect the incorporation of electron-donating groups on the ferrocenyl cyclopentadienyl (Cp) rings has on the fluoride binding properties of the receptor.

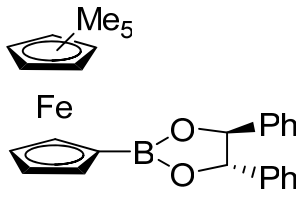

60

Compound **60** exhibits a redox potential which is shifted cathodically by 300 mV compared to the nonmethylated analog **56**. Upon fluoride complexation, the solution containing the fluoroborate [**60**-F]$^-$ rapidly changes from orange to green when the reaction is carried out under aerobic conditions. Spectroscopic and electrochemical evidence suggests that the observed color change arises from initial fluoride complexation to the boron center forming [**60**-F]$^-$ followed by aerobic oxidation of the iron center to yield the green ferrocenium zwitterion **60**-F (Figure 20). In contrast, no change is observed upon addition of Cl^-, Br^-, I^-, BF_4^-, PF_6^-, $H_2PO_4^-$, HSO_4^- or NO_3^- pointing to the selectivity of the receptor.

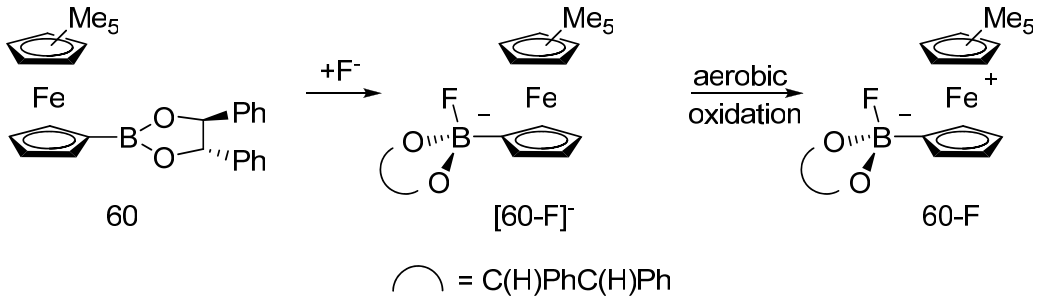

Figure 20: Fluoride binding of **60** followed by aerobic oxidation to form **60**-F.

1.9.2 Bisborylated ferrocence boronic esters

In addition to monofunctional derivatives, Aldridge has used the ferrocene backbone to develop bifunctional diboronic esters. The earliest sensor developed by Aldridge is the bidentate bis(boronic ester) **61**[100] which can bind a fluoride anion at each boron center. Indeed, reaction of **61** with two or more equivalents of fluoride in chloroform or dichloromethane under aerobic conditions leads to a drastic color change from orange to green indicating formation of the ferrocenium species [**61**-F_2]$^{-}$[100] Formation of [**61**-F_2]$^{-}$ suggests that increased borylation of the ferrocene unit is a viable alternative to permethylation to facilitate aerobic oxidation. Fluoride binding can be monitored using UV/Vis spectroscopy, as well as electrochemically. The binding constants for the first and second fluoride anions for **61** are very low, 4.1 and 9.8 M^{-1} respectively. Despite the low binding constants, **61** behaves as a remarkably selective, colorimetric and potentiometric fluoride probe.[100]

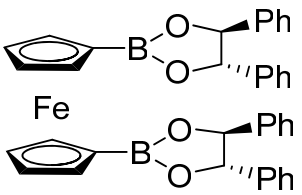

61

Several other polyborylated ferrocene derivatives have been investigated by Aldridge. Since **61** is not able to chelate the fluoride anion, Aldridge synthesized the bisborylated ferrocene **62** which features sterically less encumbered boronic ester functionalities. With the smaller boronic ester groups, it was hoped that **62** would be able to chelate a fluoride anion between the two boron centers.[98] This molecule however retains a large degree of conformational flexibility, and like **61** binds two fluoride anions, one at each boron center.

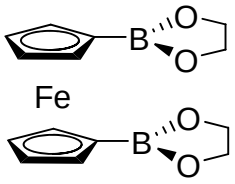

62

In an effort to determine what factors facilitate the colorimetric aerobic oxidation observed in **60** and **61** after fluoride complexation, Aldridge has synthesized bis-, tris- and tetrakis-borylated ferrocenes. First, the bis-borylated ferrocene derivatives, **63**, **64** and **65** were prepared. These compounds are capable of binding two fluoride ions, one per boron center.[98] In the presence of an excess of fluoride anions, the rate of oxidation for compound **65** was approximately twice the rate observed for the compounds which did not contain a pentamethylated Cp ring, suggesting that the rate of oxidation can be tuned by changing the electron density on the Cp substituents.[98]

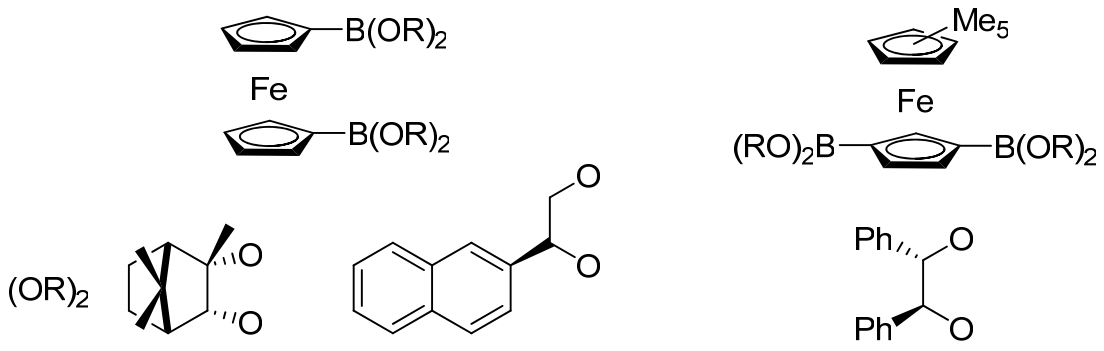

63 64 65

1.9.3 Tris- and tetrakis-borylated ferrocene boronic esters

The tris-borylated ferrocene derivatives **66**, **67** and **68** were prepared to determine if increasing the number of boronic ester groups in borylated ferrocene compounds affects the rate of the oxidation. Indeed, it was shown that compared to their bis-borylated analogs, the tris-borylated species exhibited an enhancement in their rates of oxidation by approximately one order of magnitude.[98] For example, the rate of oxidation of the tris-borylated compound **66** was found to be 5.4×10^{-2} s^{-1}, whereas a rate of 2.0×10^{-3} s^{-1} was obtained for the bis-borylated analog **61**. The same observation was made for the tetrakis-borylated species **69**, **70**, **71** and **72**, whose rates of oxidation were nearly identical to those of the tris-borylated compounds.

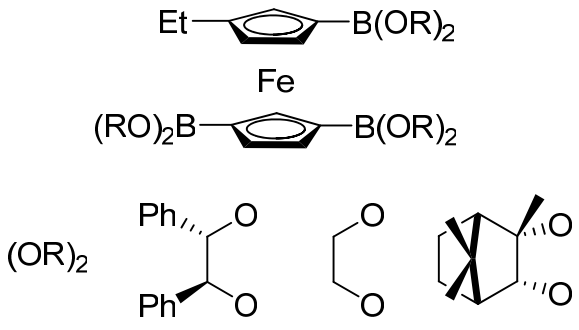

66 67 68

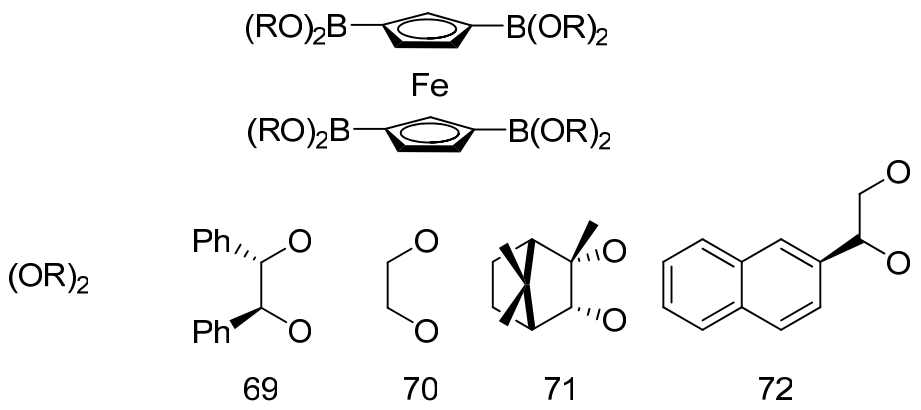

In summary, Aldridge's investigation with the polyborylated ferrocene derivatives shows that the rate of oxidation can be tuned by altering the nature of the substituents on the Cp rings. These results have also revealed that increasing the number of boronic ester moieties results in an enhancement of the oxidation rate by an order of magnitude.[98]

1.10 Silicon-based fluoride receptors

There is a rich chemistry involving the formation of silicon and fluorine (or fluoride) bonds. Most notably, silyl groups are used in organic synthesis as protecting groups for a variety of functionalities. Protection of alcohols with silicon reagents such as trimethylsilyl chloride (TMSCl) has been used exhaustively in the preparation of natural products; and, along with other silyl ethers, addition of fluoride (as TBAF) is typically the preferred method for deprotection. Fluoride-promoted deprotection is facile due to the formation of a very strong (and stable) silicon-fluorine bond. The formation of silicon-fluorine (or other halogen) bonds has become the staple for several other organometallic reactions including halide abstraction from various main group and transition metal complexes, whereby treatment with a silicon cation reagent such as trimethylsilyl triflate (TMSOTf), a halogen (often times fluoride) is abstracted and cleanly removed from the mixture as the volatile silylhalogen compound. Despite

widespread synthetic application which utilizes the formation of Si-F bonds, only recently have chemists used this paradigm in the context of fluoride sensing.

1.10.1 Fluoride ion chelation by Lewis acidic fluorosilanes

To date, several fluoride receptors which utilize Lewis acidic fluorosilyl functionalites have been prepared. Interestingly, much of this silicon chemistry parallels the chemistry previously reported with boron. One of the first examples from the group of Tamao in 1996 makes use of a bidentate-bis(fluorosilyl) Lewis acid appended to an *ortho*-phenylene scaffold. [101,102] This molecule (**73**), like bidentate diboranes[48,73], is capable of fluoride ion chelation between the two Lewis acidic silicon centers (Figure 21).[101,102]

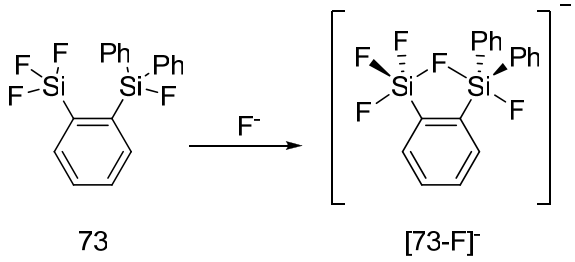

Figure 21: Fluoride anion chelation by bidentate silicon-based Lewis acid **73**.

The fluorine atom in [**73**-F]$^-$ is bridging the two silicon centers which adopt a pseudo-trigonal bipyramidal geometry. Lone pairs on the fluoride anion are donating into an empty-p type orbital located approximately 180° from the terminal fluorine atoms on the two silicon centers. Occupation of axial sites by the fluorine atoms is typical for difluorosilicate species such as $[SiMe_3F_2]^-$. The Si-$F_{(bridging)}$ distances are 1.700(3) and 2.369(3) Å for the F→SiF_3 and F→$SiPh_2F$ moieties respectivelym, which is indicative of an ionic interaction between the fluoride and silicon atoms.[101]

Remarkably, the ability of **73** to chelate the fluoride anion raises the fluoride binding constant ($K > 10^9$ M^{-1}) by at least six orders of magnitude when compared to the monofunctional derivative, $PhMeSiF_2$ ($K = 10^3$ M^{-1}) in organic solvents.[102]

More recently, Kawachi and coworkers have reported the synthesis and fluoride binding properties of heteronuclear bidentate Lewis acids which features both triarylboryl and fluorosilyl moieties.[103] Compounds **74** and **75**, like **73**, are capable of fluoride ion chelation between the two Lewis acidic sites (Figure 22). The fluoride anions in [**74**-F]$^-$ and [**75**-F]$^-$ form covalent bonds to the Lewis acidic boron atom which adopts a four-coordinate, tetrahedral geometry. The B-F distances of 1.492(4) Å and 1.514(3) Å in [**74**-F]$^-$ and [**75**-F]$^-$, respectively, are slightly longer than that observed for typical triarylfluoroborates (ca. 1.47 Å). The lengthening of the B-F bond observed in these adducts arises from the additional interaction observed between the fluoride anion and the silicon atom. This interaction is similar to what is observed in [**73**-F]$^-$ where a lone pair on the fluorine atom is donating directly into an axial site on the silicon atom which formally adopts a distorted trigonal bipyramidal geometry. The Si-F distances of 2.4385(23) Å in [**74**-F]$^-$ and 2.2481(13) Å in [**75**-F]$^-$ are similar to what was observed in [**73**-F]$^-$. In each of these adducts, the F-Si-F angles are nearly linear ranging from 175° to 176°.[103]

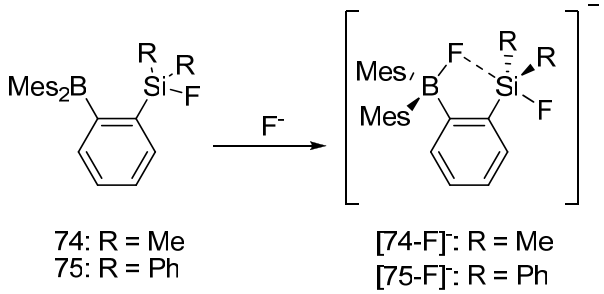

Figure 22: Fluoride anion chelation by bidentate heteronuclear Lewis acids **74** and **75**.

To further substantiate the crystallographic evidence of this interaction, the authors also studied [**75**-F]$^-$ computationally. DFT calculations at the B3LYP/6-31 G(d) level of theory were used to optimize the structure of [**75**-F]$^-$. Single point energies were calculated using MP2 with the 6-31+G(d,p) basis set for all atoms. The optimized structure was also subjected to an Atoms In Molecules (AIM) analysis which revealed a bond critical point between the silicon and fluorine atoms with an electron density, $\rho(r)$ = 3.46 × 10^{-2} e/a_0^3. This analysis attests to the strong interaction that is present between the fluorine and silicon atoms.[103]

1.10.2 Fluoride anion sensing by silylethers

During the past two years, several important contributions to the field of fluoride sensing using silicon-based systems have been investigated. A common theme which has been reported in the literature uses silylethers which mask a latent fluorophore. Addition of fluoride leads to a deprotection of the silylether functionality resulting in a turn-on phenomenon of the fluorophore.

One such example, compounds **76**, comes from the group of Lee.[104] Compounds **76** contain three silyl protected alcohol functionalities and exhibit a non-planar propeller-like structure in the solid state and in solution. Addition of fluoride leads to deprotection of the silyl ether with concomitant unmasking of the highly fluorescent planar molecule (Figure 23).[104] Planarization of **76** occurs via the formation of hydrogen-bonding interactions between the formally protected alcohols and the ketone functionalities on the central six-membered ring. This fluorometric response has also been shown to be selective for fluoride, exhibiting no turn-on phenomenon in the presence of Cl^-, Br^-, I^-, CN^-, SCN^-, NO_3^-, HSO_4^-, PF_6^-, ClO_4^- and $H_2PO_4^-$.[104]

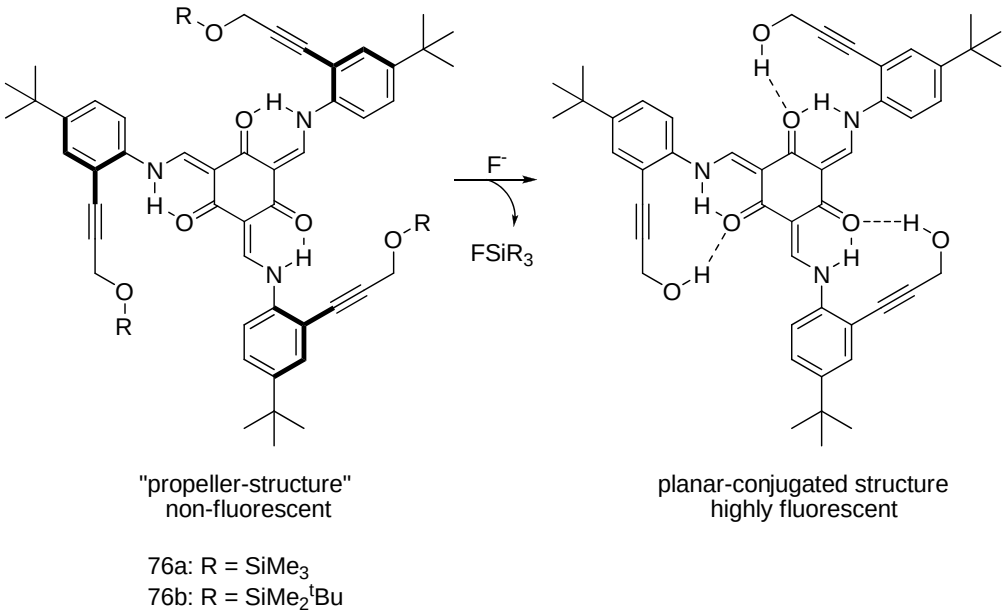

Figure 23: Fluoride induced turn-on fluorescence response of compound **76**.

Hong and coworkers have also recently developed a turn-on fluorescent receptor for fluoride which features a silyl-protected fluorophore.[105] The mechanism for inducing the turn-on response exhibited by **77** is the same as in compounds **76**, except that **77** releases the fluorophore Resorufin upon deprotection of the silyl ether (Figure 24).[105]

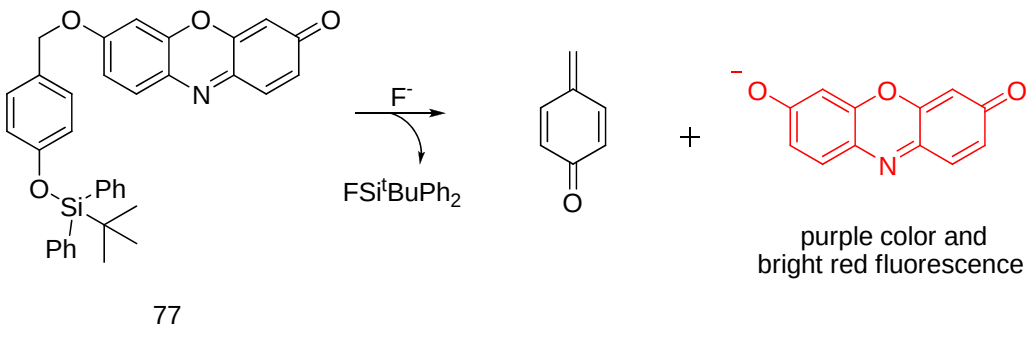

Figure 24: Fluoride induced turn-on fluorescence response of compound **77**.

The Resorufin fluorophore has a purple color in organic and aqueous media and exhibits a bright red fluorescence at 585 nm, thus its release upon fluoride-induced deprotection gives rise to both a colorimetric and fluorometric response (Figure 24).[105] Compound **77** is also highly selective for fluoride like **76**, and remarkably, this molecule functions in highly aqueous media. Indeed, treatment of **77** with NaF in acetonitrile/water (50:50 v/v) mixed solvent system lead to release of the fluorophore.

Yang has also published two recent reports highlighting fluoride-induced turn-on fluorescence sensors based on silyl-protected fluorophores.[106,107] Compounds **78**[106] and **79**[107] react with fluoride in a manner similar to compounds **76** and **77**. Both molecules are, again, highly selective for fluoride; **79**, however, is somewhat unique in that, it requires two equivalents of fluoride to elicit a drastic response, unlike the aforementioned sensors.[107]

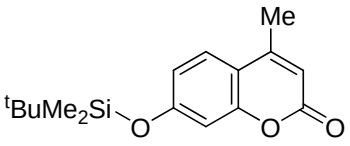

78

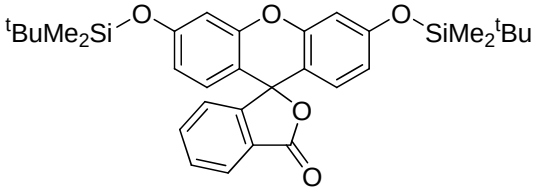

79

A cyanine chromophore has also been tethered to a silylether moiety for fluoride sensing applications. Compound **80** was reported in 2005 by Zhu *et al.*, and like compounds **76**-**79**, gives rise to a turn-on response in the presence of fluoride. The release of the cyanine chromophore is expressed by a change in color of the resulting solution from colorless to green. The cyanine chromophore in **80** contains a quinolinium moiety, making this molecule highly soluble in water, allowing for fluoride sensing in aqueous media. Fluoride sensing in water necessitates basic conditions due to

competitive protonation of the deprotected chromophore which occurs below pH = 9.0 (Figure 25).[108]

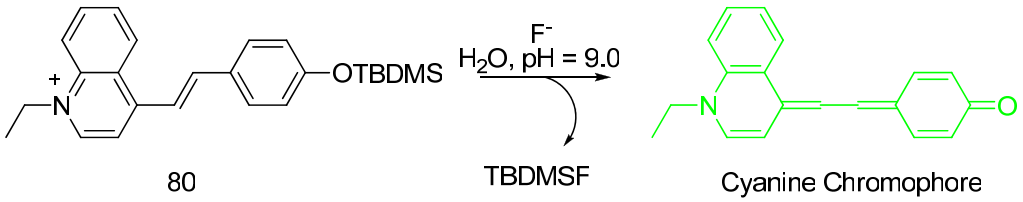

Figure 25: Fluoride induced turn-on colorimetric response of compound **80**.

1.10.3 Polymeric silylether-based fluoride sensors

Recently, polymer-supported silylether-based fluoride sensing materials have also been reported. In 2003, Swager reported the polymer-supported silylether **81**.[109] Polymer **81** can be deprotected using TBAF to generate a highly fluorescent coumarin species (Figure 26). The presence of the polymer support amplifies the fluorescence response observed in the presence of fluoride. The addition of fluoride to a solution of the polymer in THF results in a drastic increase in the fluorescence quantum yield from Φ = 0.12 to Φ = 0.30. Supporting the silylether to the polymer also results in increased sensitivity due to the enhanced fluorescence response. For example, the small molecule analog **82**, required a 100-fold higher fluoride concentration to achieve a complete fluorescence turn-on when compared to polymer **81**.

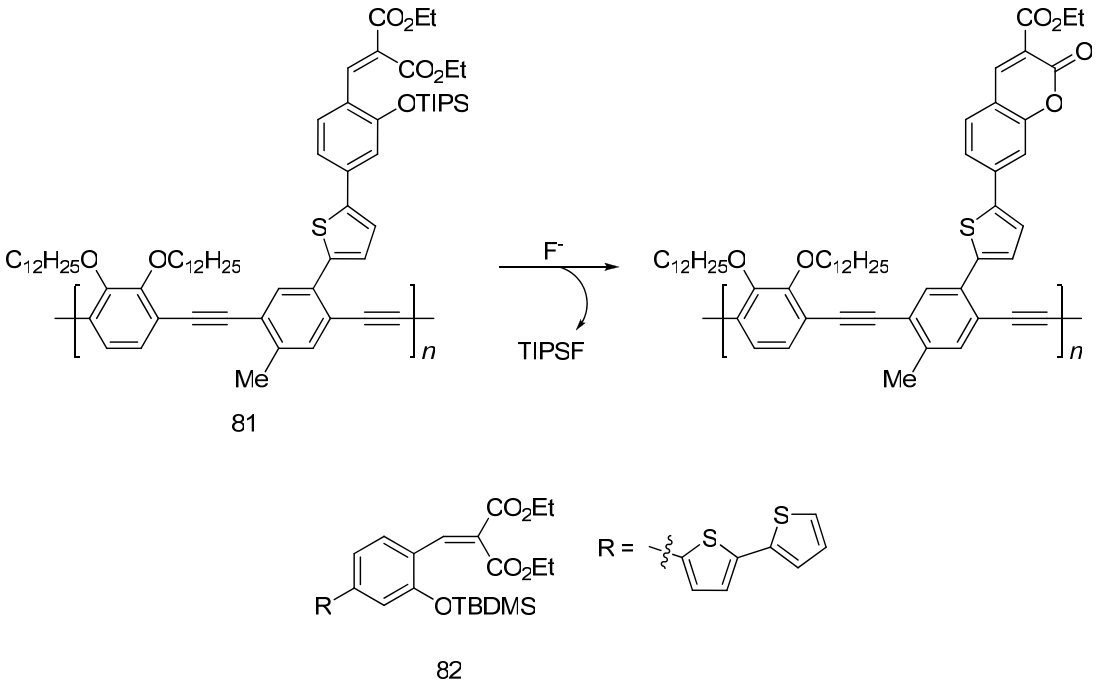

Figure 26: (top): Interaction of polymer **81** with fluoride anions. (bottom): compound **82**.

CHAPTER II

AMMONIUM TRIARYLBORANES: TUNING THE SELECTIVITY IN THE MOLECULAR RECOGNITION OF CYANIDE AND FLUORIDE IONS IN WATER*

2.1 Introduction

Cyanide is a toxic anion which binds to and deactivates the cytochrome-c oxidase enzyme with sometimes fatal consequences.[23] Because cyanide is widely available in both research and industrial settings, its use for harmful purposes or its release in the environment are sources of concern.[24] For these reasons, the development of methods that can sense this anion in water has become a topical objective. Another important nucleophilc anion is the fluoride anion. This anion is often added to drinking water and toothpastes because of its beneficial effects on dental health, and is also administered in the treatment of osteoporosis.[110] However, as widely documented, excessive fluoride intake can be problematic and can lead to the development of dental or skeletal fluorosis.[111] Thus, as with cyanide, the detection of fluoride levels in water is an important task.

To date, the recognition of cyanide and fluoride ions has been successfully implemented in organic solvents using receptors that hydrogen bond with the guest.[6-11,22,26,27,112-114] Such receptors are however challenged in the presence of water which interferes with the host-guest interactions. An added complication exists for the cyanide ion whose competititve protonation ($pK_{a(HCN)}$ = 9.3) complicates its capture in neutral water. Despite these challenges, recent efforts have afforded a number of receptors[115-121] which sometimes function in water.[116,117,120,122] Most of the cyanide receptors are

---

* Reprinted in part with permission from, "Ammonium Boranes for the Selective Complexation of Cyanide or Fluoride Ions in Water"; Hudnall, T. W.; and Gabbaï, F. P.; *J. Am. Chem. Soc.*, **2007**, *129*, 11978-11986, Copyright 2007 by the American Chemical Society.

electrophilic organic reagents which undergo C-C bond forming reactions with cyanide. Some of these reactions necessitate basic pH, and their reversibilty had not always been well documented. Other cyanide receptors or probes with interesting properties include boronic acids,[35,123-126] boron-subphthalocyanines,[122,127] zinc-porphyrins,[128,129] iron-hemes,[130] and transition metal complexes.[131] For fluoride ions, the high hydration enthalpy of -504 kJ/mol[6] is certainly one of the factors making recognition of this anion in aqueous solution especially difficult.[22,113] In order to circumvent these difficulties, several groups are currently studying receptors whose fluoride binding site is a Lewis acidic element such as boron,[29-37] aluminum[132] or tin.[133] Recent advances in this area suggest that cationic boranes[85,86,88,134] such as [**18**]$^+$, [**19**b]$^+$ and [**20**]$^+$ may be particularly well adapted for fluoride caputre in water. Indeed, [**18**]$^+$[85] and [**19**b]$^+$[87] promote the transfer of fluoride ions from water into organic or solid phases while [**20**]$^+$ binds fluoride ions in H_2O/MeOH 90:10 vol. with a binding constant of 1000 (±100) M^{-1}.[88]

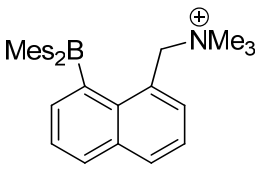

[18]$^+$

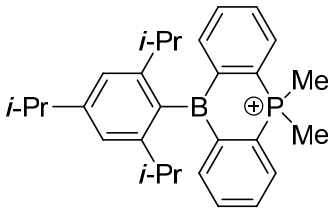

[19b]$^+$

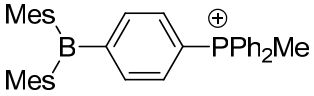

[20]$^+$

It has long been established that triarylboranes interact with cyanide to form the corresponding cyanoborate complexes. For example, the $[Ph_3BCN]^-$ anion can be used for the precipitation of cesium ions from water.[45] This simple observation suggests that water stable triarylboranes could be used for the complexation of cyanide in water. While this possibility has long gone unnoticed, the group of Jäkle showed recently that polymers containing pendant triarylboranes can serve to probe cyanide in organic solvents.[49] Hoping to achieve the molecular recognition of cyanide in water, we have

now turned our attention to cationic boron-based receptors. Based on the results that we have obtained on the recognition of fluoride ions,[88] we hypothesized that cationic boranes may be particularly well adapted for cyanide complexation because of favorable coulombic host-guest attractions. This chapter is dedicated to the synthesis, structures and cyanide/fluoride binding properties of novel cationic boranes that feature ammonium groups.

2.2 Synthesis, structures and anion binding studies of water-stable ammonium boranes

The ammonium borane triflate salts [**83**]OTf and [**84**]OTf could be easily obtained by reaction of the known 4- and 2-dimesitylboryl-*N*,*N*-dimethylanilines[135-137] with MeOTf in diethyl ether (Figure 27). These salts dissolve in polar solvents such as acetone, acetonitrile and DMSO but are insoluble in hydrocarbon solvents and diethyl ether. $[\mathbf{83}]^+$ and $[\mathbf{84}]^+$ are hygroscopic colorless solids which have been characterized by NMR spectroscopy and elemental analysis. The ^{1}H NMR spectra of $[\mathbf{83}]^+$ ($CDCl_3$) and $[\mathbf{84}]^+$ (acetone-d_6) feature all expected resonances for the aromatic CH groups of the phenylene core. The aryl and methyl proton resonances of the two mesityl groups of $[\mathbf{84}]^+$ are split into broad multiple signals thus indicating the existence of a congested structure. The proton resonance of the trimethylammonium group in $[\mathbf{83}]^+$ and $[\mathbf{84}]^+$ appears at 3.74 ppm ($CDCl_3$) and 3.75 ppm (acetone-d_6), respectively. The broad ^{11}B NMR signals at 74 ppm for $[\mathbf{83}]^+$ and 66 ppm for $[\mathbf{84}]^+$ ($CDCl_3$), respectively, are characteristic of triaryl boranes.

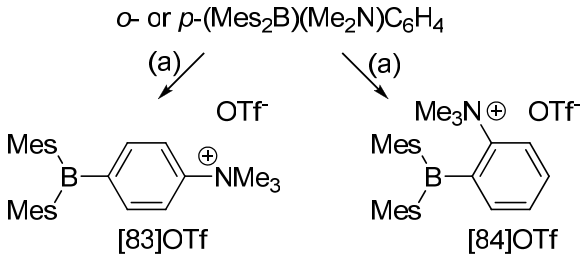

Figure 27: (a) Et_2O, MeOTf, 78% for [**83**]OTf and 39% for [**84**]OTf.

The crystal structures of [**83**][OTf] and [**84**][OTf] have been determined (Table 5, Figure 28 and Figure 29). Salt [**83**][OTf] crystallizes in the triclinic space group $P\bar{1}$ as a toluene solvate with two molecules in the asymmetric unit (Figure 28). Both molecules have very similar structures and do not form unusually short contacts with the triflate anions. Both molecules feature a trigonal planar boron center as indicated by the sum of the C_{aryl}-B-C_{aryl} angles ($\Sigma_{(C\text{-}B\text{-}C)}$ = 360°). All carbon-boron bond distances fall in the 1.557(4)-1.580(4) Å range and are comparable to those found in the starting material.[136,137] Salt [**84**][OTf] crystallizes in the monoclinic $P2_1/c$ space group with one molecule in the asymmetric unit (Figure 29). As for [**84**]$^+$, the boron center is trigonal planar ($\Sigma_{(C\text{-}B\text{-}C)}$ = 359.7°) and does not interact with the triflate anion. The boron center of the *ortho*-derivative [**84**]$^+$ is separated from the methyl carbon atom C(7) by only 3.175(7) Å. This short separation indicates that the unsaturated boron center is sterically encumbered. This conclusion is in agreement with: i) the large B(1)-C(1)-C(2) angle (135.8(4)°) which substantially deviates from the value of 126.95º observed in the starting borane 2-dimesitylboryl-*N*,*N*-dimethylaniline;[135] ii) the elongated C(1)-C(2) bond of 1.426(6) Å. Despite these distortions, the boron-carbon bonds which are in the 1.574(7)-1.582(7) Å range remain within the norm.[135]

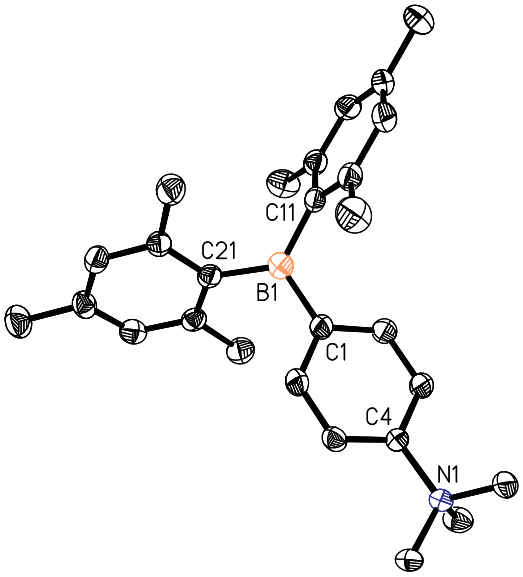

Figure 28: ORTEP view of [**83**]$^{+}$ in [**83**]OTf-0.5(toluene) (50% ellipsoid, H-atoms omitted for clarity).

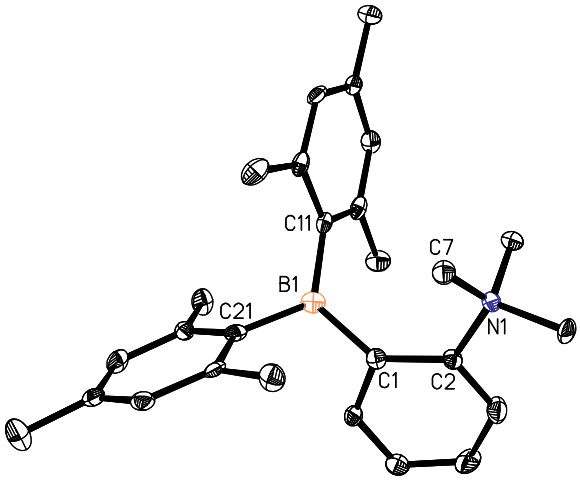

Figure 29: ORTEP view of [**84**]$^{+}$ in [**84**]OTf (50% ellipsoid, H-atoms omitted for clarity).

Table 5: Crystal data, data collection, and structure refinement for [**83**][OTf]-0.5(Toluene), and [**84**][OTf].

	[**83**][OTf]-	[**84**][OTf]
	Crystal data	
Formula	$C_{31.50}H_{39}BF_3NO_3S$	$C_{28}H_{35}BF_3NO_3S$
M_r	579.51	533.44
crystal size (mm^3)	0.23 × 0.20 × 0.20	0.22 × 0.16 × 0.13
crystal system	Triclinic	Monoclinic
Space group	$P\bar{1}$	$P2_1/c$
A (Å)	8.9107(8)	14.061(4)
B (Å)	16.1875(15)	12.976(3)
C (Å)	23.213(2)	16.329(4)
A (°)	109.8110(10)	
β (°)	95.6030(10)	113.423(5)
Γ (°)	90.4530(10)	
V ($Å^3$)	3132.1(5)	2733.8(12)
Z	4	4
ρ_{calc} (g cm^{-3})	1.229	1.296
μ (mm^{-1})	0.153	0.169
F(000)	1228	1128
	Data Collection	
T (K)	110(2)	110(2)
scan mode	ω	ω
hkl range	-11 → +11, -21 → +21, -30 → +30	-16 → +15, -14 → +14, -12 → +18
measd reflns	29051	11848
unique reflns [R_{int}]	14466 [0.0394]	4286 [0.0819]
reflns used for	14466	4286
	Refinement	
refined parameters	730	335
GOF on F^2	1.024	1.024
R1,[a] wR2[b] all data	0.1094, 0.1172	0.1105, 0.1604
ρ_{fin} (max/min) (e Å$^-$	0.399, -0.363	0.520, -0.461

[a] $R1 = \sum||Fo| - |Fc||/\sum|Fo|$. [b] $wR2 = \{[\sum w(Fo^2 - Fc^2)^2]/[\sum w(Fo^2)^2]\}^{1/2}$.

2.3 Theoretical studies of [**83**]$^+$ and [**84**]$^+$

The structures of cations [**83**]$^+$ and [**84**]$^+$ have been optimized using DFT methods (B3LYP, 6-31g(d) for all aromatic carbon, boron and nitrogen atoms, 6-31g for all other atoms) and subjected to single point energy calculations using the Polarizable Continuum Model[138,139] (PCM) with water as a solvent. Inspection of the frontier orbitals shows that the lowest unoccupied molecular orbital (LUMO) bears an important contribution from the boron-empty p-orbital, while the highest occupied molecular orbital (HOMO) is localized on the mesityl rings (Figure 30). The energy of the LUMO

in the *ortho*-isomer [**84**]$^+$ (-2.12 ev) is lower than in the *para*-isomer [**83**]$^+$ (-2.02 eV), which suggests that [**84**]$^+$ is a stronger Lewis acid. Since the ammonium moiety is closer to the boron center in [**84**]$^+$ than in [**83**]$^+$, the higher Lewis acidity of [**84**]$^+$ can also be anticipated on the basis of a simple inductive effect argument. The energies of the LUMOs in [**83**]$^+$ and [**84**]$^+$ are also substantially lower than those calculated for the LUMO of Mes_2BPh (-1.58 ev) at the same level of theory and with the same solvation model. This last comparison indicates that the positive charge of the cationic boranes substantially increases their Lewis acidity.[86]

In H_2O/DMSO 60:40 vol., the UV spectra of [**83**]$^+$ and [**84**]$^+$ feature a broad absorption band at 320nm (ε_{320} = 9104) for [**83**]$^+$ (Figure 31) and 321 nm (ε_{321} = 9200) for [**84**]$^+$ (Figure 32). TD-DFT calculations carried out using the PCM/water solvation model suggest that the low energy edge of the absorption spectrum is, in fact, dominated by the HOMO-LUMO transition. Because of the localization of the frontier orbitals, the HOMO-LUMO transition can be regarded as an intramolecular "ligand-to-element" charge-transfer transition. In agreement with this view, we note that both [**83**]$^+$ and [**84**]$^+$ give rise to a bright fluorescence whose maximum wavelength depends on the polarity of the solvent (Figure 31, Figure 32). Like other boron-based charge transfer chromophores,[52,140-142] both [**83**]$^+$ and [**84**]$^+$ show positive fluorosolvatochromism, suggesting that the exited state dipole of these molecules is larger than their ground state dipole.[140,143,144]

	HOMO	LUMO
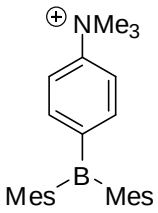 [**83**]$^+$	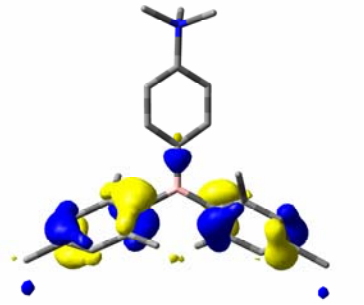 E = -6.18 eV	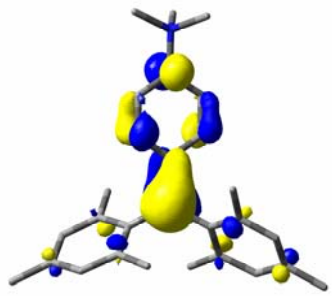 E = -2.02 eV
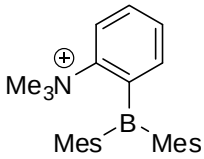 [**84**]$^+$	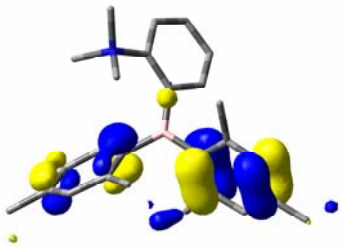 E = -6.38 eV	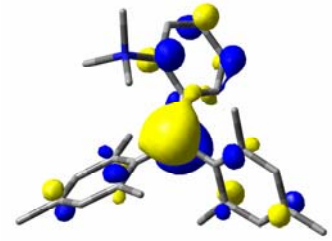 E = -2.12 eV

Figure 30: HOMO and LUMO of [**83**]$^+$ and [**84**]$^+$ (isodensity value = 0.05, H-atoms omitted for clarity).

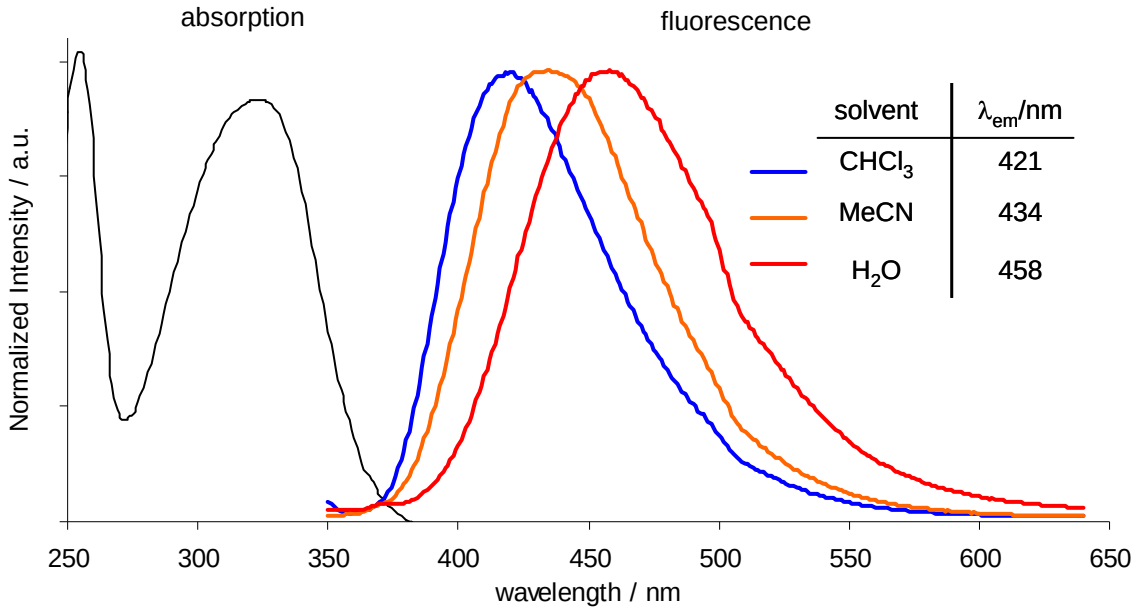

Figure 31: Absorption (in H_2O: DMSO 6:4) and emission spectra of [**83**]$^+$.

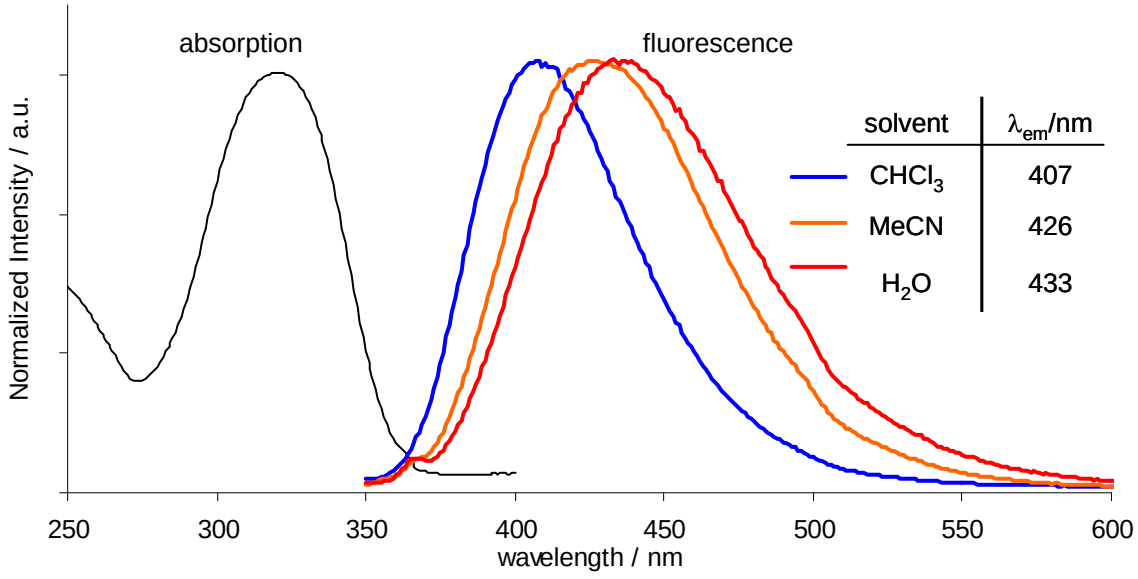

Figure 32: Absorption (in H_2O: DMSO 6:4) and emission spectra of [**84**]$^+$.

2.4 Cyanide and fluoride ion complexation in organic solvents

Salts [**83**]OTf and [**84**]OTf are converted into their corresponding cyanide complexes **83**-CN (Figure 34, Table 6) and **84**-CN (Figure 36, Table 6) upon reaction with NaCN in MeOH (Figure 33). Analogously, the fluoride complexes **83**-F (Figure 35, Table 6) and **84**-F (Figure 37, Table 6) form quantitatively when [**83**]OTf and [**84**]OTf are allowed to react with TBAF in $CHCl_3$ (Figure 33). These salts have been characterized by NMR spectroscopy and elemental analysis. In all cases, the ^{11}B NMR signal is in the expected range for a four-coordinate boron center (-12.9 ppm for **83**-CN, -14.2 ppm for **84**-CN, 5.1 ppm for **83**-F, 7.3 ppm for **84**-F). For the fluoride complexes **83**-F and **84**-F, the ^{19}F NMR signals appear at -170 and -158 ppm, respectively, which are close to that observed in compounds featuring triarylfluoroborate moieties.[46,48,59,88,145] The ^{1}H NMR spectra of **83**-F and **83**-CN feature four distinct resonances corresponding to the hydrogen nuclei of the *para*-phenylene ring. The inequivalence of these signals indicates that rotation about the B-C bond connecting the boron atom to the *para*-phenylene moiety is restricted because of steric effects. The IR spectra of **83**-CN and **84**-CN also feature intense cyanide stretching bands at 2162 cm^{-1} and 2167 cm^{-1}, respectively.

The crystal structures of all four adducts have been determined (Table 6). These compounds crystallize in the monoclinic space group $P2_1/n$ for **83**-CN (Figure 34, Table 6), triclinic $P\bar{1}$ for **1**-F (Figure 35, Table 6) and monoclinic $P2_1$ for both **84**-CN and **84**-F (Figure 36 and Figure 37, Table 6). In all of the anion adducts, the sum of the C_{aryl}-B-C_{aryl} angles ($\Sigma_{(C\text{-}B\text{-}C)}$ = 323.5° for **83**-CN, 341.2° for **83**-F, 338.1° for **84**-CN and 337.5° for **84**-F) indicates substantial pyramidalization of the boron atom. In **83**-CN, the B(1)-C(10) bond connecting the carbon atom of the cyanide anion to the boron center (1.618(8) Å) is comparable to those typically found in triarylcyanoborate anions such as $[Ph_3BCN]^-$ (1.65 Å).[146] This value is similar to that in **84**-CN (B(1)-C(7) = is 1.616(19) Å). The same type of comment can be made about the B(1)-F(1) bond lengths found in **83**-F and **84**-F (1.495(10) and 1.465(3) (4) Å respectively) which are comparable to those found in triarylfluoroborate anions (1.47 Å).[88,145]

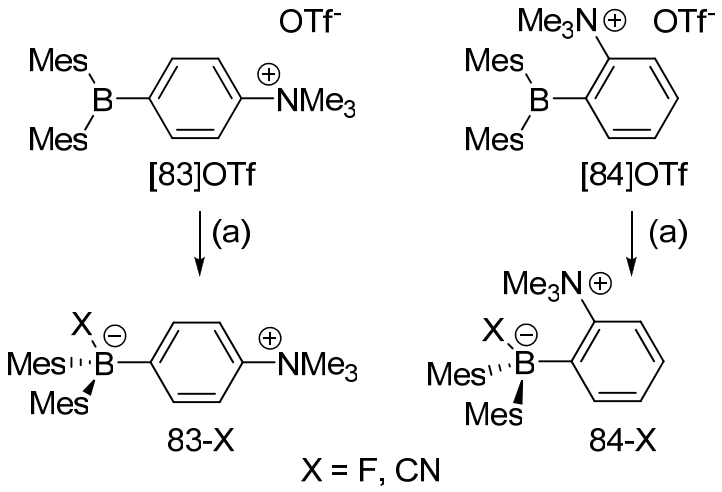

Figure 33: (a) X = F: TBAF in $CHCl_3$,, 94% for **83**-F and 88% for **84**-F; X = CN: NaCN, $MeOH$,, 95% for **83**-CN and 68% for **84**-CN.

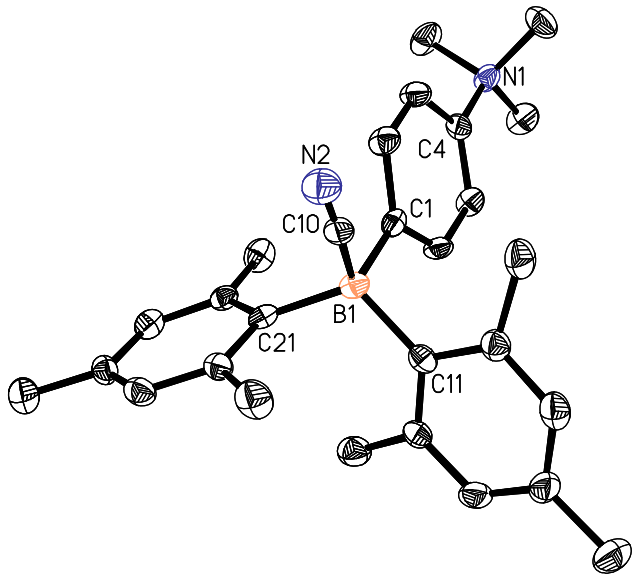

Figure 34: ORTEP view of **83**-CN (50% ellipsoid, H-atoms omitted for clarity).

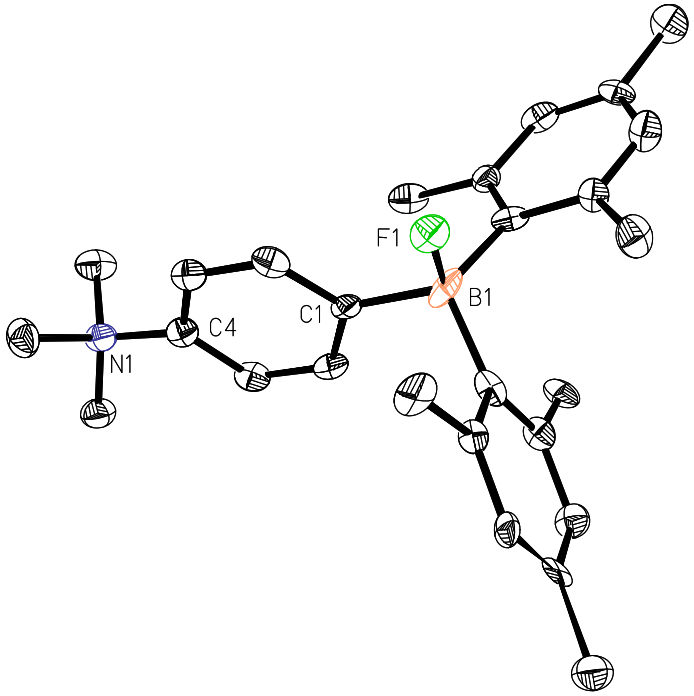

Figure 35: ORTEP view of **83**-F (50% ellipsoid, H-atoms omitted for clarity).

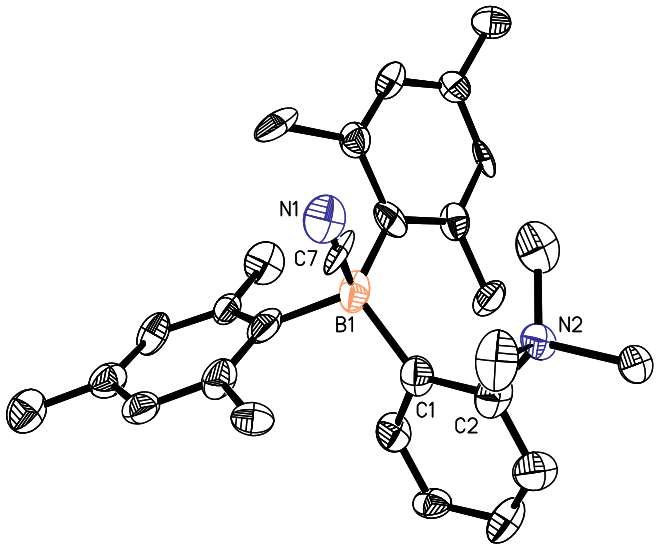

Figure 36: ORTEP view of **84**-CN (50% ellipsoid, H-atoms omitted for clarity).

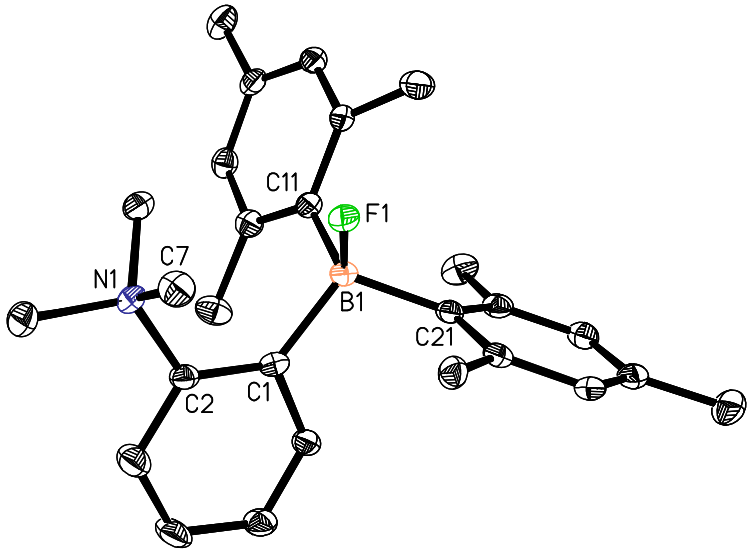

Figure 37: ORTEP view of **84**-F (50% ellipsoid, H-atoms omitted for clarity).

The most dramatic feature in the structures of both **84**-CN and **84**-F concerns the B(1)-C(1)-C(2) angles of 134.2(11)° for the cyanide complex and 132.4(2)° for the fluoride complex which remain much larger than the ideal value of 120°. The large angles are comparable to that present in [**84**]$^+$ (135.8(4)°), indicating that the pyramidalization of the boron center does not allow for a great deal of steric relief. The short distance of 2.964(3) Å separating the F(1) fluorine atom from the C(7) methyl carbon atom provides additional evidence for the steric constraints present in the fluoride derivative. In **84**-CN, there are no unsually short distances separating either the carbon atom C(7) or the nitrogen atom N(1) from the ammonium group, which are separated by more than 3 Å, however the larger B(1)-C(1)-C(2) angle of 134.2(11)° (which is nearly identical to that observed in [**84**]$^+$) allows the C-N vector to point up and away from the trimethylammonium moiety. Despite this observation, this large angle which deviates by nearly 15° from the idealized 120° attests to the steric congestion present in this molecule.

Table 6: Crystal data, data collection, and structure refinement for **83**-CN, **83**-F, **84**-CN and **84**-F.

	83-CN-Acetone	**83**-F	**84**-CN	**84**-F
		Crystal data		
Formula	$C_{31}H_{41}BN_2O$	$C_{27}H_{35}BFN$	$C_{28}H_{35}BN_2$	$C_{27}H_{35}BFN$
M_r	468.47	403.37	410.39	403.37
crystal size (mm^3)	0.28 × 0.10 × 0.08	0.12 × 0.11 × 0.11	0.19 × 0.19 × 0.15	0.29 ×0.21 × 0.20
crystal system	Monoclinic	Triclinic	Monoclinic	Monoclinic
Space group	$P2_1/n$	$P\bar{1}$	$P2_1$	$P2_1$
a (Å)	9.3438(17)	9.788(2)	8.3210(10)	8.4441(11)
b (Å)	12.777(2)	10.026(2)	15.116(3)	15.338(2)
c (Å)	23.658(4)	12.946(3)	9.2710(10)	8.8250(11)
α (°)		83.82(3)		
β (°)	99.547(2)	86.69(3)	95.281(4)	95.774(2)
γ (°)		65.57(3)		
V ($Å^3$)	2785.4(9)	1149.9(4)	1161.2(3)	1137.2(3)
Z	4	2	2	2
ρ_{calc} (g cm^{-3})	1.117	1.165	1.114	1.178
μ (mm^{-1})	0.066	0.071	0.067	0.072
F(000)	1016	436	444	436
	Data Collection			
T (K)	110(2)	110(2)	110(2)	110(2)
Scan mode	ω	ω	ω	ω
hkl range	-8 → +8, -11 → +11, -20 → +20	-9 → +8, -9 → +5, -12 → +12	-8 → +8, -15 → +15, -0 → +9	-10 → +9, -20 → +19, -11 → +11
measd reflns	12791	3373	2325	8020
unique reflns [R_{int}]	2017 [0.0502]	2111 [0.0973]	2240 [0.0608]	4989 [0.0710]
reflns used for	2017	2111	2240	4989
		Refinement		
refined parameters	316	274	289	271
GOF on F^2	1.002	1.006	1.016	1.004
R1,[a] wR2[b] all data	0.0622, 0.1364	0.1448, 0.2142	0.1488, 0.2408	0.0668, 0.1485
ρ_{fin} (max/min) (e Å$^-$	0.276, -0.236	0.356, -0.494	0.278, -0.290	0.321, -0.282

[a] $R1 = \sum||Fo| - |Fc||/\sum|Fo|$. [b] $wR2 = \{[\sum w(Fo^2 - Fc^2)^2]/[\sum w(Fo^2)^2]\}^{1/2}$.

2.5 Anion complexation in aqueous solution

The anion binding properties of [**83**]$^+$ and [**84**]$^+$ have been investigated in aqueous solution using UV-vis spectroscopy. This technique is particularly well adapted because binding of a nucleophile to the boron center disrupts the frontier orbitals of the borane, ultimately leading to drastic changes of their photophysical properties.[145] Remarkably, the UV-vis absorption spectrum of [**83**]$^+$ in H2O/MeOH 90:10 vol. is not affected in the presence of fluoride ions, while addition of cyanide induces a rapid quenching of the band at 320 nm followed by precipitation of **83**-CN (Figure 38).

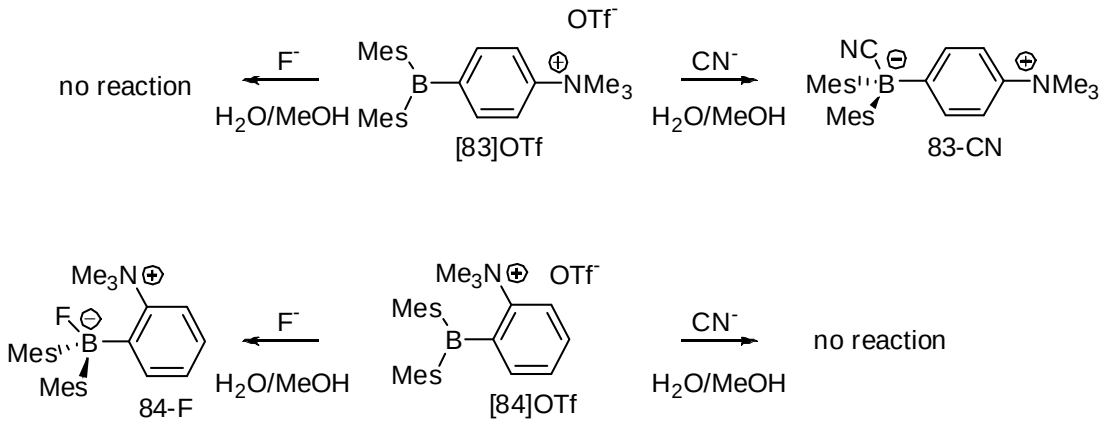

Figure 38: Reactivity of [**83**]$^+$ and [**84**]$^+$ with CN^- and F^- in H_2O/MeOH (9:1, v/v).

In buffered H2O/DMSO 60:40 vol. (HEPES 6 mM, pH 7), precipitation does not occur (Figure 39). Because of the low acidity of HCN, the cyanide binding constant of [**83**]$^+$ can only be determined if one considers the competing protonation of the anion. To this end, we measured the pK_a of HCN in H_2O/DMSO 60:40 vol. by a potentiometric titration and found it equal to 9.3 ±(0.01). Based on this value, analysis of the titration data[147] indicates that the cyanide binding constant of [**83**]$^+$ is equal to 3.9(±0.1) × 10^8 M^{-1} at pH 7 (Figure 39). These experiments show that [**83**]$^+$ has a very high affinity for cyanide, which is bound selectively over fluoride in aqueous solution (Figure 38). Since Mes_3B does not complex cyanide under these conditions, the elevated cyanide binding constant of [**83**]$^+$ probably results from favorable Coulombic effects which increase the Lewis acidity of [**83**]$^+$ by contributing electrostatically to the receptor-anion interaction. Interestingly, however, the observed selectivity indicates that these Coulombic effects are not sufficiently intense to permit fluoride binding in aqueous solution. A factor contributing to this selectivity is the high hydration enthalpy and the associated low basicity of fluoride ($\Delta H°_{hyd}$ = -504 kJ/mol, $pK_{a(HF)}$ = 3.18), which this ammonium borane receptor is unable to overcome. Because of its high cyanide binding constant, [**83**]$^+$ can be used for the naked eye detection of cyanide in the μM range. For example, the

fluorescence of a 5 μM solution of [**83**]$^{+}$ in H_2O/MeOH 90:10 vol. is quenched in the presence of one equivalent of cyanide as shown in Figure 40.

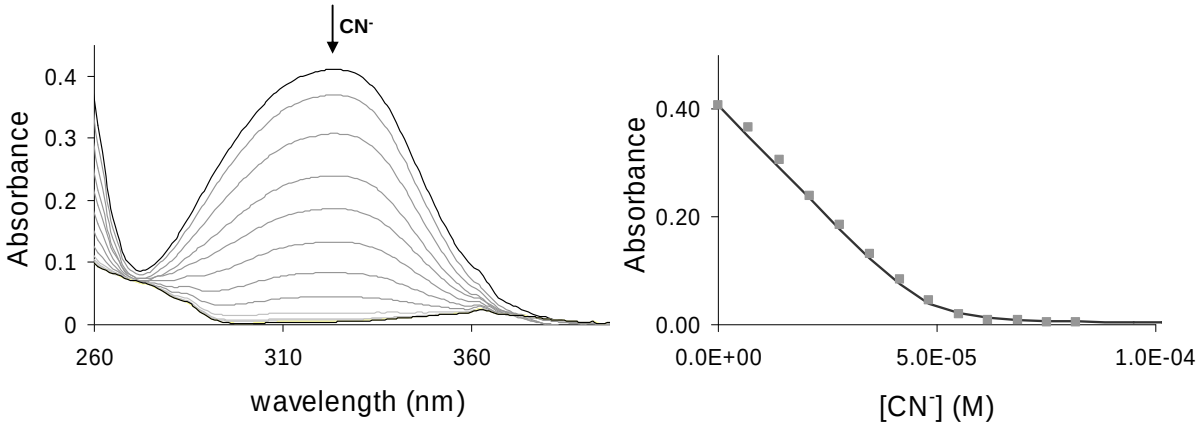

Figure 39: Changes in the UV-vis absorption spectra of a solution of: [**83**]OTf (3 mL, 5 × 10^{-5} M in H_2O/DMSO 60:40 vol.; HEPES 6 mM, pH 7) upon addition of a NaCN solution (3 × 10^{-3} M in H_2O).

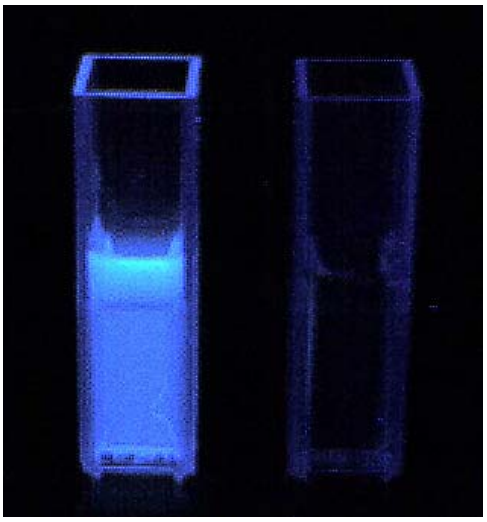

Figure 40: Fluorescence of a 5 μM solution of [**83**]$^+$ in H_2O/MeOH 90:10 vol. before (left) and after (right) addition of one equivalent of cyanide. The cells are illuminated with a hand-held UV lamp.

Remarkably, the UV-vis absorption spectrum of [**84**]$^+$ in H_2O/MeOH 90:10 vol. is not affected in the presence of cyanide, while addition of fluoride ions induces a rapid quenching of the band at 321 nm followed by precipitation of **84**-F (Figure 38). When the same experiment was repeated in buffered H_2O/DMSO 60:40 vol. (HEPES 6 mM, pH 7), precipitation does not occur and a fluoride binding constant of 900 (±50) M^{-1} can be calculated (Figure 41). This observation indicates that [**84**]$^+$ is a selective receptor for fluoride ions in aqueous solution. In this case, the selectivity most probably arises from the steric crowding of the boron binding pocket which interferes with the binding of the larger cyanide ion. Since cyanide binding to [**84**]$^+$ occurs in organic solvents, the observed lack of affinity of [**84**]$^+$ for cyanide in aqueous solution must also be the result of the increased protonation and solvation of the anion in aqueous media.

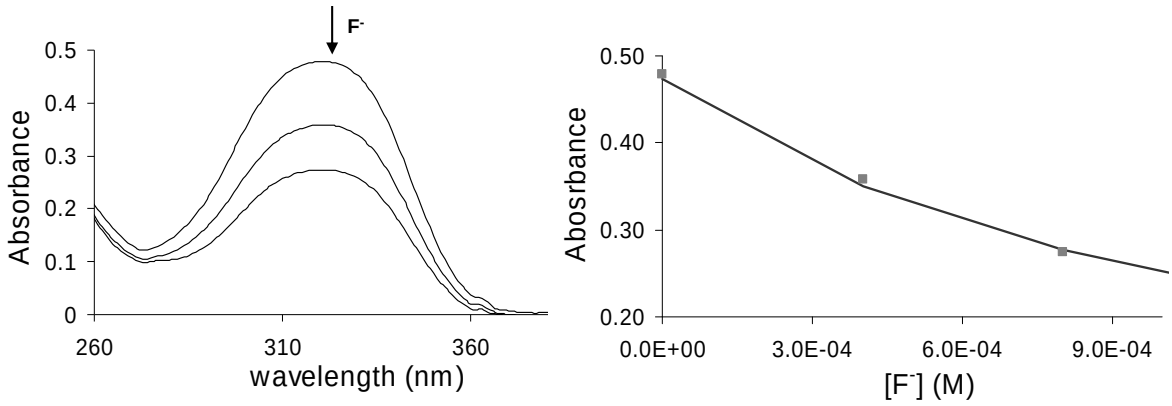

Figure 41: Changes in the UV-vis absorption spectra of a solution of: [**84**]OTf (3 mL, 5 × 10^{-5} M in H_2O/DMSO 60:40 vol.; HEPES 6 mM, pH 7) upon addition of a NaF solution (0.3 M in H_2O).

These experiments also allow us to draw some conclusions about the respective anion affinity of [**83**]$^+$ and [**84**]$^+$. As only [**84**]$^+$ binds fluoride, it can be concluded that the presence of the trimethylammonium group *ortho* to the boron center leads to an increase in the Lewis acidity of the derivative. This conclusion is in agreement with the computational results, which suggest that the LUMO in [**84**]$^+$ has a lower energy than in [**83**]$^+$ (Figure 30) . Thus for fluoride, the anion affinity seems to be governed by the Lewis acidity of the boron center. A different set of rules seem to apply to the larger cyanide anion. For this anion, steric effects appear to supersede the apparent higher Lewis acidity of [**84**]$^+$ and prevent coordination of the cyanide anion to the sterically hindered boron center. Accordingly, the reduced steric congestion of the boron center in [**83**]$^+$ makes coordination of the cyanide anion possible. It is also important to note that, unlike [**83**]$^+$ or [**84**]$^+$, neutral boranes such as Mes_3B do not complex fluoride or cyanide ions in H_2O/MeOH 90:10 vol. or H_2O/DMSO 60:40 vol.. This difference in reactivity indicates that the charge of [**83**]$^+$ or [**84**]$^+$ plays a determining role in increasing the Lewis acidity of these derivatives.

In order to test the anion binding selectivity of [**83**]$^+$ and [**84**]$^+$, their absorption spectrum has been monitored upon addition of various anions including Cl^-, Br^-, I^-, OAc^-,

NO_3^-, and HSO_4^-. Despite the addition of an 80-fold excess of anions, the absorbance of the band at 320 nm for [**83**]$^+$ and 321 nm for [**84**]$^+$ show no or negligible quenching in the presence of these anions, confirming the selectivity of these receptors (Figure 44). The absorption spectra of [**83**]$^+$ and [**84**]$^+$ are also unaltered when a neutral phosphate buffer is used indicating that binding of $H_2PO_4^-$ does not occur. Finally, cyanide binding to [**83**]$^+$ is reversible and can be modulated by adjusting the pH. Thus, when the pH of a solution containing **83**-CN is lowered from 7 to 0.5, the absorption at 320 nm increases indicating liberation of the cyanide anion and regeneration of free [**83**]$^+$ (Figure 42). Finally, addition of an aqueous solution of Al^{3+} to a solution containing **84**-F leads to complete regeneration of [**84**]$^+$ showing that fluoride binding is reversible (Figure 43).[88]

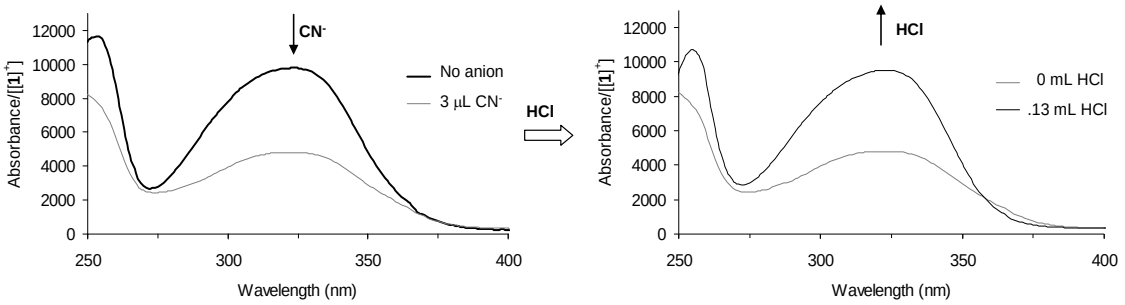

Figure 42: Changes in the UV-vis absorption spectrum of a solution of [**83**][OTf] (3 mL, 5.25 x 10^{-5} M) in H_2O/DMSO (60:40 vol.) after addition of a NaCN solution (left, 3.0 x 10^{-2} M in H_2O)followed by the acidification with HCl to pH 0.5 (right).

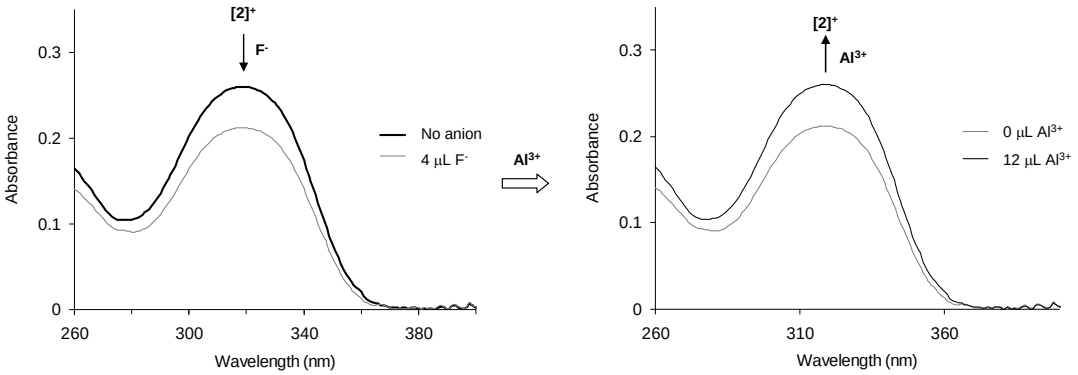

Figure 43: Changes in the UV-vis absorption spectrum of a solution of [**84**][OTf] (3 mL, 3.32 x 10^{-5} M) in H_2O/DMSO (60:40 vol.) after addition of a NaF solution (left, 3.0 x 10^{-1} M in H_2O) followed by successive additions of an aqueous $AlCl_3$ solution (right, 0.01 M).

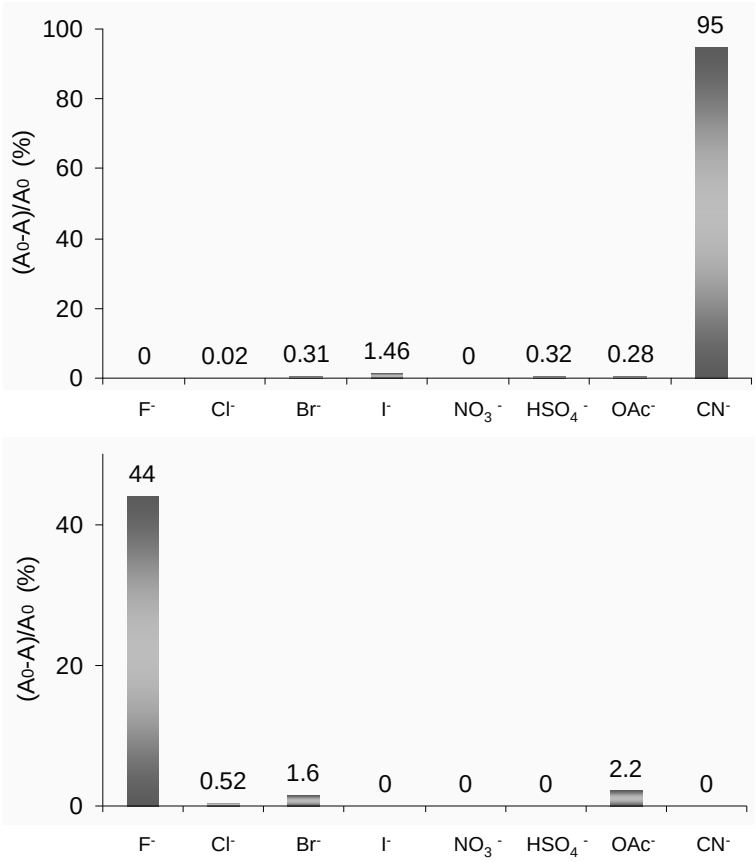

Figure 44: Top: Percent decrease of the absorbance of a solution of [**83**][OTf] (5.2 x 10^{-5} M) in H_2O/DMSO (60:40 vol.) at 320 nm in the presence of 80 equivalents of various anions. Bottom: Percent decrease of the absorbance of a solution of [**84**][OTf] (4.9 x 10^{-5} M) in H_2O/DMSO (60:40 vol.) at 321 nm in the presence of 80 equivalents of various anions.

2.6 Attempted synthesis of weakly solvated, water stable ammonium boranes

The formation of a neutral species by combination of a cation and an anion occurs at the expense of the solvation of both the cation and the anion. For this reason, highly solvated ions such as lithium or fluoride are difficult to complex in aqueous environments. In turn, it can be anticipated that the anion binding properties of a given family of cationic boranes will be increased if their solvation energy is actually decreased. In order to verify this hypothesis, we would like to determine if a decrease in the hydrophilicity of cationic boranes could be used to increase their anion affinity.

With this in mind, a series of aminoboranes, namely *p*-(Mes_2B)C_6H_4(NEt_2) (**85**), *p*-(Mes_2B)C_6H_4(NBu_2) (**86**) *p*-(Mes_2B)C_6H_4(NBn_2) (**87**), and *p*-(Mes_2B)C_6H_4(NPh_2) (**88**)[148] have been prepared in view of their conversion into the corresponding ammonium derivatives. Compounds **85-87** which had not been previously described, were synthesized by lithiation of the respective bromide derivatives in diethyl ether at room temperature followed by treatment with dimesitylboron fluoride. These new amino-boranes have been characterized by NMR spectroscopy and single crystal X-ray diffraction analysis in the case of **86** and **85**.

The diethylamino derivative, **85**, crystallizes in the triclinic space group $P\bar{1}$ with two molecules in the asymmetric unit (Figure 45, Table 7). Both independent molecules feature trigonal planar boron and nitrogen centers ($\Sigma_{(C\text{-}B\text{-}C)}$ = 360° (both molecules), and $\Sigma_{(C\text{-}N\text{-}C)}$ = 360° (molecule A) and 359.9° (molecule B)). All of the boron-carbon bonds are within the expected range 1.568(14)-1.609(13) Å and all the carbon-nitrogen bonds are within the norm (1.371(11)-1.387(10) Å for the N-C_{Ph} bonds and 1.446(10)-1.494(11) Å for the N-C_{Alk} bonds). Compound **85** exhibits all of the expected peaks in the ^{1}H NMR including the characteristic coupled triplet and quartet for the ethyl groups and the doublet of doublets corresponding to the *para*-substituted phenyl ring.

Compound **86** crystallizes in the monoclinic $P2_1/n$ space group (Figure 46, Table 7) and is structurally similar to **85** featuring trigonal planar boron and nitrogen centers as indicated by the sum of the C_{aryl}-B-C_{aryl} angles ($\Sigma_{(C\text{-}B\text{-}C)}$ = 360°) and C-N-C angles ($\Sigma_{(C\text{-}N\text{-}C)}$ = 358.3°). The planar geometry about the nitrogen atom is characteristic of *para*-substituted amino-triarylborane derivatives, and is indicative of participation of the nitrogen lone pair into the extended π-system.[148] Planarization of the nitrogen atom is also concomitant with a shortening of the nitrogen-carbon$_{aryl}$ bond (N(1)-C(12) = 1.361(7) Å) compared to the other N-C distances (1.463(7)-1.471(7) Å). All other atomic distances are within the norm. The ^{1}H NMR spectrum of **86** exhibits all of the expected peaks pertaining to this compound. In particular, the four peaks corresponding to the butyl groups are clearly identified along with the expected doublet of doublets for the *para*-substituted phenyl ring.

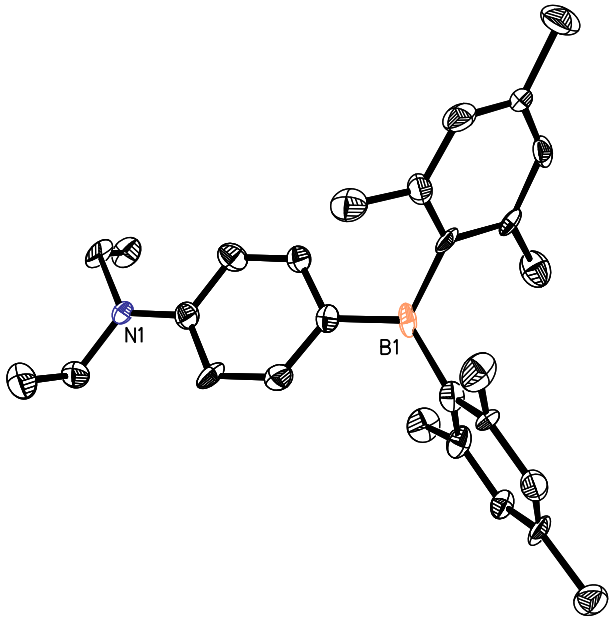

Figure 45: ORTEP view of **85** (50% ellipsoid, H-atoms omitted for clarity).

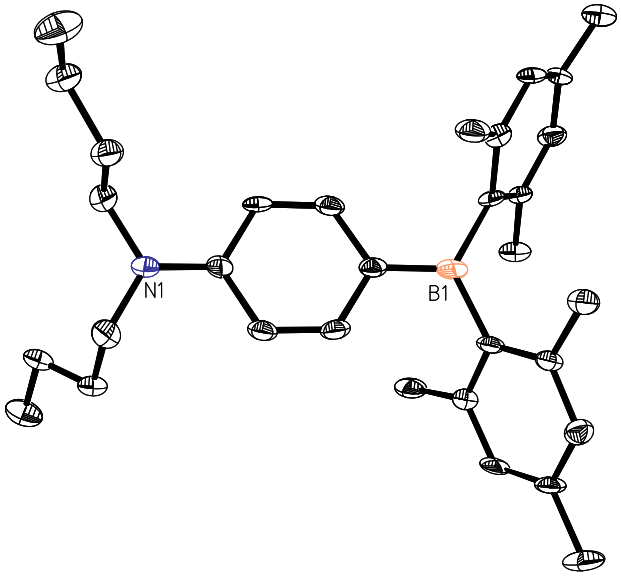

Figure 46: ORTEP view of **86** (50% ellipsoid, H-atoms omitted for clarity).

The dibenzylaminoborane, **87**, was isolated as a waxy solid. The ^{1}H spectrum exhibits all expected resonances for this compound with a diagnostic singlet at 4.66 ppm for the benzylic protons. The aromatic region features a doublet of doublets for the *para*-substituted phenyl ring. Single crystals of **87** have been elusive due to the waxy nature of this particular aminoborane, and no further characterization beyond ^{1}H NMR spectroscopy has been carried out.

In the course of this work, we obtained single crystals of **88**. Since the crystal structure of this compound has not been reported, a suitable single crystal was subjected to an X-ray analysis. Compound **88** crystallizes in the monoclinic space group $P2_1/n$ (Figure 47, Table 7). The boron and nitrogen atoms adopt the expected trigonal planar geometries, ($\Sigma_{(C\text{-}B\text{-}C)}$ = 359.95° and $\Sigma_{(C\text{-}N\text{-}C)}$ = 357.42°), typical of the aminophenyl-dimesitylboryl compounds. The nitrogen-carbon distances range from 1.414(3)-1.435(3) Å which are within the norm for triarylamines, and the boron-carbon bonds range from 1.552(3) to 1.589(3) Å. All other atomic distances are within the norm.

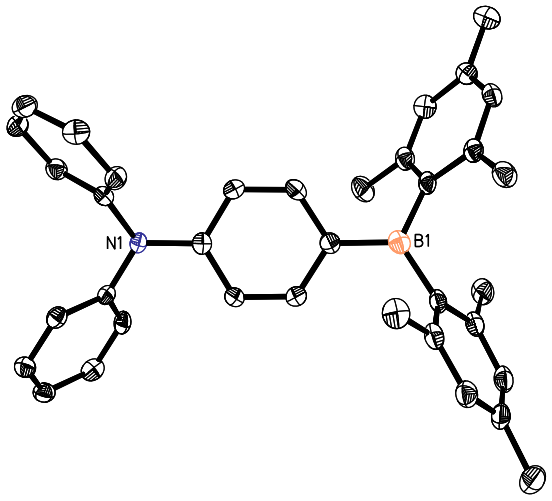

Figure 47: ORTEP view of **88** (50% ellipsoid, H-atoms omitted for clarity).

Table 7 Crystal data, data collection, and structure refinement for **85**, **86** and **88**.

	85	**86**	**88**
	Crystal data		
Formula	$C_{28}H_{36}BN$	$C_{32}H_{44}BN$	$C_{36}H_{36}BN$
M_r	397.39	453.49	493.47
crystal size (mm^3)	0.27× 0.23× 0.14	0.13 × 0.10 × 0.08	0.31 × 0.25 × 0.24
crystal system	Triclinic	Monoclinic	Monoclinic
space group	$P\bar{1}$	$P2_1/n$	$P2_1/n$
A (Å)	12.628(3)	11.712(2)	8.866(5)
B (Å)	14.109(3)	11.996(2)	34.047(17)
C (Å)	14.994(3)	19.898(4)	9.610(5)
A (°)	67.48(3)		
β (°)	89.46(3)	92.08(3)	100.561(8)
Γ (°)	83.38(3)		
V ($Å^3$)	2441.3(8)	2786.6(10)	2852(3)
Z	4	4	4
ρ_{calc} (g cm^{-3})	1.081	1.081	1.149
μ (mm^{-1})	0.061	0.061	0.065
F(000)	864	992	1056
	Data Collection		
T (K)	110(2)	110(2)	110(2)
scan mode	ω	ω	ω
hkl range	-13 → +14, -16 → +14, -17 → +17	-11 → +11, -11 → +11, -19 → +19	-11 → +11, -32 → +31, -2 → +12
measd reflns	10823	15658	8833
unique reflns [R_{int}]	7500[0.1075]	2602[0.0617]	5263[0.0303]
reflns used for	7500	2602	5263
	Refinement		
refined parameters	542	307	343
GOF on F^2	1.009	1.004	1.007
R1,[a] wR2[b] all data	0.2444, 0.4216	0.0971, 0.2149	0.0798, 0.1463
ρ_{fin} (max/min) (e Å$^-$	0.650, -0.562	0.499, -0.429	0.438, -0.320

[a] $R1 = \sum||Fo| - |Fc||/\sum|Fo|$. [b] $wR2 = \{[\sum w(Fo^2 - Fc^2)^2]/[\sum w(Fo^2)^2]\}^{1/2}$.

2.7 Alkylation reactions

The aminoboranes **85** and **86** slowly react with MeOTf in diethyl ether to afford low yields of the corresponding ammonium triflates [**89**]OTf and [**90**]OTf, respectively (Figure 48). The ^{1}H NMR spectra of [**89**]OTf, and the dibutyl derivative [**90**]OTf in $CDCl_3$ feature all expected resonances for the aromatic CH groups of the phenylene core. The alkyl groups on the nitrogen atoms for each salt give rise to two sets of proton resonances for each ethyl (in $[\mathbf{89}]^+$) or butyl (in $[\mathbf{90}]^+$) group indicating hindered rotation

about the N-$C_{Phenylene}$ bond. Both salts also display characteristic broad ^{11}B signals at 78 and 81 ppm for [**89**]$^+$ and [**90**]$^+$ respectively.

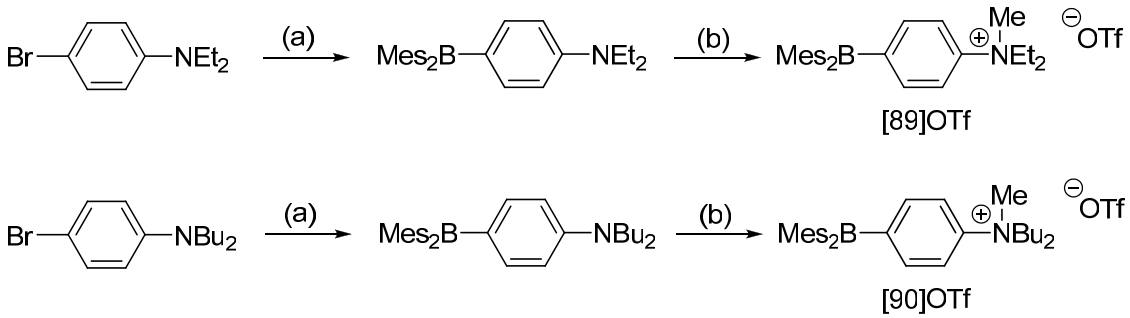

Figure 48: (a) Et_2O, ^{n}BuLi, Mes_2BF; (b) Et_2O, MeOTf, 62% for [**89**]$^+$ and 83% for [**90**]$^+$.

In the presence of water, [**89**]$^+$ and [**90**]$^+$ slowly undergo demethylation over a period of several hours to their respective aminoborane derivatives, as observed by both ^1H NMR and UV/vis spectroscopy. Demethylation of these salts is also observed in a variety of organic solvents (including chloroform, methanol and acetonitrile) over extended periods of time. The instability of these cationic boranes has precluded crystallization of these species.

Alkylation of the aminoboranes **87** and **88** was also considered. Unfortunately, methylation of the aminoboranes **87** and **88** could not be achieved with $[Me_3O]^+[BF_4]^-$, MeOTf or MeI suggesting that the strong electron withdrawing nature of the *para*-dimesitylboryl moiety renders the nitrogen atom considerably less nucleophilic than in the corresponding amines.[148]

2.8 Isolation of protonated aminoboranes

We were able to isolate the ammonium triflate salts, [*p*-$(Mes_2B)C_6H_4(NHMe_2)]^+$ ([**91**]$^+$) and [*p*-$(Mes_2B)C_6H_4(NHBu_2)]^+$ ([**92**]$^+$) from the reaction of the corresponding

aminoboranes with MeOTf in Et_2O. Formation of these ammonium boranes most likely results from the presence of triflic acid formed by hydrolysis of MeOTf in the reaction mixture. The ^{1}H NMR spectrum of [**91**]$^+$ exhibits a doublet at 3.29 ppm (J = 11.5 Hz)[149] corresponding to the methyl groups on the nitrogen atom of the ammonium moiety which are coupled to the N-*H* proton. Accordingly, the N-*H* resonance of the ammonium group is detected at a characteristic down-field shift of 11.57 ppm.[149]

The two salts have been characterized by single crystal X-ray diffraction analysis (Figure 49 and Figure 50, Table 8). The protonated dimethylammonium borane, [**91**]$^+$, crystallizes in the monoclinic space group C_2/c (Figure 49, Table 8). Most notably, the nitrogen atom N(1) exhibits substantial pyramidalization ($\Sigma_{(C\text{-}N\text{-}C)}$ = 336.6°) indicating that its lone pair is no longer conjugated with the π-system of the aromatic ring. In agreement with this assessment, we note that the N-C_{Ph} bond is substantially longer (N(1)-C(14) = 1.476(8) Å) than that observed in *p*-(Mes_2B)-C_6H_4-(NMe_2) (1.368(1) Å).[148] The boron atom remains trigonal planar ($\Sigma_{(C\text{-}B\text{-}C)}$ = 360°) and does not form any short contacts with the triflate anion. Compound [**92**]$^+$ crystallizes in the triclinic space group $P\bar{1}$ with two independent molecules in the asymmetric unit (Figure 50, Table 8). As for [**92**]$^+$, the nitrogen atom of each molecule adopts a tetrahedral geometry ($\Sigma_{(C\text{-}N\text{-}C)}$ = 337.4° (molecule A) and 334.8° (molecule B)) and the N-C_{Ph} bonds are lengthened (N-C_{Ph} = 1.487(6) Å (molecule A) and 1.495(6) Å (molecule B)) when compared to **86** (N-C_{Ph} = 1.361(7) Å). Both boron centers remain tricoordinate and are not neutralized by the triflate counter anions which display no appreciable interactions with any other atoms in the molecules.

Table 8: Crystal data, data collection, and structure refinement for [**91**][OTf] and [**92**][OTf].

	[**91**]OTf	[**92**]OTf
	Crystal data	
Formula	$C_{27}H_{33}BF_3NO_3S$	$C_{33}H_{45}BF_3NO_3S$
M_r	519.41	603.57
crystal size (mm^3)	0.23 × 0.19 × 0.09	0.14 × 0.13 × 0.11
crystal system	Monoclinic	Triclinic
Space group	*C*2/*c*	$P\bar{1}$
a (Å)	37.969(8)	8.877(8)
b (Å)	8.3772(18)	12.142(10)
c (Å)	18,743(4)	31.22(3)
α (°)		80.524(11)
β (°)	114.472(10)	87.421(11)
γ (°)		86.731(11)
V ($Å^3$)	5426(2)	3311(5)
Z	8	4
ρ_{calc} (g cm^{-3})	1.272	1.211
μ (mm^{-1})	0.168	0.147
F(000)	2192	1288
	Data Collection	
T (K)	110(2)	110(2)
scan mode	ω	ω
hkl range	-25 → +36, -9 → +8, -18 → +15	-10 → +10, -13 → +13, -35 → +35
measd reflns	8159	28932
unique reflns [R_{int}]	2520 [0.0553]	10374[0.2337]
Reflns used for	2520	10374
	Refinement	
refined parameters	325	757
GOF on F^2	1.009	1.0007
R1,[a] wR2[b] all data	0.0981, 0.1725	0.1354, 0.2166
ρ_{fin} (max/min) (e $Å^{-3}$)	0.529, -0.394	0.643, -0.650

[a] $R1 = \sum||Fo| - |Fc||/\sum|Fo|$. [b] $wR2 = \{[\sum w(Fo^2 - Fc^2)^2]/[\sum w(Fo^2)^2]\}^{1/2}$.

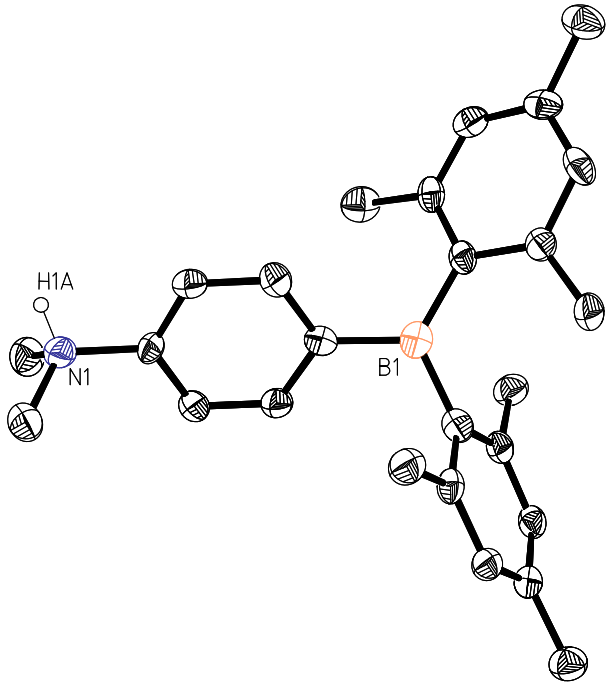

Figure 49: ORTEP view of [**91**]$^{+}$ in [**91**]OTf (right) (50% ellipsoid, H-atoms omitted).

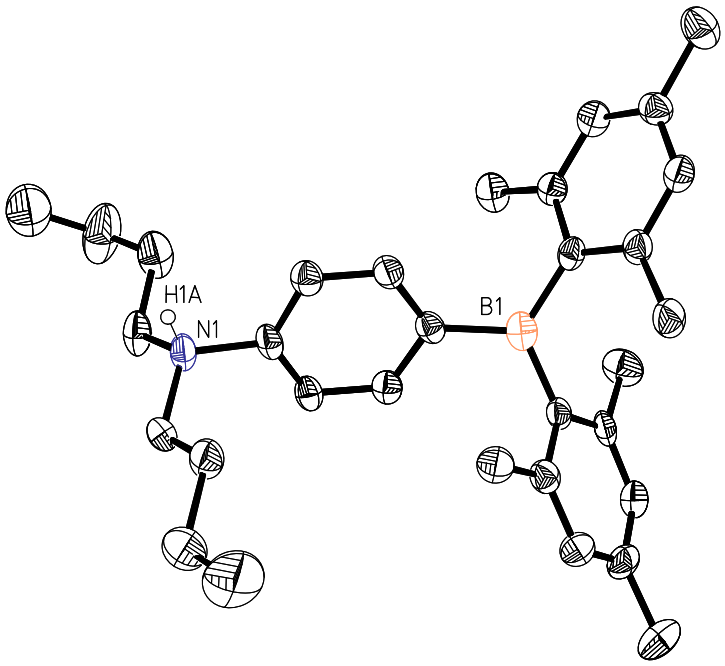

Figure 50: ORTEP view of [**92**]$^{+}$ in [**92**]OTf (right) (50% ellipsoid, H-atoms omitted).

2.9 Conclusion

This work demonstrates that cationic boranes such as [**83**]$^+$ serve as selective receptors for cyanide in water at neutral pH. While many cyanide receptors are known, few are effective in aqueous solution at neutral pH, conditions under which the cyanide anion exists mostly in a protonated form. The unusual cyanide binding properties of [**83**]$^+$ can be assigned to favorable Coulombic effects, which increase the Lewis acidity of the boron atom and strengthen the receptor-cyanide interaction. Another important aspect of this work concerns the anion binding selectivity of these cationic boranes which can be tuned using both steric and electronic effects. Indeed, when the trimethylammonium functionality is positioned *ortho* to the boron center as in [**84**]$^+$, the Lewis acidity of the ammonium borane is increased, making fluoride binding possible. However, in this case, the increased steric crowding of the boron center prevents coordination of the larger cyanide anion.

The efforts to investigate the role solvation of the cationic borane plays in anion complexation provided a plethora of new amino and ammonium boranes. While these studies were inconclusive in terms of answering any of our hypotheses regarding borane solvation and its effect on anion binding, they did provide valuable knowledge about the reactivity of many of these species. The structures obtained for [**91**]$^+$ and [**92**]$^+$ provide crystallographic evidence that these aminoboryl derivatives are sensitive to protonation. The aqueous studies with compounds [**89**]$^+$ and [**90**]$^+$ indicate that demethylation occurs, suggesting that decreasing the solubility of these receptors may inherently destabilize them.

2.10 Experimental section

General Considerations. 4-(dimesitylboryl)-*N,N*-dimethylaniline and 2-(dimesityl boryl)-*N,N*-dimethylaniline were synthesized by published procedures.[135-137] 4-Bromo-*N,N*-dimethylaniline was purchased from Oakwood Products Inc, methyl triflate, dimesitylboron fluoride and *N,N*-dimethylaniline from Aldrich, and *n*-$Bu_4NF{\cdot}3H_2O$ (TBAF) from Fluka. Et_2O and THF were dried by reflux over Na/K.

Hexane was dried by passing in a column charged with activated alumina. Air-sensitive compounds were handled under a N_2 atmosphere using standard Schlenk and glovebox techniques. UV-vis and fluorescence spectra were recorded on a HP8453 and an Aminco-Bowman 2 Luminescence spectrophotometer, respectively. IR spectra were obtained using a Bruker Tensor 37 Infrared spectrophotometer. Elemental analyses were performed at Atlantic Microlab (Norcross, GA). NMR spectra were recorded on a Varian Unity Inova 400 FT NMR (399.59 MHz for ^{1}H, 375.99 MHz for ^{19}F, 128.19 MHz for ^{11}B, 100.45 MHz for ^{13}C) spectrometer at ambient temperature. Chemical shifts δ are given in ppm, and are referenced against external Me_4Si (^{1}H, ^{13}C), $BF_3{\cdot}Et_2O$ (^{11}B), and $CFCl_3$ (^{19}F). Potentiometric titrations were carried out using a SympHony Gel-Filled Combination Electrode from VWR International with a PHM290 pH Stat Controller from Radiometer Analytical. Melting points were measured on samples in sealed capillaries and are uncorrected.

Crystallography. Colorless single crystals of [**83**]OTf-0.5(Toluene) could be obtained by slow evaporation of a 1:1 toluene:CH_2Cl_2 solution. Colorless single crystals could be obtained by vapor diffusion of hexane into a concentrated dichloromethane solution [**84**]OTf. Single crystals of **83-**CN-Acetone were obtained by crystallization from a concentrated acetone solution. Single crystals of **83-**F, **84-**CN and **84-**F were obtained by vapor diffusion of hexane into concentrated acetone solutions. Single crystals of **85**, **86** and **88** were obtained by cooling of concentrated hexane solutions to -40 °C for several hours. Single crystals of [**91**]OTF and [**92**]OTf were obtained by vapor diffusion of hexane into concentrated chloroform solutions. The crystallographic measurements were obtained using either a Siemens SMART or APEX-II CCD area detector diffractometers, with a graphite-monochromated Mo-K_α radiation (λ = 0.71069 Å). A specimen of suitable size and quality were selected and mounted onto glass fiber with apiezon grease. The structure was solved by direct methods, which successfully located most of the non-hydrogen atoms. Subsequent refinement on F^2 using the SHELXTL/PC package (version 5.1) allowed location of the remaining non-hydrogen

atoms.

Synthesis of [83]OTf. Methyl triflate (0.53 g, 3.25 mmol) was added to a solution of 4-(dimesitylboryl)-*N,N*-dimethylaniline (1.20 g, 3.25 mmol) in Et_2O (30 mL) at room temperature. The mixture was stirred overnight which resulted in the formation of a white solid. The solid formed was collected by filtration, washed with Et_2O (3 x 10 mL), and dried in under vacuum to afford [**83**]OTf as a white powder (1.35 g, 78% yield). [**83**]OTf is hygroscopic and captures water when exposed to air. Analysis of the crystal structure revealed inclusion of one molecule of toluene in the asymmetric unit. mp. 210 ºC. ^{1}H NMR (399.9 MHz, $CDCl_3$): δ 1.93 (s, 12H, Mes-CH_3), 2.29 (s, 6H, Mes-CH_3), 3.75 (s, 9H, N-CH_3), 6.81 (s, 4H, Mes-C*H*), 7.64-7.72 (m, 4H, phenyl-C*H*). ^{13}C NMR (100.5 MHz, $CDCl_3$): δ 21.22, 23.45 (Mes-*C*H_3), 57.32(N-*C*H_3), 118.64 (Mes-*o*-*C*), 128.53 (Mes-*C*H), 138.05 (phenyl-*C*H), 139.75 (Mes-*p*-*C*), 140.71 (phenyl-*C*H), 148.89 (B-*C*Mes) B-C_{phenyl}, N-C_{phenyl}, and *C*F_3 carbon peaks were not observed. ^{11}B NMR (128.2 MHz, $CDCl_3$): δ +74. ^{19}F NMR (375.9 MHz, $CDCl_3$): δ -78.3. UV-vis ($CHCl_3$): λ_{max}/nm (log ε) 335 (3.93). Anal. Calcd for $C_{28}H_{38}BNSO_{4.5}F_3$ ([**83**]OTf-1.5H_2O): C, 61.71; H, 7.16. Found: C, 61.61; H, 6.72.

Synthesis of [84]OTf. Methyl triflate (0.15 mL, .948 mmol) was added to a solution of 2-(dimesitylboryl)-*N,N*-dimethylaniline (0.35 g, .948 mmol) in Et_2O (15 mL) at room temperature. The mixture was stirred overnight which resulted in the formation of a white solid. The solid formed was collected by filtration, washed with Et_2O (3 x 10 mL), and dried in under vacuum to afford [**2**]OTf as a white powder (0.198 g, 39% yield). mp. 219 ºC. ^{1}H NMR (399.9 MHz, $CDCl_3$): δ 1.37 (bs, 3H, Mes-CH_3), 1.84 (bs, 3H, Mes-CH_3), 1.95 (bs, 3H, Mes-CH_3), 2.20 (bs, 3H, Mes-CH_3), 2.26 (bs, 6H, Mes-CH_3), 3.55 (s, 9H, N-CH_3), 6.66-6.88 (bm, 4H, Mes-C*H*), 7.43 (d, 2H, $^3J_{H\text{-}H}$ = 4.4 Hz, phenyl-C*H*), 7.72 (m, 1H, $^3J_{H\text{-}H}$ = 4.0 Hz, phenyl-C*H*), 8.08 (d, 1H, $^3J_{H\text{-}H}$ = 4.4 Hz, phenyl-C*H*). ^{13}C NMR (100.5 MHz, $CDCl_3$): δ 21.18 (2C, Mes-*p*-CH_3), 22.55 (1C, Mes-*o*-*C*H_3), 23.19 (2C, Mes-*o*-*C*H_3), 24.74 (1C, Mes-*o*-*C*H_3), 58.25 (N-*C*H_3), 120.50

(q, $^{1}J_{C\text{-}F}$ = 319.69 Hz, *C*F_3), 122.63 (phenyl-*C*H), 129.42 (bs, Mes-*C*Me), 129.66 (bs, Mes-*C*Me), 129.91 (bs, Mes-*C*Me), 130.19 (bs, Mes-*C*Me), 130.49 (phenyl-*C*H), 133.53 (phenyl-*C*H), 135.52 (phenyl-*C*H), 140.01 (bs, B-*C*Mes), 140.65 (bs, N-C_{phenyl}), 141.38 (bs, Mes-*C*Me), 141.71 (Mes-*C*Me), 141.96 (phenyl-*C*B), 143.13 (bs, B-*C*Mes), 150.66 (4C, Mes-*C*H) . ^{11}B NMR (128.2 MHz, $CDCl_3$): δ +67.6. ^{19}F NMR (375.9 MHz, $CDCl_3$): δ -74.4. UV-vis ($CHCl_3$): λ_{max}/nm (log ε) 328 (4.08). Anal. Calcd for $C_{28}H_{35}BNSO_3F_3$: C, 63.04; H, 6.61. Found: C, 62.82; H, 6.75.

Synthesis of 83-F. Addition of a solution of TBAF (60 mg, 0.187 mmol) in chloroform (10 mL) to a solution of [**83**]OTf (100 mg, 0.187 mmol) in chloroform (10 mL) resulted in the formation of a precipitate. After stirring for 30 min, the mixture was filtered. This solid was washed with chloroform and dried under vacuum to afford **83**-F-0.5($CHCl_3$) as a white powder (71 mg, 94% yield. mp. 260 ºC. ^{1}H NMR (400 MHz, acetonitrile-d_3): δ 1.85 (s, 12H, Mes-CH_3), 2.12 (s, 6H, Mes-CH_3), 3.45 (s, 9H, N-CH_3), 6.45 (s, 4H, Mes-C*H*), 7.02-7.48 (bm, 4H, phenyl-C*H*). ^{13}C NMR (100.5 MHz, acetonitrile-d_3): δ 20.85 (Mes-*C*H_3), 25.30 (Mes-*C*H_3), 57.79 (N-*C*H_3), 117.00 (Mes-*o*-*C*Me), 123.41 (phenyl-*C*B), 129.11 (Mes-*C*H), 132.69 (phenyl-*C*H), 134.21(B-*C*Mes), 135.66 (Mes-*p*-*C*Me), 142.10 (phenyl-*C*H), 144.07 (phenyl-*C*N). ^{11}B NMR (128.2 MHz, acetonitrile-d_3): δ 5.1 ^{19}F NMR (375.9 MHz, acetonitrile-d_3): δ -169.9 (bs) Anal. Calcd for $C_{27.5}H_{35.5}BNFCl_{1.5}$ (**83**-F-0.5($CHCl_3$): C, 71.32; H, 7.73. Found: C, 72.44; H, 7.94.

Synthesis of 84-F. **84**-F was prepared in a 88% yield by following the procedure used for **83**-F and was recrystallized from acetonitrile to afford **84**-F-MeCN. mp. 273 ºC. ^{1}H NMR (400 MHz, acetone-d_6): δ 1.82 (bs, 12H, Mes-CH_3), 2.11 (s, 6H, Mes-CH_3), 3.81 (d, 9H, $J_{F\text{-}H}$ = 2 Hz, N-CH_3), 6.49 (s, 4H, Mes-C*H*), 7.02 (t, 1H, $^{3}J_{H\text{-}H}$ = 7.2 Hz phenyl-C*H*), 7.12 (t, 1H, $^{3}J_{H\text{-}H}$ = 7.6 Hz phenyl-C*H*), 7.62 (d, 1H,$^{3}J_{H\text{-}H}$ = 7.6 Hz phenyl-C*H*), 7.67 (d, 1H, $^{3}J_{H\text{-}H}$ = 8.4 Hz phenyl-C*H*). ^{13}C NMR (100.5 MHz, acetone-d_6): δ 20.88 (Mes-*C*H_3), 25.56 (Mes-*C*H_3), 57.89 (d, $J_{F\text{-}C}$ = 12.6 Hz, N-*C*H_3), 118.85 (phenyl-*C*H), 126.69 (phenyl-*C*H), 128.39 (phenyl-*C*H), 129.63 (bs, 8C, Mes-o-*C*Me,

Mes-*C*H), 132.96 (phenyl-*C*H), 142.02 (d, J_{F-C} = 6.9 Hz, B-*C*Mes), 153.15 (phenyl-*C*NMe$_3$). Phenyl-*C*B carbon peak was not observed. ^{11}B NMR (128.2 MHz, acetone-d$_6$): δ 7.3 ^{19}F NMR (375.9 MHz, acetone-d$_6$): δ -157.9 (bs) Anal. Calcd for $C_{29}H_{38}BN_2F$ (**84**-F-MeCN): C, 78.37; H, 8.62. Found: C, 78.72; H, 8.52.

Synthesis of 83-CN. Addition of a solution of NaCN (9.2 mg, 187 mmol) in methanol (10 mL) to a solution of [**83**]OTf (100 mg, 0.187 mmol) in methanol (10 mL) resulted in the formation of a precipitate. After stirring for 30 min, the mixture was filtered. This solid was washed with methanol (3 x 10 mL) and dried under vacuum to afford **83**-CN-MeOH as a white powder (99 mg, 95% yield). Analysis of the crystal structure revealed inclusion of one acetone molecule in the asymmetric unit. mp 405 °C (dec). ^{1}H NMR (399.9 MHz, acetone-*d*$_6$): δ 1.90 (s, 12H, Mes-C*H*$_3$), 2.11 (s, 6H, Mes-C*H*$_3$), 3.29 (s, 3H, MeOH), 3.71 (s, 9H, N-C*H*$_3$), 6.49 (s, 4H, Mes-C*H*), 7.18 (bs, 1H, phenyl-C*H*), 7.37 (bs, 1H, phenyl-C*H*), 7.69 (bs, 1, phenyl-C*H*), 8.29 (bs, 1H, phenyl-C*H*). ^{13}C NMR (100.5 MHz, DMSO-*d*$_6$): δ 20.44 (Mes-*p*-*C*H$_3$), 25.30 (Mes-*o*-*C*H$_3$, 56.26 (N-*C*H$_3$), 79.89 (B-*C*N), 116.98 (Mes-*C*H), 128.62 (phenyl-*C*H), 131.37 (Mes-*o*-*C*Me), 135.63 (bs, B-*C*Mes), 136.53 (bs, B-*C*phenyl), 140.86 (phenyl-*C*H), 141.02 (N-*C*phenyl), 143.69 (Mes-*p*-*C*Me). ^{11}B NMR (128.2 MHz, $CDCl_3$): δ -12.9. IR ν_{CN} = 2162 cm^{-1}. Anal Calcd for $C_{29}H_{39}BON_2$ (**83**-CN-MeOH): C, 78.72; H, 8.88. Found: C, 78.83; H, 8.47.

Synthesis of 84-CN. **84**-CN was prepared by following the procedure used for **83**-CN. **84**-CN-MeCN was isolated in a 68% by recrystallization from hot acetonitrile. mp 329 °C (dec). ^{1}H NMR (399.9 MHz, DMSO-*d*$_6$): δ 1.77 (bs, 12H, Mes-C*H*$_3$), 2.11 (s, 6H, Mes-C*H*$_3$), 3.72 (s, 9H, N-C*H*$_3$), 6.53 (s, 4H, Mes-C*H*), 6.99 (t, 1H, $^3J_{H-H}$ = 7.2 Hz phenyl-C*H*), 7.22 (t, 1H, $^3J_{H-H}$ = 8.4 Hz phenyl-C*H*), 7.46 (d, 1, $^3J_{H-H}$ = 7.6 Hz phenyl-C*H*), 7.73 (d, 1H, $^3J_{H-H}$ = 8.8 Hz phenyl-C*H*). ^{13}C NMR (100.5 MHz, DMSO-*d*$_6$): δ 20.34 (Mes-*p*-*C*Me), 25.45 (Mes-*o*-*C*Me), 57.65 (N-*C*Me), 120.18 (phenyl-*C*H), 120.40 (B-*C*N), 126.66 (phenyl-*C*H), 127.44 (phenyl-*C*H), 127.78 (phenyl-*C*H), 129.33 (Mes-

*C*H), 130.06 (phenyl-*C*B), 132.40 (Mes-*p*-*C*Me), 137.25 (B-*C*Mes), 140.16 (B-*C*Mes), 141.96 (phenyl-*C*N), 142.08 (Mes-*o*-*C*Me), 152.05 (Mes-*o*-*C*Me). ^{11}B NMR (128.2 MHz, $CDCl_3$): δ -14.2. IR ν_{CN} = 2167 cm^{-1}. Anal Calcd for. $C_{30}H_{38}BN_3$ (**84**-CN-MeCN): C, 79.81; H, 8.48. Found: C, 80.42; H, 8.49.

Synthesis of 85. 4-bromo-*N,N*-diethylaniline (1.0 g, 3.52 mmol) was dissolved in Et_2O (10 mL) and treated with BuLi (1.5 mL, 2.58 M in hexanes, 3.87 mmol) at room temperature. The solution was stirred for 5 minutes at room temperature then treated with dimesitylboron fluoride (1.04 g, 3.87 mmol) in Et_2O (5 mL) and then heated to reflux for 2 hours. The solution was then cooled and the solvent removed *in vacuo*. The bright yellow residue was extracted with hexanes (3 x 10 mL) and filtered over Celite. The hexane solution was concentrated to 5 mL and cooled to -40 °C for 12 hours resulting in crystallization of **85** as a yellow solid. (541 mg 62% yield). mp 109-111 °C (dec). ^{1}H NMR (399.9 MHz, $CDCl_3$): δ 1.17 (t, 6H, ^3J = 7.2 Hz, Et-C*H*$_3$), 2.06 (s, 12H, Mes-C*H*$_3$), 2.28 (s, 6H, Mes-C*H*$_3$), 3.38 (q, 4H, ^3J = 7.2 Hz, Et-C*H*$_2$), 6.53 (d, 2H, ^3J = 8.9 Hz phenyl-C*H*), 6.78 (s, 4H, Mes-C*H*), 7.38 (d, 2H, ^3J = 8.9 Hz phenyl-C*H*). Anal Calcd for. $C_{28}H_{32}BN$: C, 84.62; H, 9.13. Found: C, 84.15; H, 9.13.

Synthesis of 86. **86** was prepared by following the procedure to synthesize **85**, starting from 4-bromo-*N,N*-dibutylaniline (1.0 g, 3.52 mmol) to yield the title compound as a yellow crystalline solid. (706 mg, 44% yield). mp 118-120 °C (dec). ^{1}H NMR (399.9 MHz, $CDCl_3$): δ 0.94 (t, 6H, ^3J = 7.6 Hz, Bu-C*H*$_3$), 1.33 (m, 4H, Bu-C*H*$_2$), 1.58 (m, 4H, Bu-C*H*$_2$), 2.07 (s, 12H, Mes-C*H*$_3$), 2.28 (s, 6H, Mes-C*H*$_3$), 3.34 (m, 4H, Bu-C*H*$_2$), 6.51 (d, 2H, ^3J = 9.2 Hz phenyl-C*H*), 6.79 (s, 4H, Mes-C*H*), 7.39 (d, 2H, ^3J = 9.2 Hz phenyl-C*H*).

Synthesis of 87. **87** was prepared by following the procedure to synthesize **86**, starting from 4-bromo-*N,N*-dibenzylaniline (500 mg, 1.42 mmol) to yield the title compound as a waxy yellow solid (541 mg 62% yield). mp 74-76 °C. ^{1}H NMR (399.9

MHz, $CDCl_3$): δ 2.03 (s, 12H, Mes-CH_3), 2.26 (s, 6H, Mes-CH_3), 4.66 (s, 4H, Bn-CH_2), 6.66 (d, 2H, ^3J = 8.5 Hz phenyl-C*H*), 6.76 (s, 4H, Mes-C*H*), 7.20-7.22 (m, 5H, phenyl-C*H*), 7.20-7.22 (m, 5H, phenyl-C*H*), 7.35 (d, 2H, ^3J = 8.5 Hz phenyl-C*H*).

Synthesis of [89]OTf. [**89**]OTf was prepared by following procedure to synthesize [**83**]OTf and [**84**]OTf starting from **85**, (100 mg, .251 mmol) to yield the title compound as a white powder (117 mg, 83% yield). mp. 155-159 ºC. ^{1}H NMR (399.9 MHz, $CDCl_3$): δ 1.11 (m, 3H, Et-CH_3), 1.18 (t, 3H, ^3J = 7 Hz, Et-CH_3) 1.94 (s, 12H, Mes-CH_3), 2.29 (s, 6H, Mes-CH_3), 3.32-3.41 (bm, 1H, Bu-CH_2), 3.52 (bs, 2H, Bu-CH_2), 3.78-3.82 (bm, 1H, Bu-CH_2), 4.02-4.17 (bm, 3H, N-CH_3), 6.81 (s, 4H, Mes-C*H*), 7.41 (d, 1H, $^3J_{H\text{-}H}$ = 8.5 Hz, phenyl-C*H*), 7.48 (d, 1H, $^3J_{H\text{-}H}$ = 8.5 Hz, phenyl-C*H*) 7.65 (d, 1H, $^3J_{H\text{-}H}$ = 8.5 Hz, phenyl-C*H*), 7.69 (d, 1H, $^3J_{H\text{-}H}$ = 8.5 Hz, phenyl-C*H*). ^{13}C NMR (100.5 MHz, $CDCl_3$): δ 8.68, 10.32 21.25, 23.39, 45.43, 54.46, 64.79, 120.66, 121.71, 126.87, 128.52, 128.58, 137.88, 139.73, 139.86, 140.66, 140.69, 142.36. ^{11}B NMR (128.2 MHz, $CDCl_3$): δ 78.

Synthesis of [90]OTf. [**90**]OTf was prepared by following procedure to synthesize [**83**]OTf and [**84**]OTf starting from **86**, (300 mg, 1.06 mmol) to yield the title compound as a white powder (298 mg, 62% yield). mp. 176-177 ºC. ^{1}H NMR (399.9 MHz, $CDCl_3$): δ 0.83 (t, 6H, ^3J = 7.5 Hz, Bu-CH_3), 1.16-1.36 (bm, 6H, Bu-CH_2), 1.71-1.79 (bm, 2H, Bu-CH_2), 1.94 (s, 12H, Mes-CH_3), 2.29 (s, 6H, Mes-CH_3), 3.14-3.32 (bm, 4H, N-CH_3, Bu-CH_2), 3.53 (bs, 1H, Bu-CH_2), 3.58-3.67 (bm, 3H, Bu-CH_2), 6.82 (s, 4H, Mes-C*H*), 7.41 (d, 2H, $^3J_{H\text{-}H}$ = 8.5 Hz, phenyl-C*H*), 7.64 (d, 1H, $^3J_{H\text{-}H}$ = 8.5 Hz, phenyl-C*H*). ^{11}B NMR (128.2 MHz, $CDCl_3$): δ 81.2.

Synthesis of [91]OTf. [**91**]OTf was synthesized in a small NMR scale reaction by treatment of *p*-(Mes_2B)-C_6H_4-(NMe_2) with hydrolyzed BuOTf in ether (5 mL). Yield is not optimized for this compound. mp. 172-174 ºC. ^{1}H NMR (399.9 MHz, $CDCl_3$): δ 1.93 (12H, Mes-CH_3), 2.29 (s, 6H, Mes-CH_3), 3.29 (d, 6H, ^3J = 11.5 Hz, N-CH_3), 6.81

(s, 4H, Mes-C*H*), 7.50 (d, 2H, ^3J = 8.0 Hz, phenyl-C*H*), 7.65 (d, 2H, ^3J = 8.0 Hz, phenyl-C*H*), 11.57 (bs, 1H, N-*H*). ^{13}C NMR (125.70 MHz, $CDCl_3$): δ 21.23, 23.47, 47.33, 119.50, 128.50, 138.23, 138.71, 140.70, 144.15. B-C_{ipso} carbon peaks not observed.

Synthesis of [92]OTf. [**92**]OTf was crystallized directly from a diethyl ether solution of **86** with hydrolyzed MeOTf. Only single-crystal X-ray diffraction analysis was obtained for this molecule.

UV-vis Titration Experiments. Compound $[\mathbf{83}]^+$ was titrated in a H_2O/DMSO mixed solvendt system. A solution of [**83**]OTf (3.0 mL, 4.8739×10^{-5} M, in buffered H_2O/DMSO 6/4 vol. (HEPES 0.01 M in H_2O, pH 7) was titrated with incremental amounts of cyanide anions by addition of a solution of NaCN in H_2O (3.0×10^{-3} M). The absorption was monitored at λ_{max} = 320 nm (ε = 8376). The experimental data obtained was fitted by hand to a 1:1 binding isotherm using the following derivation (Figure 51).

The experimental data obtained (Table 9) was fitted by hand using the derivation in Figure 51. This fit yielded a $K_{rel} > 2.00(\pm 0.5) \times 10^{-1}$ M^{-1}. Since K_a for HCN = 5×10^{-10} M^{-1} => the stability constant of **83**-CN, $K_{\mathbf{83}^+} > 3.9 \times 10^8$ M^{-1}. In order to fit the above equation and solve for $K_{\mathbf{83}^+}$, the pH of the H_2O/DMSO 6/4 (HEPES 0.01 M in H_2O, pH 7) solvent mixture was verified to remain at pH 7 using a standard pH electrode, and the pK_a of HCN in H_2O/DMSO 6/4 was determined analytically to be 9.3 ± (0.01) by potentiometrically titrating a NaCN solution (0.100 M, H_2O/DMSO (6/4 vol.)) with a 0.100 M HCl solution

[83]$^+$	+	H^+	+	NaCN	⇔	**83-CN**	+	HCN
[83]$^+_0$ – x		H^+		$NaCN_0$ – x – y		X		Y

K_{1+} = **83-CN** /([**83**$^+$**]*** [NaCN]) = x/[(**83**$^+_0$ – x) * ($NaCN_0$ – x – y)]

K_2 = HCN /([H^+]*[NaCN]) = y/[(H^+) * ($NaCN_0$ – x – y)] = 1/K_a of HCN

=> K_{rel} = K_{1+}/K_2 = [x * (H^+)]/ [y * (**83**$^+_0$ – x)]

K_{1+} and K_2 are very large, and there is therefore, very little free cyanide anion.

=> As a result, the following approximation can be made: [NaCN] = x + y

=> Therefore y = [NaCN]-x

=> K_{rel} = [x * (H^+)]/ [([NaCN]-x) * (**83**$^+_0$ – x)]

=> ([NaCN]-x)*(**83**$^+_0$ – x) = x*([H^+]/K_{rel}) = [NaCN]*[**83**$^+_0$] + x^2 – x*([NaCN] + [**83**$^+_0$]

=> x^2 – x*([NaCN] + [**83**$^+_0$]) – x*([H^+]/K_{rel}) + [**83**$^+_0$]*[NaCN] = 0

=> x^2 – x*([NaCN] + [**83**$^+_0$] + ([H^+]/K_{rel})) + [**83**$^+_0$]*[NaCN] = 0

a -b c

=> x = [-b – $(D)^{1/2}$]/2a with D = b^2 -4ac

=> Abs_{calc} = (**83**$^+_0$ – x) * ε

Figure 51: Derivation of the cyanide titration isotherm for [**83**]$^+$.

Table 9: Absorbance of a solution of [**83**]$^+$ after successive additions of cyanide in buffered H_2O/DMSO 6/4 vol. (HEPES 0.01 M in H_2O, pH 7).

$C_{Fluoride}$	Abs_{exp}	Abs_{calc}	$C_{Fluoride}$	Abs_{exp}	Abs_{calc}
0.0000E00	4.08E-01	4.08E-01	4.8213E-05	4.47E-02	3.80E-02
6.9837E-06	3.67E-01	3.49E-01	5.4974E-05	1.93E-02	2.00E-02
1.3935E-05	3.06E-01	2.91E-01	6.1704E-05	9.62E-03	1.25E-02
2.0854E-05	2.39E-01	2.34E-01	6.8404E-05	7.64E-03	8.93E-03
2.7741E-05	1.86E-01	1.77E-01	7.5073E-05	5.17E-03	6.89E-03
3.4596E-05	1.32E-01	1.23E-01	8.1712E-05	4.38E-03	5.60E-03
4.1420E-05	8.33E-02	7.42E-02	---	---	---

Compound [**84**]$^+$ was also titrated in a H_2O/DMSO mixed solvent system. A solution of [**84**]OTf (3.0 mL, 5.1500×10^{-5} M, in buffered H_2O/DMSO 6/4 vol. (HEPES 0.01 M in H_2O, pH 7) was titrated with incremental amounts of fluoride anions by addition of a solution of NaF in H_2O (3.01×10^{-1} M). The absorption was monitored at λ_{max} = 320 nm (ε = 9200). The experimental data obtained was fitted by hand to a 1:1 binding isotherm to afford a stability constant for **84**-F of $K = 910 \pm (50)$ M^{-1}. (Table 10).

Table 10: Absorbance of a solution of [**84**]$^+$ after successive additions of fluoride in buffered H_2O/DMSO 6/4 vol. (HEPES 0.01 M in H_2O, pH 7).

$C_{Fluoride}$	Abs_{exp}	Abs_{calc}
0.00E+00	4.79E-01	4.74E-01
4.01E-04	3.58E-01	3.50E-01
8.01E-04	2.74E-01	2.76E-01

CHAPTER III

A BIDENTATE PHOSPHONIUM BORANE LEWIS ACID*

3.1 Introduction

Due to applications in dental care as well as in the treatment of osteoporosis, the introduction of fluoride anions in drinking water, toothpastes and medications has become widespread. This recent trend is raising concerns because high doses of fluoride have been associated to dental and skeletal fluorosis, among other diseases.[5] As a result, discovering methods for the recognition of this anion has become a topical research objective.[6-11,150] One of the most successful strategies adopted to date relies on the use of fluorophilic boron compounds.[31,35,37,49,52,53,55,59,98,145] Bidentate boranes[58] such as **14**[68] and **15**[61] are among the best receptors thus far identified. Their high fluorophilicity results from cooperative effects involving the neighboring Lewis acidic centers which both interact with the fluoride ion to form a chelate complex. Such bifunctional boranes are however supplanted by cationic boranes such as $[\mathbf{20}]^+$, whose enhanced fluorophilicity arises from favorable Coulombic effects.[85,88] In principle, boron-based receptors that are bidentate and cationic, should capitalize on both Coulombic and cooperative effects, leading to a further enhancement of their fluoride affinity. In this chapter, we provide a dramatic illustration of this principle in the fluoride binding properties of $[1\text{-}Mes_2B\text{-}2\text{-}MePh_2P\text{-}(C_6H_4)]^+$ ($[\mathbf{93}]^+$), the *ortho*-isomer of $[\mathbf{20}]^+$. We also demonstrate that the latent phosphorus-centered Lewis acidity of the phosphonium moiety[151-154] can be harnessed to enhance fluoride binding via chelation.

---

* Reprinted in part with permission from, "Fluoride Ion Chelation by a Bidentate Phosphonium/Borane Lewis Acid"; Hudnall, T. W.; Kim, Y.-M.; Bebbington, M. W. P.; Bourissou, D.; Gabbaï, F. P. *J. Am. Chem. Soc.*, **2008**, *in press*, Copyright 2008 by the American Chemical Society.

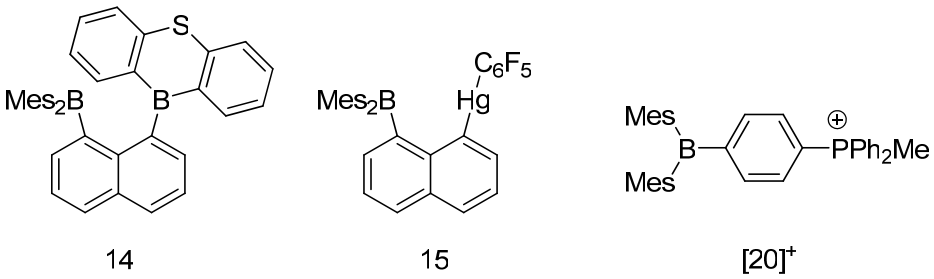

14 15 [20]+

3.2 Synthesis of a bidentate phosphonium/borane Lewis acid

The iodide salt of [**93**]$^+$ could be easily obtained by reaction of the corresponding neutral phosphinoborane 1-Mes_2B-2-Ph_2P-(C_6H_4)[155-157], **94** , with methyl iodide in dichloromethane (Figure 52). This salt has been characterized by multinuclear NMR spectroscopy, as well as by single crystal X-ray diffraction (Figure 53, Table 11). The ^{1}H NMR of [**93**]I displays broad multiple signals for the protons on the mesityl substituents, indicative of a congested structure about the boron center. The phosphorus bound methyl group gives rise to a characteristic doublet ($^2J_{H\text{-}P}$ = 13.5 Hz) at 2.86 ppm, and the ^{31}P NMR resonance appears at 23.9 ppm. In $CHCl_3$, [**93**]I features a broad absorption band at 347 nm corresponding to the triarylborane chromophore. Observation of this band indicates that the boron center remains coordinatively unsaturated as in the case of the *para*-isomer [**20**]I[88]. In the crystal, the boron center of [**93**]$^+$ is trigonal planar ($\Sigma_{(C\text{-}B\text{-}C)}$ = 359.7°) and is separated from the phosphorus atom P(1) by only 3.494(3) Å. This short separation indicates that the unsaturated boron center is sterically encumbered. This conclusion is in agreement with: i) the large B(1)-C(1)-C(2) angle (130.1(3)°), which substantially deviates from the ideal value of 120º; ii) the elongated C(1)-C(2) bond of 1.462(4) Å. Distortions are also evident in the coordination geometry of the phosphorus atom with the sum of the C(2)-P(1)-C(30),

C(30)-P(1)-C(41), C(41)-P(1)-C(2) angles α equal to 335.2° rather than 328.4°, which would be expected if the phosphorus adopted a regular tetrahedral geometry.

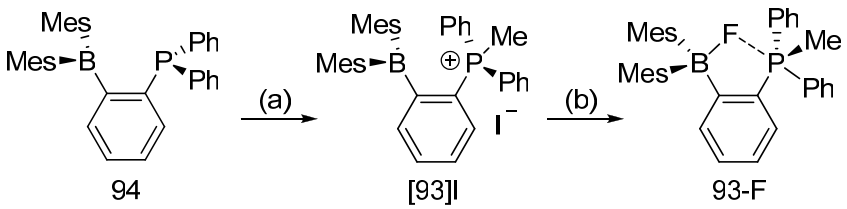

Figure 52: Synthesis of [**93**]I and **93**-F; (a) MeI, CH_2Cl_2, 25 °C, 87%. (b) TASF, $CHCl_3$, 25 °C, 91%.

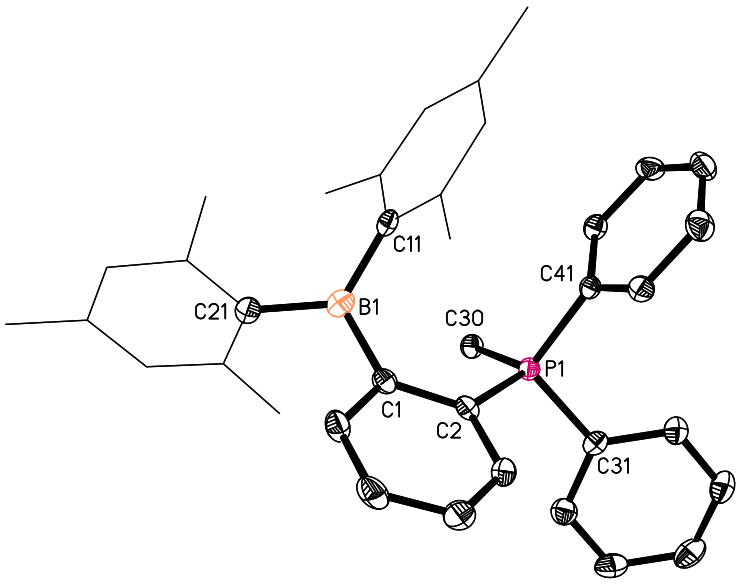

Figure 53: ORTEP view of [**93**]$^+$ in [**93**]I, (50% ellipsoids, H atoms are omitted and mesityl substituents drawn as thin lines for clarity).

3.3 Fluoride binding studies of [**93**]$^+$

With this new cationic borane in hand, we became eager to compare its fluoride binding properties to those of its para isomer [**20**]$^+$. Remarkably, when equimolar amounts of [**93**]I and **20**-F were mixed in $CDCl_3$, ^{31}P NMR spectroscopy indicated quantitative formation of [**20**]$^+$ along with a new species assigned to **93**-F, which is characterized by a doublet at 28.3 ppm (Figure 54). Encouraged by these results, we decided to compare the fluoride binding constants (K) of [**20**]$^+$ and [**93**]$^+$. First we investigated the stability of [**93**]$^+$ in water over a wide pH range by UV-vis spectroscopy. Surprisingly, [**93**]$^+$ decomposes over a period of several hours in water above pH 3.5. Because of this limitation, fluoride titrations of [**20**]$^+$ and [**93**]$^+$ were carried out in MeOH by monitoring the absorbance of the boron-centered chromophore upon fluoride addition. Fitting of the resulting isotherms to a 1:1 binding model, indicates that the fluoride binding constant of [**93**]$^+$ ($K > 10^6$ M^{-1}) exceeds the measurable range and is at least four orders of magnitude higher than that measured for [**20**]$^+$ (K = 400 (±50) M^{-1}). In an effort to identify the origin of this difference, we isolated **93**-F from the reaction of [**93**]I with $[S(NMe_2)_3][Me_3SiF_2]$ (TASF) and proceeded with its characterization (Figure 52). The ^{11}B NMR signal of the four coordinate boron center of **93**-F appears at 5.7 ppm, and the ^{19}F NMR spectrum features a broad signal at -158 ppm, which is comparable to the chemical shift observed in other triarylfluoroborate complexes.[88] The ^{31}P NMR signal at 28.3 ppm appears as a doublet because of coupling to the fluorine nucleus ($J_{P\text{-}F}$ = 24.3 Hz). Observation of this down-field shifted doublet indicates that the boron-bound fluorine atom interacts directly with the phosphorus atom in solution. Altogether, these spectroscopic features suggest that the fluorine atom may actually be chelated by the boryl and phosphonium moieties of [**93**]$^+$.

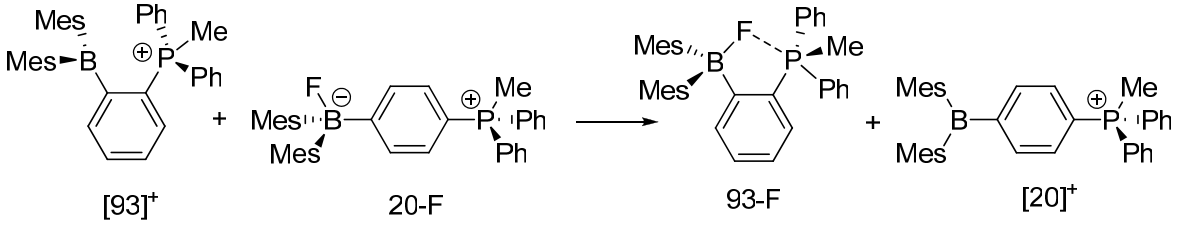

Figure 54: Competition experiment between **20**-F and [**93**]$^+$ in $CDCl_3$.

This conclusion was confirmed by determination of the X-ray crystal structure of **93**-F (Figure 55, Table 11). This structure shows that the boron-bound fluorine atom F(1) is located only 2.666(2) Å away from the P(1) atom, which is well within the sum of the van der Waals radii of the two elements (ca 3.45 Å)[158]. Another conspicuous feature concerns the F(1)-P(1)-C(31) angle of 176.36(9)°, indicating that the fluorine atom occupies an axial coordination site directly opposite from a phenyl ring. In agreement with this view, we note: a slight elongation of the P(1)-C(31) bond (1.813(3) Å) when compared to the P(1)-C(41) bond (1.796(3) Å); a notable increase in the sum of angle α on going from [**93**]$^+$ to **93**-F (α = 340.4° in **93**-F vs 335.2° in [**93**]$^+$). Altogether, the structural and spectroscopic results support the presence of a B-F→P interaction, which may be at the origin of the increased fluorophilicity of [**93**]$^+$. These structural results establish that the phosphorus atom of [**93**]$^+$ is acting as a Lewis acid, an intrinsic property of phosphonium cations that has so far only been rarely exploited.

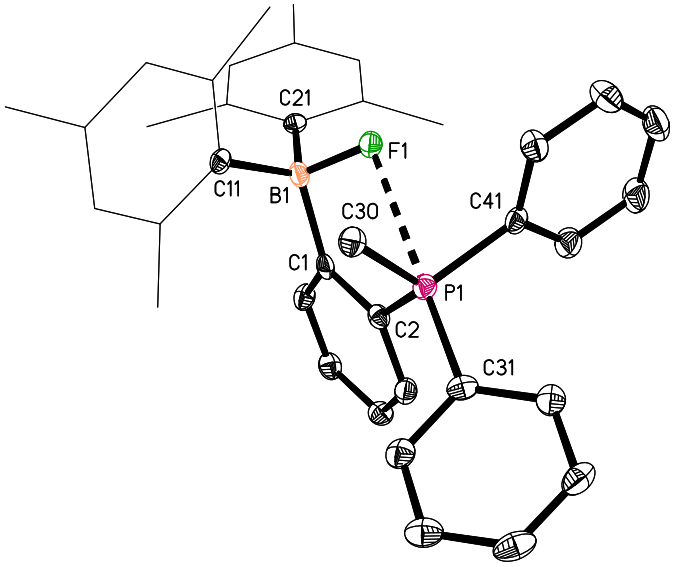

Figure 55: ORTEP view of **93**-F (50% ellipsoids, H atoms are omitted and mesityl substituents drawn as thin lines for clarity).

The DFT optimized structure of **93**-F is in excellent agreement with that experimentally determined (Figure 56). In particular, the P(1)-F(1) separation of 2.665 Å is close to that observed in the crystal (2.666(2) Å). Atoms In Molecules (AIM) [159] calculations show the presence of a bond path between the P(1) and F(1) atoms with an electron density $\rho(r)$ of 2.05×10^{-2} e bohr^{-3} at the BCP (Figure 57).

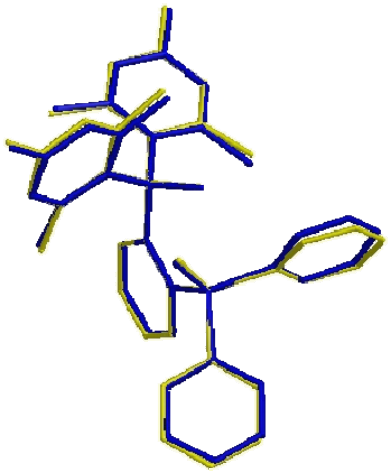

Figure 56: Overlay of crystal structure (blue) and optimized structure (yellow) of **93**-F.

The presence of this interaction can be further asserted through a Natural Bond Orbital (NBO) analysis performed at the optimized geometry. This analysis identifies a donor-acceptor interaction involving a fluorine lone-pair as a donor and the phosphorus-carbon σ^*-orbital as the acceptor (Figure 57). Moreover, a deletion calculation carried out by zeroing the Kohn-Sham matrix elements corresponding to the $lp_{(F)} \rightarrow \sigma^*_{(P\text{-}C)}$ interaction leads to an increase of the total energy of the molecule by 5.0 kcal/mol. There is also a weak hydrogen-bond interaction between a proton on the phosphonium methyl group (H(30A)) and the fluorine atom, F(1), which may help stabilize **93**-F. The AIM[159] analysis of this interaction shows the presence of a bond path between the H(30A) and F(1) atoms with an electron density $\rho(r)$ of 1.63×10^{-2} e bohr^{-3} at the BCP (Figure 58). Further insight in the increased fluorophilicity of [**93**]$^+$ was gained from a computation of the enthalpy for the reaction shown in (Figure 54). To this end, molecules [**20**]$^+$, [**93**]$^+$, **20**-F were optimized at the level of theory used for **93**-F. Each molecule was then subjected to a single point energy calculation (6-311+g(2d,p) basis set for all atoms) using the polarizable continuum model (PCM) with methanol as a solvent. The relative enthalpies obtained from these calculations afforded ΔH = -7.6 kcal/mol for the reaction shown in (Figure 54). The exothermicity computed for this

reaction is in line with experimental findings, and indicates that the fluoride ion affinity (FIA) of [**93**]$^+$ significantly exceeds that of [**20**]$^+$. Furthermore, [**20**]$^+$ and [**93**]$^+$ have virtually identical LUMO energies (-2.57 eV for [**20**]$^+$ and -2.56 eV for [**93**]$^+$), suggesting that inductive effects in these cationic boranes do not play a major role in the increased FIA of [**93**]$^+$.

Table 11: Crystal data, data collection, and structure refinement for [**93**]I-MeOH and **93**-F.

	[**93**]I-MeOH	**93**-F
	Crystal data	
Formula	$C_{38}H_{43}BIOP$	$C_{37}H_{39}BFP$
M_r	684.40	554.46
Crystal size (mm^3)	0.19 × 0.17 × 0.09	0.21 × 0.19 × 0.16
Crystal system	Monoclinic	Triclinic
Space group	$P2_1/c$	$P\bar{1}$
a (Å)	17.290(2)	10.8310(14)
b (Å)	8.6503(12)	11.5758(15)
c (Å)	23.517(3)	12.4242(16)
α (°)	90.000	85.161(2)
β (°)	109.7030(10)	75.771(3)
γ (°)	90.000	83.546(3)
V ($Å^3$)	3311.5(8)	1497.8(3)
Z	4	2
ρ_{calc} (g cm^{-3})	1.373	1.207
μ (mm^{-1})	1.044	0.123
F(000)	1408	580
	Data Collection	
T (K)	110(2)	110(2)
scan mode	ω	ω
hkl range	-19 → +19, -9 → +9 -26 → +26	-12 → +9, -13 → +13, -14 → +13
measd reflns	28126	6881
Unique reflns [R_{int}]	5191 [0.0384]	4653 [0.0381]
reflns used for refinement	5191	4653
	Refinement	
Refined parameters	381	361
GOF on F^2	1.003	1.008
R1,[a] wR2[b] all data	0.0314, 0.0944	0.0698, 0.1137
ρ_{fin} (max/min) (e $Å^{-3}$)	0.580, -0.365	0.352, -0.352

[a] $R1 = \sum||Fo| - |Fc||/\sum|Fo|$. [b] $wR2 = \{[\sum w(Fo^2 - Fc^2)^2]/[\sum w(Fo^2)^2]\}^{1/2}$.

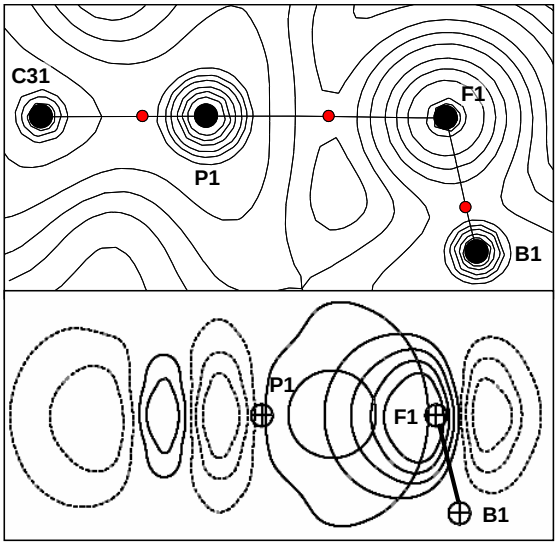

Figure 57: AIM and NBO analyses of the B-F→P interaction in **93**-F. Top: AIM electron density map with relevant bond paths and bond critical points. Bottom: NBO contour plot showing the $lp_{(F)} \rightarrow \sigma^*_{(P\text{-}C)}$ interaction.

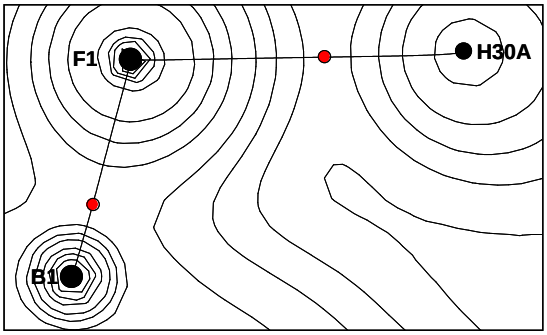

Figure 58: AIM electron density map of the B-F···H interaction in **93**-F with relevant bond paths and bond critical points.

3.4 Other anion binding studies of $[\mathbf{93}]^+$

We investigated the interaction of $[\mathbf{93}]^+$ with Cl^-, Br^-, CN^-, OAc^-, N_3^-, and OH^- and were surprised to find that in addition to fluoride, $[\mathbf{93}]^+$ forms adducts with cyanide, azide and acetate. The cyanide adduct, **93**-CN and the azide adduct **93**-N_3 have been

characterized by NMR spectroscopy as well as X-ray crystallography (Figure 59, Figure 60, Table 12). Single crystals of the acetate adduct **93**-OAc have not been forthcoming and only ^{1}H NMR has been used to characterize this species.

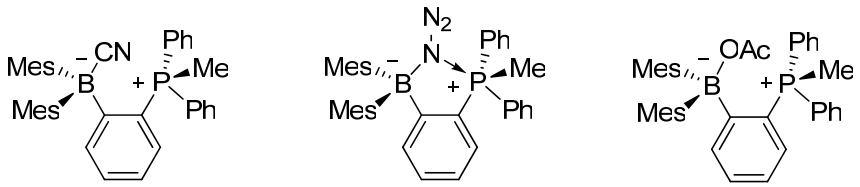

These three adducts can be prepared in good yields by treating [**93**]I with the corresponding sodium salt in MeOH at room temperature. Stirring for half an hour results in precipitation of the respective adduct as a white powder which can be isolated by filtration. **93**-CN crystallizes in the monoclinic $P2_1/n$ space group (Figure 59, Table 12). As with **93**-F, the cyanide anion is bound to the boron atom (B(1)-C(7) = 1.629(5) Å, which is slightly longer when compared to **83**-CN and **84**-CN, whose B-CN lengths are 1.618(8) and 1.616(19) Å respectively), resulting in a highly pyramidalized four-coordinate boron center ($\Sigma_{(C\text{-}B\text{-}C)}$ = 340.2°). Additionally, the ^{11}B NMR chemical shift appears at -17.5 ppm, which is similar to **83**-CN and **84**-CN. The sum of the angle α on phosphorus indicates that there may only be a weak interaction with the cyanide anion (α= 337.6° in **93**-CN vs 335.2° in [**93**]$^{+}$), which is also in agreement with the ^{31}P resonance that is shifted downfield relative to [**93**]$^{+}$ at 27.7 ppm. This is corroborated by the large distance between the carbon of the cyanide anion, C(7), and P(1), which are separated by 3.234(3) Å. The large B(1)-C(1)-C(2) angle of 129.5(3)° deviates from the idealized 120°, indicating that complexation of the cyanide anion does not offer a great deal of steric relief to the molecule. In agreement with this assessment are the broad

multiple signals which are observed for the aromatic protons and the methyl groups on the mesityl substituents in the ^{1}H NMR spectrum of **93**-CN.

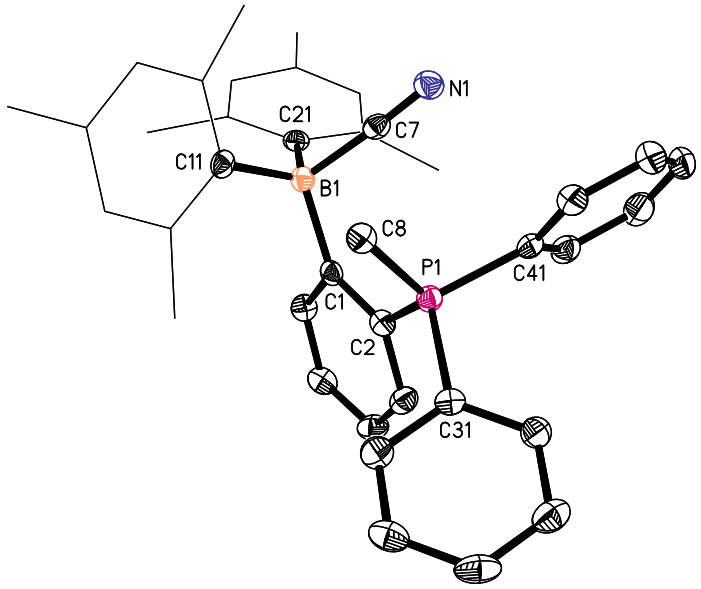

Figure 59: ORTEP view of **93**-CN, (50 % ellipsoids, H-atoms omitted and mesityl substituents drawn as thin lines for clarity).

The crystal structure of the azide adduct (**93**-N_3) is very similar to that observed for **93**-CN. **93**-N_3 crystallizes in the monoclinic $P2_1/c$ space group (Figure 60, Table 12), and the boron is tetrahedral due to coordination of the azide anion ($\Sigma_{(C\text{-}B\text{-}C)}$ = 342.7°). In agreement with this view, we note that the ^{11}B NMR resonance observed at -14.8 ppm is characteristic of sp^3 boron centers, and the B(1)-N(1) distance of 1.614(11) Å is close to that observed in **16**-N_3 (1.627(3)-1.630(3) Å)[73], which is indicative of a covalent interaction between the boron and azide anion. As with the fluoride adduct **93**-F, there appears to be an interaction between the azide and phosphonium moieties as evidenced by; i) (α= 340.2° in **93**-N_3, α= 340.5° in **93**-F); ii) the ^{31}P NMR resonance at 25.5 ppm. The ^{1}H NMR of **93**-N_3 exhibits all of the expected resonances with the phosphorus-

bound methyl group resonance appearing as a doublet ($J_{H\text{-}P}$ = 14 Hz) at 2.11 ppm which is shifted upfield relative to [**93**]I.

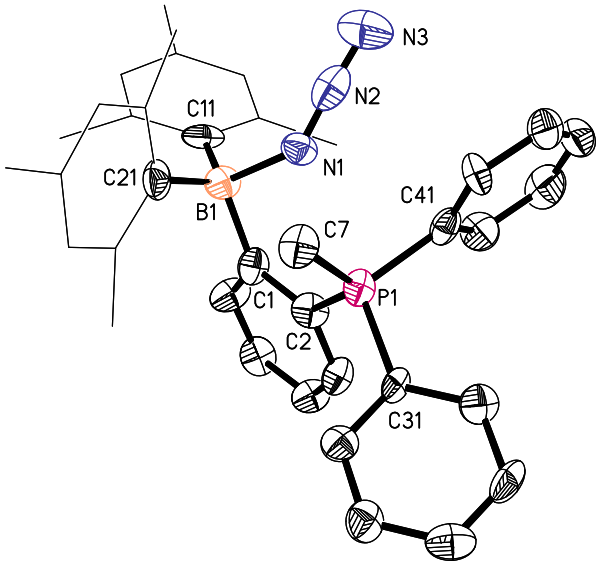

Figure 60: ORTEP view of **93**-N_3, (50 % ellipsoids, H-atoms omitted and mesityl substituents drawn as thin lines for clarity).

Crystallographic evidence of **93**-OAc has not been obtained, however, the ^{1}H NMR is also nearly identical to that observed with **93**-F and **93**-N_3 including the upfield-shifted phosphorus methyl resonance which appears as a doublet $J_{H\text{-}P}$ = 14 Hz at 2.21 ppm. The ^{31}P NMR signal at 20.8 ppm is shifted upfield relative to [**93**]$^{+}$, and the ^{11}B NMR resonance at -3.2 ppm is indicative of a four-coordinate boron center, suggesting that the acetate anion is indeed coordinated to the boron atom of **93**-OAc.

Since we found that [**93**]$^{+}$ is not stable in water at pH above 3.5, we were interested to see if [**93**]$^{+}$ was capable of hydroxide anion chelation. Interestingly, reaction of [**93**]$^{+}$ with hydroxide in MeOH/water mixed solvent does not lead to the corresponding hydroxide adduct **93**-OH. Instead, formation of a phosphine oxide by hydrolysis of a P-

C_{Ph} bond is observed leading to the formation of the phosphine oxide borane complex **95** (Figure 61).

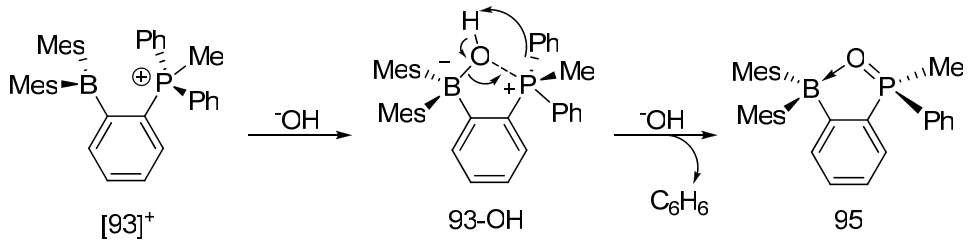

Figure 61: Reaction of [**93**]$^{+}$ with hydroxide anions leading to the formation of the phosphine oxide borane **95**.

The mechanism depicted in Figure 61 is speculated; however, at this time there is no spectroscopic evidence to support the initial formation of **93**-OH. Compound **95** however has been isolated and fully characterized by multinuclear NMR spectroscopy and X-ray diffraction analysis. Compound **95** crystallizes in the monoclinic space group $P2_1/c$ (Figure 62, Table 12). The crystal structure confirms the presence of a phosphine oxide moiety in which a phenyl ring has been displaced from the phosphorus atom. The ^{31}P NMR chemical shift of 62.5 ppm is significantly shifted downfield when compared to methyldiphenylphosphine oxide (^{31}P NMR chemical shift = 30.5 ppm).[160] This downfield shift can be explained by a dative interaction observed between the boron and oxygen atoms. Further evidence to support this proposal include i) the P(1)-O(1) distance of 1.5310(16) Å which is significantly longer than typical phosphine oxides (P-O_{avg} = 1.48 Å); ii) the large degree of pyrimidalization observed at the boron center ($\Sigma_{(C\text{-}B\text{-}C)}$ = 344.23°); iii) the short B(1)-O(1) distance of 1.644(3) Å; and iv) the ^{11}B NMR chemical shift at 9.8 ppm which indicative of a four-coordinate boron atom.

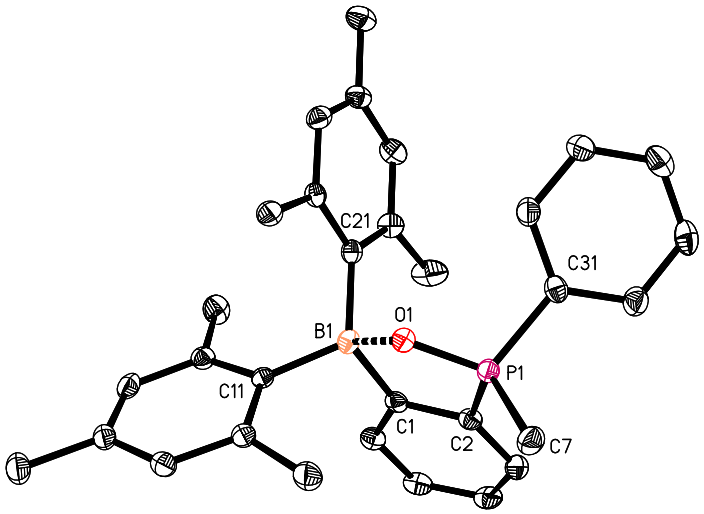

Figure 62: ORTEP view of **95**, (50 % ellipsoids, H-atoms omitted for clarity).

The ^{1}H NMR of **95** is also interesting, exhibiting two sets of peaks corresponding to the mesityl substituents which are inequivalent by virtue of the chiral phosphorus center. The phosphorus methyl resonance is also shifted significantly upfield and appears as a doublet ($J_{H\text{-}P}$ = 13.2 Hz) at 1.96 ppm.

Table 12: Crystal data, data collection, and structure refinement for **93**-CN and **93**-N_3 and **95**.

	93-CN	**93**-N_3	**95**
		Crystal data	
Formula	$C_{38}H_{39}BNP$	$C_{37}H_{39}BN_3P$	$C_{31}H_{34}BOP$
M_r	551.48	567.49	464.36
Crystal size	0.30 × 0.21 × 0.08	0.12 × 0.05 × 0.05	0.38 × 0.29 × 0.26
Crystal	Monoclinic	Monoclinic	Monoclinic
Space group	$P2_1/n$	$P2_1/c$	$P2_1/c$
a (Å)	17.044(3)	17.684(8)	9.1095(17)
b (Å)	10.570(2)	8.937(4)	14.850(3)
c (Å)	17.554(4)	25.3657(8)	19.059(3)
α (°)			
β (°)	107.202(2)	128.99(2)	98.127(4)
γ (°)			
V (Å^3)	3021.10(10)	3115(2)	2552.4(8)
Z	4	4	4
ρ_{calc} (g cm^{-3})	1.213	1.210	1.208
μ (mm^{-1})	0.119	0.119	0.130
F(000)	1176	1208	992
		Data Collection	
T (K)	110(2)	110(2)	110(2)
Scan mode	ω	ω	ω
hkl range	-19 → +19, -12 → +12 -20 → +20	-19 → +19, -9 → +9, -27 → +27	-12 → +8, -19 → +19, -25 → +22
measd reflns	25809	22748	15784
Unique	4730 [0.0598]	4070 [0.2084]	6221 [0.0531]
reflns used for	4730	4070	6221
		Refinement	
Refined	370	379	307
GOF on F^2	1.006	1.005	1.008
R1,[a] wR2[b]	0.0694, 0.1312	0.2033, 0.1669	0.0852, 0.1207
ρ_{fin} (max/min)	0.555, -0.435	0.381, -0.323	0.552, -0.529

[a] $R1 = \sum||Fo| - |Fc||/\sum|Fo|$. [b] $wR2 = \{[\sum w(Fo^2 - Fc^2)^2]/[\sum w(Fo^2)^2]\}^{1/2}$.

3.5 Conclusion

This chapter reports the synthesis, characterization and anion binding studies of the novel bidentate phosphonium/borane Lewis acid $[\mathbf{93}]^+$. The results presented show how $[\mathbf{93}]^+$ is capable of anion chelation. In particular, the fluoride adduct **93**-F has been fully characterized by multinuclear NMR spectroscopy, single crystal X-ray diffraction

analysis and computationally. The results obtained from these studies are in agreement with the formation of a B-F→P^+ interaction. Moreover, this interaction leads to a substantial increase in the fluorophilicity of [**93**]$^+$ when compared to its *para* derivative [**20**]$^+$.

We have also shown how this enhanced Lewis acidity can be utilized for the complexation of a variety of anions. While [**93**]$^+$ is capable of complexing cyanide to form the cyanoborate **93**-CN, it is also capable of forming the less common azide and acetate complexes. Crystallographic data suggests that as in **93**-F, the azide anion in **93**-N_3 is actually chelated between the two Lewis acid borane and phosphonium centers. Interestingly, when [**93**]$^+$ is allowed to react with hydroxide anions, a novel reaction to form the neutral phosphine oxide borane (**95**) rather than hydroxide adduct formation is observed.

3.6 Experimental

General Considerations. 2-bromo-(diphenylphosphino)benzene was synthesized according to a reported procedure. [161,162] 2-bromoiodobezene was purchased from TCI America, methyl iodide from Across, diphenylphosphine and tetrakis(triphenylphosphine)palladium from Alfa Aesar. Tris(dimethylamino)sulfonium trimethyldifluorosilicate (TASF) and dimesitylboron fluoride were purchased from Aldrich. Et_2O and THF were dried by reflux over Na/K. Hexane and dichloromethane were dried by passing through a column charged with activated alumina. Air-sensitive compounds were handled under a N_2 atmosphere using standard Schlenk and glovebox techniques. UV-vis spectra were recorded on an Ocean Optics USB4000 spectrometer with a Ocean Optics ISS light source. Elemental analyses were performed by Atlantic Microlab (Norcross, GA). NMR spectra were recorded on a Varian Unity Inova 400 FT NMR (399.59 MHz for ^{1}H, 375.99 MHz for ^{19}F, 128.19 MHz for ^{11}B, 100.45 MHz for ^{13}C, 161.75 MHz for ^{31}P) spectrometer at ambient temperature. Chemical shifts δ are given in ppm, and are referenced against external Me_4Si (^{1}H, ^{13}C), $BF_3{\cdot}Et_2O$ (^{11}B), H_3PO_4 (^{31}P), and $CFCl_3$ (^{19}F). Melting points were measured on samples in sealed

capillaries and are uncorrected.

Crystallography. Colorless single crystals of [**93**]I-(MeOH) could be obtained by slow evaporation of a methanol solution of [**93**]I. Colorless single crystals of **93**-F could be obtained by slow evaporation of a concentrated chloroform solution. Single crystals of **93**-CN and **93**-N_3 were grown by slow evaporation of methanol solutions. Compound **95** was crystallized by slow evaporation of a concentrated acetone solution. The crystallographic measurement of [**93**]I-(MeOH), **93**-F, **93**-CN and **93**-N_3 were performed using a Bruker APEX-II CCD area detector diffractometer, with a graphite-monochromated Mo-K_α radiation (λ = 0.71069 Å); and the measurement of **95** was collected using a Bruker SMART-97 CCD area detector diffractometer, with a graphite-monochromated Mo-K_α radiation (λ = 0.71069 Å). A specimen of suitable size and quality was selected and mounted onto a nylon loop. The structure was solved by direct methods, which successfully located most of the non-hydrogen atoms. Subsequent refinement on F^2 using the SHELXTL/PC package (version 5.1) allowed location of the remaining non-hydrogen atoms.

Synthesis of 94. ^{n}BuLi (0.27 mL, 2.5 M in hexanes, 0.678 mmol) was added to an Et_2O (5 mL) solution of 2-bromo-(diphenylphosphino)benzene (0.210 g, 0.615 mmol) at room temperature. The resulting dark yellow solution was stirred for ten minutes at room temperature leading to precipitation of the corresponding lithium salt as a white crystalline solid. To this slurry was added dimesitylboron fluoride (0.182 g, 0.679 mmol) in Et_2O (5 mL). The solution was stirred overnight at room temperature. The solvent was then removed *in vacuo* and the residue was extracted with hexanes (10 mL) and dichloromethane (10 mL). Both fractions were filtered over Celite, combined and evaporated to dryness. The residue was recrystallized from Et_2O/MeOH 1:1 (v/v 10 mL total volume) to afford **94** as a white solid which was isolated by filtration and dried under vacuum (0.231 g, 74% yield). mp. 188 °C. ^{1}H NMR (399.9 MHz, $CDCl_3$): δ 1.98 (s, 6H, Mes-CH_3), 2.24 (bs, 12H, Mes-CH_3), 6.69-6.82 (m, 4H, Mes-C*H*), 6.95 (m, 2H,

phenyl-C*H*), 7.15-7.39 (m, 12H, phenyl-C*H* and phenyl-P). ^{13}C NMR (100.5 MHz, $CDCl_3$): δ 21.7, 22.9 (bs, Mes-*C*), 128.3 (bs, CH_{Ph}), 128.6 (bs, CH_{Mes}), 129.1 (bs, CH_{Ph}), 130.1 (bs, CH_{Ph}), 132.6 (bs, CH_{Ph}), 133.5 (bs, CH_{Ph}), 134.1 (bs, CH_{Ph}), 134.3 (bs, $C_{para,Mes}$), 135.8 (bs, CH_{Ph}), 139.5 (bs, $C_{ortho,Mes}$), 140.9 (bs, $C_{ipso,Mes}$), 141.4 (d, $^1J_{P\text{-}C}$ = 11 Hz, $C_{ipso,Ph}$), 134.1 (bs, CH_{Ph}), 144.0 (bs, $C_{ipso,B}$), 158.1 (d, $^1J_{P\text{-}C}$ = 42 Hz, $C_{ipso,P}$). ^{11}B NMR (128.2 MHz, $CDCl_3$): δ 75.0. ^{31}P NMR (161.75 MHz, $CDCl_3$): δ -4.2.

Synthesis of [93]I. Methyl iodide (0.03 mL, .392 mmol) was added to a solution of **94** (0.100 g, 0.196 mmol) in dichloromethane (10 mL) at room temperature. After being stirred overnight, the solution was concentrated to a volume of 3 mL. To the concentrated solution was added Et_2O (10 mL) which resulted in the precipitation of a pale yellow solid (0.111 g, 81% yield). The solid was isolated by filtration and recrystallized by vapor diffusion of hexanes into a chloroform solution (3 mL) and dried under vacuum to afford [**93**]I as chloroform solvate mp. 162 ºC (dec.). ^{1}H NMR (399.9 MHz, $CDCl_3$): δ 1.13 (bs, 3H, Mes-CH_3), 1.71 (bs, 3H, Mes-CH_3), 2.09 (bs, 6H, Mes-CH_3), 2.25 (bs, 6H, Mes-CH_3), 2.73 (d, $^2J_{HP}$ = 12 Hz, 3H, P-CH_3), 5.51(bs, 1H, Mes-C*H*), 6.75 (bs, 2H, Mes-C*H*), 6.86 (bs, 1H, Mes-C*H*), 7.18-7.75 (bm, 14H, Ar-C*H*). ^{13}C NMR (100.5 MHz, $CDCl_3$): δ 11.75 (d, $J_{P\text{-}C}$ = 57.2 Hz P-*C*H_3), 21.05, 22.76 (bs, Mes-*C*), 23.51 (bs, Mes-*C*), 24.87 (bs, Mes-*C*), 122.50 (d, $J_{P\text{-}C}$ = 85.5 Hz), 128.71, 129-131 (bs), 131.25 (d, $J_{P\text{-}C}$ = 12.9 Hz), 131.49 (bs), 132.62 (bs), 134.14 (bs), 134.41 (d, $J_{P\text{-}C}$ = 3.0 Hz), 137.01 (d, $J_{P\text{-}C}$ = 14.6 Hz), 137.85 (d, $J_{P\text{-}C}$ = 13.7 Hz), 139.89 (bs), 140.39 (bs), 140.85 (bs), 141.70 (bs), 155.31 (bs). Due to excessive signal broadening, some of the *C* atoms could not be observed. ^{11}B NMR (128.2 MHz, $CDCl_3$): not observed. ^{31}P NMR (161.75 MHz, $CDCl_3$): δ 23.9. UV-vis (MeOH): λ_{max}/nm (log ε) 372 (3.19). Anal. Calcd for $C_{38}H_{40}BPICl_3$ ([**93**]I-$CHCl_3$): C, 59.14; H, 5.22. Found: C, 58.53; H, 5.10.

Synthesis of 93-F. [**93**]I (0.050 g, 0.077 mmol) was dissolved in THF (10 mL) and treated with TASF (0.021 g, 0.077 mmol). The resulting suspension was stirred for 30 minutes then filtered. The solvent was removed *in vacuo* to yield a white residue

which was washed with Et_2O and dried under vacuum giving **93**-F as a white powder (38 mg, 91% yield). mp. 237 ºC. ^{1}H NMR (399.9 MHz, $CDCl_3$): δ 1.21-1.99 (bms, 12H, Mes-CH_3), 2.15-2.21 (bs, 6H, Mes-CH_3), 3.12 (bs, 3H, P-CH_3), 6.54(bs, 4H, Mes-C*H*), 6.85-7.60 (bm, 14H, Ar-C*H*). ^{13}C NMR (100.5 MHz, $CDCl_3$): δ 12.07 (d, $J_{P\text{-}C}$ = 56.8 Hz P-*C*H_3), 21.22, 22.27, 22.84 (bs, Mes-*C*), 23.87 (bs, Mes-*C*), 24.97 (bs, Mes-*C*), 123.03 (d, $J_{P\text{-}C}$ = 85.4 Hz), 128.06, 129-131 (bs), 131.15 (d, $J_{P\text{-}C}$ = 13.0 Hz), 131.93 (bs), 132.96 (bs), 134.14 (bs), 134.40 (d, $J_{P\text{-}C}$ = 3.4 Hz), 137.18 (d, $J_{P\text{-}C}$ = 14.1 Hz), 137.97 (d, $J_{P\text{-}C}$ = 13.8 Hz), 138.41, 140.82, 141.82 (bs) 155.56 (bs). Due to excessive signal broadening, some of the *C* atoms could not be observed. ^{11}B NMR (128.2 MHz, $CDCl_3$): δ 5.7. ^{31}P NMR (161.75 MHz, $CDCl_3$): δ 28.3 (d, $^1J_{PF}$ = 24.3 Hz). ^{19}F NMR (375.97 MHz, $CDCl_3$): δ -151.8. Anal. Calcd for $C_{37}H_{39}BPF$: C, 81.62; H, 7.22. Found: C, 81.33; H, 7.34.

Synthesis of 93-CN. [**93**]I (0.030 g, 0.046 mmol) was dissolved in MeOH (10 mL) and treated with NaCN (0.005 g, 0.092 mmol) in MeOH. The resulting solution was allowed to slowly evaporate yielding the target compound as colorless crystals. (22.5 mg, 89% yield). ^{1}H NMR (399.9 MHz, $CDCl_3$): δ 1.65 (bs, 3H, Mes-CH_3), 1.76 (bs, 3H, Mes-CH_3), 2.04 (bs, 3H, Mes-CH_3), 2.21 (bs, 9H, Mes-CH_3), 2.33 (d, $J_{H\text{-}P}$ = 13 Hz, 3H, P-CH_3), 6.59 (bs, 1H, Mes-C*H*), 6.65 (bs, 1H, Mes-C*H*), 6.75 (bs, 2H, Mes-C*H*), 6.98-7.09 (bm, 2H, Ar-C*H*), 7.27 (bm, 4H, Ar-C*H*), 7.53 (bm, 5H, Ar-C*H*), 7.59-7.72 (bm, 3H, Ar-C*H*). ^{11}B NMR (128.2 MHz, $CDCl_3$): δ -17.5. ^{31}P NMR (161.75 MHz, $CDCl_3$): δ 27.7.

Synthesis of 93-N_3. This compound was prepared using the same procedure to synthesize **93**-CN starting from [**93**]I (30 mg, 0.046 mmol). **93**-N_3 was isolated as a white powder (15.1 mg, 58% yield). ^{1}H NMR (499.88 MHz, $CDCl_3$): δ 1.76 (bs, 12H, Mes-CH_3), 2.11 (d, $J_{H\text{-}P}$ = 13 Hz, 3H, P-CH_3), 2.19 (s, 6H, Mes-CH_3), 6.57-6.79 (bm, 4H, Mes-C*H*), 6.92 (m, 1H, Ar-C*H*), 7.05 (bm, 1H, Ar-C*H*), 7.27 (bm, 5H, Ar-C*H*), 7.45 (bm, 1H, Ar-C*H*), 7.59 (bm, 3H, Ar-C*H*), 7.59-7.62 (bm, 2H, Ar-C*H*), 7.69 (bt, 1H, Ar-

C*H*). ^{11}B NMR (128.2 MHz, $CDCl_3$): δ -14.8. ^{31}P NMR (161.75 MHz, $CDCl_3$): δ 25.5.

Synthesis of 93-OAc. This compound was prepared using the same procedure to synthesize **93**-CN starting from [**93**]I (0.030 g, 0.046 mmol). **93**-OAc was isolated as a white powder (25 mg, 93% yield). ^{1}H NMR (399.9 MHz, $CDCl_3$): δ 1.79 (bs, 9H, Mes-CH_3), 1.95 (bs, 3H, Mes-CH_3), 2.15 (s, 3H, OAc-CH_3), 2.23 (d, $J_{H\text{-}P}$ = 14 Hz, 3H, P-CH_3), 2.31 (bs, 6H, Mes-CH_3), 6.55 (bs, 4H, Mes-C*H*), 6.88-6.98 (bm, 2H, Ar-C*H*), 7.27 (bs, 5H, Ar-C*H*), 7.44 (bm, 4H, Ar-C*H*), 7.53 (bm, 2H, Ar-C*H*), 7.59 (bm, 1H, Ar-C*H*). ^{11}B NMR (128.2 MHz, $CDCl_3$): δ -3.2. ^{31}P NMR (161.75 MHz, $CDCl_3$): δ 20.82.

Synthesis of 95. [**93**]I (50 mg, 0.077 mmol) was suspended in water (2 mL). MeOH was added until the suspension just became clear (about 10 drops). The solution was then treated with a saturated NaOH solution (10 drops) resulting in the precipitation of a white solid. The mixture was extracted with dichloromethane (3 x 3 mL), and the organic layers were combined, dried over $MgSO_4$ and the solvent was removed under reduced pressure. The resulting solid was then dissolved in warm acetone (8 mL). Compound **95** crystallized by slow evaporation of the acetone solution over several days as clear colorless blocks. (12.1 mg, 34% yield). ^{1}H NMR (399.9 MHz, $CDCl_3$): δ 1.77 (s, 6H, Mes-CH_3), 1.96 (d, $J_{H\text{-}P}$ = 13 Hz, 3H, P-CH_3), 2.03 (s, 6H, Mes-CH_3), 2.15 (s, 3H, Mes-CH_3), 2.20 (s, 3H, Mes-CH_3), 6.50 (s, 2H, Mes-C*H*), 6.65 (s, 2H, Mes-C*H*), 7.28 (m, 5H, Ar-C*H*), 7.37 (t, *J* = 7.6 Hz, 1H, Ar-C*H*), 7.42-7.54 (bm, 2H, Ar-C*H*), 7.61 (d, *J* = 7.6 Hz, 1H, Ar-C*H*). ^{13}C NMR (100.5 MHz, $CDCl_3$): δ 14.97 (d, $J_{C\text{-}P}$ = 69 Hz P-*C*H_3), 20.76 (Mes-*C*H_3), 20.83 (Mes-*C*H_3), 24.90 (Mes-*C*H_3), 24.96 (Mes-*C*H_3), 125.70 (d, $J_{C\text{-}P}$ = 17.2 Hz), 126.17 (d, $J_{C\text{-}P}$ = 12.7 Hz), 128.64, 128.78, 129.05, 130.26 (d, $J_{C\text{-}P}$ = 11.5 Hz), 132.07, 132.64, 133.26 (d, $J_{C\text{-}P}$ = 14.9 Hz), 133.65, 140.10, 140.85. B-*C* peaks were not observed. ^{11}B NMR (128.2 MHz, $CDCl_3$): δ 9.8. ^{31}P NMR (161.75 MHz, $CDCl_3$): δ 62.5. Anal. Calcd for $C_{31}H_{34}BPO$: C, 80.18; H, 7.38. Found: C, 79.61; H, 7.35.

UV-vis Titration Experiments. A solution of [20]I (3.0 mL, 6×10^{-5} M, MeOH) and [93]I (3.0 mL, 5.8×10^{-4} M, MeOH) was titrated with incremental amounts of fluoride anions by addition of a solution of KF in H_2O. The absorption was monitored at λ = 333 nm ($\varepsilon_{(333\ nm)}$ = 5533) for [20]I and λ = 372 nm ($\varepsilon_{(372\ nm)}$ = 1540) for [93]I. The fluoride binding constants were obtained by fitting the experimental data to a 1:1 binding isotherm (Figure 63, Table 13 for [20]I; Figure 64, Table 14 for [93]I).

Table 13: Absorbance of a solution of [**20**]$^+$ after successive additions of fluoride anions in MeOH.

$C_{Fluoride}$	Abs_{exp}	Abs_{calc}
0.00E+00	3.32E-01	3.32E-01
4.99E-04	2.87E-01	2.90E-01
9.97E-04	2.59E-01	2.59E-01
1.49E-03	2.37E-01	2.36E-01
1.99E-03	2.20E-01	2.18E-01
2.48E-03	2.06E-01	2.04E-01
2.97E-03	1.95E-01	1.93E-01
3.46E-03	1.86E-01	1.83E-01
3.95E-03	1.78E-01	1.75E-01
4.43E-03	1.70E-01	1.69E-01
4.92E-03	1.64E-01	1.63E-01
5.40E-03	1.56E-01	1.58E-01
5.88E-03	1.50E-01	1.53E-01
6.36E-03	1.46E-01	1.50E-01

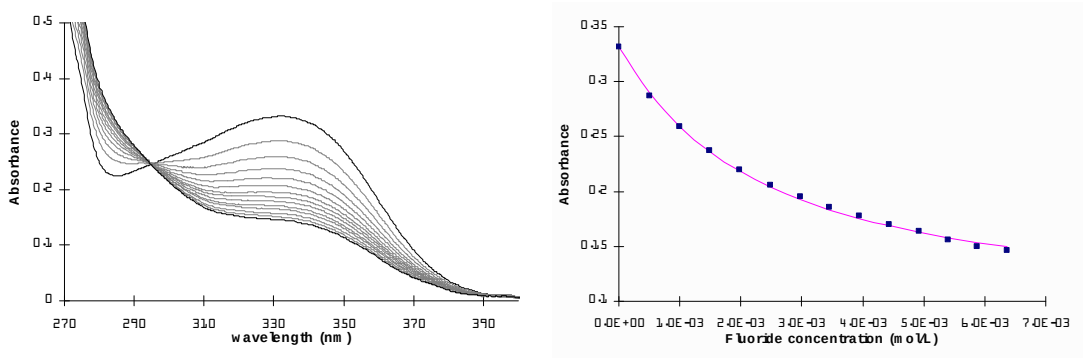

Figure 63: left: Absorbance change of a MeOH solution of [**20**]$^{+}$ after successive additions of fluoride anions; right: Experimental data and calculated 1:1 binding isotherm with K = 400 M^{-1}.

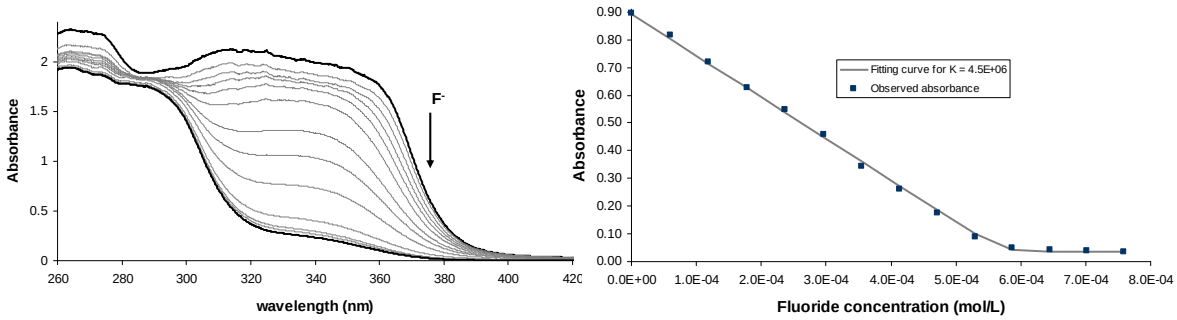

Figure 64: left: Absorbance changes of a MeOH solution of [**93**]$^{+}$ after successive additions of fluoride anions; right: Experimental data and calculated 1:1 binding isotherm with K = 4.5×10^{6} M^{-1}.

Table 14: Absorbance of a solution of $[93]^+$ after successive additions of fluoride anions in MeOH.

$C_{Fluoride}$	Abs_{exp}	Abs_{calc}
0.0000E 00	8.96E-01	8.93E-01
5.9567E-05	8.17E-01	8.04E-01
1.1894E-04	7.19E-01	7.14E-01
1.7811E-04	6.28E-01	6.25E-01
2.3709E-04	5.47E-01	5.37E-01
2.9587E-04	4.58E-01	4.48E-01
3.5446E-04	3.45E-01	3.60E-01
4.1285E-04	2.62E-01	2.73E-01
4.7105E-04	1.76E-01	1.86E-01
5.2906E-04	8.80E-02	1.01E-01
5.8689E-04	5.10E-02	4.26E-02
6.4452E-04	4.40E-02	3.66E-02
7.0196E-04	3.80E-02	3.55E-02
7.5922E-04	3.60E-02	3.50E-02

Computational Details. DFT calculations (full geometry optimization) were carried out with the Gaussian 03 program[163] using the gradient-corrected Becke exchange functional (B3LYP) and the Lee-Yang-Parr correlation functional.[164,165]

Geometry optimization (Figure 65 for [**20**]$^+$, Table 15; Figure 66, Table 16 for **20**-F; Figure 67, Table 17 for [**93**]$^+$; Figure 68, Table 18 for **93**-F) was carried out with the following mixed basis set: 6-31+g(d') for the boron and fluorine atoms,[166] 6-31+g(d) for the phosphorus atom, 6-31g basis set was used for all carbon and hydrogen atoms. [167,168] Frequency calculations, which were carried out on the optimized structure of each compound, confirmed the absence of any imaginary frequencies. The electron density of the DFT optimized structure of **93**-F was subjected to an Atoms-In Molecules analysis[169] using AIM2000.[159] The Natural Bond Orbital (NBO) analysis of **93**-F was carried out using the stand along PC version of GENNBO 5.0 program. The relative enthalpy of [**20**]$^+$, [**93**]$^+$, **20**-F, **93**-F were calculated using the aforementioned optimized geometry through single point calculations at the B3LYP/6-311+g(2d,p) level of theory[170,171] using the polarizable continuum model (PCM) and methanol as a solvent. The relative enthalpies were derived from the energy of each molecule (from the single point calculation) corrected to enthalpy by the "thermal correction to enthalpy term" obtained in the frequency calculations. The LUMO energy of [**20**]$^+$ and [**93**]$^+$ was obtained from the output file of the single point calculations (B3LYP/6-311+g(2d,p)/ PCM:solvent=MeOH).

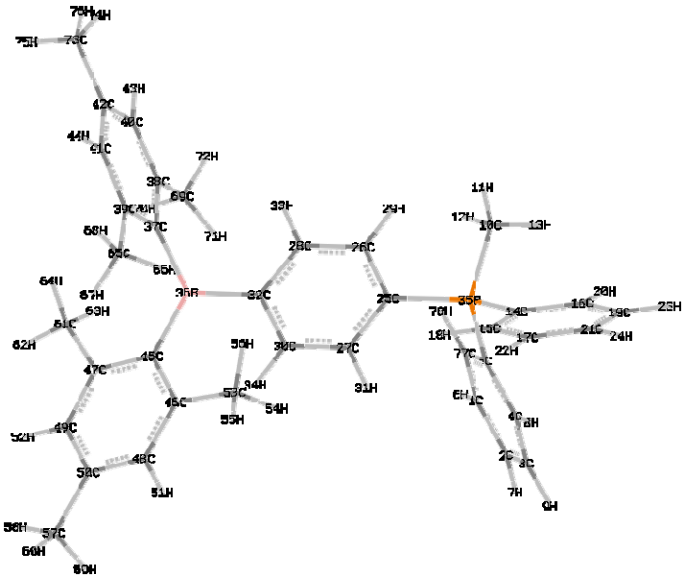

Figure 65: DFT optimized structure of [**20**]$^{+}$.

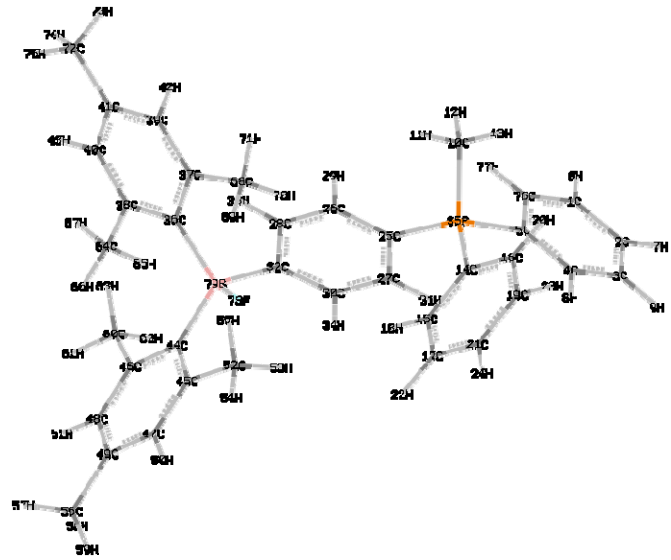

Figure 66: DFT optimized structure of **20**-F.

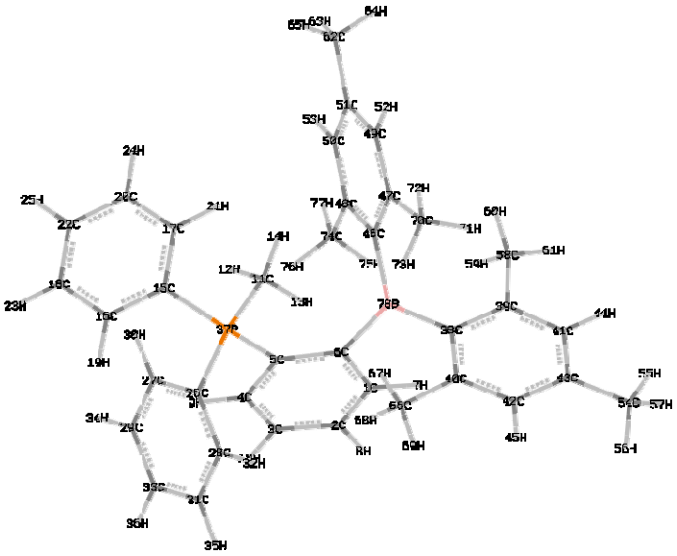

Figure 67: DFT optimized structure of [**93**]$^{+}$.

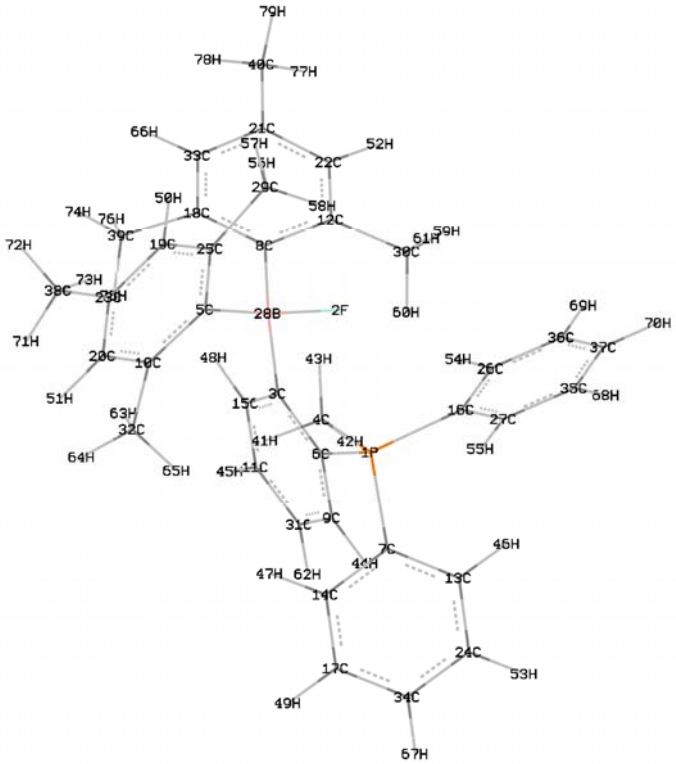

Figure 68: DFT optimized structure of **93**-F.

Table 15: Atom coordinates for the optimized structure of [**20**]$^{+}$.

Center Number	Coordinates (Angstroms) X	Y	Z	Center Number	Coordinates (Angstroms) X	Y	Z
C1	0.67202	-0.63446	2.367772	C40	2.991658	-6.42588	-5.9457
C2	1.390033	-0.18911	3.485928	C41	5.295637	-7.04557	-6.19654
C3	2.699684	0.28149	3.339353	C42	4.026343	-6.87347	-6.77185
C4	3.297786	0.31326	2.075488	H43	1.994381	-6.30717	-6.36254
C5	2.579926	-0.13119	0.947635	H44	6.114558	-7.39445	-6.82063
H6	-0.34243	-0.99982	2.481856	C45	5.442421	-6.8903	-1.4594
H7	0.928584	-0.20938	4.467113	C46	6.589533	-6.51883	-0.69606
H8	4.310526	0.685511	1.970028	C47	4.880241	-8.18572	-1.23072
H9	3.255222	0.626053	4.20436	C48	7.134644	-7.40977	0.238979
C10	2.146573	0.574707	-1.88043	C49	5.438656	-9.03124	-0.26362
H11	2.585903	0.600911	-2.88123	C50	6.571596	-8.66905	0.47876
H12	1.242836	-0.03967	-1.91095	H51	8.02552	-7.11598	0.788935
H13	1.872409	1.592367	-1.58961	H52	4.98362	-10.0033	-0.09229
C14	4.81326	0.932096	-0.68942	C53	7.30194	-5.18701	-0.87722
C15	6.098148	0.371858	-0.82719	H54	6.885076	-4.41128	-0.22147
C16	4.671027	2.329354	-0.54242	H55	8.362805	-5.28676	-0.62532
C17	7.2245	1.201486	-0.8212	H56	7.243855	-4.8106	-1.90275
H18	6.219695	-0.69909	-0.94346	C57	7.183256	-9.62264	1.479033
C19	5.80189	3.148198	-0.53819	H58	7.830512	-10.3564	0.980042
H20	3.690616	2.779992	-0.42355	H59	7.796768	-9.09361	2.215125
C21	7.078032	2.58555	-0.67873	H60	6.413842	-10.186	2.017967
H22	8.211447	0.765989	-0.93013	C61	3.662695	-8.68641	-1.98721
H23	5.688568	4.220812	-0.42701	H62	3.362248	-9.67131	-1.61784
H24	7.953445	3.225652	-0.67728	H63	2.799075	-8.01985	-1.87433
C25	3.76058	-1.7989	-1.20603	H64	3.861556	-8.77701	-3.05997
C26	4.120397	-2.05334	-2.54807	C65	6.953429	-7.01205	-4.32889
C27	3.740564	-2.86182	-0.28067	H66	7.399746	-6.09814	-3.9174
C28	4.436128	-3.35152	-2.94837	H67	6.981155	-7.76725	-3.53709
H29	4.153842	-1.25014	-3.27828	H68	7.604734	-7.35209	-5.13939
C30	4.082464	-4.15099	-0.69632	C69	1.971003	-5.7708	-3.77105
H31	3.46396	-2.68516	0.753002	H70	1.40655	-6.67348	-3.49895
C32	4.4293	-4.43392	-2.03647	H71	2.213522	-5.25203	-2.84123
H33	4.685221	-3.54003	-3.98711	H72	1.291333	-5.13317	-4.34753
H34	4.081917	-4.95811	0.028798	C73	3.794698	-7.17212	-8.23516
P35	3.343375	-0.12137	-0.69146	H74	4.419841	-6.5373	-8.87568
B36	4.790379	-5.91586	-2.50779	H75	4.046298	-8.21298	-8.47325
C37	4.488425	-6.30129	-4.00372	H76	2.750596	-7.00756	-8.5176
C38	3.197479	-6.13831	-4.58687	C77	1.260331	-0.60868	1.1016
C39	5.542839	-6.78681	-4.84397	H78	0.694418	-0.9656	0.24709

Table 16: Atom coordinates for the optimized structure of **20**-F.

Center Number	Coordinates (Angstroms) X	Y	Z	Center Number	Coordinates (Angstroms) X	Y	Z
C1	-0.21619	-0.11821	0.725408	C41	3.44477	-6.7248	-6.48489
C2	-0.07063	0.516575	1.966142	H42	1.387386	-6.63448	-5.87068
C3	1.188494	0.959922	2.383568	H43	5.578428	-6.70959	-6.73233
C4	2.306837	0.776842	1.562464	C44	5.676439	-6.98628	-1.43994
C5	2.165857	0.145751	0.313098	C45	6.819989	-6.37332	-0.85071
H6	-1.18926	-0.47435	0.405455	C46	5.671932	-8.41998	-1.46083
H7	-0.93481	0.656724	2.606713	C47	7.875614	-7.14733	-0.33037
H8	3.280245	1.115442	1.898071	C48	6.746115	-9.15636	-0.93705
H9	1.304861	1.442063	3.34817	C49	7.862691	-8.54205	-0.35965
C10	3.265156	0.85215	-2.31605	H50	8.733554	-6.63772	0.105585
H11	4.095842	0.735908	-3.01684	H51	6.705325	-10.2433	-0.98459
H12	2.346855	0.500092	-2.79366	C52	7.012979	-4.86732	-0.74949
H13	3.15522	1.912088	-2.07185	H53	6.265074	-4.39739	-0.10059
C14	5.085031	0.556748	-0.04046	H54	8.001941	-4.64375	-0.33196
C15	6.103904	-0.32479	0.368211	H55	6.947927	-4.36874	-1.72295
C16	5.258108	1.947423	0.125687	C56	8.997277	-9.35806	0.221683
C17	7.277439	0.180379	0.938888	H57	9.280765	-10.1843	-0.44224
H18	5.984314	-1.39407	0.231934	H58	9.887607	-8.74101	0.388319
C19	6.432976	2.442536	0.69659	H59	8.721711	-9.80404	1.187997
H20	4.484017	2.643642	-0.18253	C60	4.524024	-9.22684	-2.04357
C21	7.44264	1.559671	1.10316	H61	4.80089	-10.2848	-2.11831
H22	8.059359	-0.50462	1.247506	H62	3.628607	-9.1458	-1.41977
H23	6.562029	3.512413	0.820873	H63	4.242482	-8.87508	-3.04022
H24	8.355254	1.947978	1.542739	C64	6.54338	-6.44411	-4.30597
C25	3.743079	-1.83794	-1.19152	H65	6.782976	-5.61025	-3.63879
C26	4.335673	-2.24563	-2.41184	H66	6.88861	-7.35153	-3.80057
C27	3.351198	-2.82723	-0.2564	H67	7.1371	-6.32037	-5.2195
C28	4.531513	-3.59893	-2.67021	C68	1.468144	-6.32183	-3.26396
H29	4.636548	-1.51382	-3.15673	H69	1.331685	-7.19599	-2.62097
C30	3.563147	-4.17317	-0.5407	H70	1.55439	-5.46328	-2.59024
H31	2.877178	-2.54095	0.67833	H71	0.564199	-6.19219	-3.87151
C32	4.175474	-4.61002	-1.74313	C72	3.137768	-6.92451	-7.95365
H33	4.953721	-3.8936	-3.62525	H73	2.197865	-6.43594	-8.23738
H34	3.242549	-4.92698	0.169577	H74	3.934498	-6.51992	-8.58901
P35	3.576782	-0.11658	-0.79829	H75	3.035228	-7.9904	-8.20313
C36	4.028327	-6.43789	-3.66861	C76	0.894556	-0.30719	-0.09934
C37	2.685624	-6.46479	-4.16348	H77	0.775926	-0.82724	-1.04465
C38	5.063286	-6.5115	-4.6506	F78	3.221012	-6.81199	-1.24397
C39	2.423526	-6.61299	-5.5362	B79	4.324794	-6.22754	-2.0424
C40	4.759037	-6.65327	-6.01745				

Table 17: Atom coordinates for the optimized structure of [**93**]$^{+}$.

Center Number	Coordinates (Angstroms) X	Y	Z	Center Number	Coordinates (Angstroms) X	Y	Z
C1	-0.16323	-0.22196	0.171203	C40	-0.72746	-1.46125	-3.17699
C2	-0.06469	-0.53246	1.52939	C41	-2.93185	0.157897	-3.75365
C3	1.190146	-0.75556	2.101638	C42	-1.86012	-1.98716	-3.81219
C4	2.324382	-0.7016	1.291532	C43	-2.97745	-1.19674	-4.10987
C5	2.230975	-0.38975	-0.08545	H44	-3.79535	0.785815	-3.957
C6	0.966981	-0.09277	-0.67911	H45	-1.87264	-3.04066	-4.0792
H7	-1.14553	-0.05365	-0.25582	C46	1.261795	1.87646	-2.59695
H8	-0.96264	-0.60022	2.134433	C47	1.563876	2.042909	-3.99028
H9	3.290953	-0.90974	1.740429	C48	1.596337	2.957216	-1.71702
H10	1.287677	-0.98561	3.156697	C49	2.223469	3.196233	-4.43706
C11	3.856118	-0.14205	-2.69484	C50	2.22648	4.1073	-2.21973
H12	4.848609	-0.39651	-3.0792	C51	2.560957	4.246969	-3.57259
H13	3.116658	-0.74705	-3.22407	H52	2.464288	3.285216	-5.49313
H14	3.652644	0.911079	-2.88249	H53	2.44466	4.924658	-1.53719
C15	5.064376	0.512249	-0.10518	C54	-4.18535	-1.77844	-4.80638
C16	5.969768	-0.01362	0.837828	H55	-4.15236	-1.57814	-5.88581
C17	5.073618	1.895062	-0.38572	H56	-4.23936	-2.86379	-4.67704
C18	6.875361	0.833087	1.485131	H57	-5.11553	-1.34309	-4.42624
H19	5.978628	-1.07483	1.060361	C58	-1.88263	2.213427	-2.80625
C20	5.985015	2.730913	0.264613	H59	-1.6075	2.425688	-1.76693
H21	4.374514	2.326164	-1.09529	H60	-1.21732	2.808996	-3.44079
C22	6.885569	2.202737	1.198401	H61	-2.90074	2.584923	-2.9545
H23	7.571717	0.421791	2.207552	C26	3.2223	5.501617	-4.09212
H24	5.99091	3.792337	0.042717	H63	3.942183	5.277446	-4.88637
H25	7.59135	2.855989	1.699725	H64	2.478062	6.188756	-4.51619
C26	4.386139	-2.27745	-0.82547	H65	3.74593	6.04043	-3.29638
C27	5.673786	-2.60808	-1.30371	C66	0.440575	-2.40162	-2.9444
C28	3.53637	-3.30126	-0.36626	H67	1.290643	-2.16754	-3.60206
C29	6.099107	-3.93809	-1.31235	H68	0.80074	-2.36802	-1.91169
H30	6.348936	-1.83499	-1.65779	H69	0.1534	-3.43485	-3.16094
C31	3.97059	-4.63172	-0.38064	C70	1.211556	1.010138	-5.04799
H32	2.544485	-3.0691	0.001758	H71	0.142342	1.03426	-5.28502
C33	5.247929	-4.95144	-0.85137	H72	1.759727	1.213043	-5.97296
H34	7.09079	-4.18257	-1.67662	H73	1.437536	-0.01677	-4.7464
H35	3.308984	-5.41392	-0.02531	C74	1.233715	2.977549	-0.23998
H36	5.580587	-5.9836	-0.86064	H75	0.19349	2.686653	-0.06395
P37	3.838972	-0.54584	-0.92462	H76	1.859579	2.309075	0.361079
C38	-0.67153	-0.07706	-2.83061	H77	1.359067	3.987483	0.16112
C39	-1.80962	0.732648	-3.14163	B78	0.56577	0.555477	-2.08931

Table 18: Atom coordinates for the optimized structure of **93**-F.

Center Number	Coordinates (Angstroms) X	Y	Z	Center Number	Coordinates (Angstroms) X	Y	Z
P1	-0.06363	-7.3E-05	0.001331	H41	-0.11427	2.39403	0.322191
F2	-0.03761	-0.01277	2.6659	H42	-1.70254	1.750496	-0.16244
C3	2.217538	-0.02449	1.737964	H43	-1.10492	1.585611	1.531438
C4	-0.83172	1.585321	0.479151	H44	2.053315	-1.07596	-1.55655
C5	1.060642	2.178576	3.086828	H45	5.403893	-1.17313	1.111067
C6	1.678994	-0.29528	0.444969	H46	-1.37719	-1.59512	-2.17453
C7	-0.10689	0.122824	-1.83331	H47	1.163721	1.883542	-1.85962
C8	1.878409	-0.16228	4.406095	H48	4.013397	-0.20153	2.898236
C9	2.473714	-0.87308	-0.57822	H49	1.057038	2.177237	-4.30443
C10	1.717716	3.186664	2.321089	H50	-1.15474	4.280123	4.68543
C11	4.364554	-0.92752	0.912766	H51	1.845055	5.274267	1.801285
C12	1.5195	-1.50765	4.738034	H52	1.677109	-3.13285	6.136844
C13	-0.84347	-0.76996	-2.63118	H53	-1.46459	-1.2987	-4.62493
C14	0.577683	1.189579	-2.45417	H54	-2.86179	-0.16534	0.949592
C15	3.578492	-0.36545	1.918549	H55	0.369884	-2.88563	0.045399
C16	-1.15071	-1.39045	0.428503	H56	-0.07189	1.090657	5.492535
C17	0.524098	1.354216	-3.83988	H57	-1.4065	2.257798	5.544063
C18	2.768272	0.492475	5.312489	H58	-1.36415	0.975414	4.316287
C19	-0.35493	3.982627	4.009508	H59	0.680432	-3.41961	4.194402
C20	1.316964	4.535533	2.401493	H60	1.006642	-2.36899	2.805732
C21	2.811579	-1.44247	6.824866	H61	-0.38444	-2.04865	3.821542
C22	1.976603	-2.10841	5.922494	H62	4.407154	-1.63462	-1.13522
C23	0.278869	4.959627	3.232942	H63	3.702656	2.371925	1.899289
C24	-0.89322	-0.60137	-4.02106	H64	3.315173	3.862611	1.036803
C25	0.011606	2.628231	3.956258	H65	2.628622	2.31943	0.518012
C26	-2.47794	-1.17271	0.836948	H66	3.884676	0.387806	7.149837
C27	-0.662	-2.70617	0.328928	H67	-0.25238	0.587403	-5.70327
B28	1.33034	0.542154	3.009831	H68	-1.11067	-4.79927	0.551239
C29	-0.75074	1.687815	4.876594	H69	-4.32706	-2.0826	1.45742
C30	0.657307	-2.38169	3.842496	H70	-3.46412	-4.40754	1.258628
C31	3.810508	-1.18859	-0.34607	H71	0.348982	7.007015	2.526453
C32	2.897155	2.916255	1.397429	H72	0.169703	6.859203	4.279726
C33	3.208324	-0.14757	6.486162	H73	-1.21047	6.540832	3.227871
C34	-0.21213	0.458406	-4.62663	H74	4.13105	2.09433	5.791004
C35	-1.49731	-3.78816	0.622191	H75	3.703915	2.039531	4.078849
C36	-3.30729	-2.25933	1.132257	H76	2.548099	2.664456	5.242326
C37	-2.8201	-3.56668	1.023015	H77	3.437348	-3.1715	7.977295
C38	-0.12401	6.416046	3.318366	H78	4.190488	-1.64879	8.485433
C39	3.312229	1.895671	5.090088	H79	2.5083	-1.99048	8.904555
C40	3.262868	-2.09734	8.112279				

CHAPTER IV

SYNTHESIS OF *ORTHO*-BORYLATED TRIFLUOROACETANILIDES: HYBRID LEWIS ACID/HYDROGEN BOND DONOR RECEPTORS FOR FLUORIDE ANIONS*

4.1 Introduction

Sensors featuring hydrogen bond donor groups such as amides, ureas, thioureas, quanidium ions or pyrroles have long been been utilized for the molecular recognition of fluoride in organic solvents.[6-21] In addition to these receptors, which interact with fluoride anions via hydrogen-bonds, Lewis acidic triarylboranes, which form boron-fluorine covalent bonds, have also been considered.[46,58,145] Such receptors present attractive photophysical properties, and capture fluoride anions with association constants in the 10^5-10^6 M^{-1} range in organic solvents. In order to increase the binding constant of borane-based receptors, we and others have explored the use of bidentate boranes that chelate fluoride.[48,68,72,73] We also investigated heteronuclear bidentate Lewis acids and showed that the fluoride binding constant of 1-(dimesitylboron)-8-(pentafluorophenylmercury) naphthalenediyl (**15**), a hybrid boron/mercury derivative, exceeds 10^8 M^{-1} in THF.[61]

These results indicate that a weakly fluorophilic Lewis acidic site (such as mercury) may serve to assist fluoride binding at a neighboring boron center. In order to generalize this paradigm, we decided to investigate whether hydrogen bond donor groups can be used to assist triarylboryl moieties in the binding of fluoride anions. This chapter details

---

* Reprinted in part with permission from, "A hybrid Lewis acid/hydrogen bond donor receptor for fluoride"; Hudnall, T. W.; Melaïmi, M.; Gabbaï, F. P.; *Org. Lett.*, **2006**, *8(13)*, 2747-2749, Copyright 2007 by the American Chemical Society; and with permission from, "*ortho*-Borylated trifluoroacetanilides-Synthesis and fluoride ion binding properties"; Hudnall, T. W.; Bondi, J. F.; Gabbaï, F. P.; *Main Group Chemistry*, **2006**, *5(4)*, 319-327, Copyright 2006 by Taylor & Francis Journals.

the synthesis and behavior of hybrid derivatives containing both a Lewis acidic boron center and a hydrogen bond donor trifluoroacetamide group.

4.2 *o*-(Dimesitylboryl)-trifluoroacetanilide: Synthesis, structure and reactivity

Double lithiation of *o*-bromotrifluoroacetanilide[172] followed by reaction with dimesitylboron fluoride affords, after treatment with KOH, K[**96**] as a pale yellow air and water stable salt (Figure 69). The ^{11}B NMR signal of [**96**]$^-$ appears at 5 ppm which is in agreement with a tetracoordinate boron center. The structure of [**96**]$^-$ was confirmed by a single crystal X-ray analysis of [S(NMe$_2$)$_3$][**96**] (Figure 70), which was obtained from salt metathesis of K[**96**] and [S(NMe$_2$)$_3$][SiF$_2$Me$_3$]. [S(NMe$_2$)$_3$][**96**] crystallizes in the triclinic $P\bar{1}$ space group. The oxygen atom of the trifluoroacetamide functionality is indeed coordinated to the boron atom (O(1)-B(1) = 1.578(4) Å) and the boron atom adopts a tetrahedral geometry ($\Sigma_{C\text{-}B\text{-}C}$ angles = 344.0°). Coordination of the oxygen atom is concurrent with the presence of a very short N(1)-C(14) bond (1.283(4) Å).

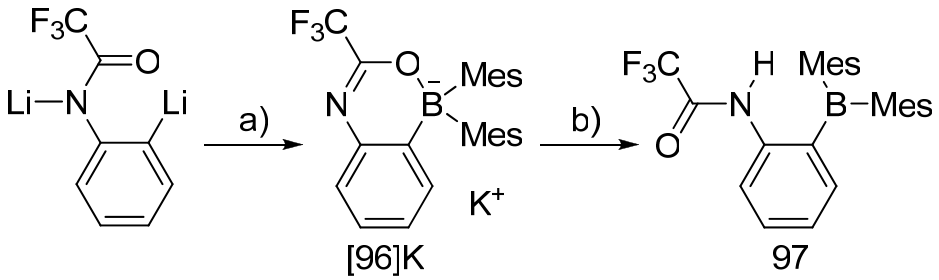

Figure 69: Synthesis of **97**, (a) Mes$_2$BF, THF, -78°C (b) KHF$_2$, H$_2$O/CHCl$_3$, 25°C.

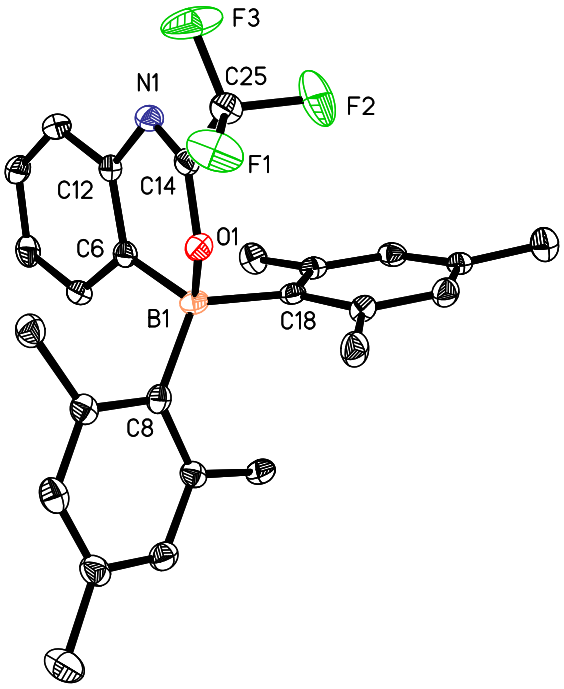

Figure 70: ORTEP view of [**96**]$^-$ in [$S(NMe_2)_3$][**96**], (50% ellipsoid, H-atoms omitted for clarity).

[K][**96**] can be easily protonated with KHF_2 to afford *o*-(dimesitylboryl) trifluoroacetanilide, **97**, (Figure 69). The presence of an uncoordinated trigonal planar boron center is confirmed by detection of a ^{11}B NMR signal at 74 ppm. Other spectroscopic features include: a ^{19}F NMR signal at -77 ppm corresponding to the trifluoromethyl group; and a broad ^1H NMR signal at 8.79 ppm corresponding to the proton of the trifluoroacetamide functionality. The structure of this compound was also studied by single crystal X-ray diffraction (Figure 71). Compound **97** also crystallizes in the triclinic $P\bar{1}$ space group. The boron atom in **97** adopts a trigonal planar geometry ($\Sigma_{(C\text{-}B\text{-}C\ angles)}$ = 359.9°). The absence of a boron-oxygen bond (B(1) and O(1) are separated by more than 5 Å) indicates that the carbonyl group of the trifluoroacetamide functionality is not sufficiently basic to neutralize the Lewis acidic boron center.

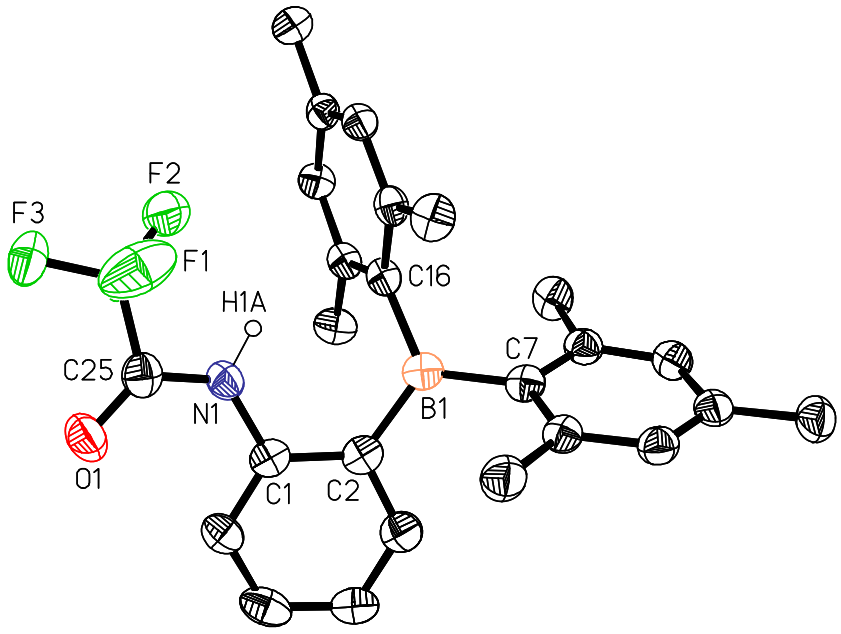

Figure 71: ORTEP view of **97**, (50% ellipsoids, H-atoms, except H(1A) are omitted for clarity).

In order to probe the Lewis acidic properties of this compound, we studied its interaction with neutral bases. We first noted that the ^{11}B NMR chemical shift of **97** is very sensitive to changes in solvent (Table 19). In $CDCl_3$, the resonance is detected at 74 ppm, indicating that the boron center remains three-coordinate. In increasingly polar solvents however, the ^{11}B NMR resonance undergoes a high-frequency shift. For example, in DMF the ^{11}B NMR resonance of **97** appears at 11 pm which is close to that of [**96**]$^-$ (5 ppm in MeOH). This upfield shift observed in the boron NMR spectrum is indicative of increasing sp^3 character of the boron atom. With this in mind, it could be postulated that the coordination environment about the boron gradually increases from three to four as the polarity of the solvent increases.

Table 19: Solvent dependence of the ^{11}B NMR chemical shift of **97** compared with that of [**96**]$^-$.

Compound	Solvent	^{11}B NMR chemical shift
97	Chloroform	74 ppm
97	Acetone	22 ppm
97	DMF	11 ppm
[**96**]$^-$	Methanol	5 ppm

While it can be argued that this observed high-frequency shift results from coordination of the carbonyl functionality of the acetone or DMF molecule to the boron center, the formation of a hydrogen-bonded complex between **97** and acetone or DMF, which directs coordination of the trifluoroacetanilide oxygen atom to the boron center, appears to be at the origin of this observation. Indeed, slow crystallization of **97** from DMF yields crystals of the hydrogen-bonded complex **97**-DMF (Figure 72, Table 20) which crystallizes in the triclinic $P\bar{1}$ space group. The N(1)···O(2) distance of 2.730(4) Å confirms the presence of a hydrogen bond between these two atoms. The resulting B(1)-O(1) distance of 1.650(5) Å is distinctly longer than that observed in [$S(NMe_2)_3$][**96**] (1.578(4) Å). It is also longer than the boron-oxygen bond observed in related derivatives such as 1,1-difluoro-3-(methylamino)-1H-2,4,1- benzoxazaborine[173] (1.520(2) Å) suggesting that it is relatively weak. Despite the weakness of this linkage, coordination of the carbonyl oxygen atom to the boron center most likely polarizes the trifluoroacetamide functionality thus increasing its hydrogen bond donor ability. Similar arguments have been used to rationalize the affinity of boronate-urea derivatives for carboxylate anions.[174]

Table 20: Crystal data, data collection, and structure refinement for $[S(NMe_2)_3]$[**96**], **97**, and **97**-DMF.

	$[S(NMe_2)_3]$[**96**]	**97**	**97**-DMF
	Crystal data		
Formula	$C_{32}H_{44}BF_3N_4O_S$	$C_{26}H_{27}BF_3N_1O_1$	$C_{29}H_{34}BF_3N_2O_2$
M_r	600.58	437.30	510.39
crystal size (mm^3)	0.32× 0.30 × 0.23	0.34× 0.20 × 0.20	0.50 × 0.45 × 0.33
crystal system	Triclinic	Triclinic	Triclinic
space group	$P\bar{1}$	$P\bar{1}$	$P\bar{1}$
a (Å)	10.181(2)	8.481(3)	10.112(4)
b (Å)	11.860(3)	11.804(4)	11.838(4)
c (Å)	14.546(3)	12.288(5)	12.303(4)
α (°)	95.399(4)	99.518(7)	96.433(6)
β (°)	107.067(4)	106.156(6)	91.218(7)
γ (°)	106.078(4)	94.747(9)	111.586(5)
V ($Å^3$)	1583.7(6)	1154.6(7)	1357.7(8)
Z	2	2	2
ρ_{calc} (g cm^{-3})	1.259	1.258	1.248
μ (mm^{-1})	0.151	0.092	0.091
F(000)	640	460	540
	Data Collection		
T (K)	110(2)	110(2)	110(2)
scan mode	ω	ω	ω
Hkl range	-11 → +11, -13 → +13 -16 → +15	-9 → +2, -8 → +10 -13 → +13	-6 → +11, -13 → +12, -13 → +13
measd reflns	7420	2407	5959
unique reflns [R_{int}]	4297 [0.0513]	2369 [0.0567]	3859 [0.0370]
reflns used for refinement	4297	2369	3859
	Refinement		
refined parameters	379	289	329
GOF on F^2	1.008	1.007	1.007
R1,[a] wR2[b] all data	0.0807, 0.1767	0.0827, 0.1341	0.0914, 0.1498
ρ_{fin} (max/min) (e $Å^{-3}$)	0.585, -0.575	0.461, -0.328	0.521, -0.366

[a] $R1 = \sum||Fo| - |Fc||/\sum|Fo|$. [b] $wR2 = \{[\sum w(Fo^2 - Fc^2)^2]/[\sum w(Fo^2)^2]\}^{1/2}$.

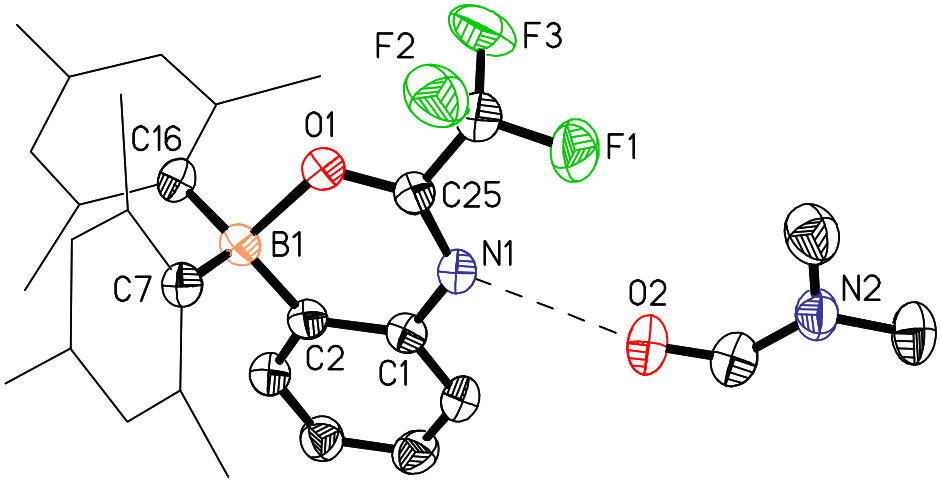

Figure 72: ORTEP view of **97**-DMF, (50% ellipsoids, H-atoms, omitted for clarity. The mesityl substituents are drawn as thin lines for clarity).

4.3 *o*-(Dimesitylboryl)-trifluoroacetanilide: Fluoride binding studies

Compound **97** readily chelates fluoride anions in a variety of solvents. For example, treatment of **97** with [*n*-Bu_4N][F] in acetone leads to formation of [*n*-Bu_4N][**97**-F] (Figure 73). The ^{11}B NMR signal of [**97**-F]$^-$ appears at 3 ppm as expected for a tetrahedral boron atom. The ^{19}F NMR spectrum features a characteristic broad signal at -164.4 ppm whose width and chemical shift is comparable to those observed in other triarylfluoroborates.[48,61,145]

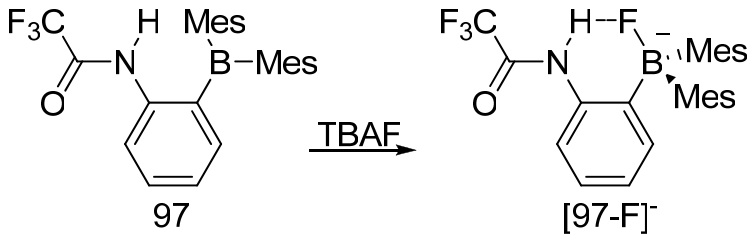

Figure 73: Reaction of **97** with TBAF to form fluoroborate [**97**-F]$^-$.

Remarkably, the amide proton is coupled to the bridging fluoride and gives rise to a doublet ($^1J_{H\text{-}F}$ = 36 Hz) at 11.43 ppm indicating the presence of a NH···F hydrogen bond. This situation is reminiscent of that observed in the zwitterionic ammonium fluoroborate [(η^5-C_5H_5)Fe{η^5-C_5H_3(BF_3)(CH_2NMe_2H)}] (**38**), which features a weak NH···FB hydrogen bond.[30] In order to confirm our assignment, we carried out a heteronuclear decoupling NMR experiment and observed that the amide proton signal collapses to a singlet upon irradiation of the ^{19}F resonance of [**97**-F]$^-$ at -164.4 ppm (Figure 74). ^1H-^{19}F Coupling in fluoride complexes of hydrogen bond donor receptors is not unprecedented and has been observed in complexes involving indole- or amide-based receptors[175,176] among others.

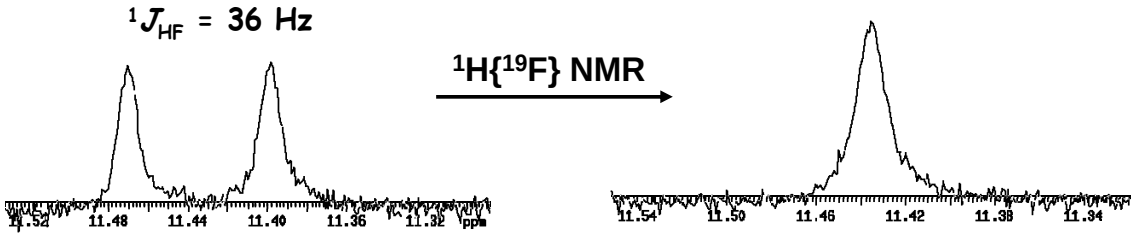

Figure 74: $^1H\{^{19}F\}$ NMR experiment carried out on the N-H resonance of [**97**-F]$^-$.

Incremental addition of fluoride to a solution of **97** in THF leads to an increase in the intensity of broad absorption bands observed below 296 nm and quenching of the broad absorption feature spanning the 300-350 nm range (Figure 75). This phenomenon is similar to that observed upon fluoride coordination to simple triarylboranes and therefore suggests the formation of [**97**-F]$^-$. In order to get a more quantitative measure of the thermodynamical stability of [**97**-F]$^-$, we monitored the absorbance at 236 nm and

found that it reaches a plateau after addition of exactly one equivalent of fluoride. These observations reflect the formation a 1:1 complex whose stability constant K is at least equal to 10^7 M^{-1} in THF (Figure 75 inset) and exceeds that reported Mes_3B ($3.3 \pm (0.4) \times 10^5$ M^{-1}).[48] Although the inductive electron withdrawing properties of the trifluoroacetamide functionality may be invoked, we propose that the high fluoride affinity of **97** results from the cooperativity of the Lewis acidic borane and the hydrogen bond donor trifluoroacetamide functionality. In order to support this hypothesis, we have computed the gas phase fluoride affinity of **97** (DFT ,B3LYP, 6-311+g(2d,p) for all atoms) and compared it to that of Mes_2BPh (which does not contain a hydrogen bond donor). The fluoride ion affinity of **97** (75.15 kcal/mol) exceeds that of Mes_2BPh (61.53 kcal/mol), corroborating the conclusions of the solution binding studies. As part of these calcuations, we also optimized the geometry of [**97**-F]$^-$ and $[Mes_2BPhF]^-$. The computed structure of [**97**-F]$^-$ (Figure 76) shows a NH$\cdots$FB hydrogen bond of 1.72 Å which is much shorter than that measured in (**38**).[30] The presence of this short hydrogen bond, which also results in a lengthening of the B-F bond (1.52 Å in [**97**-F]$^-$ vs 1.49 Å in $[Mes_2BPhF]^-$), is most likely responsible for the high fluoride binding constant displayed by **97**.

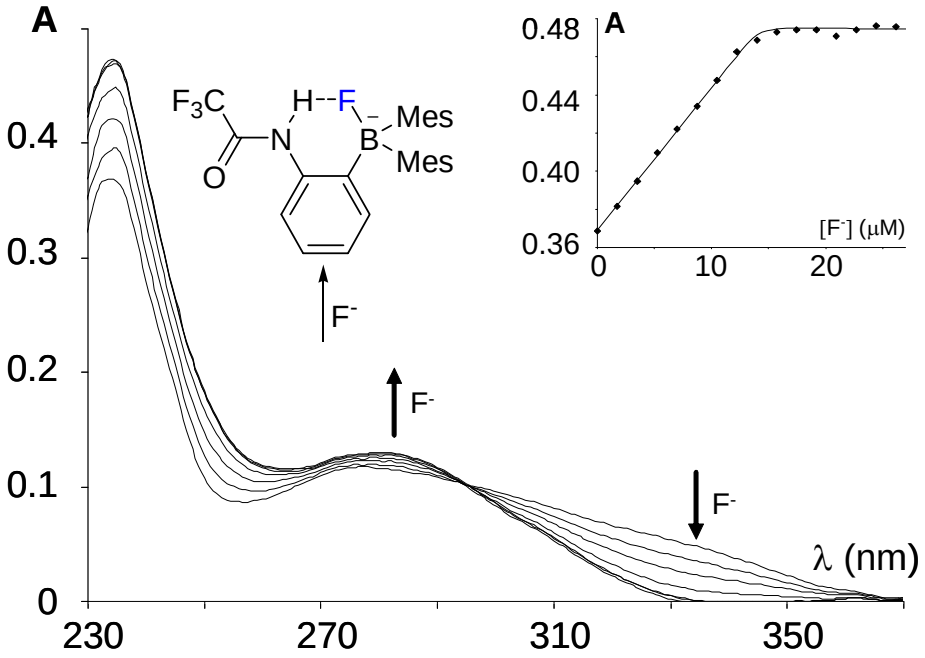

Figure 75: Spectral change accompanying the formation of [**97**-F]$^-$ upon addition of *n*Bu$_4$NF to a THF solution of **97** (1.43 ×10^{-5} M). The inset shows the absorbance at 236 nm as a function of [F$^-$] (M). The thin line corresponds to the binding isotherm calculated with K = 10^8 M^{-1}.

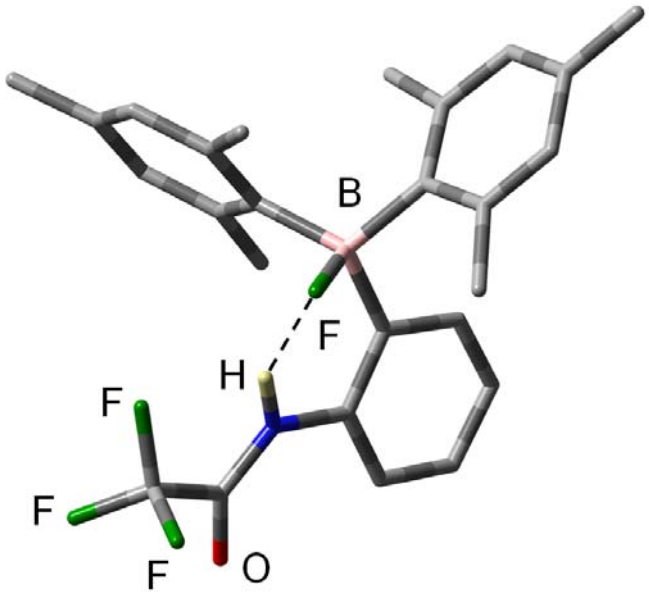

Figure 76: Tube representation of the optimized geometry of [**97**-F]$^-$. H-atoms, except N*H* are omitted for clarity.

4.4 Synthesis and characterization of *o*-(pinacolboryl)-trifluoroacetanilide and [K-dibenzo-18-crown-6-ether][*o*-(trifluoroborato)-trifluoroacetanilide]

Encouraged by the fluoride binding properties of **97**, we decided to investigate the synthesis and properties of its pinacolboryl analog. Double lithiation of *o*-bromotrifluoroacetanilide[172] followed by reaction with trimethylborate affords, after treatment with HCl, the boronic acid **98**. This boronic acid, which exists as a mixture with the corresponding boroxine (**99**), was not purified and directly converted into *o*-(pinacolboryl)trifluoroacetanilide (**100**) by treatment with pinacol in $CHCl_3$/Acetone (Figure 77). The presence of an uncoordinated trigonal planar boron center is confirmed

by detection of a ^{11}B NMR signal at 30.5 ppm. Other spectroscopic features include: a ^{19}F NMR signal at -76.5 ppm corresponding to the trifluoromethyl group; and a broad ^{1}H NMR signal at 10.55 ppm corresponding to the proton of the trifluoroacetamide functionality. The structure of this compound was also studied by single crystal X-ray diffraction (Figure 78, Table 21). Compound **100** crystallizes in the triclinic space group $P\bar{1}$ as an acetonitrile solvate. The boron atom in **100** adopts a trigonal planar geometry ($\Sigma_{C\text{-}B\text{-}O}$ angles = 360.0°) and does not interact with the carbonyl group of the trifluoroacetamide functionality. All other bond distances and angles remain typical.

Multinuclear NMR measurements indicate that compound **100** captures fluoride to form the corresponding fluoroborate adduct (Figure 79). The ^{11}B NMR signal of [**100**-F]$^-$ appears at 4.7 ppm as expected for a tetrahedral boron atom. The ^{19}F NMR spectrum features a characteristic broad signal at -158 ppm whose chemical shift is comparable to those observed in other pinacolfluoroborate anions.[38] The NH ^{1}H-NMR resonance undergoes a noticeable shift from 10.55 ppm in **100** to 12.12 ppm in [**100**-F]$^-$, in agreement with the formation of an intramolecular NH···F hydrogen bond. A similar shift was observed in the case of [**97**-F]$^-$. Despite cooling, H-F coupling could not be observed.

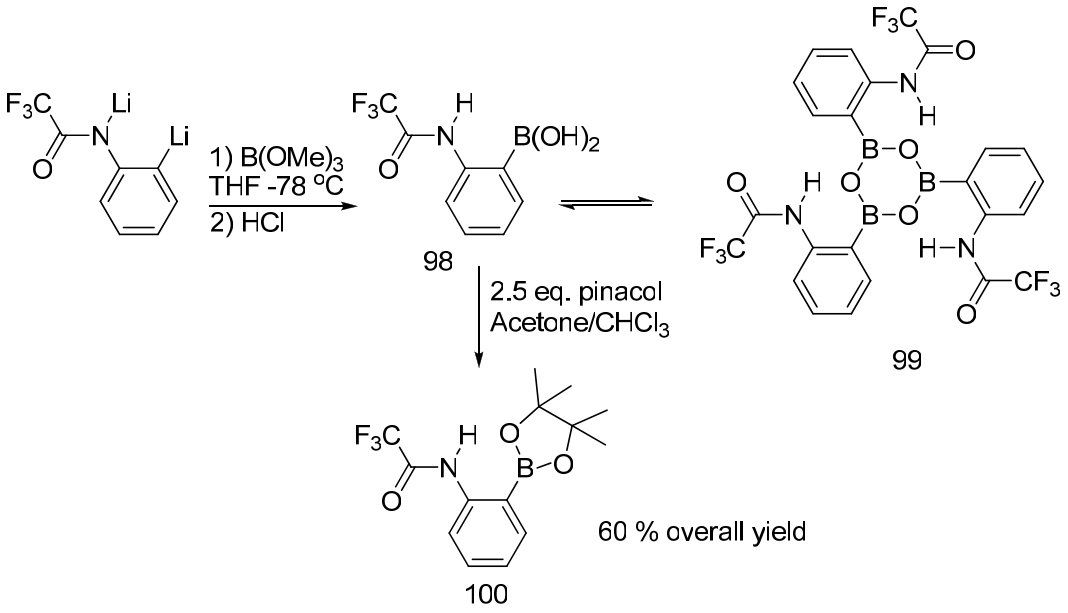

Figure 77: Synthesis of compounds **98**, **99** and **100**.

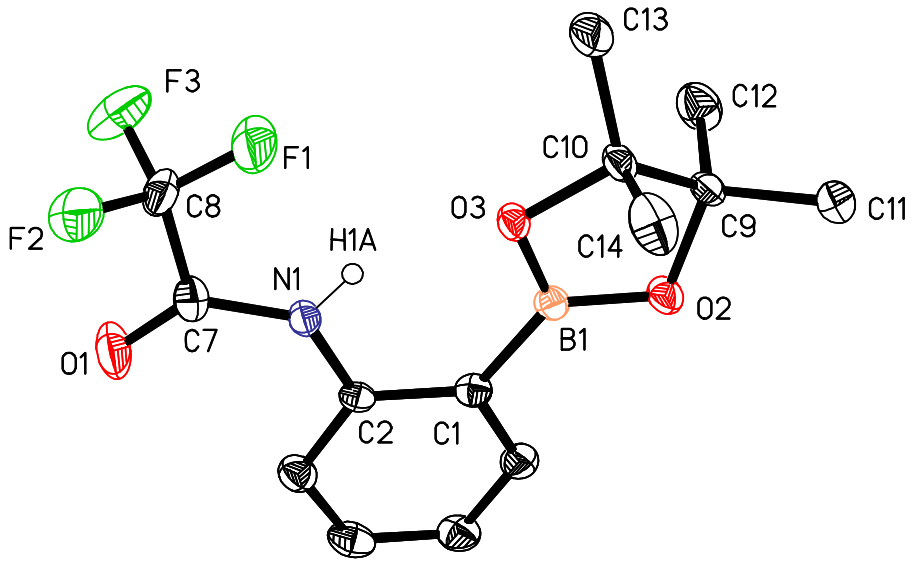

Figure 78: ORTEP view of **100**, (50% ellipsoids, H-atoms, except for H(1A), omitted for clarity).

Table 21: Crystal data, data collection, and structure refinement for **100**-MeCN and **101**-$CHCl_3$.

	100-MeCN	**101**-$CHCl_3$
	Crystal data	
Formula	$C_{16}H_{20}BF_3N_2O_3$	$C_{29}H_{30}BCl_3F_6KNO_7$
M_r	356.15	774.80
crystal size (mm^3)	0.28 × 0.07 × 0.05	0.39 × 0.21 × 0.12
crystal system	Triclinic	Triclinic
Space group	$P\bar{1}$	$P\bar{1}$
a (Å)	7.2731(13)	9.297(2)
b (Å)	10.743(2)	12.305(3)
c (Å)	11.645(2)	16.012(4)
α (°)	81.205(3)	74.901(4)
β (°)	84.419(4)	73.977(4)
Γ (°)	8 7.827(3)	75.300(4)
V ($Å^3$)	894.7(3)	1666.8(6)
Z	2	2
ρ_{calc} (g cm^{-3})	1.322	1.544
μ (mm^{-1})	0.110	0.480
F(000)	372	792
	Data Collection	
T (K)	110(2)	110(2)
scan mode	ω	ω
hkl range	-8 → +8, -11 → +11 -6 → +12	-12 → +11, -16 → +15, -21 → +10
measd reflns	4107	10539
unique reflns [R_{int}]	2563 [0.0347]	7278 [0.0304]
Reflns used for refinement	2563	7278
	Refinement	
refined parameters	245	433
GOF on F^2	1.002	1.032
R1,[a] wR2[b] all data	0.0470, 0.1156	0.0889, 0.1754
ρ_{fin} (max/min) (e $Å^{-3}$)	0.289, -0.192	1.222, -0.465

[a] $R1 = \sum||Fo| - |Fc||/\sum|Fo|$. [b] $wR2 = \{[\sum w(Fo^2 - Fc^2)^2]/[\sum w(Fo^2)^2]\}^{1/2}$.

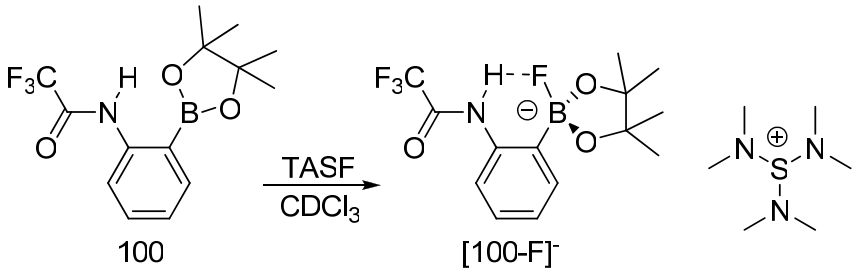

Figure 79: Formation of [**100**-F]$^-$ upon reaction of **100** with TASF in $CDCl_3$.

Compound **100** reacts KHF_2 to afford the corresponding trifluoroborate derivative which has been isolated as a dibenzo-18-crown-6 potassium salt (**101**) (Figure 80). This salt has been characterized by NMR spectroscopy and elemental analysis. The ^{11}B NMR signal at 3.7 ppm is in the expected range for an aryltrifluoroborate species. The ^{19}F NMR signals at -76.1 ppm and -136.2 ppm correspond to the trifluoromethyl and trifluoroborate groups, respectively. Interestingly, the ^{1}H NMR resonance of the proton of the trifluoroacetamide functionality appears as a quartet at 9.97 ppm ($^{1}J_{H\text{-}F}$ = 7.2 Hz, Figure 81) when cooled to -60 °C. We speculate that this quartet arises from H-F coupling involving the fluorine nuclei of the BF_3 group. The appearance of a quartet suggests that the BF_3 unit undergoes rapid rotation about the C_{aryl}-B bond while still interacting with the proton of the trifluoroacetamide functionality.

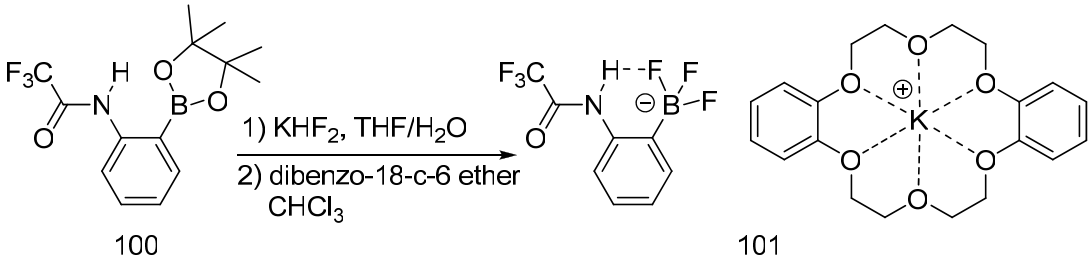

Figure 80: Synthesis of [K-dibenzo-18-c-6][*o*-(trifluoroboryl)-trifluoroacetanilide] (**101**).

$^{1}J_{H\text{-}F} = 7.2$ Hz

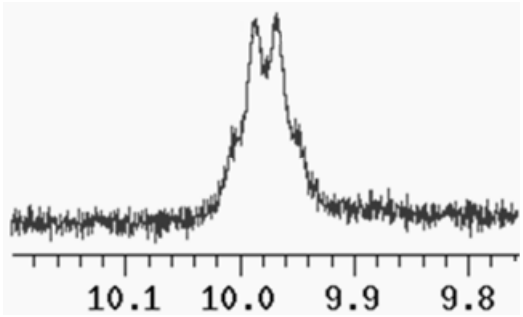

N*H* NMR signal
$CDCl_3$, -60 °C

Figure 81: Part of the ^{1}H NMR spectrum of **101** in $CDCl_3$ showing the N*H* resonance.

Crystals of **101** could be obtained from a concentrated solution of **101** in chloroform after 12 hours at -20°C. Compound **101** crystallizes in the triclinic $P\bar{1}$ space group as a chloroform solvate (Figure 82, Table 21). The boron center adopts a tetrahedral geometry ($\Sigma_{F\text{-}B\text{-}F}$ angles = 320.2°). One of the fluorine atoms of the BF_3 unit is hydrogen bonded to the proton of the trifluoroacetamide functionality. Based on the calculated position of the hydrogen atom, the resulting H···F distance is equal to 2.02 Å. This distance is longer than that computed for [**97**-F]$^-$ but shorter than that measured in [(η^5-C_5H_5)Fe{η^5-$C_5H_3(BF_3)(CH_2NMe_2H)$}].[30] Also of note is that the formation of this H(1A)···F(4) hydrogen bond appears to result in a lengthening of the B(1)-F(4) bond (1.428(4) Å) when compared to the B(1)-F(5) and B(1)-F(6) bonds (1.411(4) Å, 1.401(4) Å). Lastly, we note that two fluorine atoms interact with the potassium counterion via short contacts of 2.774(2) Å (F(4)-K(1)) and 2.940(2) Å(F(5)-K(1)). These interactions may also contribute to the lengthening of the B(1)-F(4) bond.

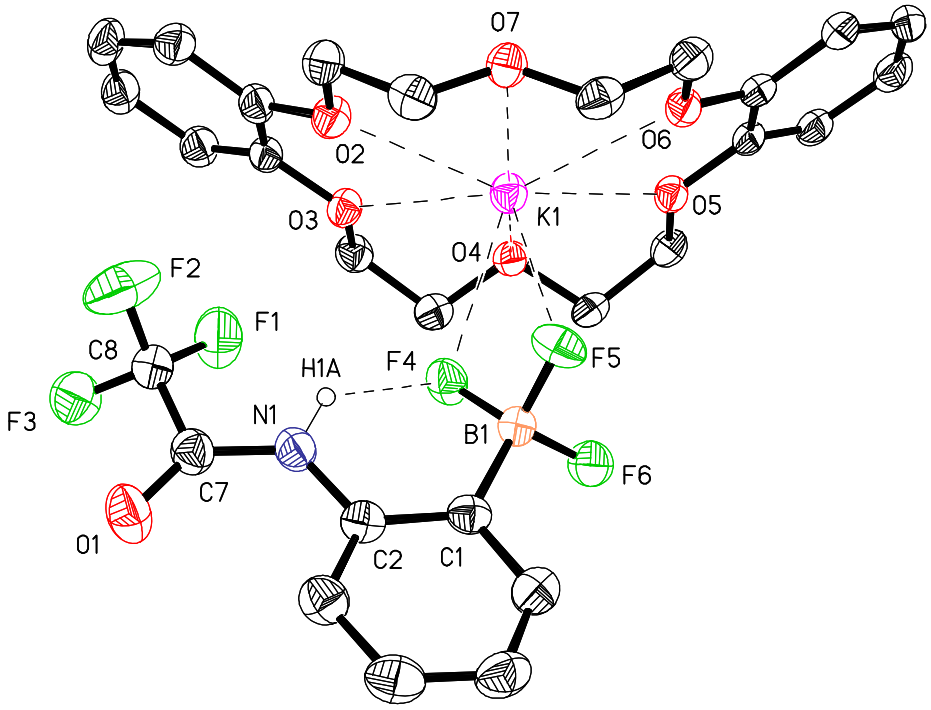

Figure 82: ORTEP view of **101** (50% ellipsoids, H-atoms, except H(1A), are omitted for clarity).

4.5 Conclusion

In this chapter we have demonstrated that hybrid receptors, which feature both a Lewis acidic site and a Brönsted acidic hydrogen-bond donor group, are capable of fluoride anion chelation. This chelation is made possible by the cooperativity of the two acidic sites. This cooperative binding leads to an enhanced affinity for fluoride anions in organic solvents over monofunctional derivatives. In fact, these receptors have exhibited binding constants which are competitive with that of chelating diboranes and chelating hybrid triarylboryl/mercury (II) derivatives.[48,61]

4.6 Experimental

General Considerations. *o*-Bromotrifluoroacetanilide was synthesized as described in the literature. Solvents were dried by reflux under N_2 over the appropriate

drying agents and freshly distilled prior to use. THF was dried over Na/K. Air-sensitive compounds were handled under a N_2 atmosphere using standard Schlenk and glovebox techniques. UV-vis spectra were recorded on a HP8430 spectrometer. Elemental analyses were performed at Atlantic Microlab (Norcross, GA). NMR spectra were recorded on Varian Unity Inova 400 FT NMR (399.63 MHz for ^{1}H, 100.50 MHz for ^{13}C, 376.03 MHz for ^{19}F, 128.22 MHz for ^{11}B) and Varian Inova 500 FT NMR (500.62 MHz for ^{1}H, 125.89 MHz for ^{13}C) spectrometers. Chemical shifts δ are given in ppm and are referenced against external Me_4Si (^{1}H, ^{13}C), BF_3-Et_2O (^{11}B), and $CFCl_3$ (^{19}F). Mass spectra were taken with a ABI Voyager-DE STR spectrometer. Melting points were measured on samples in sealed capillaries and are uncorrected.

Crystallography. The crystallographic measurements were performed using a Siemens SMART-CCD area detector diffractometer, with a graphite-monochromated Mo-K_α radiation (λ = 0.71069 Å). Specimens of suitable size and quality were selected and mounted onto glass fiber with apiezon grease. The structures were solved by direct methods, which successfully located most of the non-hydrogen atoms. Subsequent refinement on F^2 using the SHELXTL/PC package (version 5.1) allowed location of the remaining non-hydrogen atoms.

Synthesis of [**96**]K. Methyllithium (1.6M) in diethyl ether (1.2 mL, 1.9 mmol) was rapidly added to a solution of *o*-bromotrifluoroacetanilide (500 mg, 1.9 mmol) in THF (40 mL) at -78 °C. After 10 min., *t*-butyllithium (1.7 M) in pentane (2.2 mL, 3.8 mmol) was added dropwise. The mixture was stirred at -78 °C for 2 h time after which a solution of dimesitylboron fluoride (550 mg, 2.09 mmol) in THF (5 mL) was rapidly added. The mixture was allowed to warm to room temperature and stirred overnight. The reaction mixture was quenched with a saturated KOH solution (40 mL) at 0 °C. The layers were separated and the aqueous phase was extracted with ether (3 x 30 mL). The organic phases were combined, dried over magnesium sulfate, and concentrated under reduced pressure to yield a light brown oil. The residue was dissolved in chloroform (5

mL) and treated with KOH (5 mL) which resulted in the precipitation of [**96]**K as a pale yellow powder which was washed with chloroform (10 mL). Yield: 49% (720 mg). Melting point: 452 °C (decomp.) ^{1}H NMR (methanol-d_4, 400 MHz): δ 1.84 (s, 12 H, Mes-*o*-CH_3), 2.12 (s, 6 H, Mes-*p*-CH_3), 6.47 (s, 4 H, Mes-C*H*), 6.88 (m, 4 H, phenylene-C*H*). ^{13}C NMR (methanol-d_4, 100.5 MHz): δ 19.9 (Mes-*p*-*C*H$_3$), 23.8 (Mes-*o*-*C*H$_3$), 118.8 (q, $^{1}J_{CF}$ = 291.5 Hz, *C*F$_3$), 115.8 (phenylene-*C*N or *C*B), 141.2 (Mes-*o*-*C*), 121.2 (phenylene-*C*H), 124.8 (phenylene-*C*H), 132.0 (phenylene-*C*H), 133.9 (phenylene-*C*H), 143.9 (phenylene-*C*B or *C*N), 145.0 (Mes-*p*-*C*), 132.0 (Mes-*C*B), 128.3 (Mes-*m*-*C*H), 153.2 (q, $^{2}J_{CF}$ = 36 Hz, *C*O).^{11}B NMR (methanol-d_4, 128.2 MHz): δ 5. ^{19}F NMR (methanol-d_4, 376.03 MHz): δ -73.7.

Synthesis of 97. KHF_2 (50 mg, 0.630 mmol) was added to a suspension of [**96]**K (100 mg, 0.21 mmol) in a biphasic mixture of water (10 mL) and chloroform (10 mL). The mixture was stirred at room temperature for 1 hour. The phases were separated and the aqueous layer was extracted with chloroform (3 x 10 mL). The combined organic phases were dried over magnesium sulfate and concentrated under reduced pressure to afford a yellow oil. The oil was suspended in acetonitrile (1 mL). The resulting solution was frozen in liquid nitrogen and then warmed to room temperature, producing **2** as a pale yellow solid which was washed with cold acetonitrile (3 mL). Yield: 75% (41 mg). Melting point: 154-157 °C. Single crystals of **97** were grown by slow evaporation of an acetone solution. ^{1}H NMR (chloroform-*d*, 500 MHz): δ 2.01 (s, 12 H, Mes-*o*-CH_3), 2.33 (s, 6 H, Mes-*p*-CH_3), 6.86 (s, 4 H, Mes-C*H*), 7.19 (t, *J* = 10.0 Hz, 1 H, phenylene-C*H*), 7.37 (d, *J* = 10.0 Hz, 1 H, phenylene-C*H*), 7.53 (t, *J* = 10.0 Hz, 1 H, phenylene-C*H*), 8.24 (d, *J* = 10.0 Hz, 1 H, phenylene-C*H*), 8.77 (bs, 1 H, N*H*). ^{13}C NMR (chloroform-*d*, 100.5 MHz): δ 21.8 (Mes-*o*-*C*H$_3$), 23.7 (Mes-*p*-*C*H$_3$), 115.1 (q, $^{1}J_{CF}$ = 288.8 Hz, *C*F$_3$), 116.5 (phenylene-*C*N or *C*B), 120.7 (Mes-*o*-*C*), 126.4 (phenylene-*C*H), 129.3 (phenylene-*C*H), 133.3 (phenylene-*C*H), 137.0 (phenylene-*C*H), 137.8 (phenylene-*C*B or *C*N), 139.5 (Mes-*p*-*C*), 140.6 (Mes-*C*B), 141.0 (Mes-*m*-*C*H), 154.9 (q, $^{2}J_{CF}$ = 37 Hz, *C*O). ^{19}F NMR (chloroform-*d*, 376.03 MHz): δ –76.95. ^{11}B

NMR (chloroform-*d*, 128.2 MHz): δ 72. ESI-HRMS $C_{26}H_{27}BNOF_3$ 436.2050 $(M-H)^-$; found 436.2059.

Synthesis of 97-DMF. Slow evaporation of the solvent from a solution of **97** (20 mg, .046 mmol) in DMF (1 mL) at room temperature afforded colorless crystals of **97**-DMF in quantitative yield. ^{1}H NMR (chloroform-*d*, 400 MHz): δ 1.99 (s, 12 H, Mes-*o*-C*H*$_3$), 2.28 (s, 6 H, Mes-*p*-C*H*$_3$), 2.86 (s, 3 H, DMF-C*H*$_3$), 2.94 (s, 3 H, DMF-C*H*$_3$), 6.82 (s, 4 H, Mes-C*H*), 7.17 (t, *J* = 8.0 Hz, 1 H, phenylene-C*H*), 7.33 (d, *J* = 8.0 Hz, 1 H, phenylene-C*H*), 7.48 (t, *J* = 8.0 Hz, 1 H, phenylene-C*H*), 8.00 (s, 1 H, DMF-C*H*). 8.17 (d, *J* = 8.0 Hz, 1 H, phenylene-C*H*), 8.88 (bs, 1 H, N*H*). ^{19}F NMR (chloroform-*d*, 376.03 MHz): δ –76.9 (2 F, C*F*$_3$), -76.3 (1 F, C*F*$_3$). ^{11}B NMR (chloroform-*d*, 128.2 MHz): δ 47.0.

Synthesis of 100. Methyllithium (1.6 M) in diethyl ether (2.33 mL, 3.7 mmol) was rapidly added to a solution of *o*-bromotrifluoroacetanilide (1.00 g, 3.7 mmol) in THF (80 mL) at -78 °C. After 10 min., *t*-butyllithium (1.7 M) in pentane (4.39 mL, 7.4 mmol) was added dropwise. The mixture was stirred at - 78 °C for 2 h, after which trimethyl borate (1.61 mL, 14.1 mmol) was rapidly added. The mixture was allowed to warm to room temperature and stirred overnight. The reaction mixture was quenched with a 10% HCl solution (40 mL) at 0 °C. The mixture was then extracted with dichloromethane (3 x 30 mL). The organic phases were combined, dried over magnesium sulfate, and concentrated under reduced pressure to afford a crude boronic acid as an off white powder which was used without further purification. To a solution of the crude solid (500 mg, 2.71 mmol) in $CHCl_3$:acetone, 20 mL (95:5 vol.) was added a large excess of pinacol (800 mg, 6.78 mmol). The solution was stirred for three hours at room temperature, after which it was extracted with distilled water (3 x 20 mL) to remove any unreacted pinacol. The organic layer was dried over magnesium sulfate, filtered and the solvent was removed under reduced pressure to afford **100** as a pale brown oil. Yield: 60% (544 mg). ^{1}H NMR ($CDCl_3$, 400 MHz): δ 1.39 (s, 12 H), 7.18 (t,

$^{3}J_{HH}$ = 7.2 Hz, 1H), 7.51 (t, $^{3}J_{HH}$ = 7.6 Hz, 1H), 7.80 (d, $^{3}J_{HH}$ = 7.6 Hz, 1H), 8.45 (d, $^{3}J_{HH}$ = 7.2 Hz, 1H), 10.55 (bs, 1H). ^{13}C NMR ($CDCl_3$, 100.5 MHz): δ 24.8 (pinacol-*C*H3), 84.9 (pinacol-*C*O), 116.1 (q, $^{1}J_{CF}$ = 287.4 Hz, *C*F_3), 119.6 (phenyl-*C*H), 124.8 (phenyl-*C*H), 133.1 (phenyl-*C*H), 136.3 (phenyl-*C*H), 142.3 (phenyl-*C*N), 154.6 (q, $^{2}J_{CF}$ = 37.2 Hz, *C*O). The carbon peak for the phenyl-B was not observed. ^{11}B NMR ($CDCl_3$, 128.2 MHz): δ 30.5. ^{19}F NMR ($CDCl_3$, 376.03 MHz): δ –76.5. Anal. Calcd for $C_{14}H_{17}O_3BNF_3$: C, 53.36; H, 5.44. Found: C, 53.49; H, 5.70.

Synthesis of 101. To a solution of **100** (250 mg, 0.8 mmol) in THF (10 mL) was added a solution of KHF_2 (372 mg, 4.8 mmol) in distilled water (2 mL). The solution was stirred at room temperature for 1 hour, after which the solvent was removed under reduced pressure. A solution of dibenzo-18-crown-6 ether (286 mg, 0.8 mmol) in dry $CHCl_3$ (15 mL) was then added to the residue, which was stirred for three hours. The solvent was then reduced to a volume of 5 mL and the reaction flask was placed in the freezer at -20 °C overnight affording clear colorless crystals of **101** as a $CHCl_3$ solvate. Yield: 54% (281 mg). mp. 406 (decomp.). ^{1}H NMR ($CDCl_3$, 400 MHz): δ 3.92 (m, 8 H), 4.11 (m, 8 H), 6.83 (m, 4 H), 6.91 (m, 5 H), 7.15 (t, $^{3}J_{HH}$ = 8 Hz, 1H), 7.51 (d, $^{3}J_{HH}$ = 8 Hz, 1H), 8.17 (d, $^{3}J_{HH}$ = 8 Hz, 1H), 9.97 (q, -60 °C, J_{HF} = 7.2 Hz, 1H). ^{13}C NMR ($CDCl_3$, 100.5 MHz): δ 66.9, 68.8, 111.4 (18-c-6 phenyl), 116.2 (q, $^{1}J_{CF}$ = 241 Hz, *C*F_3), 119.2 (phenyl-*C*H), 121.5 (18-c-6 phenyl), 124.6 (phenyl-*C*H), 127.3 (phenyl-*C*H), 129.6 (phenyl-*C*H), 134.8 (phenyl-*C*N), 146.9 (18-c-6 phenyl), 154.3 (q, $^{2}J_{CF}$ = 32.6 Hz, *C*O). The carbon peak for the phenyl-B was not observed. ^{11}B NMR ($CDCl_3$, 128.2 MHz): δ 3.7 bs. ^{19}F NMR ($CDCl_3$, 376.03 MHz): δ -76.1 (s, 3 F, C*F*$_3$), -136.2 (bs, 3 F, B*F*$_3$). Anal. Calcd for $C_{29}H_{30}O_7BNF_6Cl_3K$ (**2**-$CHCl_3$): C, 44.95; H, 3.90. Found: C, 44.96; H, 3.98.

UV-vis Titration of 97. A solution of **97** (3 mL, 1.43 x 10^{-5} M, THF) was placed in the cell and titrated with incremental amounts of fluoride anions by addition of a solution of nBu_4NF in THF (5.26 x 10^{-3} M). The absorption was monitored at λ_{max} =

236 nm (ε = 25800 for **97**, ε=33400 for [**97**-F]$^-$). The experimental data obtained was fitted to a 1:1 binding isotherm which indicated that the fluoride binding constant of **97** is greater than 10^7 M^{-1} in THF.

Reaction of 100 with F$^-$. To a solution of **100** (71 mg, 0.225 mmol) in dry $CDCl_3$ (0.5 mL) was added TASF (62 mg, 0.225 mmol). NMR measurments carried out on the resulting solution confirmed formation of [**100**-F]$^-$. ^{1}H NMR ($CDCl_3$, 500 MHz): δ 1.07 (bs, 12 H), 2.62 (s, 18 H, TAS$^+$), 6.85 (t, $^3J_{HH}$= 8 Hz, 1H), 6.90 (t, $^3J_{HH}$= 8 Hz, 1H), 7.51 (d, $^3J_{HH}$= 7 Hz, 1H), 8.09 (bs, 1H), 12.06 (s, 1H). ^{19}F NMR ($CDCl_3$, 400 MHz): δ -76.6 (C*F*$_3$), -158 (bs, B*F*). ^{11}B NMR ($CDCl_3$, 400 MHz): δ 4.7.

CHAPTER V

CATIONIC BODIPY-BASED DERIVATIVES: SYNTHETIC METHODOLOGY FOR THE PREPARATION OF TURN-ON FLUORESCENT FLUORIDE PROBES*

5.1 Introduction

In keeping with the current trend of fluoride recognition, this chapter will discuss the synthesis of a new class of boron-based fluoride receptors. As previously mentioned, fluoride recognition is attracting a great deal of interest because of its importance in dental heath, as well as its possible toxicity when administered in high doses. Because of their inherent fluorophilicity, organoboron compounds have often been considered for the complexation of fluoride.[31,36,98] For example, both neutral[49,145] and cationic triarylboranes[85,88] react with fluoride to form the corresponding fluoroborate species. The previous chapters have shown that in the case of cationic boranes, the resulting boron–fluorine interaction is strengthened by favourable Coulombic attractions leading to greater binding constants. In the examples reported in previous chapters however, fluoride binding accompanied by a turn-off response both in the absorption and emission spectra of the borane.[49,88,145] The turn-off, rather than turn-on, nature of the observed response inherently limits the sensitivity of such sensors. Because of this limitation, boron-based fluoride sensors which give a turn-on response upon fluoride binding are now attracting attention.[37,52,57,98] As part of our contribution to this area, we investigated the use of fluorescent dipyrromethene boron (BODIPY) compounds.[177,178] More specifically,

---

* Reprinted in part with permission from, "A BODIPY boronium cation for the sensing of fluoride ions"; Hudnall, T. W.; Gabbaï, F. P.; *Chem. Commun.*, **2008**, Copyright 2008 by the Royal Society of Chemistry.

we contemplated a situation in which a cationic BODIPY derivative could be prepared so that its reaction with fluoride would afford a highly fluorescent derivative.

5.2 Synthesis of a BODIPY boronium cation for the turn-on fluorescence sensing of fluoride

We have investigated the fluoride abstraction of an easily prepared BODIPY-BF_2 species using trimethylsilyltriflate (TMSOTf) in the presence of a netural donor ligand for the purpose of generating a BODIPY-boronium cation. The specific motivation of this methodology was to determine if a BODIPY-boronium cation could be prepared and then reacted with fluoride to form a highly fluorescent BODIPY-BF_2 species (Figure 83).

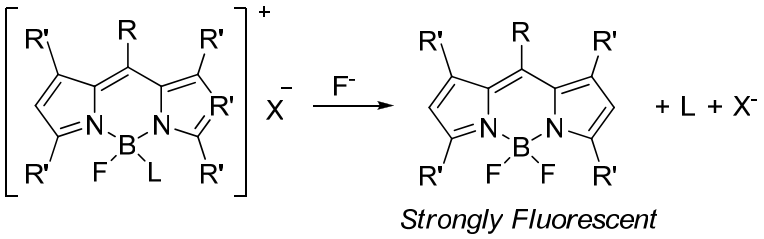

Figure 83: Conceptual scheme describing the proposed BODIPY boronium reaction with fluoride where L = neutral ligand; X^- = anion; and R, R' = hydrocarbon substituents.

The reaction of 1,3,5,7,8-pentamethylpyrromethene-borondifluoride[179] (**102**) with TMSOTf was monitored by ^1H NMR spectroscopy in $CDCl_3$ which allowed for the detection of **103** as the main product of the reaction (Figure 84).

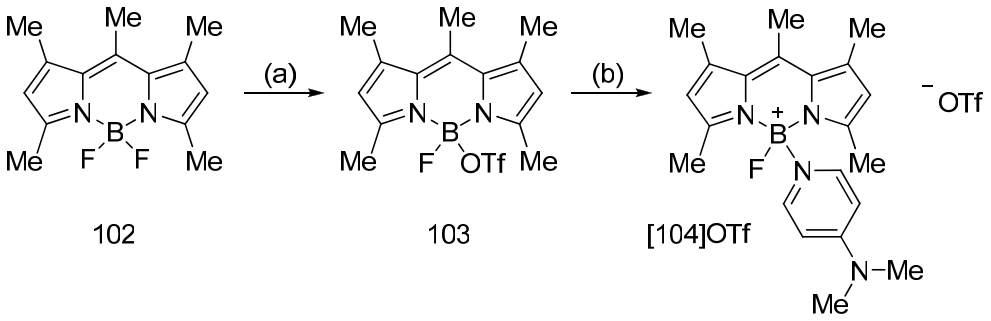

Figure 84: Synthesis of compounds **103** and [**104**]OTf; (a): TMS-OTf, toluene; (b): DMAP, DCM, RT.

Some of the salient NMR spectroscopic features of **103** include: a ^{11}B NMR resonance at 0.92 ppm in agreement with the existence of a four coordinate boron atom and a ^{19}F NMR signal at -148.96 (bs) ppm which can be compared to the value of -147.6 ppm (q, $^{1}J_{FB}$ = 33.8 Hz) measured for **102**. Compound **103** is moisture sensitive and was not isolated in bulk quantities. Single crystals of **103** could be obtained from toluene at -25°C. This derivative crystallizes in the monoclinic $P2_1/c$ space group (Figure 85, Table 22). The B(1)-F(1) bond length of 1.370(3) Å is shorter than that measured in **102** (1.395 Å)[180], suggesting an increase in the positive character of the boron center. In agreement with this view, we note that the B(1)-O(1) bond of 1.568(3) Å is somewhat longer than those observed in other four coordinate boron-triflate species featuring chelating nitrogen donor ligands.[181,182]

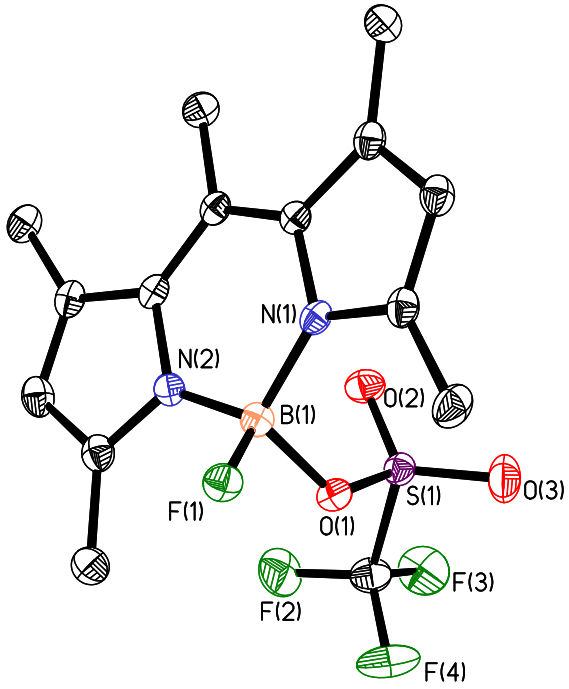

Figure 85: ORTEP view of **103**, (50% ellipsoids, hydrogen atoms omitted for clarity).

This triflate derivative (**103**) reacts quickly with DMAP to afford the boronium triflate salt [**104**]OTf (Figure 84). This salt can also be obtained in 82% yield by the one-pot reaction of **102** with TMSOTf and DMAP in refluxing toluene. When dissolved in chloroform, this salt can be washed with water without decomposing. As a solid, it is air-stable which facilitated its characterization. The ^{1}H NMR spectrum confirms the presence of a single DMAP ligand coordinated to the boron center. The ^{11}B NMR resonance at 0.91 ppm appears as a doublet as a result of coupling to the fluorine nucleus ($^{1}J_{BF}$ = 37 Hz). Likewise, the ^{19}F NMR resonance is split into a quartet because of coupling to the ^{11}B nucleus (I = 3/2). The observed coupling constant is comparable to that in **102**. This salt crystallizes in the monoclinic $P2_1/n$ space group (Figure 86, Table 22). The structure of this derivative confirms the presence of a DMAP ligand coordinated to the boron center. The B(1)−N(3) bond of 1.593(5) Å, which can be compared to that observed in DMAP-

BF_3 (1.589 Å),[183] is short thus indicating the tight coordination of the DMAP ligand. The B(1)-F(1) bond length of 1.385(5) Å is somewhat longer than in **103** indicating a less electron deficient boron center.

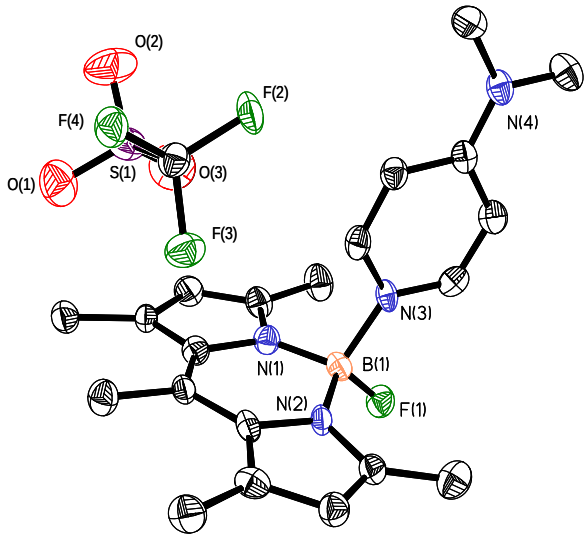

Figure 86: ORTEP view of [**104**]OTf, (50 % ellipsoids, H-atoms omitted for clarity).

As indicated by ^{1}H NMR spectroscopy, the salt [**104**]OTf reacts with tetrabutylammonium fluoride (TBAF) in $CDCl_3$ to afford **102**. No reaction is observed by ^{1}H NMR in the presence of Cl^-, Br^- or I^- salts. Since the reaction with F^- is fast and quantitative, we questioned whether it could be used for the development of a fluoride ion assay. With this in mind, we first studied the fluorescence of [**104**]$^+$ in $CHCl_3$ in the presence of I^- ions. Addition of 10 eq. of tetrabutylammonium iodide (TBAI) to a solution of [**104**]OTf (5.1×10^{-5} M) in $CHCl_3$ results in a drastic quenching of the fluorescence of [**104**]$^+$ (Figure 87), whereas addition of Cl^- or Br^- provided no fluorescence response. This quenching most probably results from an external heavy atom effect[184], whose efficacy is increased by the formation of [**104**]$^+$/I^- ion pairs (Figure 87). Remarkably, when 1 eq. of TBAF is added, the fluorescence intensity increases by

a factor f = 500%, giving a response than can be easily detected with the naked eye (Figure 87).

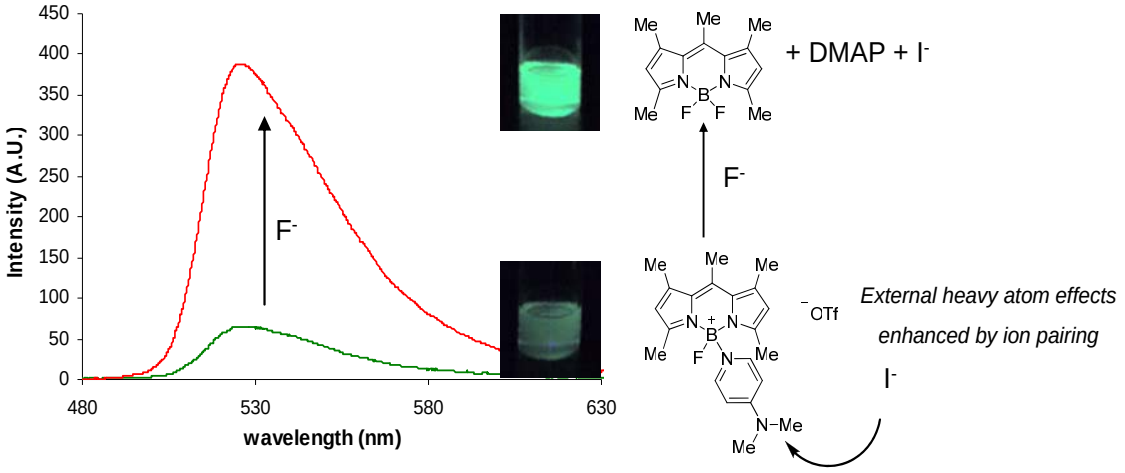

Figure 87: Left: Spectral changes in the emission spectrum of a $CHCl_3$ solution containing [**104**]OTf (5.1×10^{-5} M) and TBAI (10 eq.) upon addition of 1 eq. of TBAF. Right: pictures showing the emission of the solution before and after fluoride addition under a hand held UV lamp.

We propose that this increase results from the formation of **102** which, as a neutral compound, is not as sensitive as $[\mathbf{104}]^+$ to the external spin orbit coupling effect imparted by I^-. A much weaker response is observed upon addition of 1 eq. of Cl^- (f = 48%) or Br^- (f = 6%) ions which competes with the iodide ions in pairing with the $[\mathbf{1}\text{-DMAP}]^+$ cation. In conclusion, we describe a novel approach for the fluorescent turn-on sensing of F^- ions. This approach is based on: i) the use of a BODIPY boronium cation ($[\mathbf{104}]^+$) which is converted into a neutral BODIPY dye (**102**) in the presence of fluoride ions; ii) the greater sensitivity of cationic $[\mathbf{104}]^+$ (when compared to neutral **102**) to the external heavy atom effects imparted by I^-.

Table 22: Crystal data, data collection, and structure refinement for **103** and [**104**]OTf.

	103	**104**[OTf]
	Crystal data	
Formula	$C_{15}H_{17}BF_4N_2O_3S$	$C_{22}H_{27}BF_4N_2O_3S$
M_r	392.18	514.35
crystal size (mm^3)	0.32 × 0.26 × 0.13	0.13 × 0.10 × 0.07
crystal system	Monoclinic	Monoclinic
space group	$P2_1/c$	$P2_1/n$
a (Å)	10.715(4)	11.116(2)
b (Å)	11.143(4)	17.342(3)
c (Å)	14.078(5)	12.365(2)
α (°)	90.000	90.000
β (°)	91.037(7)	101.252(4)
γ (°)	90.000	90.000
V ($Å^3$)	1680.7(10)	2348.4(8)
Z	4	4
ρ_{calc} (g cm^{-3})	1.550	1.455
μ (mm^{-1})	0.253	0.203
F(000)	808	1072
	Data Collection	
T (K)	110(2)	110(2)
scan mode	ω	ω
hkl range	-13 → +7, -14 → +14, -18 → +18	-12 → +10, -18 → +19, -10 → +14
measd reflns	10057	10736
unique reflns [R_{int}]	4022 [0.0842]	3684 [0.0317]
reflns used for refinement	4022	3684
	Refinement	
Refined parameters	235	316
GOF on F^2	1.007	1.008
R1,[a] wR2[b] all data	0.0693, 0.1710	0.0847, 0.1319
ρ_{fin} (max/min) (e $Å^{-3}$)	0.622 -0.588	0.521, -0.478

[a] $R1 = \sum||Fo| - |Fc||/\sum|Fo|$. [b] $wR2 = \{[\sum w(Fo^2 - Fc^2)^2]/[\sum w(Fo^2)^2]\}^{1/2}$.

5.3 Synthetic methodologies for the preparation of cationic BODIPY derivatives

The results described in the preceding sections show that BODIPY triflate compounds such as **103** adopt a covalent rather than ionic structure. We questioned whether ionic compounds, which could be described as borenium ions, could be obtained if: i) the boron atom was substituted by an electon-rich aryl group rather than an electron-withdrawing fluorine atom (Figure 88); ii) the pyrromethene ligand

was substituted with electron-donating substituents.

With this in mind, we first decided to investigate mono-arylated BODIPY compounds which have been recently reported by Ziessel.[177,185,186] The synthetic methodology employed by Ziessel is challenging however, with poor control over the degree of arylation on the boron and low to modest yields. In order to avoid some of these synthetic obstacles, we developed a new synthetic methodology for preparing these mono-arylated BODIPY species. This new methodology was inspired by the recent work of Cowley *et al.* on β-diketiminate supported boron cations.[187]

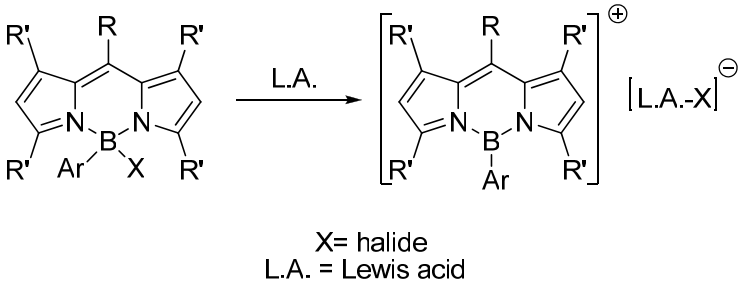

Figure 88: Proposed synthesis of arylated cationic BODIPY derivatives via halide abstraction.

Ziessel's method involves substitution of a single fluoride on a BODIPY-BF_2 species using either aryl-lithium or aryl-Grignard reagents. We proposed that the synthesis of monoarylated species could be simplified using Cowley's method reported with the β-diketiminate analogs.[187] Indeed, 3,5,3',5',6-penta- methylpyrromethene hydrochloride[188] (**105**) was deprotonated using sodium hydride (NaH), and subsequent treatment with phenylboron dichloride produced the mono-arylated boron chloride BODIPY species **106** (Figure 89).

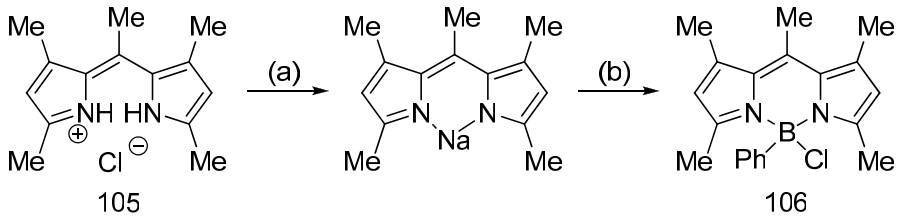

Figure 89: Synthesis of compound **106**, (a): NaH, Et_2O/Hexanes 1:1 (v/v), RT; (b): $PhBCl_2$, toluene, RT.

Dark red crystals of **106** were obtained by slow evaporation of a toluene solution under an atmosphere of N_2. BODIPY compound **106** crystallizes in the triclinic $P\bar{1}$ space group (Figure 90). All of the bond lengths and angles are within the norm for BODIPY derivatives.[180] The B(1)-Cl(1) bond length of 1.921(3) Å is similar to what Cowley has observed in similar species,[187] and the boron is tetrahedral as expected for BODIPY compounds. This is in agreement with the ^{11}B NMR resonance at 2.5 ppm which is characteristic of four-coordinate boron atoms.

Compound **106** is sensitive to moisture, and attempts at chloride abstraction were carried out in dry solvents under N_2. Chloride abstraction was attempted by treating a toluene solution of **106** with anhydrous aluminum chloride ($AlCl_3$). This resulted in the formation of a fluorescent pink solution from which a ^1H NMR spectrum revealed no discernable products. This result led us to consider if fluoride abstraction using silicon-based Lewis acids would produce the desired cationic BODIPY. To this end, the BODIPY-hydroxide complex (**107**), and subsequently the fluoride complex (**108**) were synthesized starting from compound **106** (Figure 91).

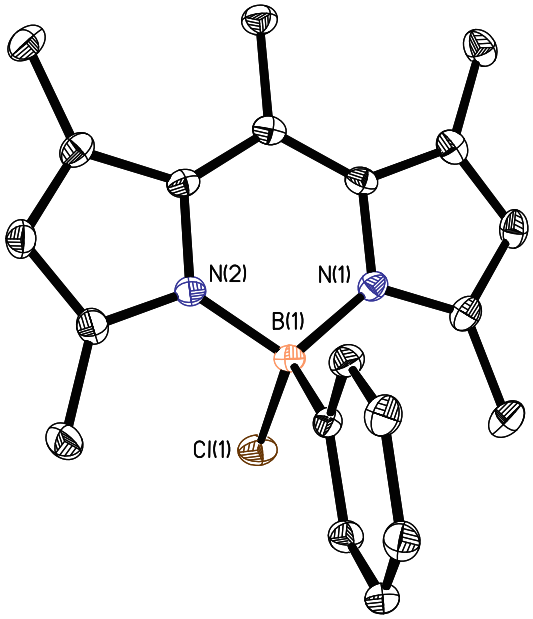

Figure 90: ORTEP view of **106** (50 % ellipsoids, H-atoms omitted for clarity).

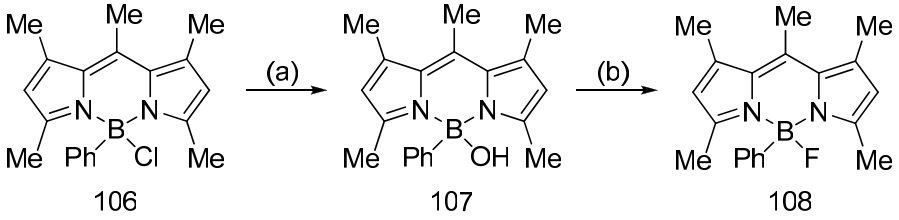

Figure 91: Synthesis of compounds **107** and **108**; (a): eluted over SiO_2 with toluene; (b): KHF_2, THF, 40 °C, 24 hrs.

A toluene solution of **106** was rapidly eluted over a plug of silica gel to yield the hydroxide derivative (**107**) in quantitative yield. Single bright red crystals of **107** were obtained by cooling a concentrated ethyl acetate (EtOAc) solution of **107** to -40 °C for several hours (Figure 92). Compound **107** crystallizes in the monoclinic $P2_1$ space group with two independent molecules in the asymmetric unit. The B-O distances of 1.412(13) Å (molecule 1) and 1.446(13) Å (molecule 2) are typical of hydroxy and

alkoxy substituted BODIPY compounds.[189] Spectroscopic data corroborates the single crystal X-ray diffraction analysis. The ^{1}H NMR spectrum exhibits all of the expected resonances, and the ^{11}B NMR chemical shift of 0.97 is indicative of sp^3 hybridization at the boron center as observed in the crystal.

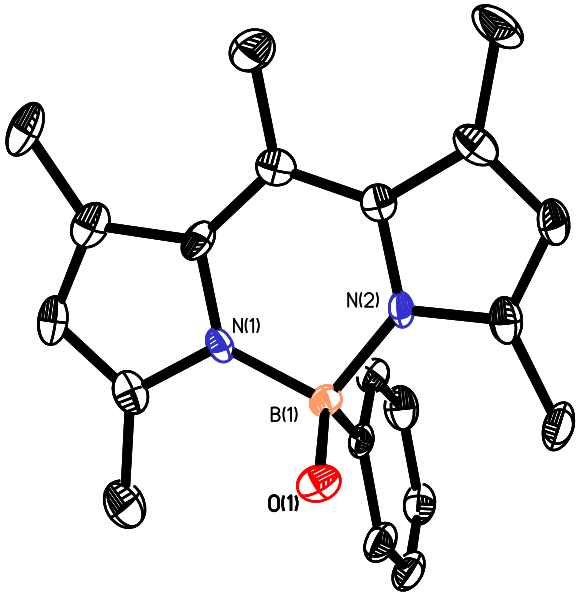

Figure 92: ORTEP view of **107**, (50 % ellipsoids, H-atoms are omitted for clarity).

Compound **107** was easily converted into the BODIPY-phenylboron fluoride species **108** by treatment with KHF_2 in THF (Figure 91). Compound **108** was obtained as an orange powder and single crystals suitable for X-ray diffraction analysis were obtained by cooling a concentrated EtOAc solution to -40 °C for several days (Figure 93, Table 23). Compound **108** crystallizes in the triclinic space group $P\bar{1}$. The B(1)-F(1) distance of 1.410(3) Å is within the norm of four-coordinate boron-fluorine bonds (ca. 1.45 Å), and the ^{19}F NMR spectrum features a broad signal at -174 ppm which is characteristic of many fluoroborate species. The boron atom adopts a tetrahedral center, which is further substantiated by the ^{11}B NMR chemical shift of 2.3 ppm.

Compound **108** is remarkably stable, and attempts at fluoride abstraction were unsuccessful even when strong silylium cations were used. Fluoride abstraction using Me_3Si-OTf or $[Et_3Si][B(C_6F_5)_4]$ resulted in unidentified products.

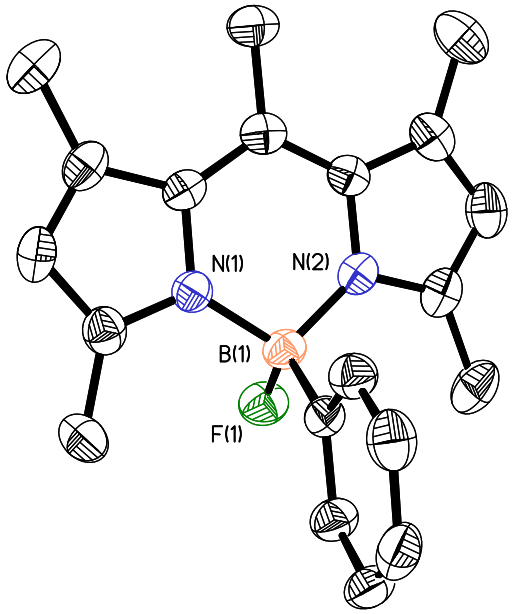

Figure 93: ORTEP view of **108**, (50 % ellipsoids, H-atoms omitted for clarity).

Faced with these difficulties, we sought compounds with increased electron density at the boron atom. Thus, the methodology used to synthesize compounds **106**-**108** was employed to prepare electron rich BODIPY species; namely, the 4-dimethylaminophenyl substituted BODIPY derivatives, **109** and **110** . Electron donation from the dimethylamino moiety should stabilize the corresponding cationic BODIPY derivative, facilitating halide abstraction.

Table 23: Crystal data, data collection, and structure refinement for **106**, **107**, and **108**.

	106	**107**	**108**
		Crystal data	
Formula	$C_{20}H_{22}BClN_2$	$C_{20}H_{23}BON_2$	$C_{20}H_{22}BFN_2$
M_r	336.66	318.21	320.21
crystal size (mm^3)	0.15 × 0.14 × 0.09	0.21 × 0.17 × 0.14	0.16 × 0.13 × 0.09
crystal system	Triclinic	Monoclinic	Triclinic
Space group	$P\bar{1}$	$P2_1$	$P\bar{1}$
a (Å)	7.667(2)	10.158(3)	7.561(3)
b (Å)	10.529(4)	14.479(5)	10.331(4)
c (Å)	11.808(3)	11.622(4)	11.652(4)
α (°)	92.059(4)		80.457(6)
β (°)	102.968(3)	98.302(7)	78.295(6)
γ (°)	111.319(3)		72.473(6)
V ($Å^3$)	858.0(4)	1691.4(9)	844.6(5)
Z	2	4	2
ρ_{calc} (g cm^{-3})	1.303	1.250	1.259
μ (mm^{-1})	0.226	0.076	0.081
F(000)	356	680	340
		Data Collection	
T (K)	110(2)	110(2)	110(2)
scan mode	ω	ω	ω
hkl range	-10 → +10, -13 → +13 -15 → +15	-7 → +10, -14 → +14, -11 → +11	-8 → +8, -11 → +11, -13 → +13
measd reflns	10015	6161	7567
unique reflns [R_{int}]	4010 [0.0315]	3852 [0.0701]	2658 [0.0352]
reflns used for refinement	4010	3852	2658
		Refinement	
refined parameters	217	415	217
GOF on F^2	1.008	1.008	1.004
R1,[a] wR2[b] all data	0.0653, 0.1807	0.1177, 0.1700	0.0745, 0.1847
ρ_{fin} (max/min) (e $Å^{-3}$)	0.641 -0.669	0.412, -0.327	0.428, -0.328

[a] $R1 = \sum||Fo| - |Fc||/\sum|Fo|$. [b] $wR2 = \{[\sum w(Fo^2 - Fc^2)^2]/[\sum w(Fo^2)^2]\}^{1/2}$.

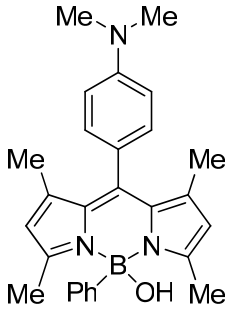

109

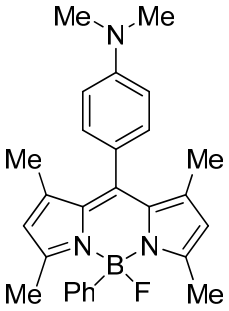

110

Compounds **109** and **110** were prepared in good yield, and single crystals could be obtained from cooling an EtOAc solution. Compound **109** crystallizes in the monoclinic space group $P2_1/c$ (Figure 94,Table 24). One important feature regarding the structure of **109** is the orientation of the 4-dimethylaminophenyl substitutent. The arene ring of this moiety is perpendicular to the π-system of the BODIPY backbone (Figure 94), indicating that the lone pair on the nitrogen atom, N(3), is not delocalized into the BODIPY system. This observation is further supported by the geometry about N(3) which exhibits a small degree of pyramidalization ($\Sigma_{(C\text{-}N\text{-}C)} = 351.2°$) when compared 4-$Me_2N$-($C_6H_4$)-$BMes_2$ whose $\Sigma_{(C\text{-}N\text{-}C)} = 360°$.[148] Also in agreement with this assessment is the environment at the boron center, which is nearly identical to that observed in compounds **107** and **108**.

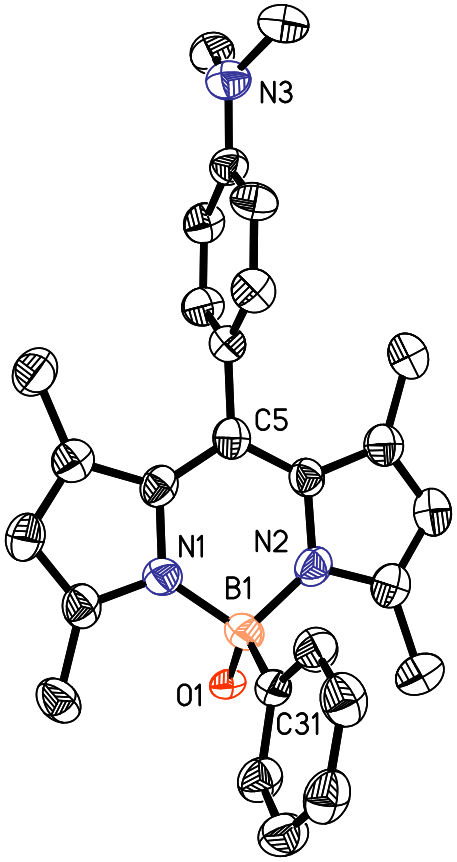

Figure 94: ORTEP of **109**, (50% ellipsoids, H-atoms are omitted for clarity).

Compound **110** also crystallizes in the monoclinic space group $P2_1/c$ (Figure 95, Table 24) and is structurally very similar to **109**. The 4-dimethylaminophenyl moiety is again perpendicular to the π-system of the BODIPY backbone (Figure 95), and the nitrogen atom N(3) exhibits a small degree of pyramidalization ($\Sigma_{(C\text{-}N\text{-}C)}$ = 351.2°). As in **109** there is no appreciable perturbation observed in the boron environment.

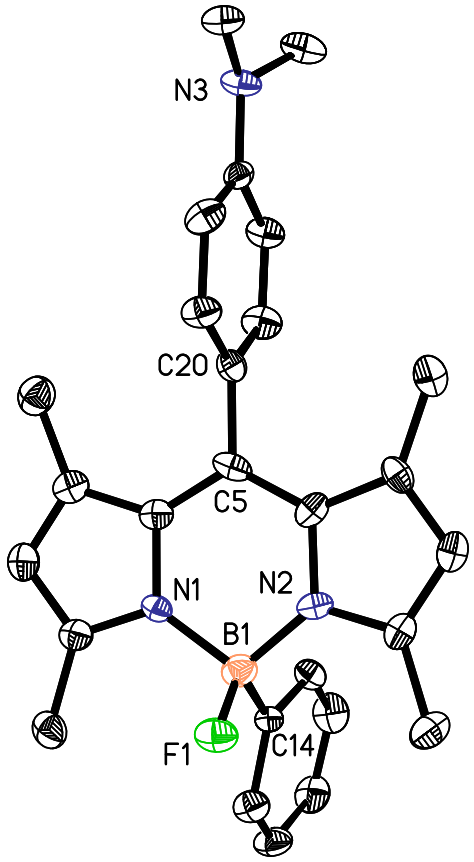

Figure 95: ORTEP of **110**, (50% ellipsoids, H-atoms are omitted for clarity).

Compound **110** exhibits all of the expected ^{1}H NMR resonances, and the ^{19}F signal appears at -173 ppm which is close to that of **108**. Based on the observation that the nitrogen lone pair is not delocalized greatly into the BODIPY π-system, it can be concluded that halide abstraction to the corresponding cationic species will not be greatly facilitated when compared to compounds **106** and **108**. Indeed, attempts to abstract the fluoride from **110** resulted, again, in intractable mixtures of unidentifiable compounds.

Table 24: Crystal data, data collection, and structure refinement for **109** and **110**.

	109	**110**
	Crystal data	
Formula	$C_{27}H_{30}BON_3$	$C_{27}H_{29}BFN_3$
M_r	423.35	425.34
crystal size (mm^3)	0.31 × 0.25 × 0.22	0.21 × 0.16 × 0.14
crystal system	Monoclinic	Monoclinic
Space group	$P2_1/c$	$P2_1/c$
a (Å)	14.482(7)	14.426(5)
b (Å)	15.441(8)	15.417(5)
c (Å)	10.881(5)	10.832(4)
α (°)		
β (°)	109.647(10)	109.705(4)
Γ (°)		
V ($Å^3$)	2291.5(19)	2268.0(13)
Z	4	4
ρ_{calc} (g cm^{-3})	1.227	1.246
μ (mm^{-1})	0.075	0.079
F(000)	904	904
	Data Collection	
T (K)	110(2)	110(2)
scan mode	ω	ω
hkl range	-13 → +13, -14 → +14, -9 → +6	-13 → +13, -14 → +14, -9 → +9
measd reflns	6085	11607
unique reflns [R_{int}]	1841 [0.0764]	1821 [0.0831]
reflns used for refinement	1841	1821
	Refinement	
refined parameters	289	289
GOF on F^2	1.006	1.008
R1,[a] wR2[b] all data	0.0998, 0.1912	0.0885, 0.1487
ρ_{fin} (max/min) (e $Å^{-3}$)	0.355 -0.332	0.419, -0.329

[a] $R1 = \sum||Fo| - |Fc||/\sum|Fo|$. [b] $wR2 = \{[\sum w(Fo^2 - Fc^2)^2]/[\sum w(Fo^2)^2]\}^{1/2}$.

5.4 Conclusions

In this chapter we described a halide abstraction methodology for the preparation of the BODIPY-boronium cation [**104**]OTf. This novel cation was synthesized by fluoride abstraction from the BODIPY-BF_2 complex **102** using TMSOTf in the presence of a neutral donor ligand (DMAP). Using [**104**]OTf, we then developed a fluoride assay which elicits a turn-on fluorescence response in the presence of this anion.

We also described new synthetic routes to mono-arylated BODIPY derivatives. A series of five new BODIPY compounds were prepared utilizing this synthetic methodology, and their conversion into cationic BODIPY-borenium derivatives was investigated. It was shown that the attempted halide abstraction of these compounds **106**, **108** and **110** led to solutions of intractable unidentified compounds. These reactions most likely do not proceed cleanly, as the corresponding cationic derivatives are not stable.

5.5 Experimental

General Considerations. 3,5,3',5',6-Pentamethylpyrromethenehydrochloride[135-137], **105**, and 1,3,5,7,8-pentamethylpyrromethene-borondifluoride[179], **102,** were prepared according to a literature procedure. Sodium hydride and dichlorophenyl borane were purchased from Aldrich and used without further purification. Potassium hydrogen difluoride (KHF_2) was purchased from Alfa Aesar. Et_2O and THF were dried by reflux over Na/K. Toluene, hexane and dichloromethane were dried by passing through a column charged with activated alumina. Air-sensitive compounds were handled under a N_2 atmosphere using standard Schlenk and glovebox techniques. UV-vis spectra were recorded on an Ocean Optics ISS-UV/VIS spectrometer equipped with an Ocean Optics USB4000 detector. Elemental analyses were performed at Atlantic Microlab (Norcross, GA). NMR spectra were recorded on a Varian Unity Inova 400 FT NMR (399.59 MHz for ^{1}H, 375.99 MHz for ^{19}F, 128.19 MHz for ^{11}B, 100.45 MHz for ^{13}C) spectrometer at ambient temperature. Chemical shifts δ are given in ppm, and are referenced against external Me_4Si (^{1}H, ^{13}C), $BF_3{\cdot}Et_2O$ (^{11}B) and $CFCl_3$ (^{19}F). Melting points were measured on samples in sealed capillaries and are uncorrected.

Crystallography. Dark red single crystals of **106** could be obtained by slow evaporation of a toluene solution. Single crystals of **107**, **108**, **109** and **110** could be obtained by cooling a concentrated EtOAc solutions to -40 °C for several hours. Single crystals of **103** were obtained by cooling a concentrated toluene solution to -40 °C for

several days, whereas crystals of [**104**]OTf were obtained by vapor diffusion of hexanes into a concentrated chloroform solution. The crystallographic measurement of **106**, and **110** were performed using a Bruker APEX-II CCD area detector diffractometer, with a graphite-monochromated Mo-K_α radiation (λ = 0.71069 Å); and compounds **103**, **104**, **107**, **108** and **109** were measured using a Bruker SMART-97 CCD instrument. A specimen of suitable size and quality was selected and mounted onto glass fiber with apiezon grease. The structure was solved by direct methods, which successfully located most of the non-hydrogen atoms. Subsequent refinement on F^2 using the SHELXTL/PC package (version 5.1) allowed location of the remaining non-hydrogen atoms.

Synthesis of 103. **102** (50 mg, 0.191 mmol) was dissolved in $CDCl_3$ (0.5 mL) and treated with TMSOTf (0.069 mL, 0.382 mmol). Formation of **103** was quantitative by NMR. ^{1}H NMR (399.57 MHz, $CDCl_3$) δ 2.42 (s, 6H, C*H*$_3$-dipyrrin), 2.49 (s, 6H, C*H*$_3$-dipyrrin), 2.60 (s, 3H, C*H*$_3$-dipyrrin), 6.11 (s, 2H, C*H*-dipyrrin). ^{19}F NMR (375.97 MHz, $CDCl_3$) δ -78.05 (s, OTf), -148.96 (bs, B-*F*). ^{11}B NMR (128.20 MHz, $CDCl_3$) δ 0.92 (bs).

Synthesis of [104]OTf. **102** (100 mg, 0.382 mmol) dissolved in toluene (5 mL) was treated with TMSOTf (0.138 mL, 0.763 mmol) and DMAP (93.1 mg, 0.763 mmol). The resulting mixture was heated to 80 °C and stirred for 12 hours. The solvent was then removed *in vacuo* and the residue was disolved in dichloromethane (30 mL) and washed with distilled water (30 mL). After drying over $MgSO_4$, reduction of the volume to 5 mL followed by addition of hexanes (15 mL) resulted in the precipitation of an orange solid. This solid was washed with hexanes (3 x 5 mL) and dried *in vacuo* to afford [**104**]OTf (161 mg, 82% yield). ^{1}H NMR (499.91 MHz, $CDCl_3$) δ 2.12 (s, 6H, C*H*$_3$-dipyrrin), 2.47 (s, 6H, C*H*$_3$-dipyrrin), 2.73 (s, 3H, C*H*$_3$-dipyrrin), 3.19 (s, 6H, N(C*H*$_3$)$_2$), 6.07 (s, 2H, C*H*-dipyrrin), 6.86 (d, ^3J = 7.5 Hz, 2H, C*H*-DMAP), 7.89 (d, ^3J = 7.5 Hz, 2H, C*H*-DMAP). ^{13}C NMR (125.7 MHz, $CDCl_3$) δ 14.63, 16.86, 17.54, 107.55, 122.98, 132.51, 141.64, 143.98, 153.70, 156.60. ^{19}F NMR (375.99 MHz, $CDCl_3$) δ -

78.09 (OTf), -167.71 (q, $^{1}J_{F\text{-}B}$ = 37 Hz). ^{11}B NMR (128.20 MHz, $CDCl_3$) δ 0.91 (d, $^{1}J_{B\text{-}F}$ = 37 Hz). [**104**]OTf is hygroscopic and water could not be completely removed for elemental analysis. (Found: C, 49.87; H, 5.13. $C_{22}H_{29}BF_4N_4SO_4$ ([**104**]OTf • H_2O) requires C, 49.63; H, 5.49%).

Synthesis of 106. **105** (100 mg, 0.40 mmol) was dissolved in 5 mL of a Et_2O/hexanes (1:1, v:v) solvent mixture. To this solution, NaH (20 mg, 0.83 mmol) was added slowly at room temperature in a drybox. The suspension was stirred overnight in the drybox, the solvent was then removed *in vacuo*. The resulting residue was extracted with hexanes, filtered, and the solvent was again removed *in vacuo*. The sodium salt of **1** was then taken into a drybox, dissolved in toluene (10 mL) and $PhBCl_2$ (380 mg, 2.4 mmol) was added slowly, which resulted in the appearance of a green fluorescence. The solution was stirred in the drybox overnight then filtered over Celite. Slow evaporation of the toluene produced a crop of dark red crystals of **106** (75 mg, 56 % yield, *not optimized*). ^{1}H NMR (399.59 MHz, $CDCl_3$): δ 1.93 (s, 6H, dipyrrin-CH_3), 2.44 (s, 6H, dipyrrin-CH_3), 2.67 (s, 3H, dipyrrin-CH_3), 5.97 (s, 2H, dipyrrin-C*H*), 7.17-7.22 (m, 3H, phenyl-C*H*), 7.55 (d, 2H, ^{2}J = 8.0 Hz, phenyl-C*H*). ^{13}C NMR (100. 48 MHz, $CDCl_3$): δ 16.36, 16.73, 17.74, 122.60, 126.47, 126.93, 131.45, 133.29, 140.24, 141.38, 154.73. B-*C* peak not observed. ^{11}B NMR (128.20 MHz, $CDCl_3$): δ 2.53.

Synthesis of 107. A freshly prepared solution of **106** (prepared using 100 mg of **105**) in toluene (10 mL) was quickly eluted over a short plug of silica gel. The solvent was removed under reduced pressure to afford an orange-red residue, which was recrystallized at -40 °C in EtOAc (5 mL). The resulting red-orange microcrystalline solid was collected by filtration and dried *in vacuo* to give **107** (69 mg, 97 % yield). ^{1}H NMR (399.59 MHz, $CDCl_3$): δ 2.18 (s, 6H, dipyrrin-CH_3), 2.43 (s, 6H, dipyrrin-CH_3), 2.65 (s, 3H, dipyrrin-CH_3), 5.93 (s, 2H, dipyrrin-C*H*), 7.07(m, 1H, phenyl-C*H*), 7.13 (t, 2H, ^{2}J = 6.0 Hz, phenyl-C*H*), 7.31 (d, 2H, ^{2}J = 7.0 Hz, phenyl-C*H*). ^{13}C NMR (100. 48 MHz, $CDCl_3$): δ 16.47, 16.81, 17.77, 122.54, 126.51, 126.90, 131.65, 133.49, 140.54,

141.41, 154.34. B-*C* peak not observed. ^{11}B NMR (128.20 MHz, $CDCl_3$): δ 0.97. Anal. Calcd for $C_{20}H_{24}BO_{1.5}N_2$ (**107** 0.5 H_2O): C, 73.41; H, 7.39. Found: C, 73.77; H, 7.41.

Synthesis of 108. A THF (5 mL) solution of **107** (50 mg, 0.157 mmol) was treated with KHF_2 (74 mg, 0.943 mmol) and stirred for 24 hours. The reaction mixture was then quenched with water (10 mL) and extracted with dichloromethane (3 × 5 mL). The organic layers were combined, dried over $MgSO_4$, and filtered. The solvent was removed under reduced pressure and the residue was recrystallized at -40 °C from EtOAc (5 mL) to afford **108** as a bright orange crystalline solid (46 mg, 91% yield). ^{1}H NMR (399.59 MHz, $CDCl_3$): δ 2.15 (s, 6H, dipyrrin-C*H*$_3$), 2.42 (s, 6H, dipyrrin-C*H*$_3$), 2.66 (s, 3H, dipyrrin-C*H*$_3$), 5.94 (s, 2H, dipyrrin-C*H*), 7.10(t, 1H, ^2J = 4.5 Hz, phenyl-C*H*), 7.15 (t, 2H, ^2J = 7.0 Hz, phenyl-C*H*), 7.31 (d, 2H, ^2J = 7.0 Hz, phenyl-C*H*). ^{13}C NMR (100. 48 MHz, $CDCl_3$): δ 16.50, 16.81, 17.79, 122.49, 126.53, 126.92, 131.61, 133.51, 140.52, 141.44, 154.38. B-*C* peak not observed. ^{19}F NMR (375.97 MHz, $CDCl_3$): δ -174.17 ^{11}B NMR (128.20 MHz, $CDCl_3$): δ 2.51. Anal. Calcd for $C_{20}H_{22}BFN_2$: C, 75.02; H, 6.93. Found: C, 74.95; H, 6.96.

Synthesis of 109. 2,4-dimethylpyrrole (298 mg, 3.13 mmol) was dissolved in 300 mL of dichloromethane. To this solution, 4-dimethylaminobenzaldehyde (381 mg, 2.55 mmol) was added followed by two drops of trifluoroacetic acid. The resulting solution became dark red, and was stirred for three hours at room temperature. The red solution was then treated with *p*-chloranil (491 mg, 2.00 mmol) in dichloromethane (250 mL) and stirred for 15 minutes. Dry triethylamine (1.0 mL, 13.6 mmol) was then added followed by dropwise addition of phenylboron dichloride (1.49 g, 9.38 mmol) in Et_2O (10 mL) which resulted in a green fluorescent solution. The solution was stirred overnight then quenched with water (2 × 300 mL). After each wash the organic layer was separated and then dried over $MgSO_4$. The solvent was removed *in vacuo* and then chromatographed on silica eluting with chloroform until all of the green fluorescent material had eluted (followed using a hand-held UV lamp). The solvent was again

removed under reduced pressure. This residue was subjected to column chromatography over a small column of silica gel using toluene:hexanes (80:20 v/v) as the eluent (followed using a UV lamp). The fractions with the green fluorescence were combined and the solvent removed to afford **109** as an orange solid (310 mg, 29% yield). ^{1}H NMR (399.59 MHz, $CDCl_3$): δ 1.49 (s, 6H, dipyrrin-CH_3), 2.17 (s, 6H, dipyrrin-CH_3), 3.02 (s, 6H, N-CH_3), 5.85 (s, 2H, dipyrrin-C*H*), 6.80 (t, 2H, ^{2}J = 8.5 Hz, phenyl-C*H*), 7.09-7.25 (m, 5H, phenyl-C*H*), 7.42 (d, 2H, ^{2}J = 7.0 Hz, phenyl-C*H*). ^{13}C NMR (100. 48 MHz, $CDCl_3$): δ 16.36, 16.73, 17.74, 122.60, 126.47, 126.93, 131.45, 133.29, 140.24, 141.38, 154.73. B-*C* peak not observed. ^{11}B NMR (128.20 MHz, $CDCl_3$): δ 2.53.

Synthesis of 110. 110 Was prepared following the same method used to prepare **108**, starting from compound **109** (100 mg). (86 mg, 86% yield). ^{1}H NMR (399.59 MHz, $CDCl_3$): δ 1.49 (s, 6H, dipyrrin-CH_3), 2.16 (s, 6H, dipyrrin-CH_3), 3.02 (s, 3H, dipyrrin-CH_3), 5.85 (s, 2H, dipyrrin-C*H*), 6.80 (t, 2H, ^{2}J = 8.5 Hz, phenyl-C*H*), 7.09-7.25 (m, 5H, phenyl-C*H*), 7.42 (d, 2H, ^{2}J = 7.0 Hz, phenyl-C*H*). ^{13}C NMR (100. 48 MHz, $CDCl_3$): δ 16.36, 16.73, 17.74, 122.60, 126.47, 126.93, 131.45, 133.29, 140.24, 141.38, 154.73. B-*C* peak not observed. ^{19}F NMR (375.97 MHz, $CDCl_3$): δ -173.9. ^{11}B NMR (128.20 MHz, $CDCl_3$): δ 2.51.

CHAPTER VI

COLORIMETRIC SILICON REAGENTS FOR THE DETECTION OF FLUORIDE ANIONS AT PHYSIOLOGICAL PH

6.1 Introduction

This chapter is concerned with the development of a new class of receptors for the molecular recognition of fluoride. The development of sensors for fluoride anions, which are competent in aqueous environments, continues to attract a great deal of attention. Fluoride, primarily used in dental health and in the treatment of osteoporosis[110], is a biologically beneficial anion. However, at high doses, this anion may become toxic, leading to diseases such as skeletal fluorosis.[111] Therefore, the development of methods for the recognition of fluoride anions in water at neutral or physiological pH remains a topical objective. Under these conditions, the fluoride anion is efficiently hydrated, (ΔH_{hyd} = -504 kJ mol^{-1}),[6] impeding its capture by molecular receptors and its reaction with electrophilic reagents.[22,113] One of the current approaches of fluoride recognition that has been successfully implemented in organic solvents relies on the fluoride induced deprotection of silylated alcohols.[104,105,106,107] To our knowledge, however, these reactions have only been carried out successfully in organic solvents or aqueous solution, but not in pure water.

As indicated by our recent reports on boron-based fluoride receptors, the incorporation of cationic moieties into the receptor results in a drastic increase of the fluoride ion affinity, making fluoride binding in water possible. Hoping to benefit from similar effects, we have now decided to investigate cationic examples of silicon-based receptors whose reaction with fluoride in water could be facilitated by favorable Coulombic attractions. In this chapter we report the synthesis of a series of cationic silyl ethers, as well as their reaction with fluoride in organic solvents and water. Also included are some efforts aimed at synthesizing neutral Lewis acidic fluorosilane receptors for fluoride sensing applications.

6.2 Synthesis and structures of cationic silyl ether derivatives

The first series of cationic silyl ethers are reminiscent of work carried out by Lakowicz and coworkers on quinolinium boronic acids.[91] Indeed the quinolinium silyl ethers, [**111**]$^+$, [**112**]$^+$ and [**113**]$^+$ could be prepared as triflate salts in modest yield over two steps. The synthesis of these species began with silylation of 8-hydroxyquinoline followed by methylation of the nitrogen atom with methyl triflate (MeOTf) (Figure 96).

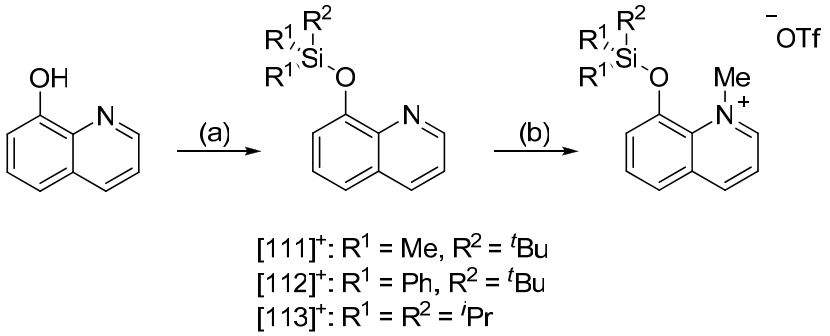

Figure 96: Synthesis of quinolinum silyl ether derivatives [**111**]OTf, [**112**]OTf and [**113**]OTf; (a): R_3SiCl, imidazole, DCM 12 h RT; (b): MeOTf, Et_2O 12 h RT.

Compounds [**111**]$^+$-[**113**]$^+$ are air and water stable salts which can be stored on the benchtop for extended periods of time. Compound [**111**]$^+$ exhibits all of the salient ^{1}H NMR signals and is especially informative as it confirms the presence of the ^{t}BuMe$_2$Si (TBDMS) group. The methyl substituent on the cationic nitrogen appears at 4.94 ppm which is characteristic of *N*-methylquinolinium species. The crystal structure of [**111**]OTf has also been determined. This salt crystallizes in the in *C*2/c space group (Figure 97, Table 25). Inspection of the structure confirms the proposed connectivity and also indicates that there are no unusually short contacts between the anion and cation.

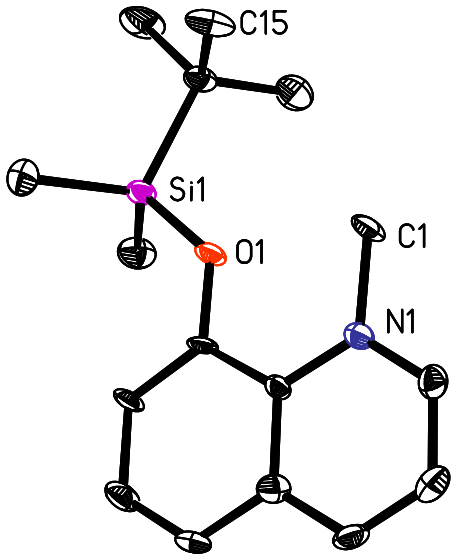

Figure 97: ORTEP view of [**111**]$^+$ in [**111**]OTf, (50 % ellipsoids, H-atoms omitted for clarity).

The triflate salts [**112**]OTf and [**113**]OTf have also been characterized by heteronuclear NMR spectroscopy and single crystal X-ray diffraction analysis. The proton NMR spectra confirm the presence of the *t*-butyl-diphenyl silyl (TBDPS) and triisopropyl silyl (TIPS) moieties present in [**112**]$^+$ and [**113**]$^+$ respectively. Compound [**112**]OTf crystallizes in the monoclinic space group $P2_1/c$ (Figure 98, Table 25) and [**113**]OTf crystallizes in the triclinic space group $P\bar{1}$ (Figure 99, Table 25).

The structure of [**112**]$^+$ is nearly identical to that observed in [**111**]$^+$ with the exception of the two phenyl groups on the silicon atom instead of methyl groups. The *t*-butyl group is pointing upward and away from the quinoline backbone as in [**111**]$^+$, and there are also no short contacts observed between the cation and the triflate counter anion in this structure. Likewise, the crystal structure of [**113**]$^+$ reveals no short contacts between the cation and anion.

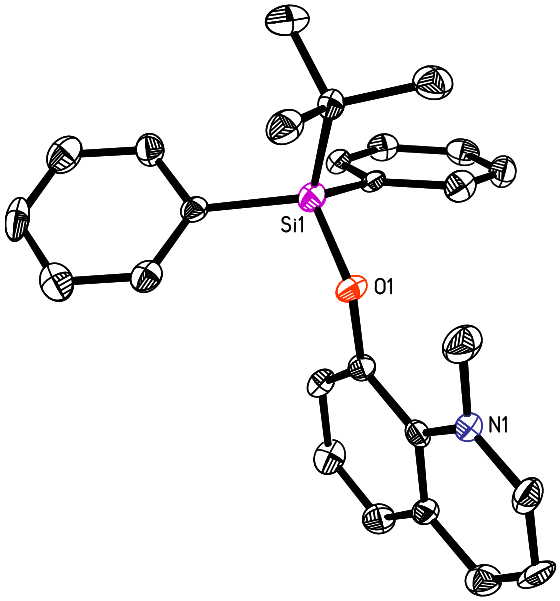

Figure 98: ORTEP view of [**112**]$^{+}$ in [**112**]OTf, (50 % ellipsoids, H-atoms omitted for clarity).

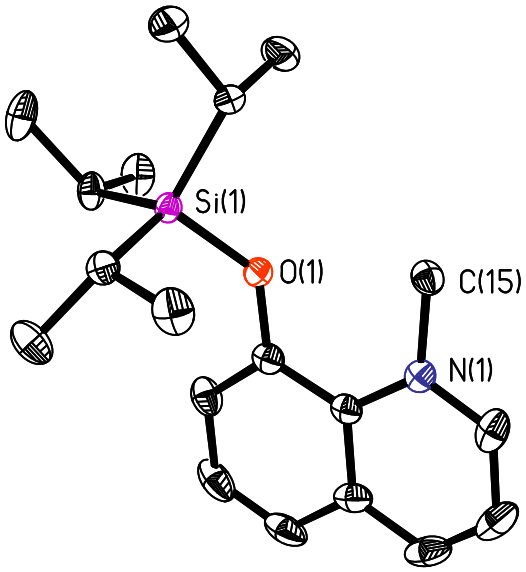

Figure 99: ORTEP view of [**113**]$^{+}$ in [**113**]OTf, (50 % ellipsoids, H-atoms omitted for clarity).

Table 25: Crystal data, data collection and structure refinement for [**111**]OTf, [**112**]OTf and [**113**]OTf.

	[**111**]OTf	[**112**]OTf	[**113**]OTf
	Crystal data		
Formula	$C_{17}H_{24}F_3NO_4SSi$	$C_{27}H_{28}F_3NO_4SSi$	$C_{20}H_{30}F_3NO_4SSi$
M_r	423.52	547.65	465.60
crystal size (mm^3)	0.18 × 0.16 × 0.13	0.18 × 0.15 × 0.13	0.35 × 0.33 × 0.28
crystal system	Monoclinc	Monoclinic	Triclinic
Space group	*C*2/c	$P2_1/c$	$P\bar{1}$
a (Å)	20.871(19)	11.8447(15)	8.7035(12)
b (Å)	10.595(8)	12.1411(15)	11.3451(15)
c (Å)	18.134(13)	18.199(2)	12.3874(17)
α (°)			110.643(2)
β (°)	95.45(3)	98.158(3)	94.214(2)
γ (°)			97.228(3)
V ($Å^3$)	3992(6)	2590.7(6)	1126.3(3)
Z	8	4	2
ρ_{calc} (g cm^{-3})	1.409	1.404	1.373
μ (mm^{-1})	0.272	0.228	0.248
F(000)	1776	1144	492
	Data Collection		
T (K)	110(2)	110(2)	110(2)
scan mode	ω	ω	ω
hkl range	-22 → +22, -10 → +11 -14 → +19	-10 → +10, -10 → +11, -15 → +16	-11 → +8, -15 → +10, -13 → +16
measd reflns	8153	7097	7114
unique reflns [R_{int}]	2768 [0.1624]	2087 [0.0487]	5181 [0.0397]
reflns used for refinement	2768	2087	5181
	Refinement		
refined parameters	244	334	271
GOF on F^2	1.006	1.006	1.006
R1,[a] wR2[b] all data	0.0983, 0.1195	0.0425, 0.0585	0.0653, 0.1114
ρ_{fin} (max/min) (e $Å^{-3}$)	0.489, -0.555	0.159, -0.201	0.489, -0.355

[a] $R1 = \sum||Fo| - |Fc||/\sum|Fo|$. [b] $wR2 = \{[\sum w(Fo^2 - Fc^2)^2]/[\sum w(Fo^2)^2]\}^{1/2}$.

Compounds [**111**]$^+$-[**113**]$^+$ are partially soluble in water at low concentrations, but suffer from slow hydrolysis of their respective silyl ether moieties over a period of several hours. Remarkably, all three cations give rise to a colorimetric response in the presence of fluoride anions in chloroform, changing from pale-yellow to deep-purple. This reaction can be monitored by ^{1}H NMR, which exhibits the formation of the fluorosilane due to deprotection of the alcohol functionality. In water however, only

compound [**111**]$^+$ undergoes a clean fluoride induced deprotection. This has led us to investigate the interaction of [**111**]$^+$ with fluoride ions in water at physiological pH (7.5).

We have also investigated the fluoride sensing of an ammonium-naphthlenediyl silyl ether in physiological conditions. Compound [**114**]$^+$ (synthesized by Sirinan Kulchat) could be obtained as a triflate salt in two steps by methylation of 5-(dimethylamino)-1-naphthalenol with MeOTf followed by treatment of the resulting ammonium salt with ^{t}BuMe$_2$SiCl (TBDMSCl) in acetonitrile with imidazole as a base. This salt is an air stable solid which can be stored for extended periods of time. [**114**]OTf has been fully characterized by elemental analysis and NMR spectroscopy. The ^{1}H NMR spectrum is especially informative, confirming the presence of the TBDMS group. The nitrogen bound methyl groups are also readily detected at 4.08 ppm in $CDCl_3$.

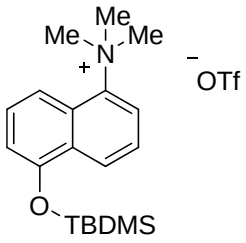

[114]OTf

6.3 Theoretical investigation of [**111**]$^+$ and [**114**]$^+$

The structures of [**111**]$^+$ and [**114**]$^+$ have been optimized using DFT methods at the B3LYP/6-31G* by a postdoctoral researcher in the Gabbaï group, Dr. Chammi Palehepitiya Gamage. In the case of [**111**]$^+$, the computed structure closely matched that observed in the crystal. The electrostatic potential maps of these derivatives indicate an accumulation of positive character around the quaternized nitrogen atom (Figure 100).

In the case of [**111**]$^+$, this positive area is located in closer proximity to the silicon center than in [**114**]$^+$.

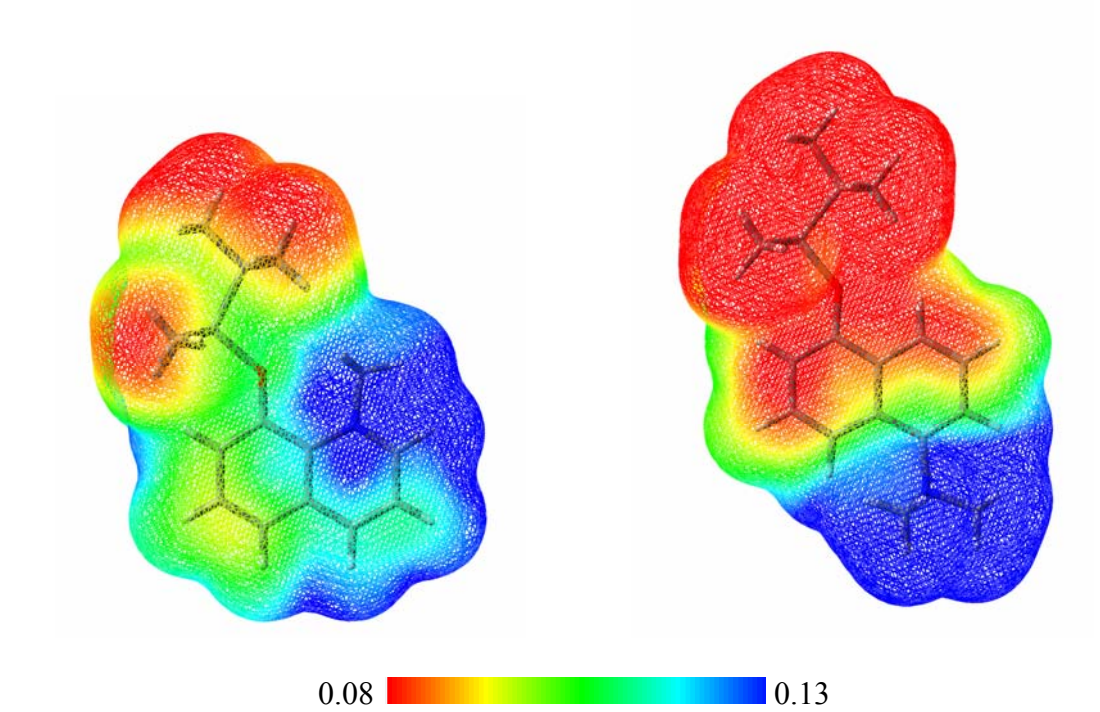

Figure 100: Electrostatic potential maps of [**111**]$^+$ (left) and [**114**]$^+$ (right).

6.4 Fluoride sensing studies of [**111**]$^+$ and [**114**]$^+$

Both of these compounds undergo rapid desilylation when treated with TBAF in chloroform. These reactions can be conveniently monitored by ^{1}H NMR spectroscopy which indicates formation of TBDMSF and the corresponding zwitterions **115** and **116** (Figure 101). In both cases, this reaction results in the development of a distinct color, caused by the absorbance of the zwitterions **115** and **116**, respectively. In turn, [**111**]$^+$ and [**114**]$^+$ are useful colorimetric indicators for fluoride in $CHCl_3$. The reaction can be followed spectrometrically which confirms the appearance of new absorption bands corresponding to the zwitterions **115** and **116** (Figure 102).

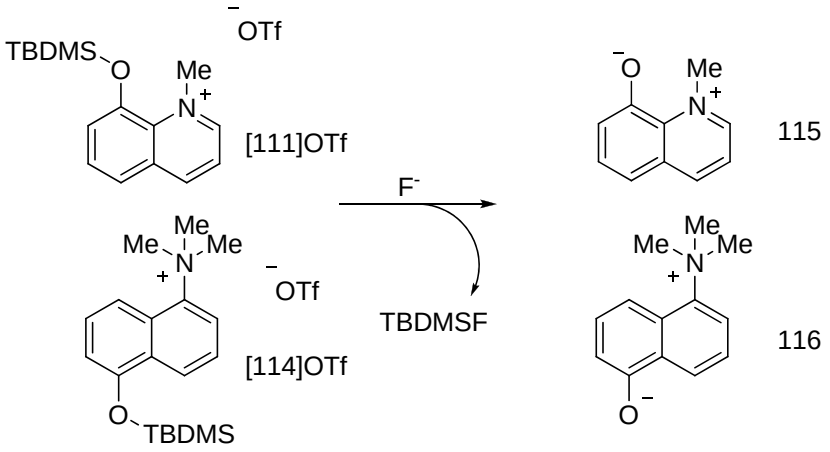

Figure 101: Fluoride induced silyl ether deprotection and formation of zwitterions **115** and **116**.

Next, we decided to determine if this desilylation would also occur in water. In the case of [**114**]$^+$, only a sluggish desilylation reaction was observed at pH 7.5 suggesting that this cationic silyl ether may not be ideally suited for sensing fluoride in water. In the case of [**111**]$^+$, addition of KF to an aqueous solution of [**111**]OTf at pH 7.5 induces a rapid color change from pale-yellow to dark yellow-orange which was assigned to the formation of zwitterion **115**. This assignment was confirmed by comparison of: i) the ^{1}H NMR spectrum of pure **115** and that of a mixture of [**111**]OTf and KF in D_2O; ii) the absorption spectrum of pure **115** and that of a mixture of [**111**]OTf and KF in water at pH 7.5 (Figure 103). As indicated by a potentiometric titration, the pKa of **115** is equal to 6.8±2 indicating that the zwitterionic form indeed dominates at pH 7.5. The low reactivity of [**114**]$^+$ toward fluoride when compared to [**111**]$^+$ may be explained by considering the electrostatic potential maps of both cations. In [**111**]$^+$, the more positively charged part of the surface is located near the silicon atom and may help guide the fluoride anion to the reaction center.

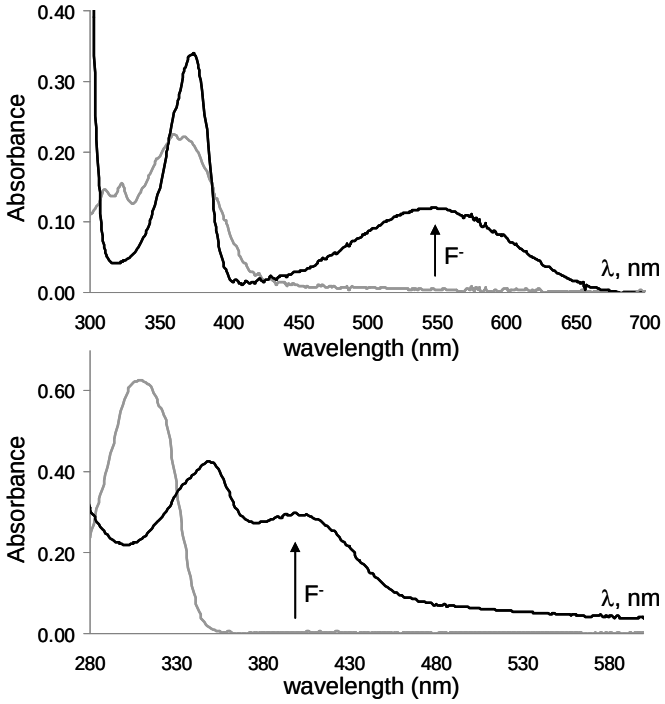

Figure 102: UV-vis spectral changes of a solution of [**111**]$^+$ (top) and [**114**]$^+$ (bottom) in $CHCl_3$ upon addition of fluoride anions.

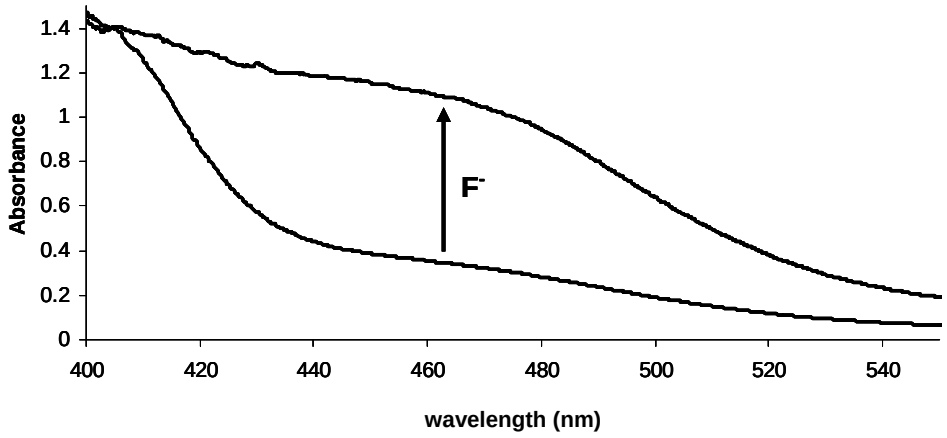

Figure 103: UV-vis spectral changes of a solution of [**111**]$^+$ in pH 7.5 buffered water upon addition of fluoride anions.

Kinetics studies carried out at pH 7.5 (EPPS 10mM) indicate that the desilylation of [**111**]$^+$ follows second-order kinetics with a first-order dependence in both [**111**]$^+$ and [F^-] with a second order rate constant k_2 = 6.00±0.6 $M^{-1}s^{-1}$. Hydroxide-induced desilylation also occurs. However, it is relatively slow and does not preclude the use of [**111**]$^+$ as an indicator for fluoride in water. For example, a 1 mM solution of F^- and [**111**]$^+$ at pH 7.5 quickly develops a dark yellow-orange color within 2 minutes, while the control solution containing only [**111**]$^+$ remains colorless. Moreover, addition of Cl^-, Br^-, I^-, NO_3^- or HSO_4^- to the control solution does not accelerate the desilylation reaction, suggesting that [**111**]$^+$ is a selective indicator for fluoride.

6.5 Synthetic attempts toward a novel, hybrid amide-fluorosilane fluoride sensor

We have also attempted to determine if hydrogen-bond donor groups can aid a Lewis acidic fluorosilane moiety in the complexation of fluoride anions via chelation. To this end, we have attempted to synthesize an *ortho*-fluorosilane substituted trifluoroacetanilide. In our efforts, we have been able to synthesize the siloxane derivative, **117**, and we have converted it into the corresponding fluorosilane **118**, which has been characterized by ^1H and ^{19}F NMR (Figure 104). Compound **117** was synthesized by dilithiation of *o*-bromotrifluoroacetanilide followed by treatment with chlorodimethylsilane ($HSiMe_2Cl$) in THF.

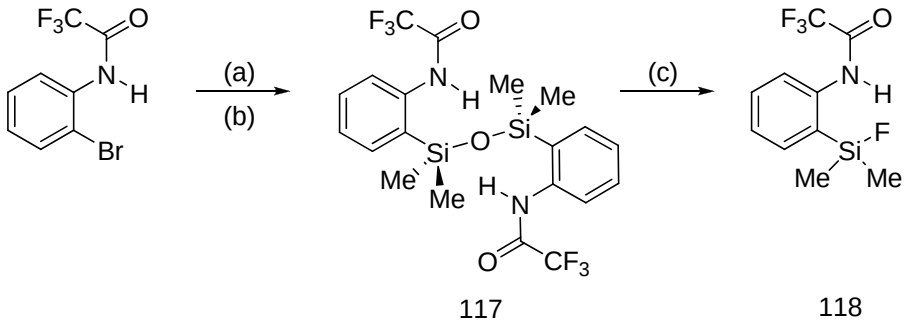

Figure 104: Synthesis of **117** and **118**. (a): MeLi, ^{t}BuLi, THF -78 °C; (b): $HSiMe_2Cl$; $NH_4Cl_{(aq)}$; (c): $BF_3{\cdot}Et_2O$, $NaHCO_{3(aq)}$.

The siloxane has been fully characterized by multinuclear NMR spectroscopy, as well as single crystal X-ray diffraction analysis. Compound **117** crystallizes in the monoclinic space group $P2_1/c$ (Figure 105, Table 26). There are no short interactions present and the connectivity shown in Figure 104 is corroborated.

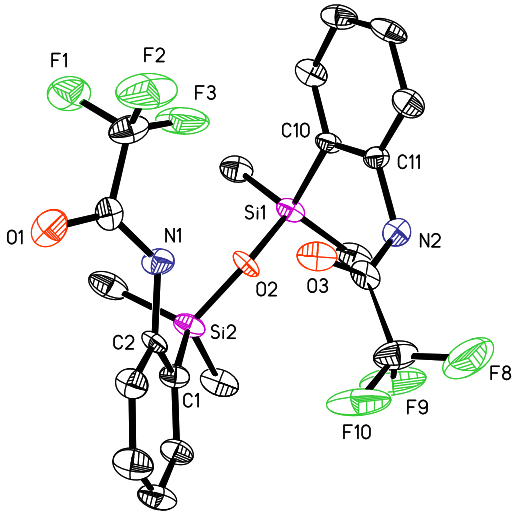

Figure 105: ORTEP of **117**, (50 % ellipsoids, H-atoms omitted for clarity).

Table 26: Crystal data, data collection and structure refinement for **117**.

117	
Crystal data	
Formula	$C_{20}H_{22}F_6N_2O_3Si_2$
M_r	508.58
crystal size (mm^3)	0.19 × 0.10 × 0.04
crystal system	Monoclinc
Space group	$P2_1/c$
a (Å)	17.378(5)
b (Å)	7.997(5)
c (Å)	18.071(5)
α (°)	
β (°)	108.761(5)
γ (°)	
V ($Å^3$)	2377.9(18)
Z	4
ρ_{calc} (g cm^{-3})	1.421
μ (mm^{-1})	0.220
F(000)	1776
Data Collection	
T (K)	110(2)
Scan mode	ω
hkl range	-15 → +15, -6 → +7, -13 → +16
measd reflns	6325
unique reflns [R_{int}]	1919 [0.0828]
reflns used for refinement	1919
Refinement	
refined parameters	298
GOF on F^2	1.009
R1,[a] wR2[b] all data	0.0780, 0.1068
ρ_{fin} (max/min) (e $Å^{-3}$)	0.222, -0.303

[a] $R1 = \sum||Fo| - |Fc||/\sum|Fo|$. [b] $wR2 = \{[\sum w(Fo^2 - Fc^2)^2]/[\sum w(Fo^2)^2]\}^{1/2}$

Compound **117** can be easily converted into the fluorosilane **118** by treatment with $BF_3{\cdot}Et_2O$. Fluorosilane **118** was isolated as a colorless oil which has been fully characterized by multinuclear NMR spectroscopy as well as elemental analysis. Some of the salient spectroscopic features of **118** include a ^{19}F signal at -154.8 ppm corresponding to the Si-F moiety; which is split into a doublet of septets due to coupling to the two methyl groups, as well as the N-H proton with $^1J_{H\text{-}F}$ and $^3J_{H\text{-}F}$ coupling constants equal to 11.3 Hz and 7.5 Hz respectively. Accordingly, the Si-Me_2 methyl groups appear as a doublet in the ^1H NMR spectrum of **118**. The Si-F coupling constant

of 278.2 Hz could also be determined from the silicon satellites observed in the ^{19}F NMR, or from the $^{29}Si\{^{1}H\}$ NMR which exhibited a doublet at 26.6 ppm. Although **118** could not be crystallized, spectroscopic evidence suggests the formation of an NH···FSi bridge.

The reaction of **118** with TBAF in $CDCl_3$ was also monitored spectroscopically. ^{1}H and ^{19}F NMR data indicate fluoride complexation to the Lewis acidic silicon center and formation of a pentacoordinate difluorosilicate species **119**. The collapse of the doublet in the ^{1}H NMR spectrum of **118** for the silicon bound methyl groups to a singlet upon fluoride addition is in agreement with the formation of a 5-coordinate difluorosilicate species in which the two fluoride anions occupy axial positions.

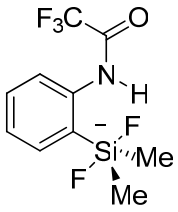

119

6.6 Conclusion

In summary, we describe a cationic silyl ether ($[\mathbf{111}]^{+}$) which functions as a colorimetric reagent for fluoride in water under physiological conditions. These results attest to the marked enhancement in fluoride affinity that can be achieved by incorporating a cationic moiety in the fluoride receptor. We have also reported a variety of other cationic silyl ethers which are highly soluble in water. Further research in this area may lead to several new promising species which are competent fluoride indicators at physiological pH.

Additionally, we developed a novel siloxane, which has been converted into a Lewis acidic fluorosilane moiety. Spectroscopic studies suggest that compound **118**

features a NH···FSi bridging motif, is similar to those seen in the boron derivatives [**97**-F]$^-$ and **101**. Initial spectroscopic results indicate that this new fluorosilane is a competent Lewis acid for fluoride recognition.

6.7 Experimental

General Considerations. 8-hydroxyquinoline was purchased from TCI America, methyl triflate, imidazole, potassium fluoride and *tert*-butyldimethylsilyl chloride from Aldrich; and *n*-$Bu_4NF{\cdot}3H_2O$ (TBAF) from Fluka. Et_2O was dried by reflux over Na/K. Dichloromethane was dried by passing through a column charged with activated alumina. Air-sensitive compounds were handled under a N_2 atmosphere using standard Schlenk and glovebox techniques. UV-vis spectra were recorded on a HP8453 spectrophotometer. Elemental analyses were performed at Atlantic Microlab (Norcross, GA). NMR spectra were recorded on a Varian Unity Inova 500 FT NMR (499.88 MHz for ^1H) and on a Varian Unity Inova 400 FT NMR (375.99 MHz for ^{19}F and 100.45 MHz for ^{13}C) spectrometer at ambient temperature. Chemical shifts δ are given in ppm, and are referenced against external Me_4Si (^1H, ^{13}C), and $CFCl_3$ (^{19}F). Potentiometric titrations were carried out using a SympHony Gel-Filled Combination Electrode from VWR International with a PHM290 pH Stat Controller from Radiometer Analytical.

Crystallography. Colorless single crystals of [**111**]OTf, [**112**]OTf and [**113**]OTf could be obtained by slow diffusion of pentane into concentrated DCM solutions of the triflate salts. Single crystals of **117** were obtained by cooling a concentrated hexane solution to -40 °C for several hours. The crystallographic measurements were performed using a Siemens SMART-CCD area detector diffractometer, with a graphite-monochromated Mo-K_α radiation (λ = 0.71069 Å). A specimen of suitable size and quality was selected and mounted onto glass fiber with apiezon grease. The structure was solved by direct methods, which successfully located most of the non-hydrogen atoms. Subsequent refinement on F^2 using the SHELXTL/PC

package (version 5.1) allowed location of the remaining non-hydrogen atoms.

Synthesis of [111]OTf. To a nitrogen purged 250 mL Schlenk flask was added 8-hydroxyquinoline (2.995 g, 20.6 mmol), imidazole (1.542 g, 22.6 mmol) and *tert*-butyl-dimethylsilyl chloride (3.446 g, 22.9 mmol). The solids were then dissolved in 100 mL of dry dichloromethane. The reaction mixture was stirred under nitrogen at room temperature for 12 hours. The reaction mixture was then quenched with distilled water (100 mL). The organic phase was separated and the aqueous layer was extracted with dichloromethane (3 x 20 mL). The organic phases were combined and dried over magnesium sulfate and then filtered. The solvent was removed by rotary evaporation affording a light brown oil. The resulting oil (500 mg) was dissolved in Et_2O (10 mL) and treated with an excess of methyl triflate (320 mg, 1.95 mmol) at room temperature. The mixture was stirred overnight, which resulted in the formation of a white solid. The solid was collected by filtration, washed with Et_2O (3 x 10 mL), and dried under vacuum to afford [111]OTf as a white powder (711 mg, 87% yield). ^{1}H NMR (499.88 MHz, $CDCl_3$): δ 0.43 (s, 6H, Si-CH_3), 1.04 (s, 9H, Si-^{t}Bu-CH_3), 4.94 (s, 3H, N-CH_3), 7.45 (dd, 1H, $^3J_{H\text{-}H}$ = 6.0 Hz, Ar-C*H*), 7.72-7.78 (m, 2H, Ar-C*H*), 7.99 (td, 1H, $^3J_{H\text{-}H}$ = 6.8 Hz, Ar-C*H*), 8.85 (d, 1H, $^3J_{H\text{-}H}$ = 8.5 Hz, Ar-C*H*), 9.48 (d, 1H, $^3J_{H\text{-}H}$ = 6.0 Hz, Ar-C*H*). ^{13}C NMR (100.5 MHz, $CDCl_3$): δ 3.91 (Si-*C*H_3), 18.86 (Si-*C*$(CH_3)_3$), 25.96 (Si-C(*C*$H_3)_3$), 52.54 (N-*C*H_3), 122.46, 122.98, 123.17, 130.45, 131.82, 132.43, 147.42, 147.78, 152.74 (Ar-*C*). *C*F_3 carbon peak was not observed. ^{19}F NMR (375.97 MHz, $CDCl_3$): δ -78.04. Anal Calcd for $C_{17}H_{24}NSiSF_3O_4$: C, 48.21; H, 5.71. Found: C, 47.98; H, 5.71.

Synthesis of [112]OTf. [**112**]OTf was prepared in 82 % yield using the same method as [**111**]OTf starting from 8-hydroxyquinoline and *tert*-butyldiphenylsilyl chloride. ^{1}H NMR (499.88 MHz, $CDCl_3$): δ 0.43 (s, 6H, Si-CH_3), 5.05 (s, 3H, N-CH_3), 7.45 (dd, 1H, $^3J_{H\text{-}H}$ = 6.0 Hz, Ar-C*H*), 7.54-7.62 (m, 2H, Ar-C*H*), 7.72-7.78 (m, 5H, Ar-C*H*), 7.99 (td, 1H, $^3J_{H\text{-}H}$ = 6.8 Hz, Ar-C*H*), 8.85 (d, 1H, $^3J_{H\text{-}H}$ = 8.5 Hz, Ar-C*H*), 9.48 (d, 1H, $^3J_{H\text{-}H}$ = 6.0 Hz, Ar-C*H*). ^{13}C NMR (100.5 MHz, $CDCl_3$): δ 2.76 (Si-*C*H_3), 53.22 (N-

CH_3), 122.46, 122.98, 123.17, 123.56, 125.55, 126.01, 130.45, 131.82, 132.43, 147.42, 147.78, 152.74 (Ar-*C*). *C*F_3 carbon peak was not observed. ^{19}F NMR (375.97 MHz, $CDCl_3$): δ -78.07. Anal Calcd for $C_{27}H_{30}NSiSF_3O_5$ ([**112**]OTf · H_2O): C, 57.33; H, 5.35. Found: C, 57.57; H, 4.98.

Synthesis of [113]OTf. [**113**]OTf was prepared in 76 % yield using the same method as [**111**]OTf starting from 8-hydroxyquinoline and triisopropylsilyl chloride.

Synthesis of [114]OTf. 5-(*N,N*-dimethylamino)-1-naphthol (which was prepared over two steps by stepwise methylation of 5-amino-1-naphthol with MeI, 63 % over both steps) (550 mg, 2.907 mmol) was dissolved in dichloromethane (20 mL) and treated with an excess of MeOTf (390 μL, 3.488 mmol) at room temperature. The resulting solution was stirred overnight, concentrated, followed by the addition of hexanes, precipitating 5-(trimethylamonium)-1-naphthol triflate, which was isolated by filtration (80 % yield). A 100 mL Schlenk flask was charged with 5-(trimethylammonium)-1-naphthol triflate (600 mg, 1.709 mmol), imidazole (128 mg, 1.880 mmol) and TBDMSCl (390 μL, 3.488 mmol). This mixture was dissolved in acetonitrile (20 mL) and stirred under nitrogen for 12 hours at room temperature. The solvent was then removed *in vacuo*, and the residue was extracted with chloroform and washed with water. The organic layer was dried over $MgSO_4$, and then concentrated. Addition of pentane (50 mL) led to the precipitation of [**114**]OTf as a pale gray solid. (520 mg, 68% yield). ^{1}H NMR (299.94 MHz, $CDCl_3$): δ 0.34 (s, 6H, Si-CH_3), 1.09 (s, 9H, Si-^{t}BuCH_3), 4.08 (s, 9H, N-CH_3), 7.04 (d, 1H, *J* = 7.5 Hz, Ar-C*H*), 7.60 (m, 1H, Ar-C*H*), 7.68 (m, 1H, Ar-C*H*), 7.82 (d, 1H, *J* = 9.0 Hz, Ar-C*H*), 7.92 (d, 1H, *J* = 7.2 Hz, Ar-C*H*), 8.04 (d, *J* = 8.4 Hz, Ar-C*H*). ^{19}F NMR (376.03 MHz, $CDCl_3$): δ -78.85. Anal. Calcd. for $C_{20}H_{22}N_2O_3F_6Si_2$: C, 47.23; H, 4.36. Found: C, 47.21; H, 4.31.

Synthesis of 117. Methyllithium (1.6 M, 5.83 mL, 9.32 mmol) in diethyl ether was rapidly added to a solution of *o*-bromotrifluoroacetanilide (2.5 g, 9.32 mmol) in

THF (80 mL) at -78 °C. After 10 minutes, *t*-butyllithium (1.5 M, 12.425 mL, 18.64 mmol) in pentane was added dropwise. The yellow mixture was stirred at -78 °C for 2 hours time, after which chlorodimethylsilane (2.5 mL, 23.3 mmol) was rapidly added. The solution was removed from the dry ice bath after 20 minutes and was allowed to warm to room temperature. After stirring for 1 hour, the mixture was quenched with 40 mL of distilled water. The layers were separated and aqueous phase was extracted with ether (3 × 40 mL). The organic layers were combined, dried over $MgSO_4$ and then the solvents were removed *in vacuo* affording a yellow oil. The residue was treated with hexanes (5 mL) to induce crystallization. The hexane mixture was cooled to -40 °C for 12 hours producing large colorless crystals of **117**, which were washed with cold hexanes (3 × 5 mL) and dried *in vacuo*. (1.78 g, 75% yield). ^{1}H NMR (499.97 MHz, $CDCl_3$): δ 0.42 (s, 6H, Si-C*H*$_3$), 7.24 (t, 1H, ^{3}J= 7.5 Hz, Ar-C*H*), 7.41 (d, 1H, ^{3}J= 7.5 Hz, Ar-C*H*), 7.48 (t, 1H, ^{3}J = 8.0 Hz, Ar-C*H*), 7.99 (d, 1H, ^{3}J = 8.0 Hz, Ar-C*H*), 8.63 (bs, 1H, N*H*). ^{13}C NMR (125.7 MHz, $CDCl_3$): δ 0.58 (Si-*C*H$_3$), 116.85, 122.70, 126.25, 129.00, 131.55, 134.04, 139.69, 154.82 (q, $J_{C\text{-}F}$ = 37.3 Hz, carbonyl-*C*F$_3$). ^{19}F NMR (376.03 MHz, $CDCl_3$): δ -75.85. ^{29}Si NMR (79.39 MHz, $CDCl_3$): δ 6.78. Anal. Calcd. for $C_{20}H_{22}N_2O_3F_6Si_2$: C, 47.23; H, 4.36. Found: C, 47.21; H, 4.31.

Synthesis of 118. To a solution of **117** (400 mg, 0.786 mmol) in Et_2O(20 mL) cooled to -78 °C was rapidly added $BF_3{\cdot}Et_2O$ (0.20 mL, 1.572 mmol). The reaction was stirred under nitrogen for 2 hours and then allowed to warm to room temperature, where it was stirred for 1 hour more. The solution was then quenched with a saturated solution of sodium bicarbonate (20 mL). The layers were separated and the aqueous phase was extracted with ether (3 × 20 mL). The organic phases were combined, dried over $MgSO_4$ and the solvents removed *in vacuo* affording **118** as a dark yellow oil, which was washed with cold hexanes (3 × 5 mL). (273 mg, 68% yield). ^{1}H NMR (499.97 MHz, $CDCl_3$): δ 0.58 (d, $J_{H\text{-}F}$ = 7.8 Hz, 6H, SiF-C*H*$_3$), 7.32 (t, 1H, ^{3}J= 7.5 Hz, Ar-C*H*), 7.47 (d, 1H, ^{3}J= 7.5 Hz, Ar-C*H*), 7.53 (t, 1H, ^{3}J = 8.0 Hz, Ar-C*H*), 8.05 (d, 1H, ^{3}J = 8.0 Hz, Ar-C*H*), 8.83 (bs, 1H, N*H*). ^{13}C NMR (100.5 MHz, $CDCl_3$): δ -0.70 (d, Si-*C*H$_3$), 115.9

(q), 122.80, 126.22 (d), 127.52 (d), 131.81, 133.90 (d), 139.69, 155.2 (q, $J_{C\text{-}F}$ = 37.3 Hz, carbonyl-CF_3). ^{19}F NMR (376.03 MHz, $CDCl_3$): δ -76.03 (s, 3F), -154.85 (m, 1F, $^1J_{H\text{-}F}$ = 11.3 Hz). ^{29}Si NMR (79.39 MHz, $CDCl_3$): δ 26.62 (d, $^1J_{Si\text{-}F}$ = 278.2 Hz). Anal. Calcd. for $C_{10}H_{11}NOF_4Si$: C, 45.28; H, 4.18. Found: C, 45.66; H, 4.26.

CHAPTER VII

SUMMARY

7.1 Fluoride and cyanide sensing using ammonium triarylboranes

With the recognition of aqueous fluoride and cyanide ions as an objective, we have investigated the synthesis and anion binding properties of several ammonium triarylboranes. In particular, two isomeric ammonium boranes, namely [*p*-$(Mes_2B)C_6H_4(NMe_3)]^+$ (**[83]**$^+$) and [*o*-$(Mes_2B)C_6H_4(NMe_3)]^+$ ([**84**]$^+$), which could be obtained by reaction of the known 4- and 2-dimesitylboryl-*N*,*N*-dimethylaniline respectively with MeOTf, have been investigated both experimentally and computationally. They both react with both fluoride and cyanide ions in organic solvents to afford the corresponding fluoroborate/ or cyanoborate/ammonium zwitterions **83**-F, **83**-CN, **84**-F, and **84**-CN. In aqueous solution, however, these cationic boranes behave as remarkably selective receptors. Indeed, [**83**]$^+$ only complexes cyanide ions while [**84**]$^+$ only complexes fluoride ions. In H_2O/DMSO 60:40 vol. (HEPES 6 mM, pH 7), the cyanide binding constant of [**83**]$^+$ and the fluoride binding constant of [**84**]$^+$ are respectively equal to $3.9(\pm0.1) \times 10^8$ M^{-1} and 900 ($\pm$50) M^{-1}.

Structural and computational studies indicate that both steric and electronic effects contribute to the unusual selectivity displayed by these cationic boranes. Owing to favorable Coulombic effects, the *para*-derivative [**83**]$^+$ has a very high affinity for cyanide; yet these effects are not sufficiently intense to allow complexation of the more efficiently hydrated and less basic fluoride anion. In the case of the *ortho*-derivative [**84**]$^+$, the proximity of the ammonium moiety leads to an increase in the Lewis acidity of the boron center thus making fluoride binding possible. However, steric effects prevent cyanide coordination to the boron center of [**84**]$^+$. Finally, cations [**83**]$^+$ and [**84**]$^+$ bind their dedicated anions reversibly and show a negligible response in the presence of other common anions including Cl^-, Br^-, I^-, NO_3^-, OAc^-, $H_2PO_4^-$, and HSO_4^-.

In an effort to ascertain the role solvation of the cationic borane plays on anion

binding, we have investigated ammonium boranes featuring longer alkyl substituents on the nitrogen atom. The specific goal of lengthening the alkyl substituents on the nitrogen atoms is to desolvate the ammonium borane species. In this context, [*p*-(Mes_2B)C_6H_4(NEt_2Me)]$^+$ [**89**]$^+$ and [*p*-(Mes_2B)C_6H_4(NBu_2Me)]$^+$ [**90**]$^+$ have also been synthesized by methylation of their respective amino borane derivatives. Unlike the trimethylated ammonium boranes, these cationic derivatives are incompatible in aqueous media, undergoing slow demethylation to their corresponding amino borane compounds. Attemps to methylate the known compound, *p*-(Mes_2B)C_6H_4(NPh_2) (**88**), and another new derivative that we synthesized, *p*-(Mes_2B)C_6H_4(NBn_2) (**87**), were also undertaken, however the poor nucleophilicity of the nitrogen lone pair in these molecules prohibited alkylation.

7.2 Synthesis of a novel bidentate phosphonium/triarylborane Lewis acid

The phosphonium borane [1-Mes_2B-2-$MePh_2P$-(C_6H_4)]$^+$ ([**93**]$^+$) has been synthesized as an iodide salt by alkylation of 1-Mes_2B-2-Ph_2P-(C_6H_4) (**94**) with MeI. This novel cationic borane complexes fluoride to afford the corresponding zwitterionic fluoroborate complex 1-FMes_2B-2-$MePh_2P$-(C_6H_4) (**93**-F) with a binding constant in MeOH which exceeds that of 1-Mes_2B-4-$MePh_2P$-(C_6H_4) ([**20**]$^+$) by at least 4 orders of magnitude. Structural and computational results indicate that the high fluorophilicity of [**93**]$^+$ arises from both Coulombic and cooperative effects, which lead to the formation of a B−F→P interaction with a F→P distance of 2.666(2) Å. These results, which are supported by NBO and AIM analyses, show that the latent phosphorus-centered Lewis acidity of the phosphonium moiety in [**93**]$^+$ can be exploited to enhance fluoride binding via chelation.

Remarkably, the Lewis acidic nature of the phosphonium moiety in [**93**]$^+$ can also be exploited to chelate a number of other anionic guests in addition to fluoride. Indeed, treatment of [**93**]I with azide and acetate (as their sodium salts) in methanol leads to the formation of **93**-N_3 and **93**-OAc. Crystallographic and spectroscopic data obtained on compound **93**-N_3 indicate a dative interaction between the boron-bound nitrogen atom

(N(1)) of the azide anion and the phosphorus atom of the phosphonium functionality. As with our other cationic boranes, we have been able to obtain the cyanide adduct **93**-CN. Crystallographic evidence reveals that unlike with fluoride and azide, there is no appreciable interaction observed between the cyanide anion and the phosphorus center which are separated by more than 3.2 Å.

Finally, due to the instability of [**93**]$^+$ in water at neutral or basic pH, we investigated the reaction of [**93**]$^+$ with hydroxide. To our surprise, rather than formation of the expected hydroxide adduct, hydrolysis of a P-C_{Ph} bond leading to the formation of the phosphine oxide triarylborane (**95**) was observed.

7.3 Novel hybrid, bidentate hydrogen bond donor/boryl receptors for fluoride

To verify if hydrogen bond donor groups can assist fluoride binding at the boron center of triarylboranes, *o*-(dimesitylboryl)trifluoroacetanilide (**97**) has been synthesized. Reaction of this new borane with [*n*-Bu_4N][F] in acetone affords the corresponding fluoroborate [**97**-F]$^-$ complex whose stability constant exceeds that of [Mes_3BF]$^-$ by at least two orders of magnitude. Presumably, the higher fluoride affinity of **97** results from the cooperativity of the Lewis acidic boron center and the hydrogen bond donor trifluoroacetamide group.

The *o*-(pinacolboryl)trifluoroacetanilide (**100**) has also been synthesized and structurally characterized. As indicated by NMR spectroscopy, this novel derivative reacts with fluoride to afford the corresponding fluoroborate derivative [**100**-F]$^-$ in which the boron-bound fluorine atom forms a hydrogen bond with the proton of the trifluoroacetamide functionality. Compound **100** reacts with KHF_2 to afford the corresponding trifluoroborate derivative which has been isolated as a dibenzo-18-crown-6 potassium salt (**101**). The crystal structure and the ^{1}H NMR spectrum of this salt confirm the presence of a B-F---H-N hydrogen bond which has been hypothesized in complexes [**97**-F]$^-$ and [**100**-F]$^-$.

7.4 Novel synthetic methodologies for the preparation of cationic BODIPY turn-on sensors for fluoride

We have developed a synthetic method for the preparation of novel, highly fluorescent BODIPY boronium cations. Indeed, treatment of 1,3,5,7,8-pentamethylpyrromethene-borondifluoride (**102**) with trimethylsilyl triflate results in abstraction of a fluoride followed by subsequent coordination of the triflate to yield **103**. This novel BODIPY species is sensitive to water, but has been fully characterized. Treatment of **103** with DMAP leads to the formation of the BODIPY boronium cation [**104**]OTf. In the presence of iodide ions, [**104**]OTf reacts with fluoride ions to afford the corresponding brightly fluorescent difluoride **102**.

We also questioned whether we could prepare ionic compounds in which the triflate was not bound to the boron center. Our efforts to prepare these desired cations, which could be described as borenium ions, were focused on introducing an electron rich aryl group rather than an electron withdrawing fluorine atom at the boron center. To this end, a new synthetic methodology was developed to prepare compounds **106**, **107** and **108**. All of our efforts at abstracting the chloride from **106** or the fluoride from **108** yielded intractable mixtures of unidentified products. We hypothesized that the resulting cations might be unstable, and to enhance the stability of the resulting cationic species, we decided to introduce electron donating substituents into the dipyrromethene backbone.

Using our new method, we prepared two more novel BODIPY compounds, which feature *p*-dimethylaminophenyl substituents at the 5 position of the BODIPY core. Compounds **109** and **110** have been fully characterized, and attempts of fluoride abstraction from **110** were also carried out. As with the other monoarylated species, our efforts to form the BODIPY borenium cation were unsuccessful.

7.5 Synthesis of neutral and cationic silicon-based fluoride probes

The majority of the work presented in this dissertation has been focused on the development of boron centered Lewis acids, which serve as molecular receptors for

fluoride or cyanide anions. We have also exploited the use of silicon-based Lewis acids to this end. We have synthesized a number of cationic silyl ethers, which are competent fluoride sensors in physiological conditions (pH 7.5). Two of these novel cationic silyl ethers, namely [**111**]$^+$ and [**114**]$^+$ exhibit a colorimetric response to fluoride anions in organic solvents. The observed color change from pale-yellow to deep-purple has been attributed to the fluoride-induced deprotection of the alcohol which generates the colored zwitterionic species **115** and **116**.

In water, cation [**111**]$^+$ undergoes facile deprotection in the presence of fluoride at physiological pH. In constrast, cation [**114**]$^+$ displays sluggish desilylation. Since [**111**]$^+$ is an adequate sensor for fluoride in water, we studied the kinetics of the reaction of [**111**]$^+$ with fluoride and found the reaction to be second order overall with a first-order dependence on both [**111**]$^+$ and fluoride.

We have also shown that, as with the boron-based Lewis acids, a trifluoroacetamide group can aid in the chelation of fluoride anions to a Lewis acidic fluorosilane moiety. Compound **117** was prepared from the double lithiation of 2-bromotrifluoroacetanilide, followed by treatment with $HSiMe_2Cl$. Subsequent treatment with $BF_3{\cdot}Et_2O$ led to the formation of the novel fluorosilane Lewis acid **118**. Spectroscopic evidence suggests that like the boron derivatives **97** and **100**, fluorosilane **118** is able to complex fluoride anions forming the difluorosilicate [**119**]$^-$ which may feature a NH···FSi bridging interaction.

7.6 Conclusion

The work presented in this dissertation details the synthesis of a variety of novel main group Lewis acids which serve as molecular receptors for fluoride and cyanide anions. Due to their widespread application and documented toxicity, the interest in developing molecular receptors for these anions continues to grow. The Lewis acids that have been reported in this work have been some of the first examples reported in the literature of selective sensors for fluoride and cyanide which function in neutral water. Continued research in this area may potentially lead to the development of more potent,

and more selective receptors for a variety of biologically relevant anions such as fluoride, cyanide or even azide.

Future work in the area of cationic boranes should include further investigation into what role solvation of the cationic hosts plays in their anion affinity. Since it has proven to be difficult to functionalize the aminoboranes, work in the area of the phosphonium boranes should be considered. The phosphinoboranes can be easily alkylated with alkyl iodide reagents, and a series of increasingly hydrophobic phosphonium boranes should be investigated.

In addition to studying the solvation of these Lewis acids, it would be of great importance to look at increasing the number of cationic moieties in these receptors. One ultimate goal of this research would be to develop borane-based Lewis acids which may be competitive with tris(pentafluorophenyl)borane in terms of Lewis acid strength, but which are inherently more stable to neutralization by water. Indeed, there is much work in this particular area which should be undertaken.

Finally, since several competent receptors have been developed, the focus of this research can also be turned to applications. Indeed, some of the cationic silyl ether receptors are currently being tested in a variety of biological assays by the U.S. Army Institute for Chemical Defense. They are investigating the use of these derivatives to monitor the efficacy of a variety of compounds being investigated to neutralize warfare agents.

REFERENCES

1. Matsuo, S.; Kiyomiya, K.-i.; Kurebe, M.; Mechanism of toxic action of fluoride in dental fluorosis: whether trimeric G proteins participate in the disturbance of intracellular transport of secretory ameloblast exposed to fluoride. *Archives of Toxicology* **1998**, *72*, 798-806.
2. Briancon, D.; Fluoride and osteoporosis: an overview. *Revue du rhumatisme* **1997**, *64*, 78-81.
3. CDC Water fluoridation reporting system. December 31, 2002.; *Centers for Disease Control* **2002**.
4. Fluorine and fluorides. *Environmental Health Criteria 36, IPCS International Programme on Chemical Safety, World Health Organization* **1984**.
5. Fluorides. *Environmental Health Criteria 227, IPCS International Programme on Chemical Safety, World Health Organization* **2002**.
6. Schmidtchen, F. P.; Berger, M.; Artificial organic host molecules for anions. *Chemical Reviews* **1997**, *97*, 1609-1646.
7. Martinez-Manez, R.; Sancenon, F.; Fluorogenic and chromogenic chemosensors and reagents for anions. *Chemical Reviews* **2003**, *103*, 4419-4476.
8. Choi, K.; Hamilton, A. D.; Macrocyclic anion receptors based on directed hydrogen bonding interactions. *Coordination Chemistry Reviews* **2003**, *240*, 101-110.
9. Bondy, C. R.; Loeb, S. J.; Amide based receptors for anions. *Coordination Chemistry Reviews* **2003**, *240*, 77-99.
10. Gale, P. A.; Anion and ion-pair receptor chemistry: highlights from 2000 and 2001. *Coordination Chemistry Reviews* **2003**, *240*, 191-221.
11. Sessler, J. L.; Camiolo, S.; Gale, P. A.; Pyrrolic and polypyrrolic anion binding agents. *Coordination Chemistry Reviews* **2003**, *240*, 17-55.
12. Sessler, J. L.; Davis, J. M.; Sapphyrins: Versatile anion binding agents. *Accounts of Chemical Research* **2001**, *34*, 989-997.

13. Beer, P. D.; Gale, P. A.; Anion recognition and sensing: the state of the art and future perspectives. *Angewandte Chemie, International Edition* **2001**, *40*, 486-516.
14. Gale, P. A.; Anion receptor chemistry: highlights from 1999. *Coordination Chemistry Reviews* **2001**, *213*, 79-128.
15. Gale, P. A.; Anzenbacher, P., Jr.; Sessler, J. L.; Calixpyrroles II. *Coordination Chemistry Reviews* **2001**, *222*, 57-102.
16. Gale, P. A.; Anion coordination and anion-directed assembly: highlights from 1997 and 1998. *Coordination Chemistry Reviews* **2000**, *199*, 181-233.
17. Beer, P. D.; Cadman, J.; Electrochemical and optical sensing of anions by transition metal based receptors. *Coordination Chemistry Reviews* **2000**, *205*, 131-155.
18. Snowden, T. S.; Anslyn, E. V.; Anion recognition: synthetic receptors for anions and their application in sensors. *Current Opinion in Chemical Biology* **1999**, *3*, 740-746.
19. Beer, P. D.; Transition-metal receptor systems for the selective recognition and sensing of anionic guest species. *Accounts of Chemical Research* **1998**, *31*, 71-80.
20. de Silva, A. P.; Gunaratne, H. Q. N.; Gunnlaugsson, T.; Huxley, A. J. M.; McCoy, C. P.; Rademacher, J. T.; Rice, T. E.; Signaling recognition events with fluorescent sensors and switches. *Chemical Reviews* **1997**, *97*, 1515-1566.
21. Bianchi, A.; Bowman-James, K.; Garcia-Espana, E.; Editors *Supramolecular Chemistry of Anions.* Wiley-VHC; New York, NY; 1997; 481 pp.
22. Boiocchi, M.; Del Boca, L.; Gomez, D. E.; Fabbrizzi, L.; Licchelli, M.; Monzani, E.; Nature of urea-fluoride interaction: incipient and definitive proton transfer. *Journal of the American Chemical Society* **2004**, *126*, 16507-16514.
23. Holland, M. A.; Kozlowski, L. M.; Clinical features and management of cyanide poisoning. *Clinical Pharmacy* **1986**, *5*, 737-741.
24. Baud, F. J.; Cyanide: critical issues in diagnosis and treatment. *Hum Exp Toxicol.* **2007**, *26*, 191-201.

25. Sessler, J. L.; Cho, D.-G.; The benzil rearrangement reaction: trapping of a hitherto minor product and its application to the development of a selective cyanide anion indicator. *Organic Letters* **2008**, *10*, 73-75.

26. Chen, C.-L.; Chen, Y.-H.; Chen, C.-Y.; Sun, S.-S.; Dipyrrole carboxamide derived selective ratiometric probes for cyanide ion. *Organic Letters* **2006**, *8*, 5053-5056.

27. Anzenbacher, P., Jr.; Tyson, D. S.; Jursikova, K.; Castellano, F. N.; Luminescence lifetime-based sensor for cyanide and related anions. *Journal of the American Chemical Society* **2002**, *124*, 6232-6233.

28. Ekmekci, Z.; Yilmaz, M. D.; Akkaya, E. U.; A monostyryl-boradiazaindacene (BODIPY) derivative as colorimetric and fluorescent probe for cyanide ions. *Organic Letters* **2008**, *10*, 461-464.

29. Bresner, C.; Day, J. K.; Coombs, N. D.; Fallis, I. A.; Aldridge, S.; Coles, S. J.; Hursthouse, M. B.; Fluoride anion binding by cyclic boronic esters: influence of backbone chelate on receptor integrity. *Dalton Transactions* **2006**, 3660-3667.

30. Bresner, C.; Aldridge, S.; Fallis, I. A.; Jones, C.; Ooi, L.-L.; Selective electrochemical detection of hydrogen fluoride by ambiphilic ferrocene derivatives. *Angewandte Chemie, International Edition* **2005**, *44*, 3606-3609.

31. Dusemund, C.; Sandanayake, K. R. A. S.; Shinkai, S.; Selective fluoride recognition with ferroceneboronic acid. *Journal of the Chemical Society, Chemical Communications* **1995**, 333-334.

32. Yamamoto, H.; Ori, A.; Ueda, K.; Dusemund, C.; Shinkai, S.; Visual sensing of fluoride ion and saccharides utilizing a coupled redox reaction of ferrocenylboronic acids and dye molecules. *Chemical Communications* **1996**, 407-408.

33. Cooper, C. R.; Spencer, N.; James, T. D.; Selective fluorescence detection of fluoride using boronic acids. *Chemical Communications* **1998**, 1365-1366.

34. Arimori, S.; Davidson, M. G.; Fyles, T. M.; Hibbert, T. G.; James, T. D.; Kociok-Koehn, G. I.; Synthesis and structural characterisation of the first

bis(bora)calixarene: a selective, bidentate, fluorescent fluoride sensor. *Chemical Communications* **2004**, 1640-1641.

35. Badugu, R.; Lakowicz, J. R.; Geddes, C. D.; Anion sensing using quinolinium based boronic acid probes. *Current Analytical Chemistry* **2005**, *1*, 157-170.
36. Badugu, R.; Lakowicz, J. R.; Geddes, C. D.; A wavelength-ratiometric fluoride-sensitive probe based on the quinolinium nucleus and boronic acid moiety. *Sensors and Actuators, B: Chemical* **2005**, *B104*, 103-110.
37. DiCesare, N.; Lakowicz, J. R.; New sensitive and selective fluorescent probes for fluoride using boronic acids. *Analytical Biochemistry* **2002**, *301*, 111-116.
38. Neumann, T.; Dienes, Y.; Baumgartner, T.; Highly sensitive sensory materials for fluoride ions based on the dithieno[3,2-b : 2 ',3 '-d]phosphole system. *Organic Letters* **2006**, *8*, 495-497.
39. Koskela, S. J. M.; Fyles, T. M.; James, T. D.; A ditopic fluorescent sensor for potassium fluoride. *Chemical Communications* **2005**, 945-947.
40. Shiratori, H.; Ohno, T.; Nozaki, K.; Osuka, A.; Change of electron-transfer path-selectivity in a triad by F--coordination at a boronate-ester bridge. *Chemical Communications* **1999**, 2181-2182.
41. Yamaguchi, S.; Akiyama, S.; Tamao, K.; A new approach to photophysical properties control of main group element pi-electron compounds based on the coordination number change. *Journal of Organometallic Chemistry* **2002**, *652*, 3-9.
42. Entwistle, C. D.; Marder, T. B.; Applications of three-coordinate organoboron compounds and polymers in optoelectronics. *Chemistry of Materials* **2004**, *16*, 4574-4585.
43. Entwistle, C. D.; Marder, T. B.; Boron chemistry lights the way: optical properties of molecular and polymeric systems. *Angewandte Chemie-International Edition* **2002**, *41*, 2927-2931.
44. Jäkle, F. *Boron: Organoboranes in Encyclopedia of Inorganic Chemistry.* 2nd ed.; Wiley, Chichester, 2005.

45. Bauman, A.; Sodium triphenylcyanoborate - Caesignost - a selective reagent for separating cesium-137 in environmental samples. *Mikrochimica Acta* **1977**, *1*, 69-72.

46. Yamaguchi, S.; Akiyama, S.; Tamao, K.; Tri-9-anthrylborane and its derivatives: new boron-containing π-electron systems with divergently extended π-conjugation through boron. *Journal of the American Chemical Society* **2000**, *122*, 6335-6336.

47. Yamaguchi, S.; Shirasaka, T.; Akiyama, S.; Tamao, K.; Dibenzoborole-containing p-electron systems: Remarkable fluorescence change based on the "On/Off" control of the pπ-π* conjugation. *Journal of the American Chemical Society* **2002**, *124*, 8816-8817.

48. Solé, S.; Gabbaï, F. P.; A bidentate borane as colorimetric fluoride ion sensor. *Chemical Communications* **2004**, 1284-1285.

49. Parab, K.; Venkatasubbaiah, K.; Jäkle, F.; Luminescent triarylborane-functionalized polystyrene: synthesis, photophysical characterization, and anion-binding studies. *Journal of the American Chemical Society* **2006**, *128*, 12879-12885.

50. Miyata, M.; Chujo, Y.; π-Conjugated organoboron polymer as an anion sensor. *Polymer Journal* **2002**, *34*, 967-969.

51. Liu, Z.-Q.; Shi, M.; Li, F.-Y.; Fang, Q.; Chen, Z.-H.; Yi, T.; Huang, C.-H.; Highly selective two-photon chemosensors for fluoride derived from organic boranes. *Organic Letters* **2005**, *7*, 5481-5484.

52. Liu, X. Y.; Bai, D. R.; Wang, S.; Charge-transfer emission in nonplanar three-coordinate organoboron compounds for fluorescent sensing of fluoride. *Angewandte Chemie, International Edition* **2006**, *45*, 5475-5478.

53. Agou, T.; Kobayashi, J.; Kawashima, T.; Dibenzophosphaborin: A hetero-π-conjugated molecule with fluorescent properties based on intramolecular charge transfer between phosphorus and boron atoms. *Organic Letters* **2005**, *7*, 4373-4376.

54. Bai, D.-R.; Liu, X.-Y.; Wang, S.; Charge-transfer emission involving three-coordinate organoboron: V-shape versus U-shape and impact of the spacer on dual emission and fluorescent sensing. *Chemistry--A European Journal* **2007**, *13*, 5713-5723.

55. Sun, Y.; Ross, N.; Zhao, S. B.; Huszarik, K.; Jia, W. L.; Wang, R. Y.; Macartney, D.; Wang, S.; Enhancing electron accepting ability of triarylboron via π-conjugation with 2,2'-bipy and metal chelation: 5,5'-bis(BMes2)-2,2'-bipy and its metal complexes. *Journal of the American Chemical Society* **2007**, *129*, 7510-7511.

56. Zhao, S.-B.; McCormick, T.; Wang, S.; Ambient-temperature metal-to-ligand charge-transfer phosphorescence facilitated by triarylboron: Bnpa and its metal complexes. *Inorganic Chemistry* **2007**, *46*, 10965-10967.

57. Yuan, M.-S.; Liu, Z.-Q.; Fang, Q.; Donor-and-acceptor substituted truxenes as multifunctional fluorescent probes. *Journal of Organic Chemistry* **2007**, *72*, 7915-7922.

58. Katz, H. E.; Hydride sponge: complexation of 1,8-naphthalenediylbis(dimethylborane) with hydride, fluoride, and hydroxide. *Journal of Organic Chemistry* **1985**, *50*, 5027-5032.

59. Williams, V. C.; Piers, W. E.; Clegg, W.; Elsegood, M. R. J.; Collins, S.; Marder, T. B.; New bifunctional perfluoroaryl boranes. Synthesis and reactivity of the ortho-phenylene-bridged diboranes 1,2-$[B(C_6F_5)_2]_2C_6X_4$ (X = H, F). *Journal of the American Chemical Society* **1999**, *121*, 3244-3245.

60. Chase, P. A.; Henderson, L. D.; Piers, W. E.; Parvez, M.; Clegg, W.; Elsegood, M. R. J.; Bifunctional perfluoroaryl boranes: synthesis and coordination chemistry with neutral Lewis base donors. *Organometallics* **2006**, *25*, 349-357.

61. Melaïmi, M.; Gabbaï, F. P.; A heteronuclear bidentate lewis acid as a phosphorescent fluoride sensor. *Journal of the American Chemical Society* **2005**, *127*, 9680-9681.

62. Melaïmi, M.; Gabbaï, F. P.; Bidentate group 13 Lewis acids with ortho-phenylene and peri-naphthalenediyl backbones. *Advances in Organometallic Chemistry* **2005**, *53*, 61-99.

63. Katz, H. E.; Hydride sponge: 1,8-naphthalenediylbis(dimethylborane). *Journal of the American Chemical Society* **1985**, *107*, 1420-1421.

64. Katz, H. E.; Anion complexation and migration in (8-silyl-1-naphthyl)boranes. Participation of hypervalent silicon. *Journal of the American Chemical Society* **1986**, *108*, 7640-7645.

65. Katz, H. E.; Recent advances in multidentate anion complexation. *Inclusion Compd.* **1991**, *4*, 391-405.

66. Gabbaï, F. P.; The charge-reverse analogy as an inspiration for the preparation of polydentate Lewis acidic boranes. *Angewandte Chemie, International Edition* **2003**, *42*, 2218-2221.

67. Piers, W. E.; Irvine, G. J.; Williams, V. C.; Highly Lewis acidic bifunctional organoboranes. *European Journal of Inorganic Chemistry* **2000**, 2131-2142.

68. Melaïmi, M.; Sole, S.; Chiu, C.-W.; Wang, H.; Gabbaï, F. P.; Structural and electrochemical investigations of the high fluoride affinity of sterically hindered 1,8-Bis(boryl)naphthalenes. *Inorganic Chemistry* **2006**, *45*, 8136-8143.

69. Bayer, M. J.; Jalisatgi, S. S.; Smart, B.; Herzog, A.; Knobler, C. B.; Hawthorne, M. F.; B-Octamethyl[12]mercuracarborand-4 as host for "Naked" fluoride ions. *Angewandte Chemie, International Edition* **2004**, *43*, 1854-1857.

70. Viets, D.; Lork, E.; Watson, P. G.; Mews, R.; [(CF3)2Hg(m-F)2Hg(CF3)2]2-: synthesis, structure, and reactivity. *Angewandte Chemie, International Edition in English* **1997**, *36*, 623-624.

71. Haneline, M. R.; Tsunoda, M.; Gabbaï, F. P.; π-Complexation of biphenyl, naphthalene, and triphenylene to trimeric perfluoro-ortho-phenylene mercury. Formation of extended binary stacks with unusual luminescent properties. *Journal of the American Chemical Society* **2002**, *124*, 3737-3742.

72. Williams, V. C.; Irvine, G. J.; Piers, W. E.; Li, Z.; Collins, S.; Clegg, W.; Elsegood, M. R. J.; Marder, T. B.; Novel trityl activators with new weakly coordinating anions derived from C_6F_4-1,2-$[B(C_6F_5)_2]_2$: synthesis, structures, and olefin polymerization behavior. *Organometallics* **2000**, *19*, 1619-1621.

73. Chai, J.; Lewis, S. P.; Collins, S.; Sciarone, T. J. J.; Henderson, L. D.; Chase, P. A.; Irvine, G. J.; Piers, W. E.; Elsegood, M. R. J.; Clegg, W.; Formation of chelated counteranions using Lewis acidic diboranes: relevance to isobutene polymerization. *Organometallics* **2007**, *26*, 5667-5679.

74. Lewis, S. P.; Taylor, N. J.; Piers, W. E.; Collins, S.; Isobutene polymerization using a chelating diborane co-initiator. *Journal of the American Chemical Society* **2003**, *125*, 14686-14687.

75. Boshra, R.; Venkatasubbaiah, K.; Doshi, A.; Lalancette, R. A.; Kakalis, L.; Jakle, F.; Simultaneous fluoride binding to ferrocene-based heteronuclear bidentate Lewis acids. *Inorganic Chemistry* **2007**, *46*, 10174-10186.

76. Amendola, V.; Esteban-Gomez, D.; Fabbrizzi, L.; Licchelli, M.; Monzani, E.; Sancenon, F.; Metal-enhanced H-bond donor tendencies of urea and thiourea toward anions: ditopic receptors for silver(I) salts. *Inorganic Chemistry* **2005**, *44*, 8690-8698.

77. Custelcean, R.; Delmau, L. H.; Moyer, B. A.; Sessler, J. L.; Cho, W. S.; Gross, D.; Bates, G. W.; Brooks, S. J.; Light, M. E.; Gale, P. A.; Calix[4]pyrrole: An old yet new ion-pair receptor. *Angewandte Chemie-International Edition* **2005**, *44*, 2537-2542.

78. Bondy, C. R.; Gale, P. A.; Loeb, S. J.; Metal-organic anion receptors: arranging urea hydrogen-bond donors to encapsulate sulfate ions. *Journal of the American Chemical Society* **2004**, *126*, 5030-5031.

79. Padilla-Tosta, M. E.; Lloris, J. M.; Martinez-Manez, R.; Pardo, T.; Sancenon, F.; Soto, J.; Marcos, M. D.; ATP recognition through a fluorescence change in a multicomponent dinuclear system containing a $Ru(Tpy)_2^{2+}$ fluorescent core and a

cyclam-Cu^{2+} complex. *European Journal of Inorganic Chemistry* **2001**, 1221-1226.

80. Beer, P. D.; Dent, S. W.; Potassium cation induced switch in anion selectivity exhibited by heteroditopic ruthenium(II) and rhenium(I) bipyridyl bis(benzo-15-crown-5) ion pair receptors. *Chemical Communications* **1998**, 825-826.
81. Beer, P. D.; Drew, M. G. B.; Knubley, R. J.; Ogden, M. I.; Synthesis and coordination chemistry of a novel bis(benzo crown-ether) substituted calix[4]arene that can simultaneously complex cations and anions. *Dalton Transactions* **1995**, 3117-3123.
82. Kinnear, K. I.; Mousley, D. P.; Arafa, E.; Lockhart, J. C.; Design and synthesis of ionophores with multiple receptor-sites - solution nuclear-magnetic-resonance studies of their interaction with chloride, sodium and potassium-ions. *Dalton Transactions* **1994**, 3637-3643.
83. Arafa, E. A.; Kinnear, K. I.; Lockhart, J. C.; New pocket ionophores with potential for simultaneous chelation of anions and cations - synthesis and scope of chelating properties. *Chemical Communications* **1992**, 61-64.
84. Liu, H.; Shao, X. B.; Jia, M.; Jiang, X. K.; Li, Z. T.; Chen, G. J.; Selective recognition of sodium cyanide and potassium cyanide by diaza-crown ether-capped Zn-porphyrin receptors in polar solvents. *Tetrahedron* **2005**, *61*, 8095-8100.
85. Chiu, C.-W.; Gabbaï, F. P.; Fluoride ion capture from water with a cationic borane. *Journal of the American Chemical Society* **2006**, *128*, 14248-14249.
86. Agou, T.; Kobayashi, J.; Kawashima, T.; Tuning of the optical properties and Lewis acidity of dibenzopnictogenaborins by modification on bridging main group elements. *Inorganic Chemistry* **2006**, *45*, 9137-9144.
87. Agou, T.; Kobayashi, J.; Kim, Y.; Gabbaï, F. P.; Kawashima, T.; Phase transfer of fluoride ion by phosphonioborins. *Chemistry Letters* **2007**, *36*, 976-977.

88. Lee, M. H.; Agou, T.; Kobayashi, J.; Kawashima, T.; Gabbaï, F. P.; Fluoride ion complexation by a cationic borane in aqueous solution. *Chemical Communications* **2007**, 1133-1135.

89. Lee, M. H.; Gabbai, F. P.; Synthesis and properties of a cationic bidentate Lewis acid. *Inorganic Chemistry* **2007**, *46*, 8132-8138.

90. Reetz, M. T.; Niemeyer, C. M.; Harms, K.; Crown ether with a Lewis acid center, a new class of heterotopic host molecule. *Angewandte Chemie* **1991**, *103*, 1515-1517.

91. Badugu, R.; Lakowicz, J. R.; Geddes, C. D.; Wavelength-ratiometric probes for the selective detection of fluoride based on the 6-aminoquinolinium nucleus and boronic acid moiety. *Journal of Fluorescence* **2004**, *14*, 693-703.

92. Galbraith, E.; Fyles, T. M.; Marken, F.; Davidson, M. G.; James, T. D.; Fluorescent boron bis(phenolate) with association response to chloride and dissociation response to fluoride. *Inorganic Chemistry* **2008**, *47*, 6236-6244.

93. Nicolas, M.; Fabre, B.; Simonet, J.; Electrochemical sensing of fluoride and sugars with a boronic acid-substituted bipyridine Fe(II) complex in solution and attached onto an electrode surface. *Electrochimica Acta* **2001**, *46*, 1179-1190.

94. Nesmeyanov, A. N.; Sazonova, V. A.; Drozd, V. N.; Ferrocenylboronic and 1,1'-ferrocenylenediboronic acids and their reactions. *Doklady Akademii Nauk SSSR* **1959**, *126*, 1004-1006.

95. Oehlke, A.; Auer, A. A.; Jahre, I.; Walfort, B.; Rueffer, T.; Zoufala, P.; Lang, H.; Spange, S.; Nitro-substituted stilbeneboronate pinacol esters and their fluoro-adducts. Fluoride ion induced polarity enhancement of arylboronate esters. *Journal of Organic Chemistry* **2007**, *72*, 4328-4339.

96. Tan, W.; Zhang, D.; Wang, Z.; Liu, C.; Zhu, D.; 4-(N,N-Dimethylamine)benzonitrile (DMABN) derivatives with boronic acid and boronate groups: new fluorescent sensors for saccharides and fluoride ion. *Journal of Materials Chemistry* **2007**, *17*, 1964-1968.

97. Nicolas, M.; Fabre, B.; Simonet, J.; Voltammetric investigation of new boronic ester-substituted triphenylamines-based redox receptors in solution and attached to an electrode surface. Effects of F- as an anionic guest. *Electrochimica Acta* **2001**, *46*, 3421-3429.

98. Day, J. K.; Bresner, C.; Coombs, N. D.; Fallis, I. A.; Ooi, L.-L.; Aldridge, S.; Colorimetric fluoride ion sensing by polyborylated ferrocenes: structural influences on thermodynamics and kinetics. *Inorganic Chemistry* **2008**, *47*, 793-804.

99. Fabre, B.; Lehmann, U.; Schluter, A. D.; Boronic ester-substituted terpyridine metal complex as a novel fluoride-sensitive redox receptor. *Electrochimica Acta* **2001**, *46*, 2855-2861.

100. Aldridge, S.; Bresner, C.; Fallis, I. A.; Coles, S. J.; Hursthouse, M. B.; Multidentate Lewis acids: synthesis, structure and mode of action of a redox-based fluoride ion sensor. *Chemical Communications* **2002**, 740-741.

101. Tamao, K.; Hayashi, T.; Ito, Y.; Shiro, M.; Pentacoordinate anionic bis(siliconates) containing a fluorine bridge between two silicon atoms. Synthesis, solid-state structures, and dynamic behavior in solution. *Organometallics* **1992**, *11*, 2099-2114.

102. Tamao, K.; Hayashi, T.; Ito, Y.; Anion complexation by bidentate Lewis acidic hosts, ortho-bis(fluorosilyl)benzenes. *Journal of Organometallic Chemistry* **1996**, *506*, 85-91.

103. Kawachi, A.; Tani, A.; Shimada, J.; Yamamoto, Y.; Synthesis of B/Si bidentate Lewis acids, o-(fluorosilyl)(dimesitylboryl)benzenes, and their fluoride ion affinity. *Journal of the American Chemical Society* **2008**, *130*, 4222-4223.

104. Jiang, X.; Vieweger, M. C.; Bollinger, J. C.; Dragnea, B.; Lee, D.; Reactivity-based fluoride detection: evolving design principles for spring-loaded turn-on fluorescent probes. *Organic Letters* **2007**, *9*, 3579-3582.

105. Kim, S. Y.; Hong, J. I.; Chromogenic and fluorescent chemodosimeter for detection of fluoride in aqueous solution. *Organic Letters* **2007**, *9*, 3109-3112.

106. Yang, X.-F.; Novel fluorogenic probe for fluoride ion based on the fluoride-induced cleavage of tert-butyldimethylsilyl ether. *Spectrochimica Acta Part A: Molecular and Biomolecular Spectroscopy* **2007**, *67*, 321-326.

107. Yang, X.-F.; Ye, S.-J.; Bai, Q.; Wang, X.-Q.; A fluorescein-based fluorogenic probe for fluoride ion based on the fluoride-induced cleavage of tert-butyldimethylsilyl ether. *Journal of Fluorescence* **2007**, *17*, 81-87.

108. Zhu, C.-Q.; Chen, J.-L.; Zheng, H.; Wu, Y.-Q.; Xu, J.-G.; A colorimetric method for fluoride determination in aqueous samples based on the hydroxyl deprotection reaction of a cyanine dye. *Analytica Chimica Acta* **2005**, *539*, 311-316.

109. Kim, T.-H.; Swager, T. M.; A fluorescent self-amplifying wavelength-responsive sensory polymer for fluoride ions. *Angewandte Chemie, International Edition* **2003**, *42*, 4803-4806.

110. Aaseth, J.; Shimshi, M.; Gabrilove, J. L.; Birketvedt, G. S.; Fluoride: a toxic or therapeutic agent in the treatment of osteoporosis? *Journal of Trace Elements in Experimental Medicine* **2004**, *17*, 83-92.

111. Carton, R. J.; Review of the 2006 United States National Research Council report: fluoride in drinking water. *Fluoride* **2006**, *39*, 163-172.

112. Worm, K.; Schmidtchen, F. P.; Molecular recognition of anions by zwitterionic host molecules in water. *Angewandte Chemie, International Edition in English* **1995**, *34*, 65-66.

113. Lin, Z.-H.; Ou, S.-J.; Duan, C.-Y.; Zhang, B.-G.; Bai, Z.-P.; Naked-eye detection of fluoride ion in water: a remarkably selective easy-to-prepare test paper. *Chemical Communications* **2006**, 624-626.

114. Sun, S.-S.; Lees, A. J.; Anion recognition through hydrogen bonding: a simple, yet highly sensitive, luminescent metal-complex receptor. *Chemical Communications* **2000**, 1687-1688.

115. Ros-Lis, J. V.; Garcia, B.; Jimenez, D.; Martinez-Manez, R.; Sancenon, F.; Soto, J.; Gonzalvo, F.; Valldecabres, M. C.; Squaraines as fluoro-chromogenic probes

for thiol-containing compounds and their application to the detection of biorelevant thiols. *Journal of the American Chemical Society* **2004**, *126*, 4064-4065.

116. Ros-Lis, J. V.; Martinez-Manez, R.; Soto, J.; A selective chromogenic reagent for cyanide determination. *Chemical Communications* **2002**, 2248-2249.
117. Garcia, F.; Garcia, J. M.; Garcia-Acosta, B.; Martinez-Manez, R.; Sancenon, F.; Soto, J.; Pyrylium-containing polymers as sensory materials for the colorimetric sensing of cyanide in water. *Chemical Communications* **2005**, 2790-2792.
118. Yang, Y.-K.; Tae, J.; Acridinium salt based fluorescent and colorimetric chemosensor for the detection of cyanide in water. *Organic Letters* **2006**, *8*, 5721-5723.
119. Tomasulo, M.; Sortino, S.; White, A. J. P.; Raymo, F. M.; Chromogenic oxazines for cyanide detection. *Journal of Organic Chemistry* **2006**, *71*, 744-753.
120. Tomasulo, M.; Raymo, F. M.; Colorimetric detection of cyanide with a chromogenic oxazine. *Organic Letters* **2005**, *7*, 4633-4636.
121. Chung, Y.; Lee, H.; Ahn, K. H.; N-acyl triazenes as tunable and selective chemodosimeters toward cyanide ion. *Journal of Organic Chemistry* **2006**, *71*, 9470-9474.
122. Ros-Lis, J. V.; Martinez-Manez, R.; Soto, J.; Subphthalocyanines as fluoro-chromogenic probes for anions and their application to the highly selective and sensitive cyanide detection. *Chemical Communications* **2005**, 5260-5262.
123. Badugu, R.; Lakowicz, J. R.; Geddes, C. D.; Cyanide-sensitive fluorescent probes. *Dyes and Pigments* **2005**, *64*, 49-55.
124. Badugu, R.; Lakowicz, J. R.; Geddes, C. D.; Excitation and emission wavelength ratiometric cyanide-sensitive probes for physiological sensing. *Analytical Biochemistry* **2004**, *327*, 82-90.
125. Badugu, R.; Lakowicz, J. R.; Geddes, C. D.; Fluorescence intensity and lifetime-based cyanide sensitive probes for physiological safeguard. *Analytica Chimica Acta* **2004**, *522*, 9-17.

126. Badugu, R.; Lakowicz, J. R.; Geddes, C. D.; Enhanced fluorescence cyanide detection at physiologically lethal levels: reduced ICT-based signal transduction *Journal of the American Chemical Society* **2005**, *127*, 3635-3641.

127. Palomares, E.; Martinez-Diaz, M. V.; Torres, T.; Coronado, E.; A highly sensitive hybrid colorimetric and fluorometric molecular probe for cyanide sensing based on a subphthalocyanine dye. *Advanced Functional Materials* **2006**, *16*, 1166-1170.

128. Liu, H.; Shao, X.-B.; Jia, M.-X.; Jiang, X.-K.; Li, Z.-T.; Chen, G.-J.; Selective recognition of sodium cyanide and potassium cyanide by diaza-crown ether-capped Zn-porphyrin receptors in polar solvents. *Tetrahedron* **2005**, *61*, 8095-8100.

129. Kim, Y.-H.; Hong, J.-I.; Ion pair recognition by Zn-porphyrin/crown ether conjugates: visible sensing of sodium cyanide. *Chemical Communications* **2002**, 512-513.

130. Poland, K.; Topoglidis, E.; Durrant, J. R.; Palomares, E.; Optical sensing of cyanide using hybrid biomolecular films. *Inorganic Chemistry Communications* **2006**, *9*, 1239-1242.

131. Chow, C.-F.; Lam, M. H. W.; Wong, W.-Y.; A heterobimetallic ruthenium(II)-copper(II) donor-acceptor complex as a chemodosimetric ensemble for selective cyanide detection. *Inorganic Chemistry* **2004**, *43*, 8387-8393.

132. Badr, I. H. A.; Meyerhoff, M. E.; Highly selective optical fluoride ion sensor with submicromolar detection limit based on aluminum(III) octaethylporphyrin in thin polymeric film. *Journal of the American Chemical Society* **2005**, *127*, 5318-5319.

133. Chaniotakis, N.; Jurkschat, K.; Mueller, D.; Perdikaki, K.; Reeske, G.; Bis[di-n-alkyl(fluoro)stannyl]methanes, (R2FSn)2CH2 (R = n-octyl, n-dodecyl): stable fluoride-selective carriers. *European Journal of Inorganic Chemistry* **2004**, 2283-2288.

134. Chiu, C.-W.; Gabbai, F. P.; A 9-borylated acridinyl radical. *Angewandte Chemie, International Edition* **2007**, *46*, 1723-1725.

135. Albrecht, K.; Kaiser, V.; Boese, R.; Adams, J.; Kaufmann, D. E.; Synthesis and properties of fluorescent organoboranes: triarylmethane-type dyes. *Perkin 2* **2000**, 2153-2157.

136. Yuan, Z.; Entwistle, C. D.; Collings, J. C.; Albesa-Jove, D.; Batsanov, A. S.; Howard, J. A. K.; Taylor, N. J.; Kaiser, H. M.; Kaufmann, D. E.; Poon, S.-Y.; Wong, W.-Y.; Jardin, C.; Fathallah, S.; Boucekkine, A.; Halet, J.-F.; Marder, T. B.; Synthesis, crystal structures, linear and nonlinear optical properties, and theoretical studies of (p-R-phenyl)-, (p-R-phenylethynyl)-, and (E)-[2-(p-R-phenyl)ethenyl]dimesitylboranes and related compounds. *Chemistry--A European Journal* **2006**, *12*, 2758-2771.

137. Yuan, Z.; Taylor, N. J.; Marder, T. B.; Williams, I. D.; Kurtz, S. K.; Cheng, L. T.; Three coordinate phosphorus and boron as p-donor and p-acceptor moieties respectively, in conjugated organic molecules for nonlinear optics; crystal and molecular structures of E-PhCH:CHB(mes)2, E-4-MeOC6H4CH:CHB(mes)2, and E-Ph2PCH:CHB(mes)2 [mes = 2,4,6-Me3C6H2]. *Journal of the Chemical Society, Chemical Communications* **1990**, 1489-1492.

138. Cossi, M.; Barone, V.; Cammi, R.; Tomasi, J.; Ab initio study of solvated molecules: a new implementation of the polarizable continuum model. *Chemical Physics Letters* **1996**, *255*, 327-335.

139. Tomasi, J.; Cammi, R.; Mennucci, B.; Medium effects on the properties of chemical systems: an overview of recent formulations in the polarizable continuum model (PCM). *International Journal of Quantum Chemistry* **1999**, *75*, 783-803.

140. Stahl, R.; Lambert, C.; Kaiser, C.; Wortmann, R.; Jakober, R.; Electrochemistry and photophysics of donor-substituted triarylboranes: symmetry breaking in ground and excited state. *Chemistry - A European Journal* **2006**, *12*, 2358-2370.

141. Yamaguchi, S.; Shirasaka, T.; Tamao, K.; Tridurylboranes extended by three arylethynyl groups as a new family of boron-based pi-electron systems. *Organic Letters* **2000**, *2*, 4129-4132.

142. Zhao, C. H.; Wakamiya, A.; Inukai, Y.; Yamaguchi, S.; Highly emissive organic solids containing 2,5-diboryl-1,4-phenylene unit. *Journal of the American Chemical Society* **2006**, *128*, 15934-15935.

143. Cavalli, V.; Silva, D. C.; Machado, C.; Machado, V. G.; Soldi, V.; The fluorosolvatochromism of Brooker's merocyanine in pure and in mixed solvents. *Journal of Fluorescence* **2006**, *16*, 77-86.

144. Baraldi, I.; Brancolini, G.; Momicchioli, F.; Ponterini, G.; Vanossi, D.; Solvent influence on absorption and fluorescence spectra of merocyanine dyes: a theoretical and experimental study. *Chemical Physics Letters* **2003**, *288*, 309-325.

145. Yamaguchi, S.; Akiyama, S.; Tamao, K.; Colorimetric fluoride ion sensing by boron-containing π-electron systems. *Journal of the American Chemical Society* **2001**, *123*, 11372-11375.

146. Kuz'mina, L. G.; Struchkov, Y. T.; Lemenovsky, D. A.; Urazowsky, I. F.; Structure of the triphenylcyanoboronate of a bis-dimethylaminomethyl[1,1-dimercurio]ferrocenophane dication. *Journal of Organometallic Chemistry* **1984**, *277*, 147-151.

147. Gabbai, F. P., A full derivation of the equation used to fit the data is provided in the experimental section.

148. Doty, J. C.; Babb, B.; Grisdale, P. J.; Glogowski, M.; Williams, J. L. R.; Boron photochemistry. IX. Synthesis and fluorescent properties of dimesitylphenylboranes. *Journal of Organometallic Chemistry* **1972**, *38*, 229-236.

149. Giger, W.; Simon, W.; Nuclear resonance spectroscopic study of protonated nitrogen compounds in trifluoroacetic acid. *Helvetica Chimica Acta* **1970**, *53*, 1609-1611.

150. Sessler, J. L.; Gale, P. A.; Cho, W.-S. *Anion Receptor Chemistry.* Royal Society of Chemistry, Cambridge, **2006**.

151. Canac, Y.; Lepetit, C.; Abdalilah, M.; Duhayon, C.; Chauvin, R.; Diaminocarbene and phosphonium ylide ligands: a systematic comparison of their donor character. *Journal of the American Chemical Society* **2008**, *130*, 8406-8413.

152. Kornath, A.; Neumann, F.; Oberhammer, H.; Tetramethylphosphonium fluoride: "naked" fluoride and phosphorane. *Inorganic Chemistry* **2003**, *42*, 2894-2901.

153. Terada, M.; Kouchi, M.; Novel metal-free Lewis acid catalysis by phosphonium salts through hypervalent interaction. *Tetrahedron* **2005**, *62*, 401-409.

154. Mukaiyama, T.; Kashiwagi, K.; Matsui, S.; A convenient synthesis of β-amino esters. The reaction of imines with ketene silyl acetals catalyzed by phosphonium salts. *Chemistry Letters* **1989**, 1397-1400.

155. Bontemps, S.; Bouhadir, G.; Miqueu, K.; Bourissou, D.; On the versatile and unusual coordination behavior of ambiphilic ligands o-R2P(Ph)BR'2. *Journal of the American Chemical Society* **2006**, *128*, 12056-12057.

156. Bebbington, M. W. P.; Bontemps, S.; Bouhadir, G.; Bourissou, D.; Photoisomerizable heterodienes derived from a phosphine borane. *Angewandte Chemie, International Edition* **2007**, *46*, 3333-3336.

157. Moebs-Sanchez, S.; Bouhadir, G.; Saffon, N.; Maron, L.; Bourissou, D.; Tracking reactive intermediates in phosphine-promoted reactions with ambiphilic phosphino-boranes. *Chemical Communications* **2008**, 3435-3437.

158. Batsanov, S. S.; Van der Waals radii of elements. *Inorganic Materials (Translation of Neorganicheskie Materialy)* **2001**, *37*, 871-885.

159. Konig, F. B.; Schonbohm, J.; Bayles, D.; AIM2000-a program to analyze and visualize atoms in molecules. *Journal of Computational Chemistry* **2001**, *22*, 545-559.

160. Lu, G.; Portscheller, J. L.; Malinakova, H. C.; Palladacycles with a metal-bonded sp3-hybridized carbon as intermediates in the synthesis of 2,2,3,4-tetrasubstituted

2H-1-benzopyrans and 1,2-dihydroquinolines. Effects of auxiliary ligands and substitution at a palladium-bonded tertiary carbon. *Organometallics* **2005**, *24*, 945-961.

161. Whited, M. T.; Rivard, E.; Peters, J. C.; Complexes of iron and cobalt with new tripodal amido-polyphosphine hybrid ligands. *Chemical Communications* **2006**, 1613-1615.

162. Harder, S.; Brandsma, L.; Kanters, J. A.; Duisenberg, A.; The structure of 2-(diphenylphosphino)phenyllithium: the significance of phosphorus-lithium bonding. *Journal of Organometallic Chemistry* **1991**, *420*, 143-154.

163. Gaussian 03, Revision C.02, M. J. Frisch, G. W. Trucks, H. B. Schlegel, G. E. Scuseria, M. A. Robb, J. R. Cheeseman, J. A. Montgomery, Jr., T. Vreven, K. N. Kudin, J. C. Burant, J. M. Millam, S. S. Iyengar, J. Tomasi, V. Barone, B. Mennucci, M. Cossi, G. Scalmani, N. Rega, G. A. Petersson, H. Nakatsuji, M. Hada, M. Ehara, K. Toyota, R. Fukuda, J. Hasegawa, M. Ishida, T. Nakajima, Y. Honda, O. Kitao, H. Nakai, M. Klene, X. Li, J. E. Knox, H. P. Hratchian, J. B. Cross, V. Bakken, C. Adamo, J. Jaramillo, R. Gomperts, R. E. Stratmann, O. Yazyev, A. J. Austin, R. Cammi, C. Pomelli, J. W. Ochterski, P. Y. Ayala, K. Morokuma, G. A. Voth, P. Salvador, J. J. Dannenberg, V. G. Zakrzewski, S. Dapprich, A. D. Daniels, M. C. Strain, O. Farkas, D. K. Malick, A. D. Rabuck, K. Raghavachari, J. B. Foresman, J. V. Ortiz, Q. Cui, A. G. Baboul, S. Clifford, J. Cioslowski, B. B. Stefanov, G. Liu, A. Liashenko, P. Piskorz, I. Komaromi, R. L. Martin, D. J. Fox, T. Keith, M. A. Al-Laham, C. Y. Peng, A. Nanayakkara, M. Challacombe, P. M. W. Gill, B. Johnson, W. Chen, M. W. Wong, C. Gonzalez, and J. A. Pople, Gaussian, Inc., Wallingford CT, 2004.

164. Lee, C. T.; Yang, W. T.; Parr, R. G.; Development of the Colle-Salvetti correlation-energy formula into a functional of the electron-density. *Physical Review B* **1988**, *37*, 785-789.

165. Miehlich, B.; Savin, A.; Stoll, H.; Preuss, H.; Results obtained with the correlation-energy density functionals of Becke and Lee, Yang and Parr. *Chemical Physics Letters* **1989**, *157*, 200-206.

166. Hariharan, P. C.; Pople, J. A.; Influence of the polarization functions on MO hydrogenation energies. *Theoretica Chimica Acta* **1973**, *28(3)*, 213-222.

167. Francl, M. M.; Pietro, W. J.; Hehre, W. J.; Binkley, J. S.; Gordon, M. S.; DeFrees, D. J.; Pople, J. A.; Self-consistent molecular orbital methods. XXIII. A polarization-type basis set for second-row elements. *Journal of Chemical Physics* **1982**, *77*, 3654-3665.

168. Hehre, W. J.; Ditchfield, R.; Pople, J. A.; Self-consistent molecular-orbital methods .12. Further extensions of Gaussian-type basis sets for use in molecular-orbital studies of organic-molecules. *Journal of Chemical Physics* **1972**, *56*, 2257-2261.

169. Bader, R. F. W. *Atoms in Molecules: A Quantum Theory*, Oxford Univ. Press; Oxford, UK; 1994.

170. Krishnan, R.; Binkley, J. S.; Seeger, R.; Pople, J. A.; Self-consistent molecular-orbital methods .20. Basis set for correlated wave-functions. *Journal of Chemical Physics* **1980**, *72*, 650-654.

171. Spitznagel, G. W.; Clark, T.; Schleyer, P. v. R.; Hehre, W. J.; Efficient diffuse function-augmented basis sets for anion calculation. Part IV. An evaluation of the performance of diffuse function-augmented basis sets for second row elements, Na-Cl. *Journal of Computational Chemistry* **1987**, *8*, 1109-1116.

172. Wender, P. A.; White, A. W.; Methodology for indole synthesis. *Tetrahedron Letters* **1981**, *22*, 1475-1478.

173. Hughes, M. P.; Smith, B. D.; Enhanced carboxylate binding using urea and amide-based receptors with internal Lewis acid coordination: a cooperative polarization effect. *Journal of Organic Chemistry* **1997**, *62*, 4492-4499.

174. Hughes, M. P.; Shang, M.; Smith, B. D.; High affinity carboxylate binding using neutral urea-based receptors with internal Lewis acid coordination. *Journal of Organic Chemistry* **1996**, *61*, 4510-4511.

175. Chang, K.-J.; Moon, D.; Lah, M. S.; Jeong, K.-S.; Indole-based macrocycles as a class of receptors for anions. *Angewandte Chemie, International Edition* **2005**, *44*, 7926-7929.

176. Kang, S. O.; Llinares, J. M.; Powell, D.; VanderVelde, D.; Bowman-James, K.; New polyamide cryptand for anion binding. *Journal of the American Chemical Society* **2003**, *125*, 10152-10153.

177. Ulrich, G.; Ziessel, R.; Harriman, A.; The chemistry of fluorescent BODIPY dyes: versatility unsurpassed. *Angewandte Chemie, International Edition* **2008**, *47*, 1184-1201.

178. Loudet, A.; Burgess, K.; BODIPY dyes and their derivatives: syntheses and spectroscopic properties. *Chemical Reviews* **2007**, *107*, 4891-4932.

179. Treibs, A.; Kreuzer, F. H.; Difluoroboryl complexes of di- and tripyrrylmethenes. *Justus Liebigs Annalen der Chemie* **1968**, *718*, 208-23.

180. Picou, C. L.; Stevens, E. D.; Shah, M.; Boyer, J. H.; Structure of 4,4-difluoro-1,3,5,7,8-pentamethyl-3a,4a-diaza-4-bora-s-indacene. *Acta Crystallographica, Section C: Crystal Structure Communications* **1990**, *C46*, 1148-1150.

181. Vidovic, D.; Findlater, M.; Cowley, A. H.; A β-diketiminate-supported boron dication. *Journal of the American Chemical Society* **2007**; *129*, 8436-8437.

182. Gates, D. P.; McWilliams, A. R.; Ziembinski, R.; Liable-Sands, L. M.; Guzei, I. A.; Yap, G. P. A.; Rheingold, A. L.; Manners, I.; Chemistry of boratophosphazenes: synthesis of borazine-phosphazene hybrid cations, and new inorganic heterocycles by skeletal substitution reactions. *Chemistry--A European Journal* **1998**, *4*, 1489-1503.

183. Lesley, M. J. G.; Woodward, A.; Taylor, N. J.; Marder, T. B.; Cazenobe, I.; Ledoux, I.; Zyss, J.; Thornton, A.; Bruce, D. W.; Kakkar, A. K.; Lewis acidic

borane adducts of pyridines and stilbazoles for nonlinear optics. *Chemistry of Materials* **1998**, *10*, 1355-1365.

184. Corma, A.; Galletero, M. S.; Garcia, H.; Palomares, E.; Rey, F.; Pyrene covalently anchored on a large external surface area zeolite as a selective heterogeneous sensor for iodide. *Chemical Communications* **2002**, 1100-1101.

185. Ulrich, G.; Goze, C.; Goeb, S.; Retailleau, P.; Ziessel, R.; New fluorescent aryl- or ethynylaryl-boron-substituted indacenes as promising dyes. *New Journal of Chemistry* **2006**, *30*, 982-986.

186. Goze, C.; Ulrich, G.; Mallon, L. J.; Allen, B. D.; Harriman, A.; Ziessel, R.; Synthesis and photophysical properties of borondipyrromethene dyes bearing aryl substituents at the boron center. *Journal of the American Chemical Society* **2006**, *128*, 10231-10239.

187. Cowley, A. H.; Lu, Z.; Jones, J. N.; Moore, J. A.; Synthesis and structure of a boron cation supported by a β-diketiminate ligand. *Journal of Organometallic Chemistry* **2004**, *689*, 2562-2564.

188. Shah, M.; Thangaraj, K.; Soong, M. L.; Wolford, L.; Boyer, J. H.; Politzer, I. R.; Pavlopoulos, T. G.; Pyrromethene-BF2 complexes as laser dyes: 1. *Heteroatom Chemistry* **1990**, *1*, 389-399.

189. Kim, H.; Burghart, A.; Welch, M. B.; Reibenspies, J.; Burgess, K.; Synthesis and spectroscopic properties of a new 4-bora-3a,4a-diaza-s-indacene (BODIPY) dye. *Chemical Communications* **1999**, 1889-1890.

VITA

Todd William Hudnall

c/o Prof. François Gabbaï
Department of Chemistry
Texas A&M University
College Station, TX 77843-3255

Education:

Ph.D. in Chemistry from Texas A&M University; Graduated: Dec. 2008
B.S. in Chemistry from Texas State University-San Marcos; Graduated: May 2004

Publications:

Hudnall, T. W.; Gabbaï, F. P. "A BODIPY boronium cation for the sensing of fluoride ions." *Chem. Commun.*; *in press.*

Hudnall, T. W.; Kim, Y.; Bebbington, M. W. P.; Bourissou, D.; Gabbaï, F. P. "Fluoride ion chelation by a bidentate phosphonium/borane Lewis acid." *J. Am. Chem. Soc.*; *in press.*

Dorsey, C. L.; Jewula, P.; Hudnall, T. W.; Hoefelmeyer, J. D.; Taylor,T. J.; Honesy, N.; Chiu, C-W.; Schulte, M.; Gabbaï, F. P. "Fluoride ion complexation by a B_2/Hg heteronuclear tridentate Lewis acid-a structural and electrochemical invest-igation." *Dalton Trans.*; *in press.*

Hudnall, T. W.; Gabbaï, F. P. "Ammonium boranes for the selective complexation of cyanide or fluoride ions in water." *J. Am. Chem. Soc.* **2007,** *129*, 11978-11986.

Hudnall, T. W.; Bondi, J. F.; Gabbaï, F. P. "*ortho*-Borylated trifluoroacet- anilides–synthesis and fluoride ion binding properties." *Main Group Chemistry.* **2006**, *5(4)*, 319-327.

Hudnall, T. W.; Melaïmi, M. A.; Gabbaï, F. P. "A hybrid Lewis acid/hydrogen bond donor receptor for fluoride." *Org. Lett.* **2006**, *8(13)*,2747-2749.

Hoppens, N. C.; Hudnall, T. W.; Foster, A.; Booth, C. J. "Aliphatic-Aromatic Copolyesters Derived from 2,2,4,4- Tetramethyl-1,3-cyclo-butanediol." *J. Polym. Sci., Part A: Polym Chem.,* **2004**, *42(14),*3473- 3478.

Awards:

Richard W. Schmude, Jr. Endowed Graduate Scholarship in Chemistry May 2008.